Nuclear Energy Research Initiative

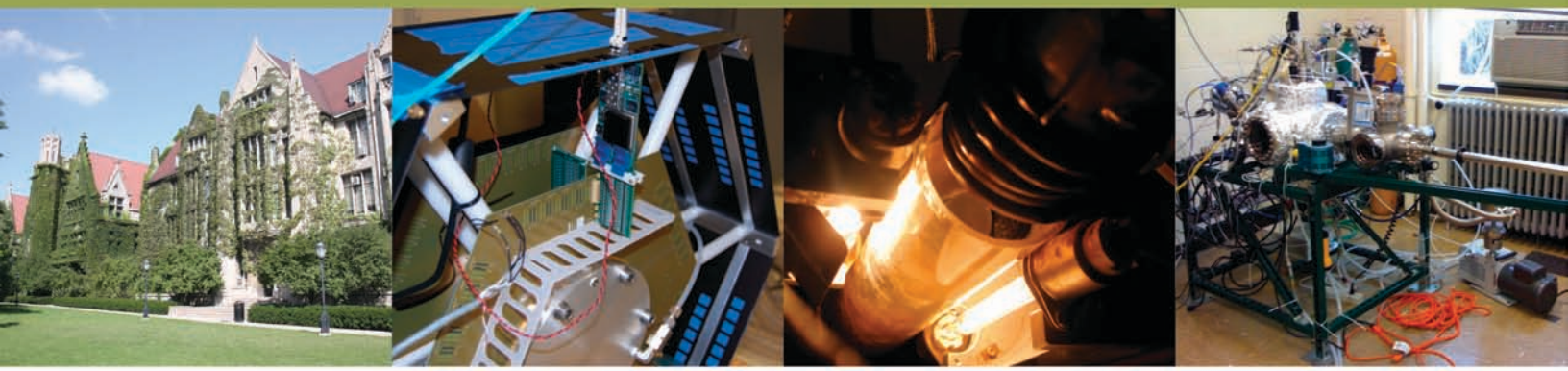

2009 Annual Report

Disclaimer

This document was prepared as an account of work sponsored by an agency of the United States Government. Neither the United States Government nor any of its employees makes any warranty, expressed or implied, or assumes any legal liability or responsibility for the accuracy, completeness, or usefulness of any information, apparatus, product, or process disclosed, or represents that its use would not infringe upon privately owned rights. Reference herein to any specific commercial product, process, or service by trade name, trademark, manufacturer, or otherwise does not necessarily constitute or imply its endorsement, recommendations, or favoring by the United States Government. The views and opinions expressed by the authors herein do not necessarily state or reflect those of the United States Government and shall not be used for advertising or product endorsement purposes.

Available to DOE, DOE contractors, and the public from the

U.S. Department of Energy
Office of Nuclear Energy
1000 Independence Avenue, S.W.
Washington, D.C. 20585

Foreword

What are the steps we must take as a nation to create new, clean energy jobs and ensure America's long-term competitiveness? What are the consequences for our climate of inaction? How can science and technology offer us new and better choices—and how can America's young people make a difference?

– U.S. Secretary of Energy Steven Chu, The White House Blog, March 8, 2010

The Nuclear Energy Research Initiative (NERI) has been addressing these questions since its inception in fiscal year (FY) 1999. The Department of Energy, Office of Nuclear Energy (DOE-NE), established NERI to support research that addresses long-term barriers to maintaining and expanding nuclear generation of electricity in this country. Towards that end, NERI has successfully encouraged, preserved, and advanced nuclear science and technology research and development.

The NERI program has evolved during its 11-year lifetime to keep pace with DOE's policies and priorities for the Nation's energy future. From its initial support of both university- and national laboratory-based research, the program has twice shifted its mission to help build the nation's academic infrastructure and harness the creativity and innovative thinking of America's young scientists. Since FY 2004, NERI has exclusively funded university-led research, with national laboratories and industry partners providing valuable contributions as collaborators. In FY 2008, NE further advanced this undertaking by creating the Nuclear Energy University Programs (NEUP), whose primary objectives are 1) to better integrate university research with technical programs and 2) to further the quality of nuclear science and engineering education. In FY 2009, NE consolidated its university support into this program. Consistent with the NEUP mission, student enrollment in nuclear engineering programs has increased fivefold since NERI's inception.

Increased university involvement has furthered NERI's successes, fostering innovative ideas in advanced nuclear energy systems, hydrogen production from nuclear power, advanced nuclear fuels and fuel cycles, non-proliferation, waste treatment, and advanced materials for reactors. Over the past 11 years, researchers have made significant contributions to each of these areas. An overview of major contributions has been included in Section 3 of the *Nuclear Energy Research Initiative 2009 Annual Report*. This report also provides updates on individual NERI projects that were active or completed in FY 2009. These updates reflect 20 projects initiated in FY 2006, 22 projects initiated in FY 2007, and 11 NERI Consortia (NERI-C) projects initiated in FY 2008. Details of projects completed before FY 2009 can be found in previous NERI annual reports. Future NE-funded university-led projects will be discussed in NEUP annual reports, the first of which will be published in fall 2010.

The results of this targeted research contribute to a robust nuclear science and engineering infrastructure, responding to the need for economical and environmentally conscious sources of energy. By promoting advanced nuclear energy systems and state-of-the-art research, NERI has enabled the United States to maintain a competitive position in the nuclear energy arena at home and abroad.

Dr. Warren F. "Pete" Miller Jr.
Assistant Secretary, Office of Nuclear Energy
U.S. Department of Energy

Table of Contents

1.0 OVERVIEW 1

2.0 RESEARCH AREAS 3

3.0 RESEARCH ACCOMPLISHMENTS 9

4.0 PARTICIPANTS: FROM INDUSTRY TO ACADEMIA 13

5.0 THE INTERNATIONAL NUCLEAR ENERGY RESEARCH INITIATIVE 19

6.0 PROJECT SUMMARIES 21

6.1 GENERATION IV NUCLEAR ENERGY SYSTEMS INITIATIVE 21

6.2 FUEL CYCLE RESEARCH AND DEVELOPMENT 77

6.3 NUCLEAR HYDROGEN INITIATIVE 157

PROJECT INDEX 185

NUCLEAR ENERGY RESEARCH INITIATIVE

1.0 Overview

The Nuclear Energy Research Initiative (NERI)

NERI is a national, research-oriented initiative managed and funded by the Department of Energy's Office of Nuclear Energy (DOE-NE). The purpose of this initiative is to sponsor university-led research and development (R&D) that addresses the principal barriers affecting the growth of nuclear energy in the United States. Since its inception in 1999, the initiative has helped foster innovative ideas in NE's primary research programs: advanced nuclear energy systems, hydrogen production from nuclear power, and advanced nuclear fuels and fuel cycles. In addition to responding to the Nation's need for current nuclear energy research to advance the development of nuclear energy technology, NERI has helped to preserve the Nation's nuclear science and engineering infrastructure. Although the NERI program is coming to a conclusion in 2010 after 11 successful years, DOE-NE support of academia will continue through the Nuclear Energy University Programs (NEUP).

To achieve the Nation's long-range goal of establishing nuclear energy as a viable and expandable energy option, NERI has the following objectives:

- To address and help overcome the potential technical and scientific obstacles to the long-term future use of nuclear energy in the United States, including non-proliferation, economics, and nuclear waste disposition.
- To advance the state of U.S. nuclear technology to maintain a competitive position in overseas and domestic markets.
- To promote and maintain a nuclear science and engineering infrastructure to meet present and future technical challenges.
- To build an infrastructure with an emphasis on nuclear education and university-led R&D, integrated with efforts of the national laboratories and industry.

The graphic on page 2 summarizes key features of the NERI program.

Inception of NERI

In January 1997, the President's Council of Advisers on Science and Technology (PCAST) reviewed the current national energy R&D portfolio and provided a strategy to ensure that the United States has a program to address the Nation's energy and environmental needs for the next century. The PCAST Energy Research and Development Panel determined that securing a viable nuclear energy option was essential to meeting future U.S. energy needs. Specifically, the panel recommended that DOE implement an R&D effort to address the principal obstacles to achieving this objective, targeting such areas as nuclear waste, proliferation, safety, and economics. DOE was to fund research through this new initiative based on a competitive selection of proposals to be submitted by national laboratories, universities, and industry.

In response to these recommendations, DOE established NERI in FY 1999. The program received Congressional appropriations to begin sponsoring innovative scientific and engineering R&D that addresses key issues affecting the future use of nuclear energy and preserves the Nation's nuclear science and technology leadership.

NERI 2009 Annual Report

This *Nuclear Energy Research Initiative 2009 Annual Report* serves to inform interested parties of progress made in NERI on a programmatic level, as well as research progress made on individual NERI projects. Following is an overview of each section:

- Section 2 presents the scope of NE R&D programs supported by NERI from program inception through FY 2009.
- Section 3 highlights major research accomplishments of the NERI program.
- Section 4 discusses NERI selection and participants, as well as the program's shift in focus to U.S. university nuclear programs, including the resulting impact.
- Section 5 presents NERI's corresponding international component, the International Nuclear Energy Research Initiative (I-NERI).
- Section 6 presents progress reports for 42 FY 2006 and FY 2007 projects, as well as the 11 NERI-C projects.

Projects are organized by their primary research area: the Generation IV Nuclear Energy Systems Initiative (Gen IV), the Fuel Cycle Research and Development (FCR&D) program, and the Nuclear Hydrogen Initiative (NHI). Numbering is designated by the fiscal year in which the award was made. At the end of the report, there is an index of NERI projects grouped by fiscal year and sequentially ordered by project number.

Additional information on the NERI program, including previous annual reports, is available on the NERI website: *http://nuclear.energy.gov/neri/neNERIresearch.html*.

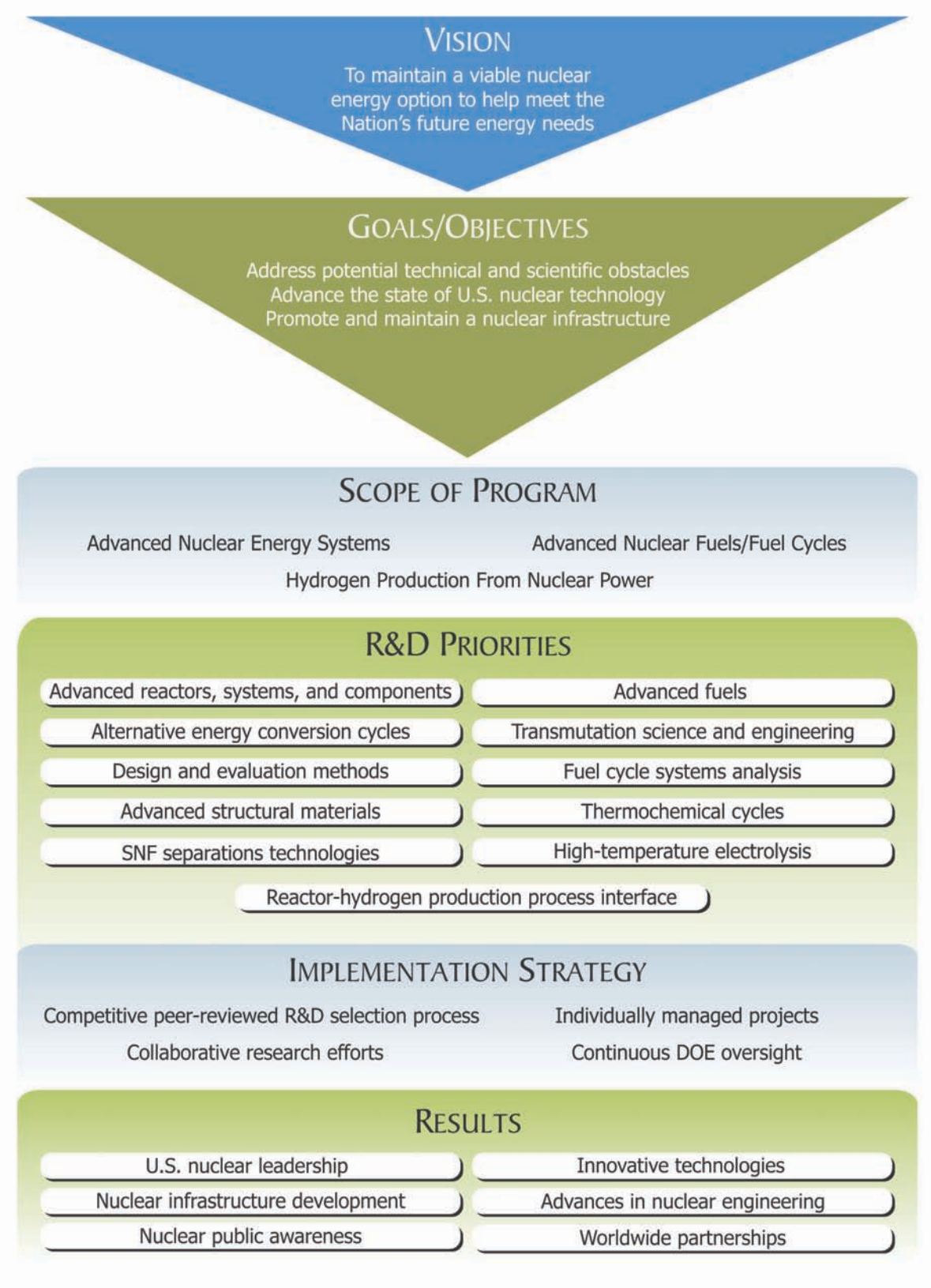

NUCLEAR ENERGY RESEARCH INITIATIVE

2.0 Research Areas

FY 2009 Focus

Current NERI research projects support two primary NE R&D programs: Gen IV and FCR&D. Several ongoing projects continue to support NHI, which was previously a stand-alone NE research area but became part of Gen IV in FY 2009. These initiatives support the revitalization of nuclear technology by developing safe, efficient technologies for future electrical power production and energy conversion systems. Following are descriptions of these programs.

Generation IV Nuclear Energy Systems Initiative

Gen IV nuclear energy systems are being developed to achieve high burnup using transmutation and recycled fuel, allowing for the efficient use of domestic uranium resources while minimizing radioactive waste. Advances in safety and physical protection will guard against possible acts of terror or diversion of nuclear materials, helping to ensure public confidence in nuclear technology.

Current advanced reactor system development efforts in the U.S. are focused on very high-temperature reactor (VHTR) technologies. In particular, research is directed towards development of the Next Generation Nuclear Plant (NGNP), a VHTR design that will concurrently produce hydrogen and generate electricity. In addition to these efforts, Gen IV includes three crosscutting programmatic areas of research—design and evaluation methods, crosscutting materials for advanced reactors, and energy conversion—that are germane to multiple reactor concepts. Current Gen IV research areas are described below.

Next Generation Nuclear Plant. Research projects focus on the validation of reactor physics and core design analysis tools, development and validation of reactor thermal-hydraulic and mechanical design analysis tools, materials research, power-conversion unit assessments, and safety and risk analysis of the VHTR. The scope of these projects also includes project design, system design and analysis methodology, and fuel development and qualification.

Sodium-Cooled Fast Reactor (SFR). The SFR system features a liquid metal fast-spectrum reactor that can operate on recycled used fuel to help manage high-level radioactive wastes, particularly plutonium and other actinides. With innovations to reduce capital cost, the mission can extend to economic electricity production. The SFR can also lead to sustainable energy production, given the proven capability of sodium reactors to utilize almost all of the energy in natural uranium. Activities under this research area focus on comparative technical and economic studies of various SFR designs, fuel-development activities, and advanced modeling and simulations techniques. Other topics include selection and testing of alloy materials and conceptual design studies of supercritical carbon dioxide secondary plant systems.

Design and Evaluation Methods. Analytical methods, modeling techniques, computer codes, and databases must be developed for Gen IV plants. In addition, methodologies must be developed to evaluate system performance against Gen IV goals.

Materials. Projects in this area include the selection, development, and qualification of structural materials necessary to design and construct advanced nuclear reactors and the coordination with similar research being conducted for FCR&D and NHI. Research plans include both crosscutting and reactor-specific materials activities.

Energy Conversion. Projects in this area focus on both the supercritical carbon dioxide Brayton cycle and the high-temperature helium Brayton cycle. A demonstration experiment and simulation model are also planned to determine plant characteristics, performance, and dynamic response. For the high-temperature helium Brayton cycle, project goals include the engineering analysis of inter-stage heating and cooling configurations, design analysis of heat exchangers and turbo-machinery, and planning of a small-scale demonstration experiment.

Fuel Cycle Research and Development

The mission of FCR&D is to enable the safe, secure, economic, and sustainable expansion of nuclear energy by conducting R&D focused on nuclear fuel recycling and waste management to meet U.S. needs. To meet the program's objectives, several technologies need to be developed to allow closing of the fuel cycle: first, technologies to separate the used nuclear fuel into products that can be reused and wastes that must be disposed of safely; second, technologies to transform the products into fuels that can be reused in reactors; and third, reactors that use the recycled fuel to produce energy. For long term sustainability, a new type of reactor is needed, using fast neutrons—initially for improved waste

management as we transition to a closed fuel cycle and address the stocks of used fuel that have accumulated, and later for resource extension as uranium resources become scarcer and more expensive.

Used-fuel treatment and recycling are critical in supporting the expansion of proliferation-resistant nuclear power. This multifaceted program involves recycling used fuel, fabricating fuel assemblies containing the removed long-lived actinides and transuranics (TRUs), burning the assemblies in a fast reactor, and developing more benign waste-disposal technologies for the remaining radioisotopes and process wastes. Advanced safeguards technologies and techniques will be developed to ensure reduced proliferation risk. Resulting technologies will satisfy requirements for a controlled, proliferation-resistant nuclear materials management system. This is accomplished by division of the program activities into key R&D campaigns:

- Separations
- Fuels
- Transmutation Science and Engineering
- Systems Analysis
- Materials Protection, Accountability, and Control Technologies (MPACT)

Separations. Separations research comprises areas such as the development of aqueous and electrochemical separations technologies; advancement of spent fuel treatment processes; improvement of temporary or permanent storage forms; treatment of spent fuel from the Experimental Breeder Reactor (EBR-II) in preparation for disposal; and conceptual planning of future spent fuel treatment plants and advanced processing technologies.

Fuels. This research area includes projects associated with advanced fuel development for light-water reactors (LWRs), Generation IV reactors, and dedicated transmuters; remote fuel fabrication evaluation; development and selection of advanced clad materials; safety analyses of different advanced fuel types; and fabrication, characterization, performance testing, post-irradiation examination, and modeling of fuels for various reactors (LWR, VHTR, fast-spectrum systems). NERI research projects are also pursuing tri-isotropic (TRISO) fuel development for the VHTR.

Transmutation Science and Engineering. Transmutation is a process by which long-lived radioactive species are converted to short-lived nuclides via nuclear capture or fission. The primary purpose of this research area is to develop an engineering basis for the transmutation of plutonium, minor actinides, and long-lived fission products. This research area explores physics and materials challenges for transmutation systems, whether they be reactors or accelerator-driven systems.

Systems Analysis. Broad systems studies, transmutation system studies and integrated model development, and fuel cycle safety assessment are all tasks within the domain of this research area. The research objectives of projects under this area are to provide analysis on fuel cycle infrastructure needs, supply recommendations on fuel types and reactor systems from the perspective of the overall fuel cycle, and perform an analysis to assist DOE in determining the need for a second repository.

Materials Protection, Accountability, and Control Technologies (MPACT). The MPACT campaign (formerly safeguards) develops technologies and analysis tools to support next-generation nuclear materials management for future U.S. fuel cycles, with particular attention to prevent diversion or misuse. Key research needs include development of new sensor materials and measurement techniques; novel methods for data integration and real-time analysis; advanced concepts for achieving real-time, online, and continuous nuclear material accountancy; and novel methods for assessing the proliferation risk associated with fuel cycles.

History of NERI Research Areas

The overall NE goal is to position nuclear energy as a viable fuel source that will help the United States sustain its growing energy needs. NERI has supported this goal since the program's inception and has helped target the R&D efforts necessary for mission success. Specific topic areas have evolved over the past 11 years, and NERI research achievements have played an integral role in that development.

In order to establish the initial focus of NERI's research efforts, DOE convened a workshop in April 1998 for nuclear community stakeholders, including national laboratory, university, and industry representatives. This workshop resulted in the focus areas below for scientific and engineering R&D.

- Reactors and fuel technologies with reduced proliferation risks
- New reactor designs to achieve improved performance, higher efficiency, and reduced cost, including low-output power reactors (for use where large reactors are not attractive)
- Advanced nuclear fuels

- New technologies for management of nuclear waste
- Fundamental nuclear science

To help guide this R&D effort and shape the future direction of nuclear energy R&D, the Secretary of the Department of Energy established an independent advisory committee, the Nuclear Energy Research Advisory Committee (NERAC). A NERAC-chartered subcommittee developed the *Long-Term Nuclear Energy Science and Technology Research Plan* to guide nuclear energy research to the year 2020. In addition, NERAC issued a report: *Technology Opportunities for Increasing the Proliferation Resistance of Global Nuclear Power Systems (TOPS)*. The Department used these reports as long-term guidance for their R&D plan and the TOPS report to guide future NERI research activities. NERAC has since then been changed to Nuclear Energy Advisory Committee (NEAC).

In May 2001, the Vice President's National Energy Policy Development Group issued the *National Energy Policy*. This policy provided the core element in the planning for DOE's nuclear energy research programs, addressing, among other areas, the R&D of advanced reactor and fuel cycle concepts, hydrogen production from nuclear energy, and the associated enabling sciences and technologies. NERI ensured its R&D focus addressed research requirements introduced in the *National Energy Policy*. Figure 1 shows a breakdown of NERI projects by research area during the program's first six years. These research projects represented the research categories described below.

Advanced Nuclear Energy Systems/New Reactor Designs and Technologies. This program element includes the investigation and preliminary development of advanced concepts for reactor and power conversion systems. These systems offer the prospect of improved performance and operation, design simplification, enhanced safety, and reduced overall cost. Projects involve innovative reactors, system and component designs, alternative power conversion cycles for terrestrial applications, new research in advanced digital instrumentation and control and automation technologies, and other important design features and characteristics.

Hydrogen Production from Nuclear Power. This program element includes R&D to identify and evaluate new and innovative concepts for producing hydrogen using nuclear reactors. This research investigates hydrogen-generation processes compatible with advanced reactor systems and integrates parameters needed to develop systems that are efficient and cost-effective. Projects in this section were integrated into either the Advanced Nuclear Energy Systems area or the Fundamental Science area, based on their technical focus.

Advanced Nuclear Fuels/Fuel Cycles. This element includes R&D to provide measurable improvements in the understanding and performance of nuclear fuel and fuel cycles with respect to safety, waste production, proliferation resistance, and economics in order to enhance the long-term viability of nuclear energy systems. This research supports Generation IV concepts by improving fuel performance, developing fuels capable of withstanding higher temperatures and more highly corrosive environments, and developing advanced proliferation-resistant fuels capable of high burnup.

Fundamental Nuclear Science. This element includes R&D in the fields of materials science and fundamental chemistry. Fundamental science research funded by NERI applies to and supports the preceding program elements in advanced nuclear engineering technology. Materials science applications include R&D on materials for use in advanced nuclear reactor systems, structures, and components (including fuel cladding) that may perform in high-radiation fields, high temperatures and pressures, and/or highly corrosive environments (such as lead-bismuth). Chemical science research may focus on developing and improving primary and secondary coolant chemistry in advanced reactors. Another research subject includes investigating nuclear isomers that could prove beneficial in civilian applications.

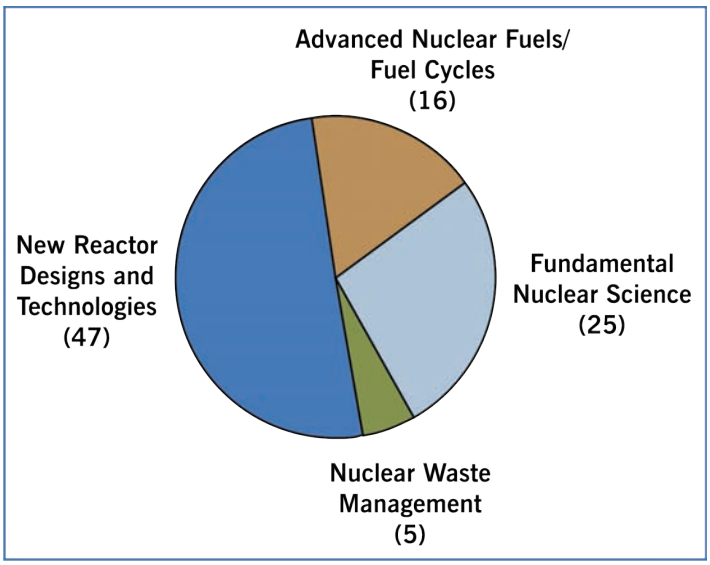

Figure 1. Distribution of NERI projects by R&D area from FY 1999 through FY 2004.

Nuclear Waste Management. NERI funded five projects in the waste management area in FY 1999. Shortly thereafter, waste management was transferred to the Office of Civilian Radioactive Waste Management (OCRWM), whereupon OCRWM assumed management for all related R&D projects.

In FY 2002, several new nuclear R&D programs were initiated: the Generation IV Nuclear Energy Systems Initiative (the equivalent of Gen IV, described above), the Advanced Fuel Cycle Initiative (which has evolved to become the FCR&D program), and the Nuclear Hydrogen Initiative (described below). NERI project selection began to focus on providing a supportive role to these programs.

Nuclear Hydrogen Initiative (NHI). The NHI mission was to develop hydrogen production technologies fueled by nuclear energy. NERI research planned under this initiative initially included projects associated with thermochemical cycles (such as sulfur-based cycles), high-temperature electrolysis (using electricity to produce hydrogen from steam), and reactor hydrogen-production process support systems. Current solicitations focus on high-temperature electrolysis as the most promising hydrogen production process. The goal is to demonstrate a process that is compatible with nuclear energy systems through scaled experiments, then to couple an engineering-scale demonstration plant with a Generation IV reactor concept. Therefore, in late FY 2009, hydrogen production was discontinued as a stand-alone program and rolled into NGNP research.

Advanced Fuel Cycle Initiative. The Advanced Fuel Cycle Initiative (AFCI), which has evolved into the FCR&D program, comprised six areas of study: separations and waste forms, transmutation fuels, transmutation science and engineering, systems analysis, advanced safeguards, and advanced modeling and simulation. The first four categories are described above as ongoing FCR&D research areas.

Advanced safeguards was the predecessor to MPACT. This area focused on development of advanced safeguards technologies and methods through improving fundamental understanding of nuclear materials and the physics of detection methods, demonstrating improved nondestructive assay technologies, creating integrated process monitoring and control technologies, and integrating and correlating information to enable near-real-time knowledge of facility operations.

Advanced modeling and simulation has become a stand-alone program area rather than an FCR&D program element. Under AFCI, this topic focused on building end-to-end codes to understand the detailed integrated performance of new nuclear systems, as well as smaller-scale material modeling work and atomistic-to-continuum multi-scale simulations to provide understanding and improved properties and models for integrated codes. Scientific codes created through this research could serve as engineering tools for industry. Researchers also developed methodologies to be used by Nuclear Energy Advanced Modeling and Simulation (NEAMS) program elements—specifically integrated performance and safety codes and fundamental methods and models—to create confidence that the simulation results are a reflection of nature and to quantify the uncertainties inherent in modeling and simulation.

In December 2002, NERAC issued *A Technology Roadmap for Generation IV Nuclear Energy Systems*. In coordination with the ten member countries in the Generation IV International Forum (GIF), six reactor system concepts were selected for further research and development: the gas-cooled fast reactor (GFR) system, the lead-alloy-cooled fast reactor (LFR) system, the molten salt reactor (MSR) system, the supercritical water-cooled reactor (SCWR) system, and the SFR and VHTR systems described above. These systems garnered the attention of both domestic and international research communities.

Gas-Cooled Fast Reactor. Projects seek to develop a safe and sustainable GFR reactor that has a closed fuel cycle, is highly efficient (using the Brayton power conversion cycle), and is capable of producing electrical power and/or hydrogen.

Lead-Alloy-Cooled Fast Reactor. Projects support production of a small nuclear energy system for deployment in remote locations and in developing countries. R&D efforts are aimed at defining and selecting the reference system, preparing a defendable safety case for the system, and licensing (e.g., through testing a demonstration reactor system).

Molten Salt Reactor. MSRs can be used for producing electricity, hydrogen, or fissile fuels, as well as actinide burning. In this design, the nuclear fuel is dissolved directly in a molten fluoride salt coolant that circulates throughout the primary system. Energy is transferred to a clean molten salt intermediate heat transport loop, then through a high-temperature Brayton power conversion cycle. The NGNP uses similar liquid salt technology in the hydrogen-production loop, so Gen IV supports many shared areas of research, such as Brayton power cycles, compact heat exchangers (HXs), and carbon composite materials.

Supercritical Water-Cooled Reactor. Projects concentrate on showing the technical feasibility of a LWR operating above the critical pressure of water, thus producing low-cost electricity. The focus of this research includes three main areas: 1) the evaluation of dynamic power/flow instabilities; 2) testing of materials for the core and vessel internals, specifically investigating corrosion and stress-corrosion cracking; and 3) investigation of basic thermal and heat transfer phenomena for the reactor.

During FY 2006 and FY 2007, NERI solicitations focused on federal R&D priorities as outlined in the *Energy Policy Act of 2005* and the *Advanced Energy Initiative of 2006*. Figure 2 provides a breakdown of NERI projects during the second half of the program. The United States began limiting its reactor development work under the Gen IV initiative to the VHTR for the NGNP and to the SFR as the advanced burner design for the Global Nuclear Energy Partnership (GNEP). Foreign collaborators are leading research on the other reactor systems under GIF. In FY 2009, domestic activities supported the reactor systems noted above through monitoring international R&D efforts, participating in related international forums, and completing ongoing research projects.

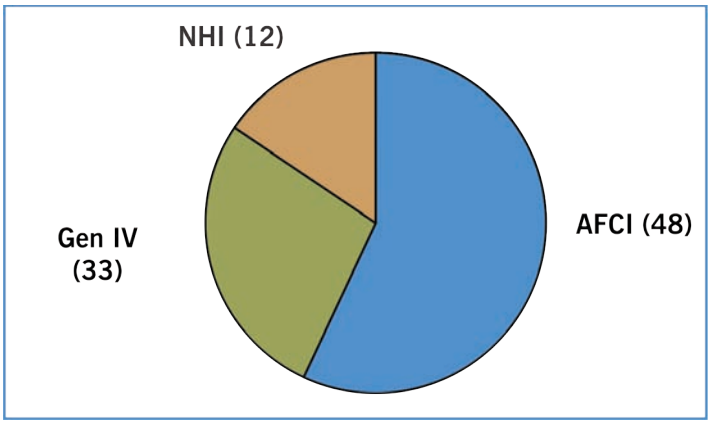

Figure 2. Distribution of NERI projects by R&D program area from FY 2005 through FY 2009.

NUCLEAR ENERGY RESEARCH INITIATIVE

3.0 Research Accomplishments

Over the past 11 years, NERI-funded projects have made significant contributions to nuclear energy R&D. The projects and findings are too numerous to cover comprehensively within the confines of this report. However, in conjunction with the research history in the previous chapter, this section provides an overview of NERI contributions and highlights some of the program's more significant successes.

Reactor Designs

NERI researchers have contributed greatly to the design of advanced nuclear reactors, improving upon existing designs and generating novel concepts for the next generation of reactors.

DOE supported research into several small reactor designs under the Gen IV program, among them the Secure Transportable Autonomous Reactor (STAR). STAR is a multi-purpose reactor design that operates with little operator interaction for the very long term. One NERI project (99-154) assessed the feasibility of a 125 MWth highly modular lead-bismuth-cooled fast-spectrum reactor concept, the encapsulated nuclear heat source (ENHS), that is characterized by low waste, exceptionally high proliferation resistance, and high uranium utilization. Three years later, researchers (02-065) investigated the feasibility of coupling the STAR-LM, a natural circulation liquid metal LFR, to an S-CO_2 Brayton cycle. They developed new core designs with a protective internal structural barrier, created a dynamic computer code to model behavior of the Brayton cycle compressors and turbine, and determined that injection of non-condensable gas above the core would significantly increase power by enhancing the natural circulation flowrate of the lead coolant. STAR-H2 is an adaptation for hydrogen and potable water production (00-060), with silicon carbide cladding and reactor internals, that is sufficient to meet the energy and water needs of 25,000 in a developing country.

Through NERI project 99-027, Westinghouse led development of the International Reactor Innovative and Secure (IRIS), a small integral primary system pressurized water reactor (PWR) with enhanced passive safety and proliferation resistance. In a later project (02-018), Westinghouse collaborated to design the Pressurizer Dynamic Test Facility, which represents a volumetrically scaled IRIS internal pressurizer used to conduct dynamic tests with steam or nitrogen as the working fluid.

Feasibility of the Gen IV SCWR design was assessed in NERI project 01-001. Researchers concluded that, because of its very large enthalpy rise along the core, the SCWR is sensitive to small variations in the flow-to-power ratio, making core design an obstacle. Another project (01-091) investigated problems preventing the SCWR's practical application, aiming to improve the reactor's efficiency.

Some projects improved upon the Gen III designs that utilities are preparing to deploy in the near term. For example, two separate projects supported construction of the AP1000. One project (00-023) contributed to development and analysis of the standard plant design, addressing pump design specifications, thermal-hydraulic conditions, and safeguards data packages used to perform safety analyses. The second project (01-094) assessed the AP1000 passive safety system core cooling performance. These researchers successfully completed 11 integral system tests and published test summary and acceptance reports for each.

Another NERI project (99-097) investigated the scientific design of two simplified boiling water reactors (SBWRs), predecessors to the ESBWR. The team developed thermal-hydraulic and neutronic systems for both compact modular (200 MWe) and full-size (1,200 MWe) SBWR designs, performing detailed core design and accident analysis.

Reactor design sped into the 21st century when a NERI project (01-069) demonstrated the feasibility and effectiveness of using full-scale, virtual reality simulation in designing Gen IV nuclear plants. Researchers used Immersive Projection Display (IPD) technology to construct a full-scale virtual mockup of a selected plant area in order to evaluate design and construction, simulate a maintenance task, and evaluate lessons learned.

Control and Monitoring Systems

A crucial part of reactor design is the ability to monitor and control plant systems. In its first year, NERI funded a project (99-119) to develop, test, and implement adaptive control strategies that recognize changes in operating data and use a decision-making module to detect system faults. Gen IV systems present new maintenance and monitoring challenges (due, for example, to longer fuel cycles). To address these challenges, three NERI teams proposed shifts in maintenance practices from outage-based maintenance to on-line inspection and monitoring. Project 99-168 focused on wireless radio-frequency technology, specifically

smart multi-sensor tag units, which they designed, fabricated, and successfully tested. Two other projects (99-306 and 01-076) developed online monitoring systems. In addition, STAR project 99-043 inspired development and demonstration of remote surveillance strategies, exploiting the plant's passive safety and autonomous operation attributes.

Other monitoring advancements supported by NERI include the constant temperature power sensor (CTPS), an in-core instrument that provides a detailed map of local nuclear power deposition and coolant thermal-hydraulic conditions during the entire life of the core (00-069); this research developed four different sensor prototypes. Project 01-039 developed and demonstrated a miniature, scintillation-based, in-core self-powered neutron flux and temperature probe. Still another project (00-100) provided design, construction, and testing of an on-line fuel burn-up monitoring system.

Reactor Safety

Severe NERI projects addressed safety as a primary topic. For example, an early project (99-200) provided important information on criticality safety and spent fuel shipment safety needed for advanced reactor fuel designs that use higher initial fuel enrichments and have larger end-of-life fuel burn-up exposures than currently operating plants. The data generated from these experiments helped verify computational methods used for reactor safety calculations, reduce the licensing burden on future reactor designs, and remove overly conservative assumptions. Another research project (00-109) applied new, nonlinear methods to assess condition change and forewarn machine failures. The resulting technology now has multiple U.S. patents, and follow-on products include software implementation of the nonlinear technology, a cost-benefit analysis of the prognostication approach, and a commercialization roadmap.

Cost Control

Several NERI projects have contributed to the goal of developing low-cost methods of generating power. Two early projects developed compact Gen IV power plant designs and layout concepts to maximize the benefits of factory fabrication, optimal packaging, transportation, and siting. Project 00-047 developed plant concepts for water, gas, or liquid metal coolant while addressing computer simulation and optimization of factory fabrication processes for each of the three reactor concepts. The second project (99-059) quantified, streamlined, and documented internal layout rules that benefit overall plant cost or licensability; created a documented set of guidelines for modularization; and developed module standards with a focus on fabricating self-contained units of a power plant that can be transported to a site and operated for 15 years or more without major maintenance. A third project (99-077) identified strategies to deliver a 40-percent reduction in capital cost and scheduling time for a future nuclear power plant utilizing information technology capabilities such as a design-to-analysis tool using computer-aided drawing.

Later projects addressed ways to lower costs during operation, such as through changes to fuels or materials. One project (02-044) used the ion beam surface treatment (IBEST) process developed at Sandia National Laboratories to incorporate boron into the outer surface of fuel cladding (rather than as an additive to fuel pellets). This procedure could represent significant cost savings and potentially lead to greater reproducibility and control of burnable fuel in the early stages of reactor operation.

Advanced Materials

In order to remain current with advancing technologies and the new generation of reactors, researchers have explored many new types of materials for use in reactor internals, fuel cladding, or structural components. NERI researchers have worked to develop, produce, characterize, and test these materials for suitability in the high-temperature, chemically harsh, radioactive environments found in the proposed new reactors. Materials investigated ranged from conventional stainless steels to advanced alloys and ceramics, often considering special surface treatments or manufacturing techniques as well.

For example, several projects investigated methods for reducing radiation-induced damage mechanisms in stainless steel. One project (99-280) did this by doping common stainless steels with small amounts of platinum, hafnium, and other elements. Several NERI projects used thermomechanical processing to alter material grain boundaries, a process which dramatically improves corrosion and creep properties. For example, project 01-084 determined that random boundary network connectivity is a major driver of intergranular stress corrosion cracking (IGSCC) in austenitic alloys. The team developed a predictive tool and established thermomechanical processing parameters for manufacturing IGSCC-resistant materials. A later project (05-151) found that grain boundary engineering (GBE) results in greater resistance to IGSCC, with the modified alloy 316L and 690 specimens tested showing 93 and 55 percent less cracking, respectively, than untreated samples.

A separate NERI project (01-137) developed physical models for radiation-induced microstructural changes in neutron-irradiated Gen IV steels. Researchers derived constitutive laws for void swelling, irradiation creep, stress-induced swelling, and changes in mechanical properties; the laws were tested and validated, then incorporated into a computer code that reproduces the observed phenomena.

Other studies focused on novel methods of material production. To create silicon carbide (SiC) ceramic materials, for example, one project (05-032) used liquid silicon infiltration of porous carbon substrates derived from cellulosic precursors. The team created net-shape, fully dense SiC ceramics for use in for high-temperature heat exchangers. Another project (06-134) expanded on results from initial national laboratory efforts to develop doped molybdenum/niobium (Mo/Nb) alloy high-temperature irradiation-resistant thermocouples, noting that pairing KW-Mo with Nb-1%Zr yielded the best thermocouple combination.

Project 05-154 addressed the corrosive nature of molten fluoride salts used as a heat transport fluid for the NGNP. After executing corrosion compatibility experiments to develop a database on the behavior of a range of candidate materials, researchers found that nickel electroplating appears to be a viable option for protecting materials against corrosion in molten fluoride salts. Another corrosion-related project (05-116) studied the roles of hydrogen and helium in damage evolution and extended this knowledge to increasingly complex iron alloy materials. Results include the finding that alloys with rhenium additions exhibit potential for corrosion resistance in the relevant atmospheres.

SCWRs were investigated early in the NERI program. Project 01-130 designed and built a test system for electrochemical and fracture mechanics studies in the extreme conditions of SCWRs, ranking candidate structural materials for susceptibility to environmentally assisted degradation. The team found a correlation between measurable oxide film properties and susceptibility to degradation in austenitic steels. Another project (01-091) sought to improve material compatibility under supercritical conditions by employing plasma-based surface modification techniques.

Nuclear Fuel Design

NERI projects have supported the development of advanced fuels to facilitate the transition towards a sustainable advanced nuclear fuel cycle. For example, one early project (01-005) found that the current generation of pressurized water reactors can increase power output up to 50 percent using high-performance, annular fuel under specified conditions; fabrication of such fuel can be accomplished by commercial techniques at a reasonable cost. Several projects, such as 99-095, investigated the use of metallic thorium/uranium (Th/U) fuel, which has good thermal and proliferation-resistant properties and can be disposed of directly. Project 99-153 studied Th/U-dioxide ceramic fuels as a means of increasing fuel utilization and proliferation-resistance, while 00-014 examined heterogeneous core design options and fuel management strategies to maximize the benefits of using thorium in PWRs. The latter developed designs for two different thorium implementation options that would significantly improve the fuel's intrinsic proliferation resistance and waste characteristics and reduce the total amount of plutonium produced: the seed-blanket unit (SBU) concept and the whole assembly seed and blanket (WASB) concept.

A number of projects have been developing and refining TRISO fuel for use in the VHTR. One such project (06-068) successfully employed the double heterogeneity factor (DHF) methodology to augment a conventional LWR lattice physics code, allowing analysis of VHTR configurations while properly accounting for the double heterogeneity in TRISO particle fuel. (Conventional lattice codes cannot analyze TRISO fuel because the integration paths cannot resolve the fuel particles.)

Other projects investigated use of minor actinides (MA) as fuel components. For example, 05-094 considered transuranic (TRU) vectors that could potentially extend VHTR refueling intervals beyond those of cores fueled by low-enriched uranium (LEU). The project confirmed that TRU-fueled VHTRs offer performance characteristics that would be difficult to achieve in analogous LEU-fueled systems, such as nearly decade-long batch mode operation without intermediate refueling, significant reductions of initial excess reactivity levels (smaller lifetime reactivity swings), and inherently higher achievable burn-up levels.

Several NERI projects have contributed to new cladding concepts, such as a continuous fiber ceramic composite cladding for water-cooled reactors (99-224). Researchers developed, tested, and irradiated two ceramic cladding materials—alumina-yttria continuous fiber ceramic composite (CFCC) and a hybrid with a high-density monolithic silicon carbide inner layer and CFCC outer layer—and demonstrated their ability to perform in harsh accident conditions. Another early project (99-229) developed a radiation-resistant SiC material with excellent thermodynamic properties to improve the economics of nuclear fuel. A SiC coating was applied to fuel cladding. In later work on SiC coatings, one project (05-030) validated and improved computational models for coating uranium

fuel pellets with carbon and SiC using the chemical vapor deposition (CVD) process in a spouting bed.

Separations

SiC is also a prime candidate for inert matrix fuel materials, and separations is being investigated as a key strategy for disposing of radioactive waste. One project (06-126) examined both topics as researchers aimed to identify a process for separating TRU species from SiC. The team ultimately selected a hot corrosion method using potassium carbonate molten salt in which SiC pellets can be completely reacted and dissolved to form water-soluble silicates in molten potassium carbonate at 1050°C after about 40 hours. Another project (02-098) sought an advanced extraction process for separating actinides and lanthanides found in acidic nitrate nuclear waste streams. Researchers developed promising ligand systems that allow for extraction of metal ions in highly acidic environments.

Transmutation

One project (05-125) designed advanced BWR fuel assemblies. Final research results showed a new implementation of lattice loading optimization of americium-241 (Am-241)-spiked bundles subjected into a core-wide BWR 3D environment. Transmutation rates of planted Am-241 exceeded 90-percent incineration levels at high burnups in a fairly uniform manner along the axial length of the bundles, indicating the viability of LWRs to efficiently destroy certain minor actinides. In another case (02-005), researchers devised a successful version of the breed and burn (B&B) gas-cooled fast reactor (GFR) concept. The project showed that spent B&B GFR fuel could be re-used as reload fuel for the same reactors by blending it with natural or depleted uranium after minimal processing. Spent B&B fuel could also be used in a PWR after 50/50 blending with UO_2 enriched to 4.4 $^{w}/_{o}$ U-235.

Hydrogen Production

Over the years, NERI has supported the development of technologies to produce hydrogen with next-generation nuclear energy systems using thermochemical or electrolysis processes. Project 05-006, for example, conducted basic research on thermodynamic measurements and physical property models of the sulfur-iodine (S-I) cycle, one of the thermochemical processes investigated. A later project (06-054) provided the scientific basis for developing high-performance electrolyzers for use in two candidate thermochemical cycles: the hybrid sulfur process and the modified calcium-bromine cycle. There are a number of challenges in making these thermochemical cycles commercially viable, but the project team made several supportive discoveries. For example, researchers investigated a novel proton exchange membrane in which conductivity is not adversely affected by concentrated sulfuric acid. This membrane would allow operation at higher current densities (i.e., higher sulfuric acid concentration at the anode), which would reduce capital cost and improve efficiency.

Project 06-027 optimized preparation of intermediate-temperature solid oxide fuel cells (IT-SOFCs), which are solid electrolyte types of fuel cells believed economically competitive thanks to high power density, fuel versatility, and variety of cell configurations. The team developed an inexpensive spray pyrolysis manufacturing process for deposition of functionally graded thin films of strontium-doped lanthanum manganite (or LSM) for use as IT-SOFC cathodes. Another project (02-030) sought to develop a plasma electrolysis technology to convert sodium metaborate into sodium borohydride using nuclear-energy-generated electricity to operate the plasma reactor. This research project tested a new technology concept, nuclear-energy-assisted plasma electrolysis, to produce hydrogen carrier materials.

This last innovative effort is one of many that demonstrate NERI's efforts to explore the cutting edge of nuclear research. While this chapter explores NERI's exciting history of contributions, Section 6 of this annual report provides summaries of NERI projects that were active or completed in FY 2009.

NUCLEAR ENERGY RESEARCH INITIATIVE

4.0 Participants: From Industry to Academia

Project Awards: A History of Success

In FY 1999, DOE's NERI program released its first solicitation. The response showed widespread awareness of the new program, with 308 R&D proposals submitted by a broad section of U.S. universities, national laboratories, and industry. The researchers selected research topics of interest and defined the scope and extent of the R&D in their proposals. The Department employed an independent expert peer review process to judge the scientific and technical merit of the R&D proposals. For those proposals judged to have the highest scientific and technical merit, the Department conducted a programmatic review to ensure conformance of selected projects with DOE policy and programmatic requirements. The two reviews resulted in award selection recommendations to the source selection official at DOE. Since its establishment, NERI has employed a similar peer-review-based process for selecting new projects, allowing objective subject matter experts to evaluate the proposals' scientific and technical merit and DOE management to ensure relevance and conformance with policy and programmatic requirements.

The initial FY 1999 procurement was completed with the award and issue of grants and laboratory work authorizations for 46 R&D projects. The research covered all NERI's designated R&D areas and represented participants from 45 organizations, including 11 foreign R&D organizations. The total cost of these research projects for the three-year period was approximately $52 million.

From FY 2000 through FY 2002, NERI continued its successful solicitation process, awarding an additional 47 NERI projects. Participants included 20 U.S. universities, 10 national laboratories, 18 private businesses, and 7 foreign R&D organizations. The total three-year cost was approximately $58 million.

In FY 2004, NE decided to focus on providing incentives exclusively for universities to concentrate on highly needed applied engineering research, better integrating the educational institutions with the research efforts and initiatives of the Department. National laboratories and private sector organizations were allowed to participate, but all the principal investigators for these projects would consist of university faculty members.

In FY 2005, 35 projects were initiated under the newly revised program, as well as an additional 25 projects in FY 2006. Participants included 38 U.S. universities, 2 foreign educational institutions, 8 national laboratories, and 7 industry partners. The total investment in these projects over their three-year term was $32.1 million. DOE awarded 22 NERI projects in FY 2007, involving 20 U.S. universities, 5 national laboratories, 2 U.S. businesses, and 1 international laboratory collaborator. Shortly thereafter, DOE awarded 11 NERI projects involving consortia (NERI-C). Participants comprised 38 U.S. universities, 7 national laboratories, and 1 U.S. business. The FY 2007 and NERI-C projects represent a $42.1 million federal government commitment to nuclear R&D during the three-year scope of these projects.

Over the past 11 years, NERI research participants have represented 64 U.S. universities, 11 national laboratories, 2 government agencies, 40 private businesses, and 37 foreign organizations. The following maps indicate the broad array of contributors to the NERI program.

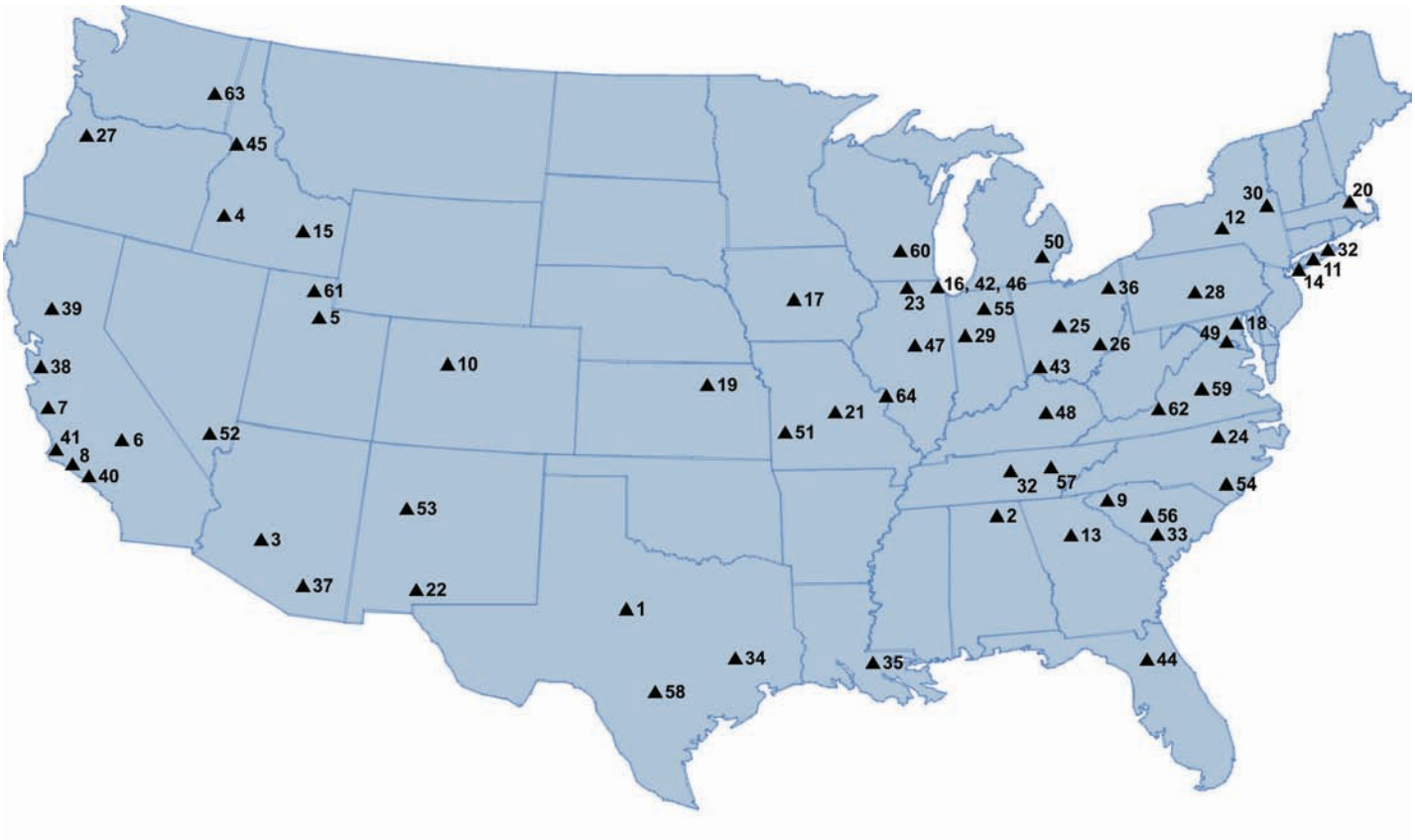

UNIVERSITY KEY

1 Abilene Christian University*
2 Alabama A&M University*
3 Arizona State University
4 Boise State University*
5 Brigham Young University*
6 California Institute of Technology*
7 California Polytechnic State University*
8 California State University, Northridge*
9 Clemson University
10 Colorado School of Mines*
11 Columbia University*
12 Cornell University*
13 Georgia Institute of Technology*
14 Hunter College (City University of New York)*
15 Idaho State University*
16 Illinois Institute of Technology
17 Iowa State University
18 Johns Hopkins University
19 Kansas State University*
20 Massachusetts Institute of Technology*
21 Missouri University of Science and Technology*
22 New Mexico State University
23 North Carolina State University*
24 Northwestern University*
25 Ohio State University*
26 Ohio University*
27 Oregon State University*
28 Pennsylvania State University*
29 Purdue University*
30 Rensselaer Polytechnic University*
31 South Carolina State University*
32 State University of New York, Stony Brook*
33 Tennessee Technological University*
34 Texas A&M University*
35 Tulane University*
36 University of Akron*
37 University of Arizona*
38 University of California, Berkeley*
39 University of California, Davis*
40 University of California, Los Angeles*
41 University of California, Santa Barbara*
42 University of Chicago*
43 University of Cincinnati*
44 University of Florida*
45 University of Idaho*
46 University of Illinois, Chicago*
47 University of Illinois, Urbana-Champaign*
48 University of Kentucky
49 University of Maryland, College Park
50 University of Michigan*
51 University of Missouri, Columbia*
52 University of Nevada, Las Vegas*
53 University of New Mexico
54 University of North Carolina, Wilmington*
55 University of Notre Dame
56 University of South Carolina*
57 University of Tennessee*
58 University of Texas, Austin*
59 University of Virginia
60 University of Wisconsin, Madison*
61 Utah State University
62 Virginia Polytechnic Institute and State University*
63 Washington State University*
64 Washington University in St. Louis*

* Indicates a FY 2009 participant

Figure 3. U.S. Universities and colleges participating in NERI projects.

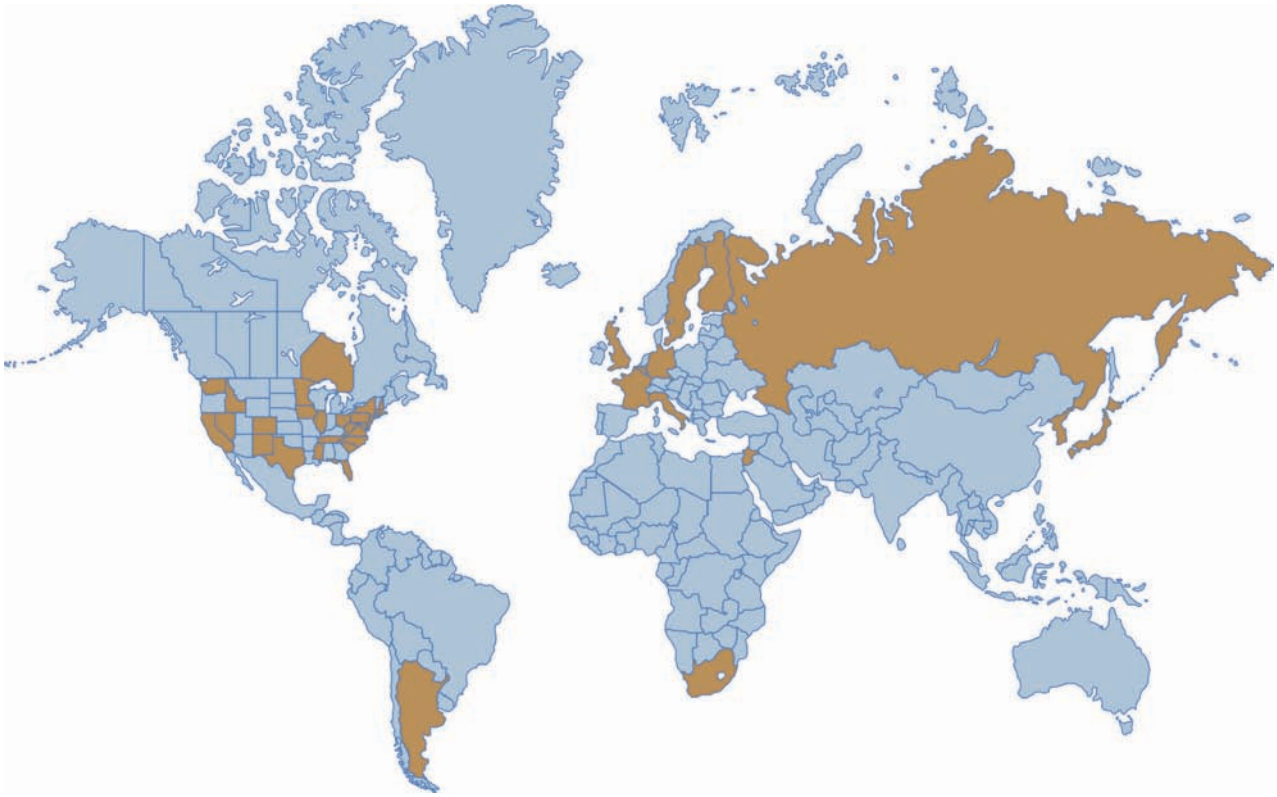

U.S. Department of Energy Laboratories
Ames Laboratory
Argonne National Laboratory*
Brookhaven National Laboratory*
Idaho National Laboratory*
Lawrence Berkeley National Laboratory*
Lawrence Livermore National Laboratory*
Los Alamos National Laboratory*
Oak Ridge National Laboratory*
Pacific Northwest National Laboratory*
Sandia National Laboratories*
Savannah River National Laboratory*

Government Agencies
National Institute of Standards and Technology
United States Nuclear Regulatory Commission

Industrial Organizations
ABB-Combustion Engineering
Aspen Technology, Inc.
Bechtel
Burns & Roe Enterprises
CEGA Corporation
Dominion Generation
Electric Power Research Institute
Eltron Research, Inc.*
Entergy Nuclear, Inc.
Florida Power and Light
Fluent, Inc.
Framatome ANP DE&S
Gamma Engineering Corporation
General Atomics*
General Electric Global Research Center
Global Nuclear Fuel
Materials Engineering Associates
McDermott Technologies
Northern Engineering and Research
Northrop Grumman Newport News
(n,p) Energy, Inc.
Pacific-Sierra Research Corporation (Veridian PSR)
Pacific Southern Electric and Gas
Panlyon Technologies
Rockwell Science Center
Siemens Power Corporation
Special Metals, Inc.
SRI International
Stress Engineering Services, Inc.*
Studsvik of America*
Swales Aerospace
Tennessee Valley Authority
TransWare Enterprises, Inc.*
United Technologies Research Center
Westinghouse Electric Company LLC*

International Collaborators
Atomic Energy of Canada (Canada)
Belgian Nuclear Research Centre (SCK/CEN)
Ben Gurion University (Israel)
British Nuclear Fuel (UK)
Chosun University (Korea)
Commissariat a l'Energie Atomique (France)*
Framatome (France)
Forschungszentrum (Germany)
Hitachi (Japan)
Hokkaido University (Japan)
Imperial College of Science, Technology, and Medicine (United Kingdom)
Institute of Physics and Power Engineering (Russia)
Italian National Agency for New Technologies, Energy and Environment (ENEA)
Japan Atomic Power Company (Japan)
Japan Nuclear Cycle Development Institute (Japan)
Korea Atomic Energy Institute (Korea)
Kurchatov Institute (Russia)
Mitsubishi Heavy Industries (Japan)
National Atomic Energy Commission and University of Cuyo (Argentina)
Nuclear Energy Agency, Organisation for Economic Co-operation and Development (OECD/NEA) (France)
PBMR, Ltd. (South Africa)
Polytechnic Institute of Milan (Italy)
The Royal Institute of Technology (Sweden)
Studsvik Scanpower Inc. (Sweden)
Tokai University (Japan)
Tokyo Institute of Technology (Japan)
Toshiba (Japan)
Toyama University (Japan)
University of Manchester (United Kingdom)
University of Rome (Italy)
University of Tokyo (Japan)
VTT Manufacturing Technology (Finland)

* Indicates a FY 2009 participant

Figure 4. Government, industrial, and international organizations participating in NERI projects.

University Focus

The preceding maps indicate the broad spectrum of NERI participants, with an emphasis on academia. One of NERI's long-term goals is to maintain the Nation's leading position in nuclear energy research by improving the nuclear science and engineering infrastructure. In FY 2004, NERI took additional steps toward achieving this goal through the cultivation of research partnerships with universities across the United States. The figures below illustrate funding allocations over time and are representative of the shift in program emphasis.

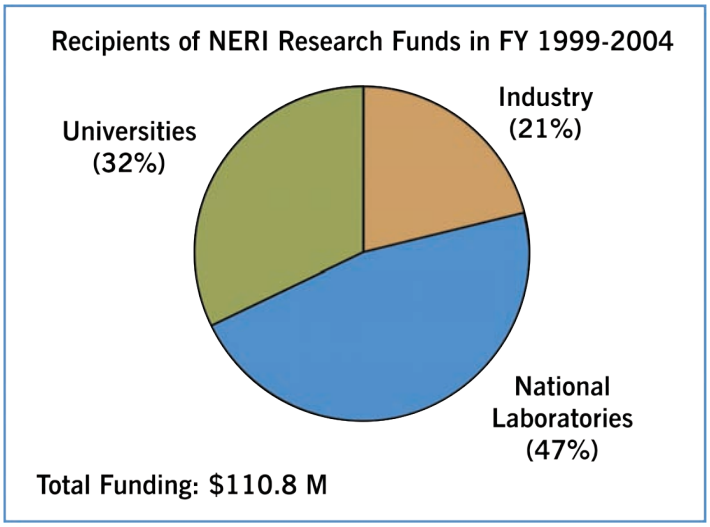

Figure 5. Distribution of NERI research funds by recipient from FY 1999 through FY 2004.

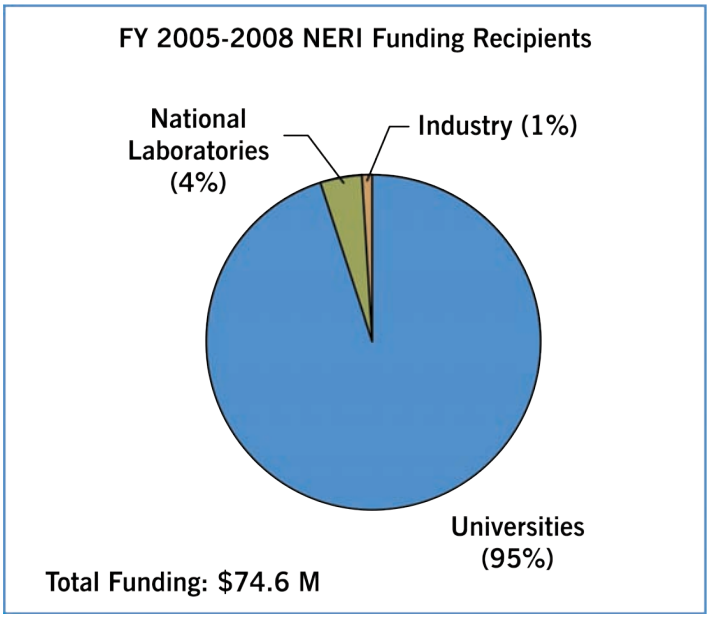

Figure 6. Distribution of NERI research funds by recipient from FY 2005 through FY 2009.

Support from the NERI program helps educational institutions remain at the forefront of science education and research, advance the important work of existing nuclear R&D programs, and create training for the next generation of nuclear scientists. Funding creative research ideas at the Nation's universities and colleges serves another purpose as well: to help solve important issues that the private sector is unable to fund alone owing to the high-risk nature of the research and/or the extended period before a return on investment is realized.

Participants in NERI's initial planning workshop recommended that NERI be viewed as a "seed program" where new nuclear-related technological and scientific concepts could be investigated. Based on this philosophy, NERI has provided universities and colleges with a competitive, peer-reviewed research program that allows faculty and students an opportunity to conduct innovative research in nuclear engineering and related areas. Of the 186 projects awarded through FY 2009, 88 percent involved U.S. universities and colleges as lead investigators or collaborators, amounting to a total of 64 institutions that have participated in NERI projects.

NERI has provided U.S. universities and colleges with the opportunity to work closely with industry and DOE national laboratories and has introduced these researchers to other nuclear energy-related government programs. In addition to research related to the Gen IV and FCR&D programs, NERI's activities are coordinated with other relevant federal government energy research programs in the DOE Office of Science, the DOE Office of Energy Efficiency and Renewable Energy, and the U.S. Nuclear Regulatory Commission. Furthermore, DOE leverages NERI program resources by encouraging no-cost collaboration with international research organizations and nuclear technology agencies. In this way, universities are given the opportunity to gain experience with international research interests and capabilities.

In FY 2008, NERI advanced its focus on U.S. universities, as shown through the establishment of NEUP, adding emphasis on integrating academic work into existing laboratory programs. The program refinements seen in NEUP further the direct support of NE goals to preserve, improve, and advance the U.S. nuclear science and engineering infrastructure.

Student Participation

One great success of NERI and other DOE programs is that nuclear-related educational opportunities at universities have significantly increased. Universities have benefited from increased research dollars, which have served as incentives for new student recruitment. This involvement has revitalized student interest in nuclear engineering. In 1998, only 500 students enrolled in U.S. universities were seeking degrees in nuclear engineering. According to a survey performed for DOE in March 2010 by the Oak Ridge Institute for Science and Education (ORISE), approximately 2,800 students—over 1,500 undergraduates and almost 1,300 graduate students—were enrolled in nuclear engineering programs during the previous fiscal year. The number of B.S. degrees granted by nuclear engineering programs was roughly double the numbers reported at the beginning of the decade.

Student participation in NERI projects has increased over time. In addition, numerous post-doctoral fellows at universities have been involved in NERI research projects. In FY 2009 alone, an estimated 93 undergraduate and 252 graduate and post-doctoral students participated in NERI R&D. Over the past few years, graduates of these programs have had higher-than-normal grade point averages, showing that these programs are training highly qualified individuals who will sustain the future growth of the nuclear power industry. Nearly 700 undergraduate, graduate, and post-doctoral students have participated in NERI projects since the program's inception (see Figure 7).

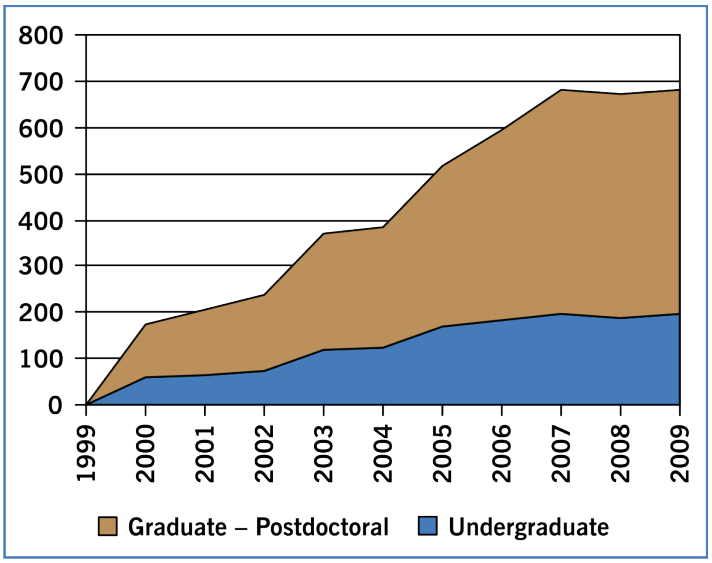

Figure 7. Cumulative NERI student participation profile from FY 1999 through FY 2009.

NUCLEAR ENERGY RESEARCH INITIATIVE

5.0 The International Nuclear Energy Research Initiative

Although the NERI program has included foreign participants, DOE is permitted to fund only domestic entities as part of this program. International participation has been supported by the foreign organizations interested in the research being conducted. Although the principal investigators are responsible for soliciting such support, foreign participation in NERI projects is contingent upon DOE approval.

Recognizing the need for an international component, PCAST issued a report in FY 1999 entitled *Powerful Partnerships: The Federal Role in International Cooperation on Energy Innovation* to promote "bilateral and multilateral research focused on advanced technologies for improving the cost, safety, waste management, and proliferation-resistance of nuclear fission energy systems." In response, DOE launched the International Nuclear Energy Research Initiative (I-NERI) for bilateral and multilateral nuclear energy research. Since FY 2001, I-NERI funding has supported 90 bilateral, cost-shared research projects with Brazil, Canada, the European Union, France, Japan, the Republic of Korea, and the Organisation for Economic Cooperation and Development (OECD).

I-NERI allows DOE to leverage federal investment and international resources by cost-sharing research with participating countries on a wide range of nuclear technology topics. This initiative enhances the influence of the United States and DOE on international policy discussions pertaining to nuclear energy's future direction. Further information, including separate annual reports for research conducted under the I-NERI program, can be found on the program website at *http://www.nuclear.energy.gov/INERI/neINERI1.html*.

NUCLEAR ENERGY RESEARCH INITIATIVE

6.0 Project Summaries and Abstracts

6.1 Generation IV Nuclear Energy Systems Initiative

There are sixteen NERI projects currently being performed under Gen IV; six of these projects were awarded in FY 2006 and ten projects (eight NERI and two NERI-C) were awarded in FY 2007.

During FY 2009, researchers worked on projects spanning most of the Gen IV program elements. In the area of advanced gas-cooled reactor fuel development, research teams are improving analytical techniques and developing online failure monitoring. Design and evaluation projects focus on improving modeling capabilities, neutronic analysis, thermal-hydraulic/heat transfer analysis, model uncertainty evaluations, and risk assessment techniques. Energy conversion projects target nuclear heat transport and supercritical CO_2 systems. Materials evaluations continue to occupy a large percentage of the Gen IV program, with studies on radiation behavior, improvement of corrosion resistance, development of advanced ceramics and metal alloys, and improvement of analytical modeling capabilities. Research is being conducted specific to reactor technologies; studies involve lead and lead-bismuth corrosion for the LFR, thermal-hydraulic modeling and materials evaluation for the SCWR, and design analysis methods and materials development for the VHTR.

Under the two NERI-C projects related to the Gen IV program, research efforts focus on NGNP and crosscutting materials-related activities. These projects involve the VHTR and structural materials.

More information about Gen IV can be found on the following website: *http://nuclear.energy.gov/genIV/neGenIV1.html.*

A summary of each project being performed under this initiative follows.

NUCLEAR ENERGY RESEARCH INITIATIVE

Directory of Generation IV Nuclear Energy Systems Initiative Project Summaries and Abstracts

FY 2006 Project Summaries

06-006 *Ab Initio*-Based Modeling of Radiation Effects in Multi-Component Alloys 23

06-046 Managing Model Data Uncertainties in Simulator Predictions for Generation IV Systems via Optimum Experimental Design 25

06-057 Uncertainty Quantification in the Reliability and Risk Assessment of Generation IV Reactors 29

06-068 An Advanced Neutronic Analysis Toolkit with In-Line Monte Carlo Capability for Very High-Temperature Reactor Analysis 33

06-100 Improving Corrosion Behavior in the Supercritical Water Reactor, Lead Fast Reactor, and Very High-Temperature Reactor Materials by Formation of a Stable Oxide....35

06-109 Multi-Scale Modeling of the Deformation of Advanced Ferritic Steels for Generation IV Nuclear Energy Systems....37

FY 2007 Project Summaries

07-003 An Advanced Integrated Diffusion/Transport Method for the Design, Analysis, and Optimization of Very-High Temperature Reactors....41

07-011 Implications of Graphite Radiation Damage on the Neutronic, Operational, and Safety Aspects of Very High-Temperature Reactors 43

07-017 Advancing the Fundamental Understanding and Scale-up of TRISO Fuel Coaters via Advanced Measurement and Computational Techniques 45

07-018 Fission Product Transport in TRISO-Coated Particle Fuels: Multi-Scale Modeling and Experiment....49

07-020 Emissivity of Candidate Materials for Very High-Temperature Reactor Applications: Role of Oxidation and Surface Modification Treatments 53

07-024 Materials and Design Methodology for Very High-Temperature Nuclear Systems....57

07-058 Experimental and Computational Fluid Dynamics Analysis of Advanced Convective Cooling Systems....61

07-069 Establishing a Scientific Basis for Optimizing Compositions, Processing Paths, and Fabrication Methods for Nanostructured Ferritic Alloys for Use in Advanced Fission Energy Systems....65

FY 2007 NERI-C Project Abstracts

08-043 A Research Program on Very High-Temperature Reactors 69

08-055 Cladding and Structural Materials for Advanced Nuclear Energy Systems 73

NUCLEAR ENERGY RESEARCH INITIATIVE

Ab Initio-Based Modeling of Radiation Effects in Multi-Component Alloys

PI: Dane Morgan, University of Wisconsin-Madison

Collaborators: None

Project Number: 06-006

Program Area: Gen IV

Project Start Date: March 2006

Project End Date: March 2010

Research Objectives

The objective of this project is to develop a highly accurate thermokinetic model for austenitic stainless steels based on fundamental quantum mechanical calculations. The model will incorporate the true temperature- and composition-dependence of the diffusion constants and provide missing information on interstitial motion.

In order to establish the critical data and computer programs to build the model, researchers will pursue the following specific tasks:

- Perform initial *ab initio* calculations of atomic-scale properties in pure elements and limited alloys.
- Develop iron-chromium-nickel (Fe-Cr-Ni) radiation-induced segregation (RIS) simulation and validation/refinement based on semi-analytic expressions for diffusion constants.
- Develop Fe-Cr-Ni RIS simulation methods based on Monte Carlo techniques.
- Perform Fe-Cr-Ni RIS simulation and validation/refinement by comparing to experiments.

Research Progress

Over the past fiscal year, the research focus was to calculate the thermokinetic parameters and diffusion constants as a function of concentration in Ni-Cr alloys. The following sections summarize the progress made in this system.

Assessing Concentration Dependence of Metal Alloys Using Kinetic Monte Carlo. Researchers developed and modified the CASM code—work initiated at the University of Michigan. This code is a flexible kinetic Monte Carlo (kMC) code to simulate diffusion of concentrated multi-component systems. First, the rersearchers the code by comparing the calculated intrinsic diffusion coefficients for dilute concentrations with intrinsic diffusion coefficients obtained from other dilute models available in the literature. Later, the code was used to assess the accuracy of the typical approach for obtaining concentration-dependent diffusion coefficients—application of the Darken and Manning approximations to dilute tracer coefficients determined with the dilute five-frequency formalism.

Figure 1 shows the ratio of true and approximate intrinsic diffusion coefficients using Darken's and Manning's approximations for a variety of solute-vacancy bindings (BE) and solute-solute interactions (BB). As the figure clearly shows, the approximate diffusion coefficients are within the error bars of the simulation except for the alloys having a solute-vacancy binding energy of J_{BV}=-30 MeV, where the true D_B decreases faster with solute concentration than the approximate values. Larger

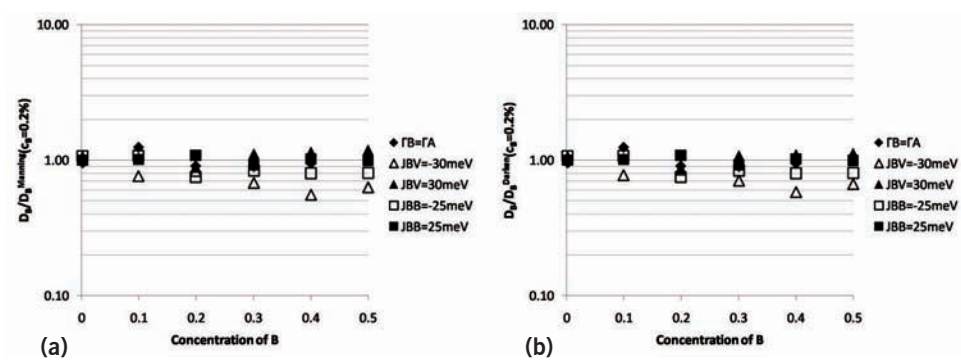

Figure 1. (a) D_B and dilute D_B^{Darken} ratios at T=800K; (b) D_B and dilute $D_B^{Manning}$ ratios at T=800K.

errors may occur for stronger interacting alloy systems or those with more than first-neighbor interactions. These results show not only that the kMC code can be used to predict concentrated diffusion coefficients from an alloy Hamiltonian, but also that analytic models based on dilute values can be very effective.

Ni-Cr-Vacancy(Va) Cluster Expansion. Later in the project, researchers applied the cluster expansion (CE) formalism to parameterize the energetics of the nickel-chromium-vacancy (Ni-Cr-Va) system by fitting *ab initio*-determined energies to effective cluster interactions (ECIs). The team used the CASM code to achieve these fits. The goal is to construct an accurate model of the energetics of the Ni-Cr-Va configurations using ECIs from two different sets of CEs, namely (a) Ni-Cr CE containing the Cr interactions in Ni and (b) Va CE containing Va-Va and Va-Cr interactions. For the Ni-Cr CEs, a total of 149 structures consisting of various Ni-Cr arrangements were used as input in a genetic algorithm for fitting; Figure 2(a) shows the resulting nine ECIs. The root mean square (rms) error of the Ni-Cr ECI's fit is 0.02 electron volts (eV). For dilute Va interactions, the Va CE is done in such a way that structures containing vacancies are referenced to a similar structure in which the Va is replaced with a Ni atom. Thus, the Cr-Cr interactions will cancel, and only Va interactions are fitted. Figure 2(b) shows the fitted ECIs for the vacancies; the fit has an rms error of 0.037 eV.

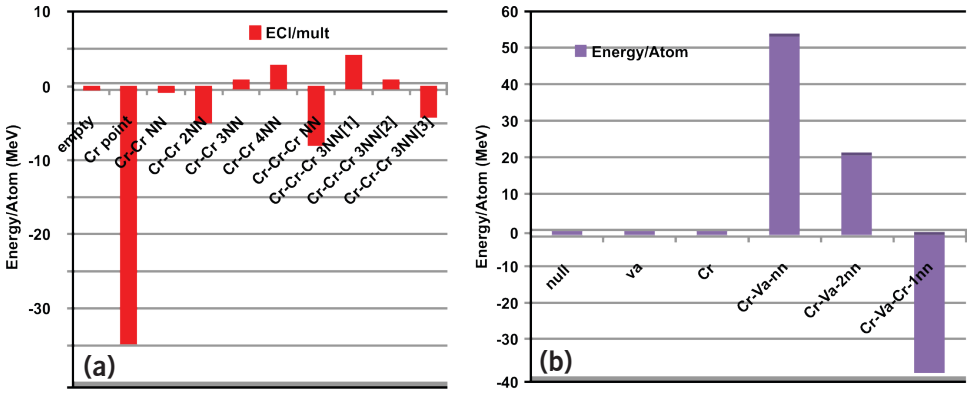

Figure 2. (a) Ni-Cr; (b) Va ECIs/atom in Ni-Cr alloy.

In order to test whether the ECIs obtained from Ni-Cr CE can accurately determine the ground states, researchers performed a grand canonical Monte Carlo simulation. Starting at T= 600K, they reduced temperature to T=10K in 10K increments for a variety of chemical potentials. As the temperature lowered, researchers expected the system to adjust concentration to the lowest energy configuration

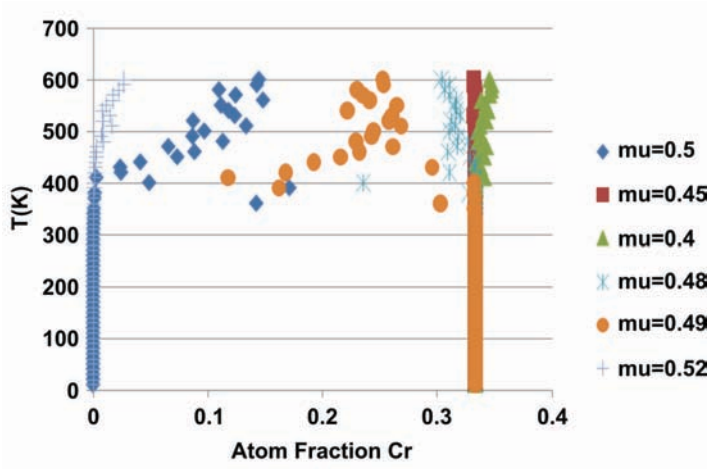

Figure 3. Compositions obtained with Ni-Cr cluster expansion and Monte Carlo (MC) by cooling into ground states using grand canonical MC simulations.

for the given chemical potential. Figure 3 shows that for the Cr range of 0%-33%, the ground states are located at 0% and 33% Cr, which is expected based on experiments. (This project restricts all calculations to Cr percentage concentrations of between 0 and 33, as fcc crystal structure is stable within this concentration regime.) This test verifies that the ECIs give the correct ground states. These ECIs can now be combined with kinetic parameterization to model diffusion in the concentrated alloy.

Planned Activities

Currently, work is in progress to determine the CE of the kinetically resolved activation barriers for Ni and Cr hops (kRA CE). The kRA ECIs contain interactions of the hopping species in the activated state and between the activated and lattice sites. Upon completion of the kRA cluster expansion, the ECIs from the three cluster expansions will be combined to parameterize a Ni-Cr-Va system. Through the remainder of the project (a no-cost extension until March 2010), researchers will use these combined ECIs in grand canonical MC and kMC codes to determine diffusion coefficients in concentrated alloys. The calculated temperature and composition-dependent diffusion constants will then be used with the previously developed rate equation code to study RIS in the Ni-Fe-Cr alloy.

NUCLEAR ENERGY RESEARCH INITIATIVE

Managing Model Data Uncertainties in Simulator Predictions for Generation IV Systems via Optimum Experimental Design

PI: Paul J. Turinsky and Hany S. Abdel-Khalik, North Carolina State University

Collaborators: Argonne National Laboratory, Idaho National Laboratory

Project Number: 06-046

Program Area: Gen IV

Project Start Date: March 2006

Project End Date: March 2010

Research Objectives

In the United States between the 1950s and 1990s, scientists performed many reactor physics and criticality benchmark experiments to provide information on the physics of operating fast reactors similar to those proposed under Generation IV (Gen IV). Uncertainties exist in simulation software used to model the nuclear core of proposed Gen IV reactors. These uncertainties are caused by uncertainties in the software data itself. All nuclear reactor designs rely on basic nuclear data, which are obtained from benchmark experiments designed to provide this information, as well as information about reactor operation. Since nuclear reactor designs are sensitive to the data provided for calculations, designers must allow margin for that data's uncertainty in order to license, build, and operate the reactors. A better understanding of sensitivity and uncertainty in the nuclear data, and perhaps further evaluation of some data, can reduce margin requirements and save money.

The objective of this project is to understand and manage uncertainties in simulation software used to model the nuclear core of proposed Gen IV reactors. Researchers will optimize experiments by determining and quantifying the uncertainties of key design attributes as a test basis to reduce model data uncertainties using Idaho National Laboratory's (INL's) Zero Power Physics Reactor (ZPPR). (The split-table, fast critical ZPPR facility was one of the test reactors operated during this time period.)[1] The team will then complete a pseudo-ZPPR experiment for the optimum design via simulation to determine observable values. The researchers will use these values to obtain adapted nuclear data.

The goal of this project is to produce the following methodologies and results, which have merit both collectively and as stand-alone methods to optimize experimental design:

- A methodology to determine covariance matrices for responses of a complex engineering system and an experimental system.
- A methodology to interpret experimental system results via adaptive simulation.
- A methodology to optimize the experimental configuration most economically appropriate for reducing the uncertainties of the complex engineering system.
- A covariance matrix originating from nuclear data uncertainties for the key design attributes of a Gen IV nuclear core.
- Optimum experimental system properties for a ZPPR experimental facility, which are most appropriate for reducing uncertainties of key design attributes of a Gen IV nuclear core.

Research Progress

The project team completed a study on integral parameter sensitivity, uncertainty, and representativity of a fast critical experiment with regard to a Gen IV fast recycle reactor concept.

This work analyzes and compares various integral parameters of the advanced burner test reactor (ABTR) design concept, published by Argonne National Laboratory (ANL) in 2006,[2] to an established benchmark, ZPPR 15 Assembly B.[3,4] The research team had previously

conducted sensitivity and uncertainty analyses for integral parameters on both reactors using the efficient subspace method (ESM) developed at North Carolina State. They compared the reactors using the representativity factor method to determine if ZPPR-15B physics adequately represents ABTR physics, then modified the computational model to include several drawers of transuranic (TRU) targets to simulate an experiment to provide additional data on minor actinide behavior in a fast reactor environment.

Since this earlier work, the team has examined a total of eight modified configurations of the ZPPR 15-B assembly. These modified configurations differ with respect to number of modified drawers, material composition of modified drawers, and instrumentation physical location. Figure 1 pictorially presents one of the eight modified configurations.

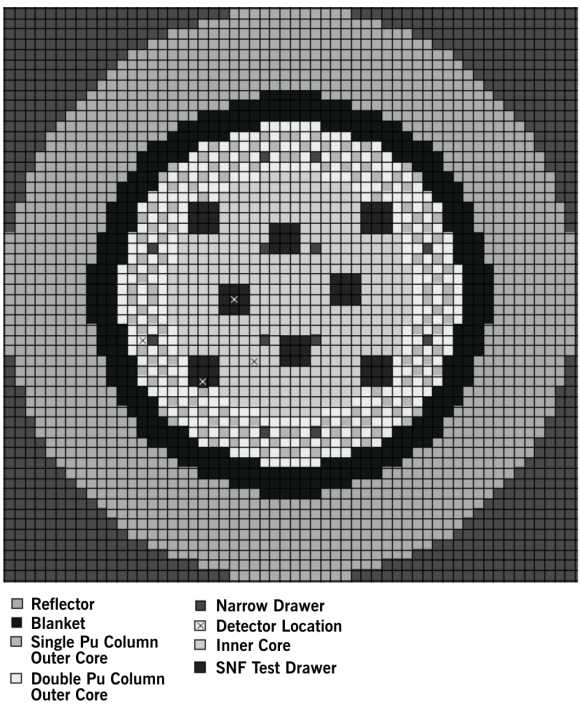

Figure 1. ZPPR-15B with mock SNF assemblies.

The team completed data assimilation of isotopic cross-sections for each modified configuration of the ZPPR 15B assembly for a 15-energy group library, which was generated using MC2-2 and utilized by the REBUS code. The covariance library is based upon that generated by a joint working group involving several DOE laboratories rather than strictly from the Evaluated Nuclear Data File/B-Versions (ENDF/B). For each modified configuration, researchers determined uncertainties of the key ABTR core attributes using the prior and posterior covariance matrices for the 15-energy group library. Table 1 shows results for a subset of modified configurations. The ABTR uncertainties were evaluated for both the start-up core and the equilibrium core. In addition to the standard core attributes of interest, Table 1 notes decay heat loads and safety parameters. As they are very much connected to the effectiveness of consuming the minor actinides, decay heat loads are of interest in waste repository studies. Safety parameters[5] are useful when determining whether the core design has sufficient passive safety characteristics to prevent core damage from occurring during the following transient conditions (all without reactor trip): loss of heat sink, transient over power, loss of flow, chilled inlet, and pump overspeed.

As expected, the project team found that certain modified assemblies are more effective in reducing certain ABTR-related uncertainties and less effective in reducing other ABTR-related uncertainties. These findings imply that, given a limited budget for ZPPR experiments, a designer would need to prioritize uncertainties to reduce, then decide which modified assemblies to construct and utilize.

Planned Activities

The project team will formulate and solve a mathematical optimization problem to maximize cost savings via margin reduction for the ABTR. Researchers will employ a formal mathematical optimization method. The problem will account for the cost offsets for building and executing critical experiments. It has proven difficult to obtain costs for the ABTR margin and for conducting experiments at ZPPR; therefore, if the information is not available, the team will develop an acceptable approximation in order to exercise the capability developed. Decision variables will be material compositions, instrumentation deployment, and types of experiments. Constraints will be imposed based upon experimental limitations. The solution to this optimization problem will yield the optimum experimental design.

This work is the final activity required for a doctorate student's degree, and this student is currently a full-time employee in industry. Therefore, the team is requesting a no-cost extension to December 31, 2010.

Table 1. Posterior relative uncertainties for the ABTR equilibrium core.

Parameter	*A Priori*	ZPPR-15B	ZPPR-TRU	ZPPR-SNF	ZPPR-ABTR
k-eff, EOC	1.0275	0.4177	0.3664	0.3684	0.3343
Void ($)	8.7075	4.2584	3.7865	4.0428	3.8320
Doppler ($/K)	4.5877	2.2084	1.9024	1.8518	2.8698
Axial Expansion	7.8448	4.5806	4.3638	4.4971	4.4248
Radial Expansion	3.7178	2.0136	1.8461	1.9165	1.9207
Peak Fluence (n/cm^2)	1.2424	0.4857	0.4075	0.4088	0.4473
Peaking Factor	0.5442	0.3502	0.3180	0.3315	0.1938
Peak Flux (n/cm^2-s)	1.3921	0.4421	0.3710	0.3830	0.2752
Peak Power Density (W/cm^3)	0.5538	0.3572	0.3240	0.3383	0.2010
Conversion Ratio	2.2458	0.2845	0.2852	0.2877	0.2535
Discharge Decay Heat Load (W)	35.4703	11.9937	10.5602	11.8948	9.7839
Heat Integral, 100 y (W-s)	59.0669	15.0336	12.8518	14.5623	12.1339
Heat Integral, 2500 y (W-s)	42.6915	10.6081	9.17405	10.3536	8.66233
Safety Parameter #1	14.2237	7.1622	6.3694	6.0627	7.5714
Safety Parameter #2	17.6832	8.2073	7.2336	6.9416	8.4823
Safety Parameter #3	14.0924	8.0533	7.5229	8.0666	7.6470
Pu-239 Fission	1.2048	0.3287	0.2407	0.2498	0.1708
U-238 Capture	2.3021	0.4736	0.4166	0.4229	0.3415
Am-241 Fission	8.1269	0.5481	0.4540	0.5296	0.3389
Am-243 Fission	6.2131	6.0110	0.6177	0.6846	0.4764
Cm-242 Fission	30.3575	30.1738	0.6013	0.8471	0.4625
Cm-244 Fission	39.4914	39.4254	0.5928	0.7639	0.4933
Cm-245 Fission	32.1604	32.0846	0.6938	0.9780	0.4354

References

[1] LeSage, L.G., "An Overview of the Argonne National Laboratory Fast Critical Experiments 1963-1990," ANL-NT-175, Argonne National Laboratory, April 2001.

[2] Chang, Y.I., Finck, P.J. and Grandy, C., "Advanced Burner Test Reactor Preconceptual Design Report," ANL-ABR-1 (ANL-AFCI-173), Argonne National Laboratory, Sept. 2006.

[3] Brumbach, S.B. and Collins, P.J., "ZPPR Progress Report for January, February and March as of March 31, 1986," ZPR Technical Memo Series No. 469, ZPR-TM-469, Argonne National Laboratory, March 1986.

[4] Brumbach, S.B. and Collins, P.J., "ZPPR Progress Report for April, May and June as of June 30, 1986," ZPR Technical Memo Series No. 470, ZPR-TM-470, Argonne National Laboratory, June 1986.

[5] Wade, D. and Fujita, E., "Trends versus Reactor Size of Passive Reactivity Shutdown and Control Performance," Nuclear Science and Engineering, 103, 182, 1989.

NUCLEAR ENERGY RESEARCH INITIATIVE

Uncertainty Quantification in the Reliability and Risk Assessment of Generation IV Reactors

PI: Karen Vierow, Texas A&M University

Collaborators: Ohio State University

Project Number: 06-057

Program Area: Gen IV

Project Start Date: March 2006

Project End Date: June 2009

Research Objectives

The goal of this project was to develop practical approaches and tools for dynamic reliability and risk assessment techniques that can be used to augment the uncertainty quantification process in probabilistic risk assessment (PRA) for Gen IV reactors. Project objectives were to 1) develop practical approaches and computationally efficient software to test event tree completeness, 2) integrate a reactor safety code with PRA, and 3) assess and propagate plant state uncertainties in the PRA analysis.

This project involved generating a practical dynamic event tree (DET) tool and assessing and quantifying uncertainty propagation. In Phase 1, the project team modified current software for DET generation and linked it to a best-estimate computer code (MELCOR). The researchers used the phenomena identification and ranking table (PIRT) technique to identify key modeling uncertainties and tested the integrated software package on select, high-risk initiating events. In Phase 2, the team improved the computational efficiency by coupling the DET generation software with stochastic and deterministic sampling schemes for epistemic uncertainty quantification and tested this new software on additional initiating events.

Research Progress

Contributions of Research to Understanding. The completed project contributes to the state-of-the-art in the PRA of existing reactors as well as future Gen IV reactors. Researchers have made the techniques and software flexible and adaptable to a variety of reactor safety codes, thereby producing a tool that is widely usable by both the designer and the regulator.

The team modified a MELCOR input deck to model a Gen IV system and extended capabilities to enable simulation of a chosen pressurized loss-of-forced-circulation event. They developed an uncertainty quantification algorithm that includes both uncertainty analysis and sensitivity analysis. The former determines the distribution of an output value, such as the figure of merit, caused by variations in the input. The latter shows to what extent variations on each input parameter affect the output value. The team constructed a two-loop algorithm for uncertainty propagation and quantification, with an inner loop treating the correlated uncertainties and an outer loop treating the uncorrelated uncertainty data.

The project has confirmed the ability to use the DET generation software (ADAPT)[1] with a reactor safety code (MELCOR)[2] for integrated analysis.

Technical Effectiveness and Economic Feasibility. One of the major additions to the software is a web-based interface for the DET generation routine. The web interface provides a more user-friendly environment for executing experiments. Functions include serving as a front end to the server and database management system, launching experiments, visualizing the current event tree status, and downloading all files associated with a particular branch. The DET-generation software has been developed in a code-neutral manner, enabling its use with a variety of reactor safety codes and simulators.

By performing experiments with various techniques and variables, the team has made the computational infrastructure more efficient with respect to the number of cases that need to be run. For the sensitivity analysis, three experiment designs were employed using full factorial, Latin hypercube, and Taguchi orthogonal arrays. Parameters were ranked by response surface, linear correlation coefficient, and partial correlation coefficient methods.

Benefit to the Public. Specific benefits of the computational infrastructure include:

- Determination of a scenario's pathway by mechanistic reactor safety codes within a probabilistic context. Each scenario sequence determined by ADAPT is a pathway.
- Reduced uncertainty in calculated plant performance parameters resulting in elimination of unnecessary conservatisms in design.
- New PRA techniques to select initiating events with the highest risk profile. If the figure of merit is low-risk, the scenarios, and hence the initiating events leading to these scenarios, can be ranked with regard to their contribution to risk. The novelty in this approach is the use of Taguchi arrays[3] to account for the epistemic uncertainties in the initiating events, which could affect the ranking.
- Timely guidance in the design and PRA-informed licensing and regulation of Gen IV systems.

Incorporation of Uncertainty Quantification Algorithm Into MELCOR. For the sensitivity analysis, the team used three experiment designs:

- A full factorial experiment (3 levels for 5 parameters = 243 simulations).
- A Latin hypercube experiment with 250 samples (sample size approximately the same as the full factorial experiment).
- A Taguchi orthogonal array experiment, with all 5 parameters at 3 levels. The team used an $L_{27}(3^5)$ orthogonal array, which required 27 MELCOR simulations.

For each experiment design, the parameters were ranked according to the following methods:

- *Linear response surface*. The output data for each design was fit to a linear polynomial of the form:

$$Y = \sum_{i=1}^{5} a_i x_i \qquad (1)$$

where Y is the output metric, the x_i's uncertain parameters, and the a_i's the fit coefficients. The importance of each parameter was determined by the absolute value of its associated fit coefficient.

- *Linear correlation coefficient (LCC)*. A LCC was calculated for each uncertain parameter with respect to the output metric:

$$r_{x_i Y} = \frac{n\sum_{j=1}^{n} x_{i,j} Y_j - \sum_{j=1}^{n} x_{i,j} \sum_{j=1}^{n} Y_j}{\sqrt{n\sum_{j=1}^{n} x_{i,j}^2 - \left(\sum_{j=1}^{n} x_{i,j}\right)^2}\sqrt{n\sum_{j=1}^{n} Y_i^2 - \left(\sum_{j=1}^{n} Y_i\right)^2}} \qquad (2)$$

where $r_{x_i Y}$ is the LCC between the output Y and the uncertain parameter x_i and n is the number of trials in the experiment design. The importance of each parameter in this method was determined by the absolute value of r for each variable.

- *Partial correlation coefficient (PCC)*. The PCCs can be calculated by first determining the correlation matrix C between all of the input variables, and between the input variables and the output metric. The PCC of an uncertain parameter x_i and the output metric Y is then determined by:

$$\rho_{x_i Y} = \frac{d_{i,6}}{\sqrt{d_{i,i} d_{6,6}}} \qquad (3)$$

where $d_{i,j}$ are the elements of $D = C^{-1}$. (Note that C will be a six-by-six matrix, five rows and columns for the input parameters and a sixth column for the output metric.) The importance of each parameter in this method was determined by the absolute value of the PCC for each variable. In addition, the Taguchi methodology has its own means to determine parameter ranking by examining the signal-to-noise (S/N) ratios of the output data.

Table 1 shows a listing of the results of the parameter rankings utilizing each experiment design and test metric. The results shown are the relative influence demonstrated by each parameter (normalized to the parameter with the strongest influence). Note that in this sensitivity study, all parameters were treated as epistemic in nature (i.e., as uncertainties in initial conditions). There is currently no standard technique for assessing a parameter's importance in an environment of mixed epistemic and aleatory uncertainties.

The results given by the Taguchi method are consistent with those of all other methods. Core power after SCRAM is predicted as the most important parameter, with the heat transfer coefficient between gas and fuel spheres the second most important. Also of note is that the response surface, LCC, and S/N ratio (Taguchi only) methods give similar relative rankings, namely that the second through

Table 1. Results of the parameter rankings.

	Response Surface	LCC	PCC	S/N Ratio
Design/Parameter				
Latin Hypercube				
1	0.002 (5)	0.002 (5)	0.009 (5)	--
2	0.052 (2)	0.103 (4)	0.520 (2)	--
3	0.014 (3)	0.028 (3)	0.161 (4)	--
4	0.006 (4)	0.029 (2)	0.165 (3)	--
5	1.000 (1)	1.000 (1)	1.000 (1)	--
Full Factorial				
1	0.020 (4)	0.038 (4)	0.155 (5)	--
2	0.055 (2)	0.143 (2)	0.459 (2)	--
3	0.024 (3)	0.037 (5)	0.224 (4)	--
4	0.010 (5)	0.080 (3)	0.254 (3)	--
5	1.000 (1)	1.000 (1)	1.000 (1)	--
Taguchi				
1	0.034 (3)	0.034 (4)	0.232 (4)	0.067 (4)
2	0.039 (2)	0.079 (2)	0.480 (2)	0.079 (2)
3	0.025 (4)	0.051 (3)	0.333 (3)	0.078 (3)
4	0.006 (5)	0.032 (5)	0.215 (5)	0.032 (5)
5	1.000 (1)	1.000 (1)	1.000 (1)	1.000 (1)

fifth most important parameters are at least one order of magnitude below the most important parameter. However, the PCC results give less separation between the most important parameter and the remainder. With regard to the PCC results, the Latin hypercube and full factorial designs give the exact same ranking, but the Taguchi method shows a different ordering for the third through fifth most important parameters. However, the difference in relative importance between these parameters is small. The PCCs tend to give a more accurate picture of the effects of a parameter on an output value than the response surface or LCC methods, since, in the PCC method, the linear effects of the other parameters are removed.

Planned Activities

The project has been completed.

References

[1] A. Hakobyan, T. Aldemir, R. Denning, S. Dunagan, D. Kunsman, B. Rutt, and U. Catalyurek, "Dynamic Generation of Accident Progression Event Trees," Nuclear Engineering and Design, 238, 3457-3467 (2008).

[2] R. O. Gauntt, R. K. Cole, S. A. Hodge, S. B. Ridriguez, R. L. Sanders, R. C. Smith, D. S. Stuart, R. M. Summers, and M. F. Young, MELCOR Computer Code Manuals, NUREG/CR-6119 (SAND 2005-5713), U.S. Nuclear Regulatory Commission, Washington, D.C. (2005).

[3] L. Sharma, T. Aldemir, and R. Parker, "Uncertainty Analysis Using Taguchi Methods With Virtual Experiments," Trans. Am. Nucl. Soc., 96 (2007).

NUCLEAR ENERGY RESEARCH INITIATIVE

An Advanced Neutronic Analysis Toolkit with In-Line Monte Carlo Capability for Very High-Temperature Reactor Analysis

PI: William R. Martin, University of Michigan

Collaborators: General Atomics, Idaho National Laboratory, Los Alamos National Laboratory, Oak Ridge National Laboratory, Studsvik of America, TransWare Enterprises, Inc.

Project Number: 06-068

Program Area: Gen IV

Project Start Date: March 2006

Project End Date: August 2009

Research Objectives

The goal of this project was to augment a conventional lattice physics code to allow the analysis of very high-temperature reactor (VHTR) configurations with tri-isotropic (TRISO) particle fuel. This project intended to establish "proof of principle" by combining the capability of the MCNP5 Monte Carlo code with the CPM3 code. The latter is a lattice physics code based on the method of characteristics (MOC) and the collision probability (CP) method. Conventional MOC-CP lattice codes such as CPM3 cannot analyze TRISO fuel because the integration paths cannot resolve the fuel particles. The final package will inherit the substantial downstream capabilities of a production MOC-CP code, such as cross-section generation for global nodal analysis and depletion, systematic preparation of cross-section sets for accident analysis, and efficient fuel cycle analyses and assessment of alternative fuel management schemes. The final product will be a validated neutronics methodology for VHTR design and analysis, including cross-section generation, global reactor analysis, depletion, and fuel management.

The primary objective has been to demonstrate that the double heterogeneity factor (DHF) methodology can be employed with a conventional light-water reactor lattice physics code such as CPM3 or HELIOS, allowing analysis of VHTR configurations while properly accounting for the double heterogeneity in the TRISO particle fuel.

Research Results

The basic idea is to use MCNP5 to perform two calculations for the geometry of interest, one with homogenized fuel compacts and one resolving the TRISO kernels. The DHF is the ratio of these two cross sections for every fine energy group and every isotope. The DHF is an effective self-shielding factor that accounts for the kernel-level heterogeneity. Researchers input these DHFs to CPM3 and use them to multiply the corresponding fine group resonance cross sections, effectively yielding MCNP5 cross sections. CPM3 then uses these adjusted microscopic resonance cross sections to perform the actual transport calculation, e.g., with CP or MOC. This methodology does not change the normal transport modules in CPM3, whether carried out by CP or MOC—only the fine group resonance cross sections. Researchers achieved several key accomplishments:

- Successfully ported DHF methodology to CPM3.
- Successfully utilized Studsvik-Scandpower to port DHF methodology to HELIOS, a production lattice physics code.
- Showed that DHF methodology works for plutonium-fueled VHTR lattices, demonstrating that it can handle the low-lying resonances of plutonium.
- Demonstrated that the DHFs are insensitive to burnup and relatively insensitive to spatial location in the fuel block and core.

Performance of CPM3 and HELIOS with DHFs. CPM3 and HELIOS were used to analyze the VHTR fuel block shown in Figure 1. Researchers used MCNP5 to compute the reference solution as well as the DHFs used in CPM3 and HELIOS. Table 1 compares these results with the reference MCNP5 case.

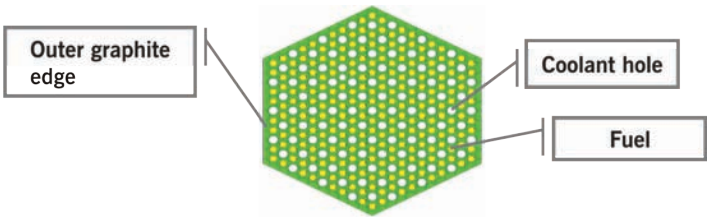

Figure 1. VHTR fuel block.

Table 1. Comparison of HELIOS and CPM3 with MCNP5 for a VHTR fuel block.

Code	Version	k_∞	% difference
MCNP5	Reference	1.4975	-
CPM3	Original	1.4409	3.8
	With DHFs	1.4970	0.03
HELIOS	Original	1.4458	3.5
	With DHFs	1.4951	.16

The results show convincingly that the DHFs allow CPM3 and HELIOS to account for the double heterogeneity due to the TRISO fuel. Without DHFs, both codes treat the TRISO fuel regions as homogeneous, and the resultant k_∞ values are low by almost 4%, totally missing the kernel-level heterogeneity. However, with DHFs from MCNP5, CPM3 agrees to within 0.03% and HELIOS to within 0.16%. Moreover, the CPM3 and HELIOS results are consistent with each other, agreeing to within 0.4% for their original versions and within 0.2% with DHFs.

Capability of DHFs to Predict Plutonium Lattices. The project team tested the ability of the DHF to analyze lattices with significant amounts of plutonium. Researchers analyzed a fuel compact cell with a fuel kernel consisting of plutonium, neptunium, and cobalt (Pu-Np-Co), representing the Pu-Np isotopics in typical used nuclear fuel from light-water reactors. The dimensions of the fuel compact cell are based on the General Atomics deep burn concept. Table 2 compares the CPM3 results with the reference MCNP5 case. These results clearly show that the original CPM3 code totally misses the kernel-level heterogeneity, under-predicting k_∞ by over 6%, whereas it agrees to within 0.1% of the reference result with DHFs.

Table 2. Comparison of CPM3 and MCNP5 for a plutonium lattice.

Code	Version	k_∞	% difference
MCNP5	Reference	1.1043	--
CPM3	Original	1.0347	6.3
	With DHFs	1.1032	0.1

Sensitivity of the DHFs to Spatial Location. DHFs were calculated for two limiting fuel block configurations—an interior fuel block and an exterior fuel block—surrounded by graphite reflectors. Figure 2 shows the two configurations.

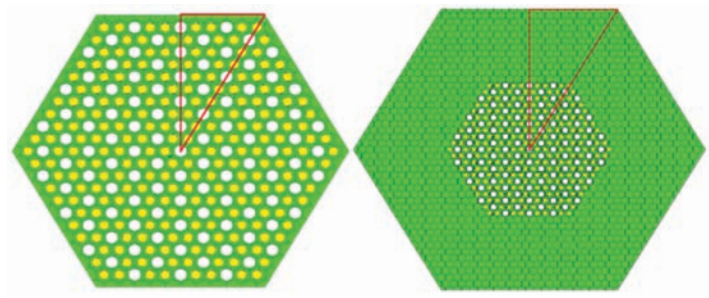

Figure 2. VHTR configurations representative of interior and exterior fuel blocks.

For the worst case, which is U-238 in Group 57, the DHFs ranged from 0.78 to 0.81 across both fuel blocks, which is less than a 4% variation in DHF. Moreover, the block average DHFs were both 0.80. These results confirm that block average DHFs are relatively insensitive to spatial location.

Sensitivity of the DHFs to Burnup. The project team used original CPM3 to deplete a fuel compact cell to 100 GWd/MT and used isotopics in MCNP5 to compute DHFs for uranium (U-235 and U-238) and plutonium (Pu-239 and Pu-240) at burnups of 0, 50, and 100 GWd/MT. The DHFs exhibited no changes to two significant figures, indicating that they are not sensitive to slow changes in composition due to burnup.

Planned Activities

The contract ended August 2009. The project team is preparing a journal article to describe the DHF methodology.

NUCLEAR ENERGY RESEARCH INITIATIVE

Improving Corrosion Behavior in the Supercritical Water Reactor, Lead Fast Reactor, and Very High-Temperature Reactor Materials by Formation of a Stable Oxide

PI: Arthur T. Motta, Penn State University

Collaborators: Los Alamos National Laboratory, University of Michigan, University of Wisconsin, Westinghouse Electric Company

Project Number: 06-100

Program Area: Gen IV

Project Start Date: March 2006

Project End Date: March 2009

Research Objectives

This project was designed to establish a technical basis for corrosion protection of candidate materials for three different types of reactors: the supercritical water reactor (SCWR), the lead fast reactor (LFR), and the very high-temperature reactor (VHTR). The materials studied included ferritic-martensitic steels, austenitic alloys, and nickel (Ni)-based alloys. In order to understand the mechanisms associated with corrosion behavior in these materials, the project team has conducted a systematic study on the nature of protective films formed during corrosion tests in simulated reactor environments. The overall objective was to understand why certain alloys exhibit better corrosion behavior than others by examining the oxide microstructure. Alloys that resist corrosion develop a protective oxide layer that limits the access of corrosive species to the underlying metal, leading to stable oxide growth. The differences between a protective and a non-protective oxide are determined by the alloy chemistry and microstructure. Very small changes in microstructure can significantly affect corrosion rate.

Research Progress

In this study, researchers used electron microscopy techniques (both scanning [SEM] and transmission [TEM]) and synchrotron radiation diffraction and fluorescence to analyze oxide layers that formed on ferritic-martensitic alloys exposed to both supercritical water (SCW) and lead-bismuth eutectic (LBE). They characterized the oxide microstructure to understand the oxidation behavior of the alloys, as shown in Figure 1.

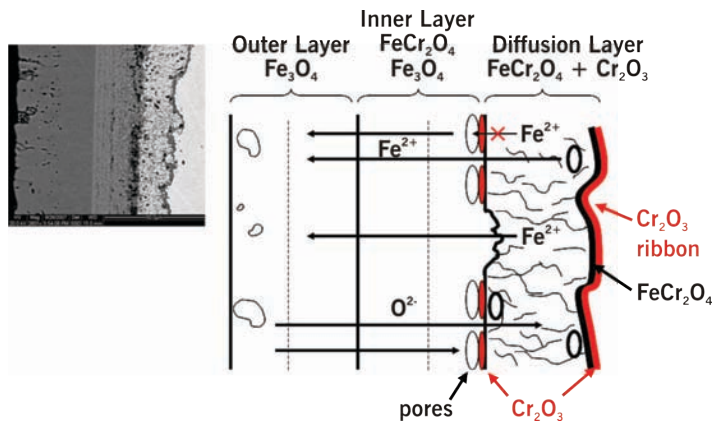

Figure 1: Oxidation mechanism in ferritic-martensitic steels in SCW.

The specific conclusions are as follows:

- The oxide formed on ferritic-martensitic steels often has a three-layer structure, with an outer layer of iron oxide (Fe_3O_4), an inner layer of spinel-iron oxide ($FeCr_2O_4$-Fe_3O_4), and a diffusion layer that often contains oxide precipitates. In the samples corroded at 500°C, the diffusion layer is essentially a solid solution of oxygen ahead of the oxide and contains few precipitates. In the 600°C samples, the diffusion layer consists of a mixture of oxide precipitates and metal grains. The TEM study shows that the outer oxide is made of large columnar grains while the inner oxide is formed of small equiaxed grains. The outer oxide columnar grains of the LBE samples tended to be smaller than those of the SCW samples, while the equiaxed inner oxide grains of the LBE samples were larger than those of the SCW samples.

- In the 9Cr-oxide dispersion-strengthened samples (9CrODS) corroded at 600°C, a chromium oxide (Cr_2O_3) film formed at the diffusion layer-metal interface between the two- and four-week samples. This continuous layer of Cr_2O_3 appeared to stop or dramatically slow oxygen diffusion beyond the ribbon and thus served as a barrier for further oxidation.

- For the SCW samples, the researchers observed chromium enrichment associated with the presence of Cr_2O_3 at the inner oxide-diffusion layer interface for the 9CrODS 600°C two-week sample, and at the diffusion layer-metal interface for the 600°C four- and six-week samples. The team observed similar enrichment for HCM12A and NF616 samples (advanced commercial steel alloys) where an yttrium layer was deposited on the surface prior to oxidation. These phenomena are linked to the rare earth element effect, which suggests that yttrium facilitates localized enrichment and segregation of chromium at grain boundaries.

- The study of the diffusion layer of HCM12A showed that oxide advancement occurs by preferential oxidation of the chromium-rich particles, likely carbides, present at the lath boundaries of the base metal. Therefore, the alloy microstructure has a strong influence on the alloy's corrosion behavior.

- Concerning oxidation behavior in SCW, two different processes form the outer oxide layer and the inner oxide layer. The outer layer is formed by the outward diffusion of Fe^{2+}, created by the metal's oxidation. These iron ions then react with the SCW to form Fe_3O_4. The inner oxide layer is formed by the inward diffusion of O^{2-}, created by the reduction of water. These oxygen anions then react with the iron or chromium cations to form the oxide. Consequently, the outer oxide-inner oxide layer interface corresponds to the original metal-solution interface. If the metal oxidizes too slowly, the number of Fe^{2+} ions created is too low to compensate for the outward migration of these cations from the inner layer, thus creating pores at the inner-diffusion layer interface.

- In SCW, the oxide dispersion-strengthened steel forms the most protective oxide (as measured by the inner oxide layer thickness) even though it has the least chromium alloying content since it has the smallest oxide thickness. This seeming discrepancy might be due to the yttrium-rich oxide nano-particles that catalyze the nucleation of a stable and protective oxide. Implanting an yttrium surface coating before oxidation positively affects corrosion resistance, a fact which further supports the above theory.

- The team found evidence for ingress of the lead-bismuth coolant into the oxide layer. Energy dispersive spectroscopy (EDS) analysis found a lead grain at the outer oxide-inner oxide interface of HT-9 (a steel alloy), and two bismuth grains at the inner oxide-metal interface of Alloy #3. SEM images show light features in the outer oxide layers of the LBE corroded samples, which can be correlated to LBE contamination. Since lead and bismuth were found individually within the oxide layer, this suggests that the lead and bismuth may separate during cool-down, or possibly upon ingress into the layer at high temperature.

Planned Activities

The project ended in September 2009, and a final report was submitted to DOE. The project team intends to publish the results in conferences and publications. Two papers are planned for the near future, one on corrosion behavior of ferritic-martensitic steels in SCW and one on such behavior in lead-bismuth.

NUCLEAR ENERGY RESEARCH INITIATIVE

Multiscale Modeling of the Deformation of Advanced Ferritic Steels for Generation IV Nuclear Energy

PI: Nasr M. Ghoniem, University of California, Los Angeles

Collaborators: California State University, Northridge

Project Number: 06-109

Program Area: Gen IV

Project Start Date: March 2006

Project End Date: March 2009

Research Objectives

The objective of this project is to design a multi-scale modeling framework to assist in the development of radiation-resistant steels with improved mechanical properties for high-temperature applications in Generation IV reactors. Researchers developed a hybrid *ab initio,* continuum model to describe the core of dislocations in iron since empirical interatomic potentials are not accurate and do not allow studies of the effects of local chemical changes in alloys. The developed model facilitates studies of dislocation core structures in steels, without ad hoc assumptions of interatomic forces. The model is applied to determine the core structure of screw dislocations in iron (Fe) and the interaction between dislocations and oxide and carbide precipitates because they control the ductility and high-temperature strength of steels. The research team developed dislocation dynamics models to simulate the mechanical properties of radiation-damaged steels as a function of the neutron dose. Single dislocation interaction with nanovoids, precipitates, and self-interstitial atom (SIA) clusters during irradiation have been developed. This information becomes the basis for a comprehensive rate theory model of radiation damage and in-reactor deformation. Using this model, the team makes predictions for in-reactor deformation, with full microstructure information linked with the deformation field.

Research Progress

Polarization-Induced Strengthening Mechanism of Copper Precipitates in α-Fe. To predict, estimate, and extend the operational life of reactor pressure-vessel steels, one needs to understand the mechanism of irradiation-induced hardening. One main reason for the hardening is nucleation and growth of copper (Cu) precipitates. Experimental observations have shown that ultrafine Cu precipitates with body-centered cubic (bcc) structure serve as obstacles to impede dislocation motion in the Fe matrix. Lozano-Perez et al. found experimental evidence of the transformation of Cu precipitates ($\sim$ 4 nm diameter) from the bcc to the 9R phase. Orowan loops form during this transformation. Recently, Nogiwa et al. showed that smaller Cu precipitates ($\sim$ 2 nm) can curve and pin dislocations without Orowan loops forming. In order to understand the difference between these observations, the research team has carried out comprehensive atomistic simulations of the interaction between dislocations with Cu precipitates of various sizes.

The research team performed molecular dynamics (MD) simulation with a system size of $12.2\times28.0\times19.9$ nm^3, using three sizes of Cu precipitate (d = 1.0 nm, 2.3 nm, and 4.4 nm) to study the size effect. After initially placing a $<111>/2$ screw dislocation 7.0 nm away from the center of the precipitate, shear stress is applied on the dislocation with strain rate $\in = 4 \times 10^7$/s. The results show that the 1.0 nm Cu precipitate does not affect the motion of the dislocation and hence does not contribute to the hardening effect. While the dislocation can penetrate into the 2.3 nm Cu precipitate, the dislocation initially becomes pinned, and finally curves as it moves out of the precipitate. The bow-out angle, $\theta = 144°$, agrees with Nogiwa's observation. Interestingly, the 2.3 nm Cu precipitate changes the dislocation core polarization. When the dislocation moves out, it undergoes a core-structure transformation from polarized to non-polarized, and the dislocation line curves in order to supply the extra stress to drive this transformation (shown in Figure 1). Thus, for the first time, research results reveal a novel polarization-induced strengthening mechanism of ultrafine Cu precipitates.

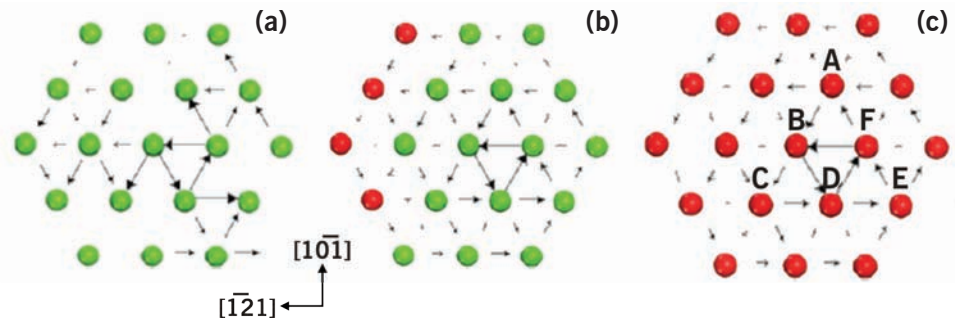

Figure 1. Dislocation core structure inside a Cu precipitate vs. diameter: (a) d = 2.3 nm, (b) d = 1.0 nm, and (c) d = 0.0 nm (pure α-Fe). Red: Fe atoms; green: Cu atoms.

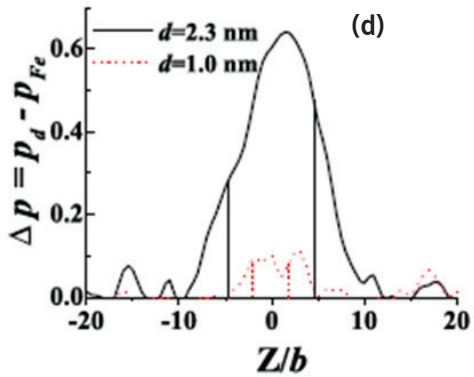

Figure 1 (d). Change of dislocation core polarization versus atomic position (normalized to Burgers vector) along the dislocation line. Solid black: 2.3 nm Cu precipitates; red dashed: 1.0 nm Cu precipitates; vertical dashed: precipitate–matrix interface.

Finally, the 4.4 nm Cu precipitate can dramatically impede the dislocation motion. As shown in Figure 2, the dislocation stops at the precipitate's center. With increasing external stress, an increasing number of Cu atoms become displaced from the perfect bcc sites. Consequently, the dislocation core spreads and expands in the precipitate. This observation is consistent with Lozano-Perez's result: the presence of the dislocation triggers the martensitic structural phase transformation, and the deformed precipitate in turn impedes the dislocations' movement.

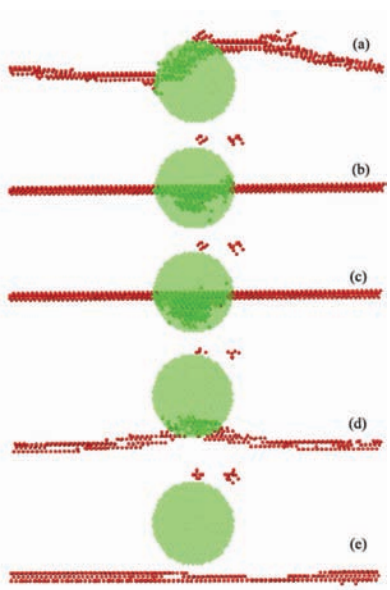

Figure 2. Snapshots of the dislocation core for the 4.4 nm Cu precipitate.

Thus, the team found two separate mechanisms responsible for the different experimental observations: 1) a polarization-induced mechanism for Cu precipitates with d ~ 2 nm, and 2) a deformation-induced mechanism for Cu precipitates with d > 4 nm.

Interaction of a Dislocation in α-Fe With an Yttrium Oxide Precipitate. Oxide-dispersion strengthened (ODS) steels are promising candidates as structural materials for applications in fission and fusion reactors. Yttrium oxide (Y_2O_3) particles dispersed in an iron matrix drastically improve the strength without adverse effects on ductility. However, the interaction between a dislocation and the Y_2O_3 particle, considered the basic strengthening mechanism in ODS steels, remains unresolved. The research objective is to employ a sequential multiscale approach that links dislocation dynamics with *ab initio* input for the generalized stacking fault (SF) energy surface (γ-surface) responsible for the lattice restoring force. As a first step, researchers have calculated the γ-surface of Y_2O_3 on the (001) plane along the [100] and [110] directions, shown in Figure 3. The team also calculated the γ-surface of the Y_2O_3 – α-Fe interface, which they employed to carry out the dislocation dynamics calculations to investigate the core structure.

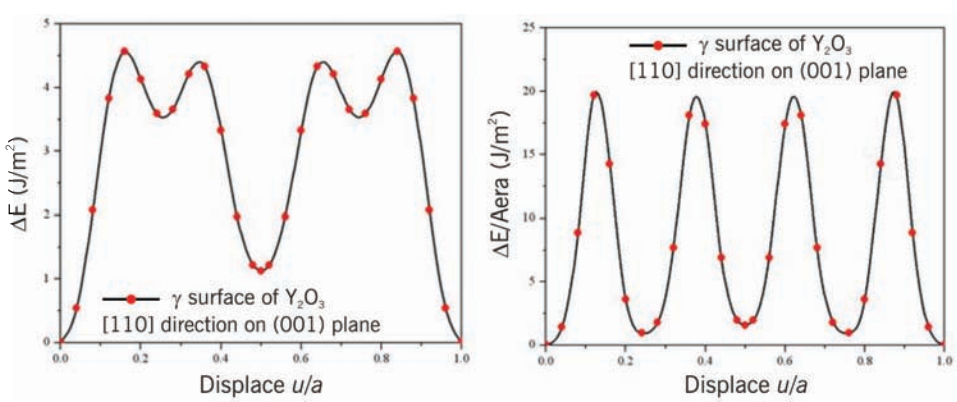

Figure 3. γ-surface of Y_2O_3 on the (001) plane. Left panel is along the [100] direction and right panel is along the [110] direction.

The Core Structure of Self-Interstitial Atoms in Cu and Fe. Researchers use the hybrid *ab initio*, continuum method of Banerjee et al. to determine the dislocation core structure of SIA clusters in bcc Fe and face-centered cubic (fcc) Cu. The project presents a hybrid extension of the Pierels-Nabarro continuum model, with lattice resistance to slip determined separately from *ab initio* calculations. This model reduces reliance on empirical potentials and facilitates predictions of how local chemistry and stress will affect defect structure.

The project team has developed a method to reconstruct the atomic arrangement and geometry of SIA clusters from the hybrid model. The results compare well with MD simulations. In Fe, the core structure does not show dependence on the self-interstitial cluster's size and is nearly identical to that of a straight edge dislocation. However, the core structure of SIA clusters in Cu is shown to depend strongly on cluster size. Small SIA clusters have non-dissociated compact dislocation cores, with strong merging of Shockley partial dislocations and a relatively narrow SF region. The Cu SIA core's compact nature is attributed to the self-energy's strong dependence on cluster size. As the number of atoms in the SIA cluster increases, Shockley partial dislocations separate and the SF region widens, rendering the SIA core structure to that of an edge dislocation. As the cluster size increases, the separation distance between the two partials widens and tends toward the value of a straight edge dislocation for cluster sizes above 400 atoms. The local stress significantly affects atomic arrangements and SF widths within Cu SIA clusters. For an SIA cluster containing 400 atoms, 1 gigapascal (GPa) shear stress delocalizes the cluster and expands the SF to 30 b, while an opposite shear stress of 2 GPa contracts the core to less than 5 b, where b is the Burgers vector magnitude. Figure 4 shows the displacement density distribution for the dislocation core of self-interstitial loops in Fe. The core structure of a straight edge dislocation is also plotted. Figure 5 shows the SIA dislocation core structure in Cu.

Crystal Plasticity Modeling of Localized Deformation. The objectives of this research are to develop an understanding of the mechanical behavior and dislocation microstructure evolution of single and polycrystals, and to delineate the physical and mechanical origins of spatially localized plastic deformation in irradiated materials. Researchers developed a rate-independent crystal plasticity model to incorporate micromechanics, crystallinity, and microstructure into a continuum description of finite strain plasticity. The research team employs a comprehensive dislocation density model based on rate theory to determine the strain hardening behavior within each plastic slip system for the fcc crystal structure. Finite strain effects and the kinematics of crystal plasticity are coupled with the dislocation density-based model via the hardening matrix in crystal plasticity. The developed material models are applied to study single and polycrystal deformation behavior in Cu. The project team is using the software system ABAQUS; team members are developing interfaces between the ABAQUS user material subroutine (umat) and the ABAQUS main code to allow further extension of the current method. Simulations carried out for polycrystals clearly illustrate the heterogeneous nature of plastic strain and the corresponding spatial heterogeneity of the mobile dislocation density. The origins of the spatial heterogeneities are essentially geometric, as a result of constraints on grain rotation (finite strain effects), geometric softening due to plastic unloading of neighboring crystals.

Planned Activities

This project is complete. The team has submitted a final report summarizing progress during the three-year project period.

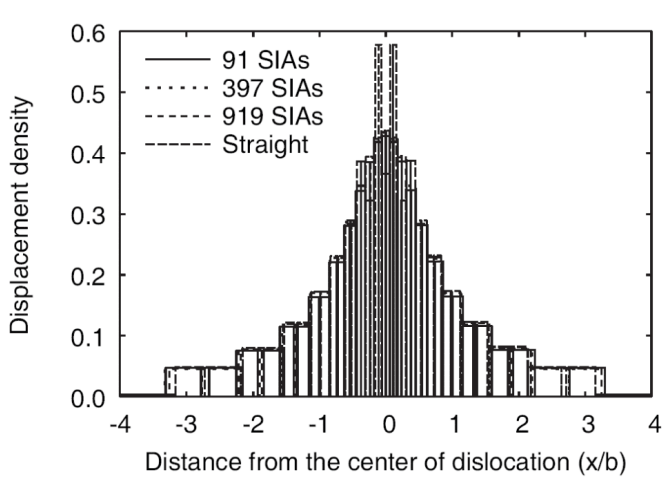

Figure 4. Displacement density distribution for the dislocation core of self-interstitial loops in Fe.

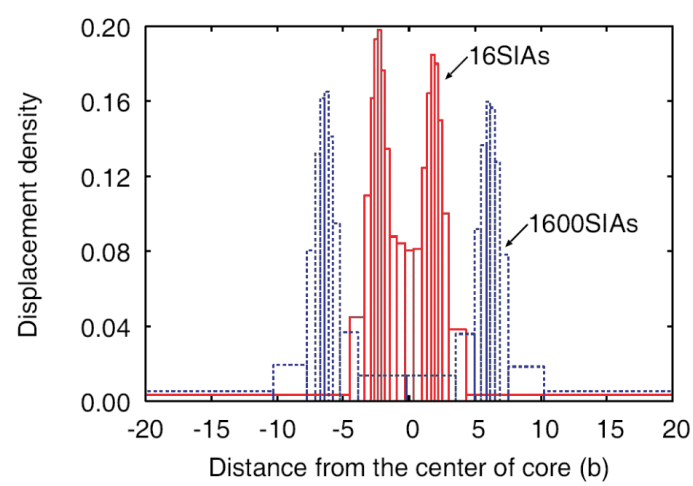

Figure 5. SIA dislocation core structure in Cu.

NUCLEAR ENERGY RESEARCH INITIATIVE

An Advanced Integrated Diffusion/Transport Method for the Design, Analysis, and Optimization of Very High-Temperature Reactors

PI: Farzad Rahnema, Georgia Institute of Technology

Collaborators: Idaho National Laboratory (INL)

Project Number: 07-003

Program Area: Gen IV

Project Start Date: July 2007

Project End Date: July 2010

Research Objectives

The main objective of this research is to develop an integrated diffusion/transport (IDT) method to substantially improve accuracy of nodal diffusion methods for design and analysis of very high-temperature reactors (VHTRs). Owing to the presence of control rods in the reflector regions of the pebble-bed reactor (PBR), traditional nodal diffusion methods are inadequate as diffusion theory breaks down in the vicinity of high neutron absorption and steep flux gradients. The proposed IDT method uses a local transport solver based on a new incident flux response expansion method in the controlled nodes, while diffusion theory is used in the rest of the core. This approach improves the accuracy of the core solution by generating transport solutions of controlled nodes while maintaining computational efficiency by using diffusion solutions in nodes where such a treatment is sufficient. The transport method will initially be developed and coupled to the reformulated three-dimensional (3D) nodal diffusion model in an INL code called CYNOD for PBR core design and fuel cycle analysis.

This method will also be extended to the prismatic VHTR. The research team expects the new method to accurately capture transport effects in highly heterogeneous regions with steep flux gradients. The calculations of these nodes with transport theory will avoid errors associated with spatial homogenization commonly used in diffusion methods in reactor core simulators.

Research Progress

During the project's second year, the team developed two-dimensional (2D) polar (r, z) and 3D cylindrical (r, Θ, z) transport methods to generate response functions for controlled regions. In addition, the team developed a 2D(r, z) PBR benchmark and conducted consistency checks. The following describes this research in more detail.

Development of the Response Function-Based Transport Method. The aim of this task was to develop a 2D(r, z) and 3D(r, Θ, z) cylindrical transport method to generate response functions, in terms of exiting partial currents and surface-averaged and node-averaged scalar fluxes, for non-multiplying regions (such as inner and outer reflectors) to couple with the diffusion method used in the fuel region.

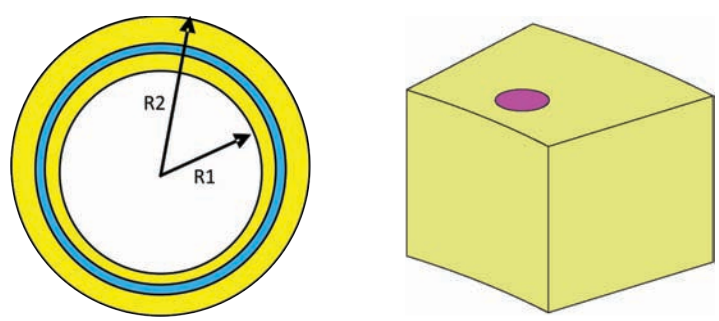

Figure 1. 2D and 3D cylindrical coarse mesh.

To generate response functions for a coarse mesh, researchers approximated the mesh boundary neutron phase space distributions. This approximation is necessary since the whole core solution is not known *a priori*. To this end, the team has developed a set of new expansion functions for an arbitrary cylindrical surface. For the (r, Θ) and (Θ, z) surfaces, the new expansion functions are a tensor product of Legendre polynomials $P_n(x)$ and Chebyshev polynomials $U_n(x)$ of the second kind:

$$f_{ijk}\left(\vec{r},\hat{\Omega}\right)=P_i\left(\vec{r}\right)U_j\left(\cos\theta\right)P_k\left(\cos\varphi\right)$$

where i, j, and k are expansion orders in spatial, polar angle, and azimuthal angle variables, respectively.

For the (r, z) surface, the new expansion functions are a tensor product of Legendre polynomials $P_n(x)$, Chebyshev polynomials $U_n(x)$ of the second kind, and orthogonal polynomial $q_i(r)$:

$$f_{ijkl}(r,z,\hat{\Omega}) = q_i(r)P_l(z)U_j(\cos\theta)P_k(\cos\varphi)$$

where polynomial $q_i(r)$ can be constructed from the following recurrence relation:

$$q_0(r) = 1$$

$$q_m(r) = rq_{m-1}(r) - \sum_{n=0}^{m-1} B_{m,n}q_n(r) \qquad m>0$$

where coefficients $B_{m,n}$ are defined as:

$$B_{m,n} = \frac{1}{A_n}\int_{R1}^{R2} 2\pi r^2 q_{m-1}(r)q_n(r)dr$$

The new expansion functions also avoid the singularity introduced by the conventional Legendre polynomial expansion since the lowest-order expansion function represents an isotropic flux. These new expansion functions serve as a boundary condition imposed on an inner/outer coarse mesh to generate response functions for coupling with diffusion solutions in fuel regions.

Development of a 2D(r, z) PBR Benchmark Problem. The project team has developed a 2D(r, z) PBR 400 benchmark problem, as shown in Figure 2. The problem consists of an inner reflector region with a diameter of 2 meters (m), an annular fuel region of 0.85 m thickness, and a controlled outer reflector region of 0.5 m thickness. The height of the benchmark problem is 4 m, and the control rod is partially inserted from the top.

To show the accuracy of the response function generation method, researchers used the response functions generated in this project to construct the outgoing partial currents and surface- and volume-averaged fluxes for Region 127. The comparisons indicate that the second order expansion in space is sufficient to reproduce the MCNP reference solutions, with a maximum error of about one percent.

Development, Implementation, and Testing of the Diffusion Method. To test the embedded response function treatment with discontinuity factors, the research team decoupled the r and z directions and tested each direction separately. The one-dimensional (1D) PBMR problem was used for testing the z direction. The decoupled z direction implementation with the CYNOD code, generated in this work, produced the same eigenvalue (keff) as in the reference solution. Researchers also tested the decoupled r direction. They obtained discontinuity factors from a finite difference fine mesh calculation in the radial direction. To obtain response functions, researchers reformulated the radial Green's function discretization in terms of partial

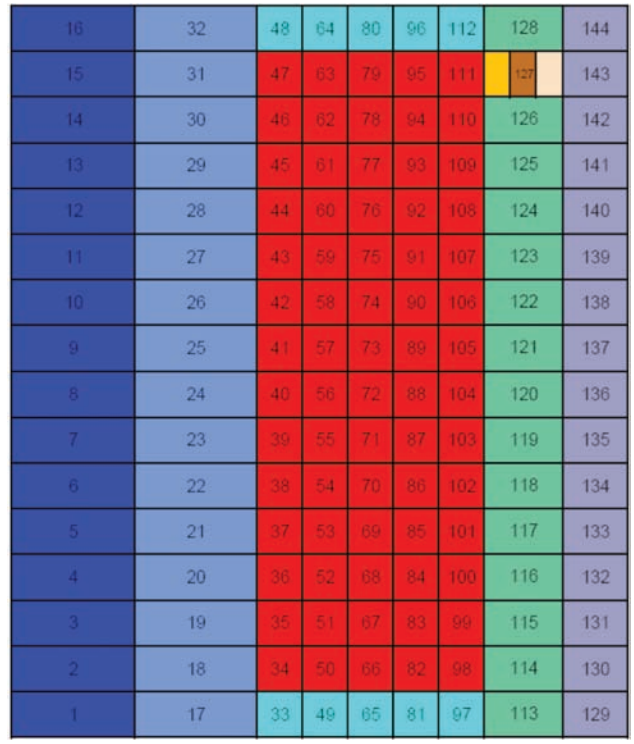

Figure 2. Geometric configuration of a 2D(r,z) PBR consisting of an inner reflector, an annular fuel region, and a controlled outer reflector.

incoming and outgoing currents. The team then programmed response functions into a MATLAB script and generated them independently. The result for the coarse mesh r direction discretization with the embedded response functions gave good agreement when compared to the fine mesh calculation of the finite difference solution.

Planned Activities

For the upcoming year, the research team plans to complete the following activities:

- Integrate results of the first two tasks (described above) into the code (CYNOD).
- Develop a 3D PBR benchmark problem.
- Test the implementation of the first activity (Bullet 1) with the 3D PBR benchmark problem.
- Develop a 2D response function-based transport method for hexagonal geometry.
- Integrate the transport method into an existing diffusion code.
- Develop a 2D prismatic VHTR benchmark problem.
- Test the result of the transport method's integration with the 2D prismatic VHTR benchmark problem.
- Write the user's manual for the modified CYNOD.

NUCLEAR ENERGY RESEARCH INITIATIVE

Implications of Graphite Radiation Damage on the Neutronic, Operational, and Safety Aspects of Very High-Temperature Reactors

PI: Ayman I. Hawari, North Carolina State University

Collaborators: Idaho National Laboratory, Oak Ridge National Laboratory

Project Number: 07-011

Program Area: Gen IV

Project Start Date: June 2007

Project End Date: May 2010

Project Description

This project entails experimental and computational investigations to study radiation effects of graphite in very high-temperature reactors (VHTRs). Researchers will use molecular dynamic and *ab initio* molecular static calculations to 1) simulate radiation damage in graphite under various irradiation and temperature conditions, 2) generate thermal neutron scattering cross sections for damaged graphite, and 3) examine the resulting microstructure to identify damage formations that may produce the Wigner effect.

In both the prismatic and pebble-bed VHTR designs, the graphite moderator is expected to reach exposure levels of 10^{21} to 10^{22} n/cm^2 over the reactor's lifetime, resulting in damage to the graphite structure. Studies of irradiated graphite show changes in thermal conductivity and heat capacity at fluences less than 10^{21} n/cm^2. These properties depend on the behavior of atomic vibrations (phonons) in the graphite solid. Certain alterations in phonon behavior would produce changes in these properties, and such alterations are likely to impact thermal neutron scattering, with implications for the VHTR's neutronic and safety behavior. Another important phenomenon pertains to published data showing that a high-temperature Wigner-like effect (greater than 1200°C) may exist in graphite. If confirmed, this effect would have direct implications on VHTR safety behavior.

Research Progress

During the past year, the project team initiated work using unirradiated and irradiated grade NBG-10 graphite samples from Oak Ridge National Laboratory (ORNL). These irradiated samples include short sections of bend bar numbers L03115-L25 (irradiated to 4.9 x 10^{25} n/m^2 at E>0.1 MeV and ~280°C) and L3124-L69 (4.7 x 10^{25} n/m^2 at E>0.1 MeV and ~700°C), as depicted in Figure 1. Researchers conducted initial measurements with a neutron powder diffractometer to investigate potential differences in sample structure. From the diffraction patterns of the irradiated and unirradiated graphite samples in Figure 2, the irradiated samples show broadening of the diffraction peaks. Researchers are in the process of interpreting these results using powder diffraction Rietveld refinement techniques.

Figure 1. Photographs of irradiated bend bar samples.

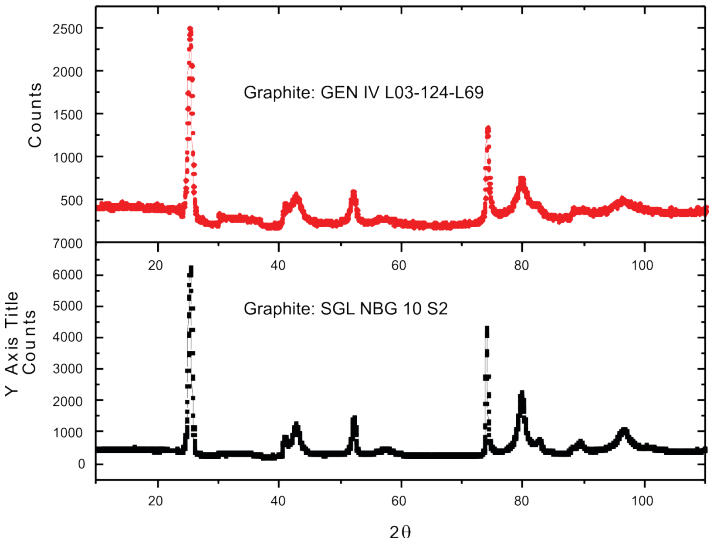

Figure 2. Neutron powder diffraction patterns for irradiated (red/top) and unirradiated (black/bottom) NBG-10 graphite samples.

Furthermore, researchers are currently performing porosity assessment measurements using sodium-based (Na-22) digital bulk positron annihilation lifetime spectrometry (PALS). Figure 3 shows the system, including the gamma-ray detectors (BaF_2 and $LaBr_3$) and data acquisition electronics. The team also measured pore size distributions for open pores using mercury intrusion porosimetry (MIP) to establish baseline comparisons between PALS and MIP. PALS is expected to be focused on nanometer (nm)-sized pores—typical sizes produced during the radiation damage stage and the subsequent stages of damage evolution. Figure 4 shows MIP information for a reactor-grade graphite sample.

Researchers established the molecular dynamics (MD) computational approach for calculating the graphite scattering law. Figure 5 shows a comparison between the scattering law (i.e., S [a, b]) calculated using MD and that generated using the NJOY/LEAPR methodology. Reasonable agreement exists at the lower β limits, although researchers are currently examining and reconciling deviations at higher β ranges.

Planned Activities

For the remainder of this project, the research team will continue further studies of the structural and dynamical aspects of unirradiated and irradiated reactor-grade graphite using neutron scattering techniques. The computational work will finalize the established MD-based approach for generating the thermal neutron scattering cross sections for graphite. The team will produce cross-section libraries suitable for VHTR design calculations.

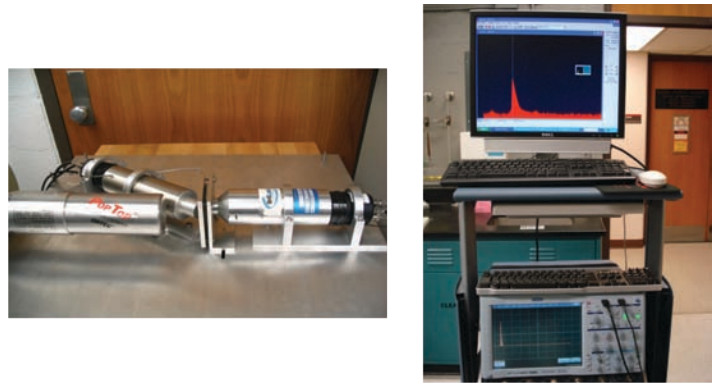

Figure 3. An Na-22-based digital bulk PALS system.

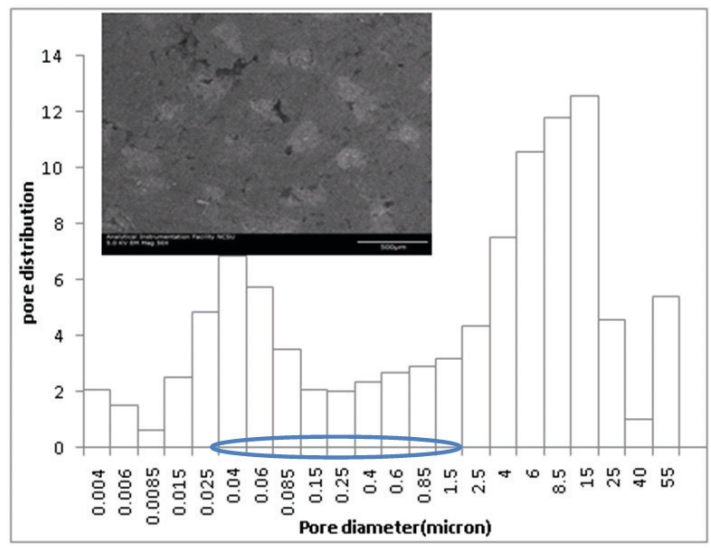

Figure 4. Pore size distribution for a reactor-grade graphite sample obtained using MIP. The circled region shows the nm-size range expected to be sensitive to PALS for both open and closed pores, important for comparing unirradiated and irradiated graphite. The inset shows an SEM image of the reactor-grade graphite structure.

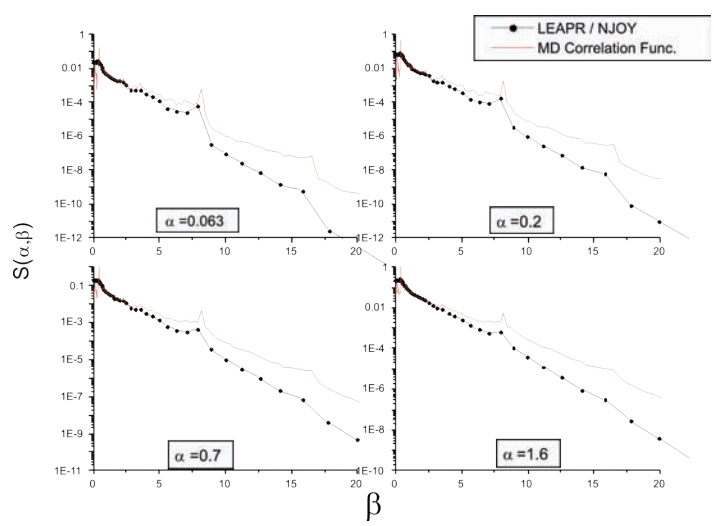

Figure 5. Room-temperature thermal scattering law of graphite calculated using the LEAPR/NJOY formalism and classical MD.

NUCLEAR ENERGY RESEARCH INITIATIVE

Advancing the Fundamental Understanding and Scale-Up of TRISO Fuel Coaters via Advanced Measurement and Computational Techniques

PI: Dr. Muthanna Al-Dahhan, Missouri University of Science and Technology[1]

Collaborators: None

Project Number: 07-017

Program Area: Gen IV

Project Start Date: October 2007

Project End Date: September 2010

Research Objectives

The overall research objectives are to 1) advance the fundamental understanding of TRISO fuel coater hydrodynamics by systematically investigating effects of design and operating variables on solids and gas dynamics, 2) evaluate the reported dimensionless groups as scaling-up factors, and 3) establish a reliable scale-up methodology for TRISO fuel particle spouted bed coaters based on maintaining hydrodynamics similarity via advanced measurement and computational techniques. Researchers will develop an on-line, non-invasive measurement technique based on gamma ray densitometry (i.e., nuclear gauge densitometry) that can be installed for coater process monitoring to ensure proper performance and operation and to facilitate the developed scale-up methodology.

To achieve these objectives, the research team will use the following research tools:

- Optical probes for solids and gas holdups and solids velocity distribution measurements and their fluctuations.
- Gamma ray densitometry for measuring radial profiles of solids and gas holdups along the bed height, spouted diameter, and fountain height. This tool also indicates the flow pattern and regime inside the bed and along its height.
- Gamma ray computed tomography (CT) for measuring the solids and gas holdup cross-sectional distribution and radial profile along the spouted bed height, spouted diameter, and fountain height.
- Radioactive particle tracking (RPT) for measuring the three-dimensional (3D) flow patterns, solids velocity, turbulent parameters, circulation time, and many others.
- Gas dynamics measurement technique for measuring the gas residence time distribution and its extent of mixing.
- Pressure transducers for measuring the pressure signal and its fluctuations, which will be analyzed statistically for flow pattern information.

The team will then use the knowledge obtained as benchmark data to evaluate the computational fluid dynamics models and their closures. Researchers will use the results to facilitate the developed scale-up methodology, to identify the conditions for hydrodynamics similarity, and to further investigate and optimize the process performance of TRISO coaters.

Research Progress

Measurements of the Optical Probe in the Spouted Bed. The team processed and analyzed measurements of a $\frac{1}{8}$-inch optical probe on 6-inch and 3-inch internal diameter spouted bed columns, using 2-mm diameter glass beads as solids material and air as the gas phase. The static bed was 16 cm high in the 3-inch columns and 32 cm high in the 6-inch columns, with an applied gas velocity of 0.74 m/s and 1 m/s, respectively. Researchers took data from three different axial positions and six radial positions, repeating experiments starting from different sides of the column to examine the system's symmetry. Figure 1 presents sample results. The operating conditions correspond to mismatch hydrodynamics (Case C in He *et al.*, 1997) with respect to the first experimental set (Case A in He *et al.*, 1997),

[1] Formerly at Washington University in St. Louis (see Planned Activities).

and resulting holdup values are expected to be different. Reynolds numbers $\frac{\rho_f d_p U}{\mu}$ and $\frac{\rho_s d_p U}{\mu}$ are the only dimensionless group differences between these two cases; all other scaling groups are kept constant. Figure 2 depicts the radial solids holdup profile for a 3-inch column. As the original probe and the electronics were found to be incapable of providing accurate results, the team could use these tools to measure the solids velocity, so the researchers designed and manufactured a new set of optical probes (see below).

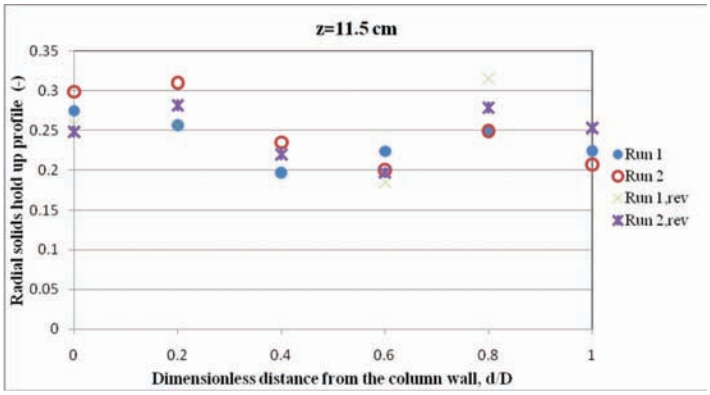

Figure 1. Radial solids holdup profiles obtained by optical probe method ($\frac{1}{8}$-inch diameter tubing) at the level z = 11.5 cm from the distributor of the 3-inch column and gas velocity U_g = 0.74 m/s.

Identification of Flow Regimes and Patterns in a Fluidized Bed Column. The team used a fluidized bed 0.45 m in diameter to evaluate the feasibility of applying gamma ray densitometry to identify flow regimes and flow patterns. Results of the study confirmed that such a technique and methodology can be applied in all gas-solid systems, including spouted beds. The sampling frequency for data acquisition was set at 10 hertz (Hz), which yielded more than 15,000 total data points. The raw data were analyzed to obtain the variance at various superficial gas velocities at ambient temperature and pressure. As illustrated in Figure 2, an increase in gas velocity indicates an increase in variance of the collected data. The variance curve changes slope between gas velocities of 12 cm/s and 13.7 cm/s, indicating the system transition from a packed state to a fluidized state; the velocity at this point is defined as the minimum fluidization velocity (mfv). Researchers conducted experiments to determine the mfv by measuring variation of bed expansion and pressure drop with superficial gas velocity in the same fluidized bed. Differences showed that close values of mfv were obtained (differences of about 10 percent or less). The variance curve changes slope again at gas velocities between 17 cm/s and 18.9 cm/s, representing the flow pattern and regime transitioning from bubbling fluidization to turbulent fluidization. Transitions between the different fluidization regimes are not usually sharp. This success indicates that the technique could be used for on-line monitoring of the flow regime and pattern in a spouted bed—a topic for future investigation.

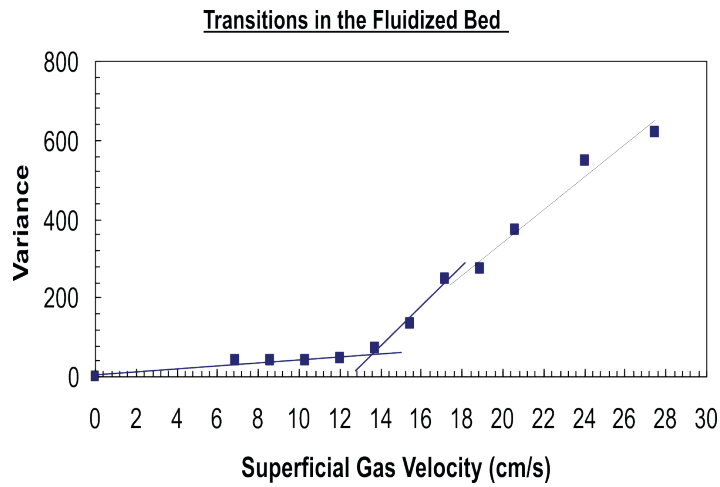

Figure 2. Effect of superficial gas velocity on the variance of nuclear gauge fluctuation (Cesium-137 source; 18-inch diameter column; low density polyethylene fluidized bed; H/D = 2; 25 inches above the distributor).

New Optical Probes. The project has acquired four newly designed optical probes (Figure 3) and an accompanying electronics system. The probes can simultaneously measure the solids concentration, void holdup, and the solid particles velocity, along with each of their fluctuations. The system consists of optical fiber probes, photoelectric converter and amplifying circuits, signal pre-processing circuits, a high-speed analog-to-digital interface card and its PV6 software. The team has initiated validation of the optical probes' measurement. Researchers are using the probes to measure the radial profile of solids and gas holdups, then making corresponding measurements using gamma ray densitometry—the technique being developed for flow pattern identification—and comparing the results.

Figure 3. Newly acquired optical probes.

Air Compressors. Missouri S&T has purchased and installed two new high-capacity and high-pressure air compressors. They can deliver the needed air flow to the four spouted bed units.

Gamma Ray Densitometry and Gamma Ray CT Techniques. The team will develop a methodology using gamma ray densitometry to identify and monitor the spouted bed coater's flow pattern and flow regime in a non-invasive manner. The measurement principle is based on the attenuation of gamma radiation, which is transmitted from a radioactive source to a radiation detector mounted directly opposite the source. The collected counts will be processed and analyzed for flow pattern identification.

Computational Fluid Dynamics (CFD) Modeling for Spouted Bed. The project is using the FLUENT Eulerian model, which can model dispersed phase distribution (solid particles, bubbles, droplets) in a liquid or gas continuous phase (primary). In the Eulerian model, every phase has its own mass, momentum, and energy conservation. The conservation equations of different phases are coupled via interfacial terms; these terms are modeled. The closer these terms are to reality, the more accurate the model. Most interfacial terms depend on particle size, and most dispersed flows are not mono-dispersed; so knowledge of representative particle diameter is essential.

The team modeled solids movements in two spouted bed reactors. The diameter and height of the first reactor are 0.15 meters and 1 meter, respectively. The gas is injected at a velocity of 1 m/s, while the column is filled to 0.32 m high with 2-mm glass beads. The diameter and height of the second reactor are 0.075 m and 1 m, respectively. The gas is injected at a velocity of 0.74 m/s while the column is again filled with glass beads.

With the same conditions, the team has implemented CFD modeling on the spouted bed of 6-inch and 3-inch diameter columns, obtaining two-dimensional (2D) contour plots for volume fraction of solids. The results describe solids' movement in the reactors (see Figure 4). Future inquiries should evaluate and validate these results through comparison with results from the optical probes, CT, and RPT.

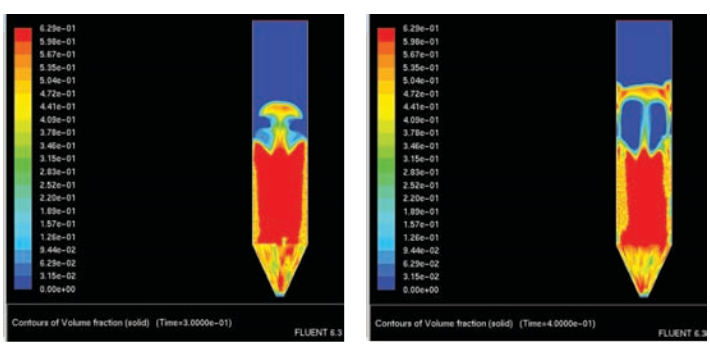

Figure 4. 2D contours of volume fraction for solids in 6-inch diameter spouted bed.

Planned Activities

The project PI recently transferred to the Missouri University of Science and Technology (Missouri S&T). Although the project lead organization remains Washington University in St. Louis, the project will be subcontracted to Missouri S&T. Dr. Al-Dahhan's joint appointment with the nuclear engineering program facilitates the use of radioactive-based techniques, and he has established two large labs dedicated to the use of radioisotope techniques. However, his transfer, along with some technical difficulties, has delayed execution of some project tasks. A no-cost extension is planned to fully complete these tasks. The following are the planned activities for the third year.

New Optical Probes and Pressure Transducers. Utilizing the spouted beds and optical probes, the team will evaluate the proposed scale-up methodology and the reported dimensionless groups for hydrodynamics similarity. Researchers will investigate effects of design and operating variables on solids and gas holdups, solids velocities, and their fluctuations. Simultaneously, the team will take pressure transducer measurements and correlate pressure signal analysis to the results and findings from the optical probes.

Gamma Ray Densitometry. Using dual source gamma ray CT, researchers will develop a gamma ray densitometry-based technique for process monitoring to ensure proper performance and scale-up achievement, determine the flow regime, and characterize on-line the bed solids and holdups.

Gas Dynamics Measurements. The team will characterize and investigate gas dynamics and dispersion using a newly developed technique based on the measurement of the dynamics of an injected gas tracer.

Computational Fluid Dynamics. Researchers will continue CFD simulations to evaluate various closures using the results as benchmark data.

Initiating RPT Measurements and Investigation. RPT technology is being assembled and developed for another project. The team will implement this technique on spouted beds.

NUCLEAR ENERGY RESEARCH INITIATIVE

Fission Product Transport in TRISO-Coated Particle Fuels: Multi-Scale Modeling and Experiment

PI: Izabela A. Szlufarska, University of Wisconsin–Madison

Collaborators: None

Project Number: 07-018

Program Area: Gen IV

Project Start Date: June 2007

Project End Date: June 2010

Research Objectives

The objective of this project is to develop a multiscale computational model of fission product transport through tristructural-isotropic (TRISO) coatings. The project team will use the model to determine fast diffusion mechanisms of silver (Ag) through the silicon carbide (SiC) TRISO coating. The model will build on the following: 1) the strength of massively parallel molecular dynamics simulations to provide a full atomistic picture of SiC microstructural features such as grain boundaries (GBs), 2) quantum mechanical approaches to determine highly accurate diffusion barriers in these structures, and 3) continuum-level theories to determine diffusion rates in macroscopic samples. The team will perform experiments to provide input for simulated microstructures (for example, information about typical GB textures) and to validate modeling predictions.

Research Progress

Modeling. In order to provide fundamental understanding of diffusion through TRISO coatings, the project team performed modeling studies of Ag interaction with SiC. The goal was to identify differences between Ag diffusivity through bulk versus GB paths.

Bulk modeling of diffusion is done by direct *ab initio* calculations of defect formation and migration energies in the cubic SiC structure. For GB studies, the team first developed an optimization scheme based on molecular dynamics simulations and empirical potentials to construct realistic GB structures. Researchers then used the optimized GB structures as input for the *ab initio* calculations for the formation energies of Ag defects and the corresponding migration barriers, performed in the framework of the density functional theory.

Diffusion of Ag Through Bulk SiC. The research team identified the key parameters that control diffusion through bulk SiC, finding that the most stable states for Ag in SiC are Ag substituted on Si with a charge of -3 (Ag_{Si}^{-3}) and Ag on Si clustered with a vacancy on C with a charge of -1 (Ag_{Si}-VC^{-1}). Formation of similar impurity-vacancy complexes is common for large impurities in carbide ceramics; e.g., the team found similar structures to be stable for cesium (Cs) in SiC, as well as for Ag and Cs in zirconium carbide (ZrC). Researchers estimated effective diffusion barriers for both Ag_{Si}^{-3} and Ag_{Si}-VC^{-1} to be approximately 9 eV. However, the lowest effective diffusion barrier for Ag in the bulk is from Ag interstitials, with a value of 7.9 eV. The migration barrier for an Ag atom is generally relatively low, just 1.9 eV for Ag on the Si sublattice and 0.9 eV for Ag interstitials. Ag's slow diffusion in the bulk is due to the large formation energy of interstitials (10.5 eV) and the large combined formation and migration energies of Si vacancies (7.8 eV).

Diffusion of Ag Through SiC Grain Boundaries. Estimates of Ag diffusion through bulk SiC are consistent with the experimentally determined bounds on bulk diffusion.[1, 2] The calculated activation energy (Q) for the bulk is approximately 7.9 eV, and the integral release measurements reported Q as approximately 2 eV. Therefore, the question is whether any physics of Ag interactions with SiC could reduce Q by 7 eV when the Ag atom diffuses along a GB instead of bulk.

To answer this question, the team investigated some of the GB structures most commonly occurring in SiC. Experiments determined that among so-called special GBs, the most common is $\sum 3$, characterized by asymmetry across the GB plane. Figure 1 shows the lowest-energy $\sum 3$ structure. Both symmetric and asymmetric $\sum 3$ structures have been observed experimentally in SiC. The team found a strong segregation tendency of Ag to GBs. For instance,

formation energy of Ag in the symmetric GB is lower than in the bulk by 2.5 to 4.5 eV. The team also did a survey of defect energies in the asymmetric structure, determining the most stable defects.

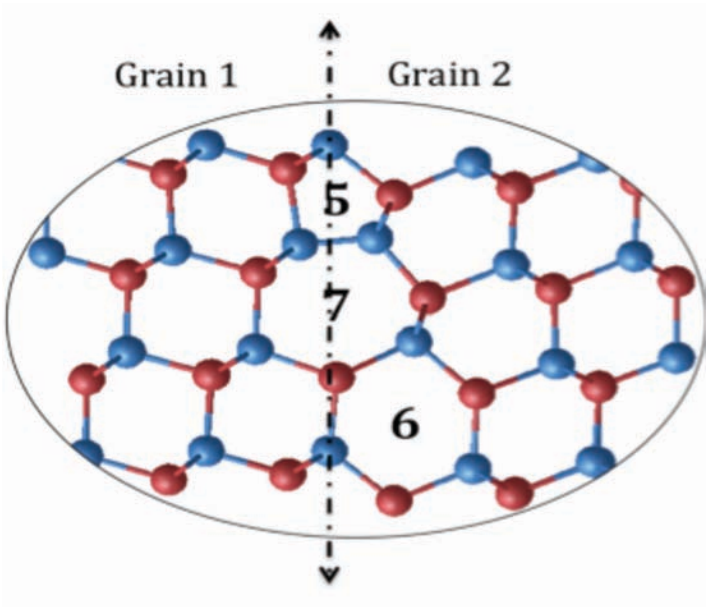

Figure 1. Asymmetric ∑3 GB structure obtained from molecular dynamics simulations.

In summary, the team found that diffusion of Ag through pristine bulk SiC is too slow to account for the integral release of Ag from TRISO. Key atomic-level parameters that control diffusion (formation energy of Si vacancy and formation energy of Ag interstitials) are significantly lowered in ∑3 GBs of SiC, which supports the hypothesis that GB diffusion is responsible for the fast release of Ag from TRISO particles. Diffusion along the symmetric ∑3 GB was found to be faster than that in the integral release measurements, while diffusion through the asymmetric ∑3 GB was found slower than in the TRISO particles, which is consistent with the fact that integral release measurements provide diffusion coefficients averaged over a microstructure.

Diffusion Couple Design. The initial diffusion couple design utilized a solid/liquid interface between Ag/SiC and Ag+10at%Si/SiC. The design resulted in oxidation of the SiC surface from residual oxygen and dissolution of Si into liquid Ag. Therefore, an alternative design was pursued to mitigate oxidation and dissolution. The new process, utilizing an instantaneous source design, deposits a sufficiently thin layer of the diffusing species (Ag) on the SiC surface so that the diffusing species enters the substrate, disallowing any dissolution issues. Oxidation is mitigated by sealing the samples in quartz tubing under UHP argon after five pump/purge cycles. Diffusion couples have been constructed and exposed to temperatures ranging from 900°C to 1200°C (Table 1). The additional advantage of the instantaneous source design is a clean exposed surface for depth profiling.

Table 1. Test matrix for completed instantaneous diffusion couple design tests.

Duration (hours)	Test Temperature				
	900°C	950°C	1000°C	1100°C	1200°C
10		•			
24		•	•	•	•
36					•
100	•				

Depth Profiling. The initial experimental design called for Rutherford backscattering spectroscopy (RBS) analysis for depth profiling, but this approach suffered from limitations on sample size and detectability (approximately 0.1 atom %). Therefore, focus was shifted to secondary ion mass spectroscopy (SIMS) analysis, which has improved depth resolution and sensitivity. The Ag/SiC system signals were analyzed for $^{28}Si^+$, $^{12}C^+$, $^{16}O^+$, and $^{107}Ag^+$. Surface layer concentration was recorded every 20 seconds, yielding an intensity (counts) verse time for each constituent atom. The SIMS signal is representative of the real composition when steady-state conditions exist and is reached when the sputter yields of each target species normalize because of conservation of mass during sputtering.[3] For most scans, steady-state conditions existed after 120 seconds or 40 nanometers (nm). Because the Ag signal's measured intensity is proportional to Ag concentration in the bulk material, the intensity can be used directly in diffusion analysis.[3]

Diffusion Analysis. Because of analysis limitations and experimental conditions, only one of the exposed instantaneous source diffusion couples provided accurate diffusion data: the 950°C 24-hour sample. In diffusion studies, competition between volume diffusion and GB diffusion exists. Three different kinetic regimes have been developed to describe the relationship: Types A, B, and C.[4] In the Ag/SiC system, Type B and C kinetics are expected. Type B kinetics, occurring with diffusion along the GB and bulk diffusion from the GB, arises when the volume diffusion distance is larger than the GB width yet smaller than the grain size. Type C kinetics occurs when the volume diffusion coefficient makes no contribution to the outcome and all transport of the diffusing species occurs by GB paths.

Calculations suggest that the kinetic regime is between Type B and Type C. To determine the appropriate kinetic regime, researchers must know the volume diffusion coefficient for the Ag diffusion in SiC. They will conduct future SIMS analysis on single-crystal 6-H SiC wafers. The analysis of the single-crystal samples will allow direct measurement of volume diffusion in SiC and a better classification of the kinetic regime.

TEM Analysis. The team has initiated an investigation of Ag penetration along individual GBs to determine if certain GBs exhibit preferential diffusion. Because of the nano-scale nature of GBs, transmission electron microscopy (TEM) analysis is preferred to scanning electron microscopy, as the former possesses better resolution and chemical sensitivity. To determine the spatial distribution of Ag in SiC, the team has conducted TEM/energy dispersive spectroscopy (EDS) analysis on the 950°C 24-hour Ag/SiC instantaneous source diffusion couple. Bright field TEM was used to identify planar GB defects along the sample interface.

EDS analysis performed along a selected GB determined the location of Ag in the sample, acquiring five separate EDS spectra. An initial spectrum was obtained using a 120-nm spot size to collect sufficient counts, with the spot size reduced to 25 nm, then to 16 nm for successive scans. Silver emits strong characteristic x-ray peaks for $L\alpha_1$, $K\alpha_1$, and $K\beta_2$ at 2.98 keV, 22.16 keV, 21.99 keV, respectively.[5] The $K\alpha_1$ and $K\beta_2$ peaks can be used for analysis.

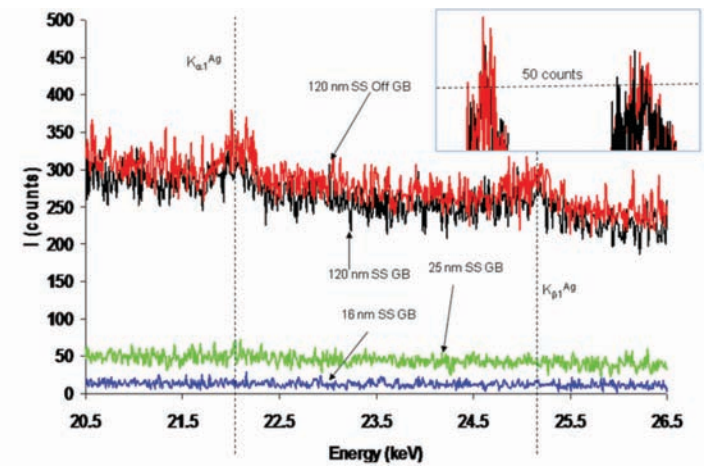

Figure 2. Montage of the EDS spectra for scans 1 through 4 on GB of energies associated with the $K\alpha_1$ and $K\beta_2$ intensities (the $K\alpha_1$ and $K\beta_2$ peaks are shown in the inset) for 120-nm spectra on- and off-GB with the background removed.

Figure 2 identifies the energy range associated with the $K\alpha_1$ and $K\beta_2$ peaks for Ag. Qualitative analysis suggests the presence of Ag in the system for both on- and off-GB scans. To conduct quantitative analysis, background noise was removed to accurately determine the peak height, shown in the inset of Figure 2. The estimated peak heights for $K\alpha_1^{Ag}$ for both scans are approximately 50 counts.

The Cliff-Lorimer ratio technique was employed to determine the concentration of Ag in the system. The calculated Ag concentration for the GB scan is approximately 0.12 at%, compared to approximately 0.05 at% for off-GB. The difference in calculated concentrations does suggest GBs are the dominant diffusion path at 950°C.

To accurately determine the spatial concentration distribution along GBs, a different technique is required. Scanning transmission electron microscopy (STEM)/EDS systems have improved sensitivity over TEM/EDS and allow EDS mapping of the sample, resulting in concentration distribution profiles necessary for directly measuring the active diffusion mechanism. A new TITAN STEM is currently being installed at the Materials Science Center user facility at the University of Wisconsin-Madison, and a proposal to use the ORNL SHaRE facility has been accepted.

Planned Activities

The team will continue modeling efforts to investigate diffusion of Ag through GBs other than $\sum 3$. Researchers will employ continuum models to estimate diffusion through a SiC microstructure with GB distribution determined experimentally and with local diffusion constants determined in atomistic simulations. Related future work will focus on additional conditions for the diffusion couple experiments. The additional diffusion couples have already been exposed and are awaiting analysis. The additional conditions will allow for calculation of diffusion energetic of the Ag/SiC system, allowing better insight into the diffusion mechanisms and comparison with the computational modeling efforts. The team plans to work with temperatures up to 1500°C.

Accurate analysis is difficult for the GB diffusion coefficient from the triple product and appropriate kinetic regime because of the lack of information on the volume diffusion and segregation coefficients. Therefore, researchers will perform SIMS analysis on 6-H SiC single-crystal diffusion couples for direct measurement of the volume diffusion coefficient. The segregation coefficient can be measured directly through *in situ* auger electron spectroscopy (AES) measurements of intergranular fracture surface.[6] The project has obtained access to appropriate AES instrumentation through the Pacific Northwest National Laboratory Environmental and Molecular Science Laboratory.

The investigation of individual GBs will illuminate fast diffusion pathways and give rise to possible GB engineering solutions. Initial TEM/EDS measurements have shown that this analysis technique does not possess adequate spatial resolution for investigating individual GBs. STEM/EDS will be pursued to improve on detectability and spatial resolution of the EDS analysis through the Oak Ridge National Laboratory SHaRE user facility.

References:

[1] Friedland, E., et al., *Study of Silver Diffusion in SiC.* J. Nucl. Mater., 2009. 389.

[2] Maclean, H.J., *Silver Transport in CVD SiC,* PhD Thesis, MIT. 2004.

[3] Feldman, L. and J. Mayer, *Fundamentals of Surface and Thin Film Analysis.* 1986: North-Holland New York.

[4] Harrison, L., *Influence of Dislocations on Diffusion Kinetics in Solids with Particular Reference to the Alkali Halides.* Transactions of the Faraday Society, 1961. 57: p. 1191-1199.

[5] Bearden, J., *X-Ray Wavelengths.* Rev. Modrn. Phys., 1967. 39(1): p. 78.

[6] Mishin, Y., et al., *Grain Boundary Diffusion: Fundamentals to Recent Developments.* International Materials Reviews, 1997. 42(4): p. 155-178.

NUCLEAR ENERGY RESEARCH INITIATIVE

Emissivity of Candidate Materials for Very High-Temperature Reactor Applications: Role of Oxidation and Surface Modification Treatments

PI: Kumar Sridharan, University of Wisconsin-Madison

Collaborators: None

Project Number: 07-020

Program Area: Gen IV

Project Start Date: April 2007

Project End Date: March 2010

Rsearch Objectives

The objectives of this project are to:

- Evaluate emissivities of candidate materials for the reactor pressure vessel (RPV) and internal components of the very high-temperature reactor (VHTR) in air and helium environments from 300°C to 900°C.
- Study the effects of emerging and commercial surface treatments on emissivity after exposure in air and helium environments at elevated temperatures.
- Expose untreated and surface-modified alloys to elevated temperatures and characterize surface oxides that form on the alloys, developing a comprehensive understanding of the relationships between emissivity, oxide characteristics, and surface treatments.
- Develop an integral separate-effects emissivity database for potential candidate materials and surface modification treatments.

Thermal radiation of heat from the RPV outer surface partially cools the vessel and its internal components. With an unexpected increase in temperature, thermal radiation becomes a significant mode of heat dissipation because of its fourth-power temperature dependence, according to the Stefan-Boltzmann equation. Energy emitted in the form of heat is directly proportional to area multiplied by temperature raised to a power of four, so if the temperature doubles, the energy emitted increases by a factor of sixteen. This energy is further affected by the radiant body's emissivity. Since oxidation inevitably occurs at these higher temperatures, material emissivity is clearly intricately related to the chemical, physical, and mechanical characteristics of the oxide scales that form on the surface, including their chemical composition, grain morphology, topography, and porosity. The growing field of surface modification provides opportunities for achieving high emissivities at high temperatures by changing topography and grain orientation or inducing controlled surface compositional changes.

Research Progress

The project team has designed and constructed equipment to measure high-temperature spectral emissivity of VHTR materials. Figure 1 shows a schematic illustration of the high-temperature spectral emissivity measurement system. The system has four major sections: the sample test chamber, central lid, optical system, and Fourier transform infrared (FTIR) spectrometer. The sample test chamber is for sample heating and atmosphere control. The optics chamber consists of a periscope system to guide the radiant heat to the FTIR spectrometer. The sample test chamber and the optics chamber are separated by a central lid that holds the optics.

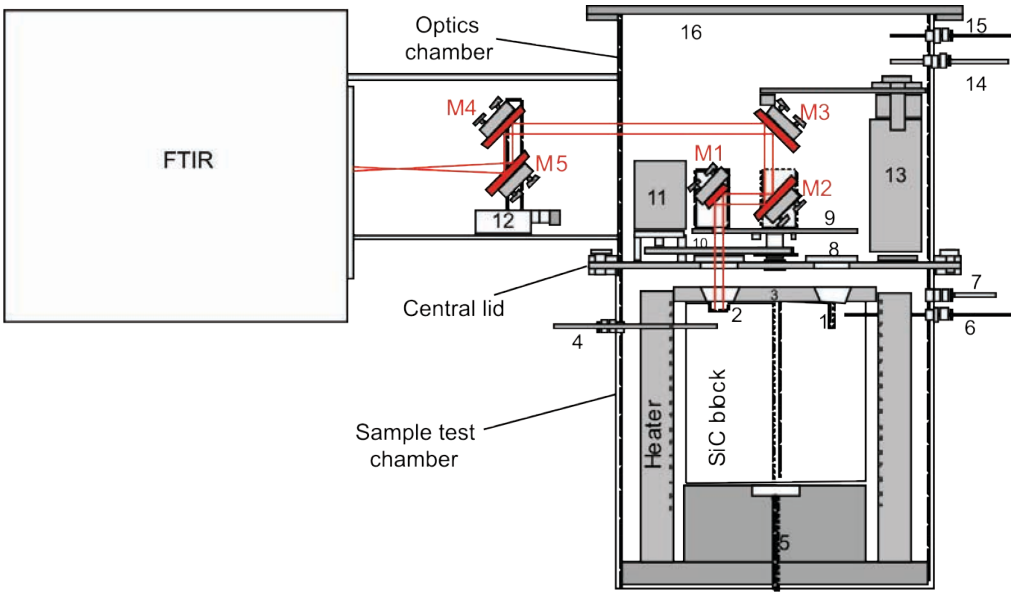

Figure 1. Schematic illustration of the high-temperature spectral emissivity measurement system. M1, M2, M3, and M4 are flat mirrors, and M5 is a parabolic mirror. M1 and M2 can rotate during emissivity measurement. The other parts are labeled as follows:

1. Blackbody hole
2. Sample holder cavity
3. Insulation board for SiC block
4. Thermocouple for sample holder
5. Gas inlet
6. Thermocouple for blackbody
7. Gas outlet
8. CaF_2 windows
9. Rotational mirror holder for mirrors M1 and M2
10. Stainless steel mini-chain for optics rotation
11. Step motor
12. Optical stage for mirrors M4 and M5
13. Vertical optical adjustment for mirror M3
14. N2 purge gas inlet
15. N2 purge gas outlet
16. Transparent plastic cover for watching optics chamber

The sample test chamber consists of a cylindrical block of monolithic silicon carbide (SiC), 203 mm in diameter and 203 mm in height. Eight holes or cavities have been machined circumferentially in this block; seven house the test samples for emissivity evaluation, and the eighth serves as the blackbody reference. Resistance heaters are installed around the SiC block. The top surface of the SiC block is covered by an insulation board to prevent heat loss and to sequester the optics from the heat emanating from the block. Eight tapered holes have been drilled in the insulation board for emissivity measurements. The sample test chamber can be readily used at temperatures up to 900°C, and higher temperatures are possible. The central lid was constructed to allow for improved cooling and evacuation capabilities of the system. The lid is made from a stainless steel plate and is bolted to the top flange of the sample test chamber. To minimize background radiation in the optics chamber and to protect optics components against high operating temperatures, the central lid is water-cooled. Eight holes have been drilled for installing CaF_2 windows, selected because of its high transmittance over the wavelength range of interest, 1 to 10 μm. The optics system consists of four flat mirrors and one parabolic mirror, all gold-coated for better reflectivity.

The FTIR spectrometer is a Bruker System model with a spectral range of 12,000 to 400 cm^{-1} that automatically scans over the entire spectrum with a high-resolution response to even weak signals. While the detector is capable of measurements from 0.8 μm to 25 μm, the CaF_2 windows limit the spectral range because the effective transmittance range of CaF_2 windows is 1 to 10 μm wavelengths, with the intensity of the signal being quite low below 2 μm.

The team used the ceramic standard to calibrate the equipment. To ensure quality assurance, the team emphasized achieving reproducibility and repeatability in emissivity data and reliably bracketing error margins. To this end, researchers performed tests on SiC, boron nitride (BN), and aluminum oxide (Al_2O_3). Figure 2 shows the reproducibility in emissivity data for BN at 600°C for three separate tests, which were performed on different days and with the optics realigned for each measurement. These measurements show spectral emissivity measurements within a five percent range. Because all the samples were placed in the same chamber, the measurement parameters are identical for all samples, and systematic measurement errors from the equipment are the same for all samples and blackbody.

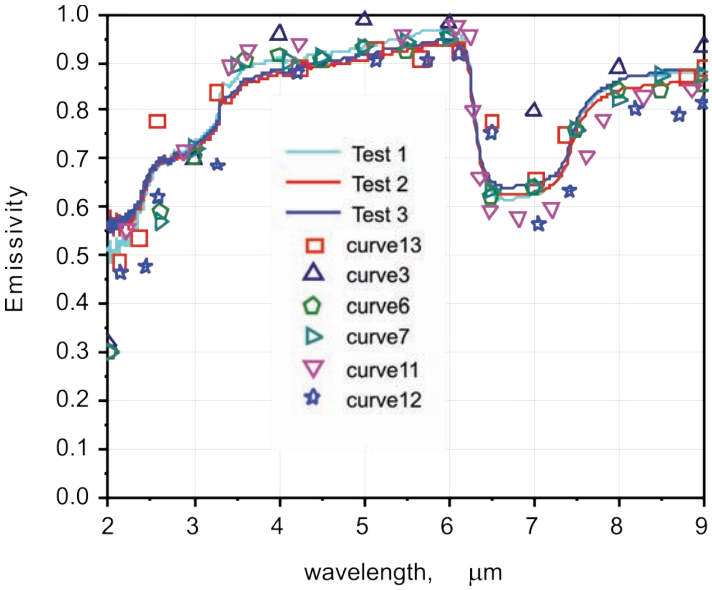

Figure 2. Spectral emissivity of BN measured at 600°C in three separate tests and comparison with literature data from the reference *Y.S. Touloukian and D.P. Dewitt, Thermophysical Properties of Matter, v. 8. Thermal and Radiative Properties, IFI/Plenum, NY, 1972*.

Researchers use scanning electron microscopy-energy dispersive spectroscopy and laser profilometry techniques to analyze the sample surfaces, correlating surface chemistry and morphology changes to the measured trends in emissivity data. Spectral emissivity measurements of surface-treated alloys are also in progress.

Researchers are also investigating how emissivity changes as surface oxidation progresses. Using Monte Carlo simulations and Maxwell's electromagnetic equations, the project team has initiated numerical modeling of emissivity that incorporates effects of oxide layers. The computer efforts use Monte Carlo sampling of emission angle and position for a sample and a blackbody. The process determines spectral sample emissivity from the optics constant and extinction coefficient of the sample and oxide layers. Of particular interest is the cutoff at which further oxide thickness does not affect emissivity. Also of note are the effects of partial oxide spallation. Surface topology is taken as flat. The oxide is assumed to be composed of a thin layer of chromium oxide (Cr_2O_3) and/or hematite (Fe_2O_3) below a thicker layer of magnetite (Fe_3O_4), a bilayered oxide structure that is typical of many chromium-containing reactor steels.

For thin layers of oxides, the emissivity is primarily a function of diffraction in the oxide film. Oxides are typically transparent in the infrared region, so the photons emitted from the substrate metal are partially transmitted through the oxide layer. At the interfaces, the light is diffracted, allowing only some wavelengths through. For larger oxide thicknesses, the photons emitted by the substrate metal are completely absorbed and the emission is dependent entirely on the oxide emissivity. Using Maxwell's electromagnetic equations and optics constants n (refractive index) and k (extinction coefficient), researchers determine the system's emissivity.

Figure 3 shows a sample result of the team's initial modeling efforts. Here, it is assumed that a 0.1-mm-thick hematite layer forms on the steel's surface, and then an outer magnetite layer grows to thicknesses of 0.1, 0.5, 1, and 2 mm. This scenario is quite typical of ferritic steels: the outer oxide layer consists of a fast-growing magnetite layer, and a thin inner hematite layer maintains a relatively low thickness. As expected, the spectral emissivity increases as the magnetite layer thickens.

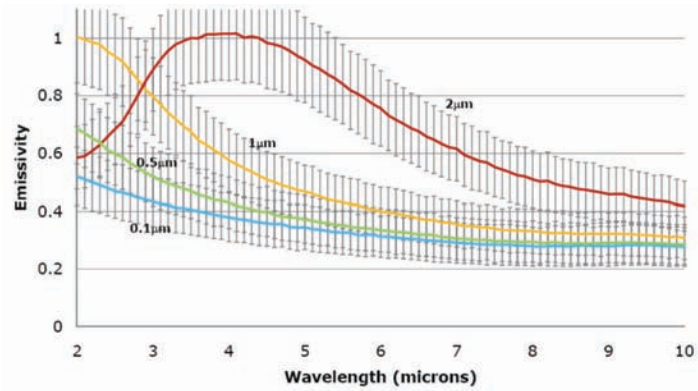

Figure 3. Numerical modeling of emissivity assuming a thin inner hematite layer of a fixed thickness (0.1 mm) and outer magnetite layer of varying thicknesses of 0.1, 0.5, 1, and 2 mm.

Planned Activities

The research team will continue emissivity evaluations on three ferritic steels (T91, SA508, and T22) and four austenitic steels (Incoloy 800H, Haynes 230, Inconel 617, and 304 stainless steel). Researchers will perform emissivity measurements after exposing the steels for up to 300 hours in air and helium. The team will continue to investigate surface treatments including shot peening and Xe^+ ion bombardment, as well as coatings of diamond-like carbon, hafnium-oxide, chromium-oxide, and silicon carbide. Detailed characterization of surface oxides and corrosion products will be performed using scanning electron microscopy, Auger electron spectroscopy, and x-ray diffraction in order to correlate surface chemistry changes to changes in emissivity. Researchers will continue efforts on theoretical modeling for prediction of spectral emissivity.

NUCLEAR ENERGY RESEARCH INITIATIVE

Materials and Design Methodology for Very High-Temperature Nuclear Systems

PI: James Stubbins, University of Illinois

Collaborators: Boise State University, Idaho National Laboratory, Massachusetts Institute of Technology, Stress Engineering Services, University of Nevada-Las Vegas

Project Number: 07-024

Program Area: Gen IV

Project Start Date: May 2007

Project End Date: April 2010

Research Objectives

The objective of this research project is to address major materials performance and design methodology issues for the design and construction of high-temperature and very high-temperature nuclear systems. This work will provide a synergy between the development of simplified, but robust, design rules for high-temperature systems and materials testing, along with performance and improvement of these systems. Such systems will have to deal with time-dependent materials properties (creep, creep-fatigue, high-temperature corrosion) in components with complex stress states, long intended service lives, and aggressive operating environments. Because routine mechanical properties data and current high-temperature design methodology do not provide adequate information for long-term, robust system design, this project will address these issues. In addition, the project team will perform high-temperature materials testing in relevant corrosive environments (such as low-oxygen, partial-pressure with substantial carbon activities) to support further code qualification of existing alloys and the development of emerging alloys.

Research Progress

During the past year, the team initiated aging tests of Alloy 617 and Alloy 230. Figure 1 shows the current status of the aging tests. The results will provide continuous information for predicting material degradation for long-term high-temperature applications. Researchers studied the microstructure evolution and associated mechanical properties for the alloys aged up to 3,000 hours. Microstructure characterization by transmission electron microscope (TEM), scanning electron microscope (SEM), and electron backscatter diffraction (EBSD) revealed the precipitation evolution process during high-temperature aging. Hardness measurement and tensile tests were in a good agreement with the microstructure evolution, showing a long-term softening process after precipitate hardening during the early aging stage. Researchers also carried out the EBSD study to investigate the mechanism of the alloys' plastic deformation at different temperatures. Figure 2 shows an example of texture analysis using EBSD. The dynamic recrystallization (DRX) was found for plastic deformation at over 800°C for both alloys.

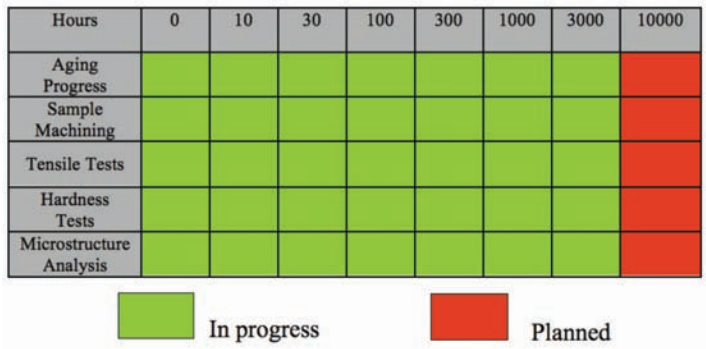

Figure 1. Aging tests plan and current progress.

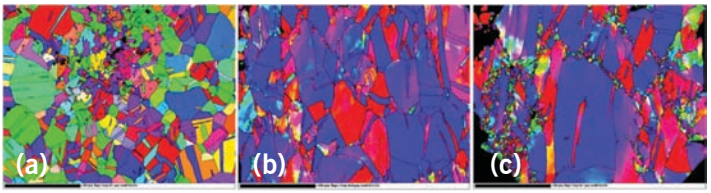

Figure 2. EBSD analysis for the plastic deformation of Alloy 617 at different temperatures: (a) no deformation; (b) plastic deformation at room temperature; (c) plastic deformation and DRX at 1000°C.

The team also performed an anisotropy study on Alloy 617 and Alloy 230 and found both materials to exhibit great in-plane anisotropy in microstructure evolution and mechanical properties. A considerable reduction of

mechanical properties was observed in transverse planes, which might therefore suffer thermal stress in the compact-type heat exchangers found in very high-temperature reactors (VHTRs), as shown in Figure 3(a). Figure 3(b) demonstrates a stress concentration distribution in transverse planes, where great boundaries ligament took place.

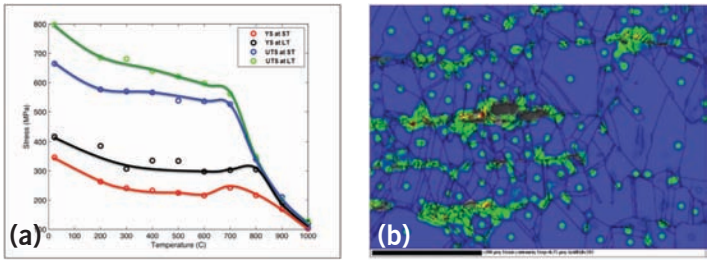

Figure 3. Anisotropy analysis of Alloy 617: (a) tensile properties at different temperatures (ST: short transverse direction, LT: long transverse direction, YS: yield stress, UTS: ultimate tensile stress); (b) strain contouring on short transverse direction after plastic deformation.

The construction of a high-temperature gas corrosion facility is nearly complete. The system will be capable of providing a continuous simulated VHTR environment for both corrosion and creep experiments. The installation of the Clarus 500 Gas Chromatography (GC), the key component of the facility, is finished and undergoing tests.

The installation of a high-temperature vacuum system is complete. The system is capable of providing an inert environment (vacuum or inert gas) for uniaxial tensile, creep, and fatigue tests. Most existing data for the mechanical tests is based on experiments performed in air; however, an inert environment is more similar to the actual atmosphere in a VHTR, and thus more reliable results can be obtained from tests done at the facility.

The extremely high temperatures foreseen in the VHTR (relative to current design practice) have generated some novel problems in the application of materials such as Alloy 617. To a large degree, these problems can be narrowed down to two complications:

- Enhanced rate dependency at around 900°C and above.
- Significantly increased sensitivity of mechanical properties to temperature, combined with numerically lower values of those properties. Together, these changes mean that point-to-point variations in properties such as creep rate and tensile strength cannot be ignored.

Firstly, these complications blur the customary simplification made in design practice between time-independent and time-dependent properties. For example, fundamental quantities, such as yield and ultimate tensile strengths, become critical functions of the test rate, so identifying single values to deal with all possible circumstances is no simple matter. Secondly, property variations during thermal cycling can no longer be easily approximated by such devices as the use of averaged or upper bounding temperatures. The experimental results shown above verify these two observations.

Work is progressing to investigate the broadened use of the isochronous approach to problems involving nonsteady loading, as well as those involving temperature-dependent property variations, either point-to-point or around a thermal cycle at a point. Researchers are addressing these questions by comparing detailed "best estimate" finite element analysis of typical component geometries under steady and cyclic loading, with simplified predictions based on the isochronous stress/strain methodology.

Planned Activities

The project initiated activities well after the intended start date because of delays in the funding cycle. For this reason, the work will extend into a fourth program year. During this next program year, the team will initiate both corrosion and creep tests in the high-temperature gas corrosion facility. Researchers will use the test results to analyze the creep-environment interaction. The team will also start creep and fatigue tests in the high-temperature vacuum system, then compare the results with existing data in air to investigate the fundamental mechanism of high-temperature creep and fatigue. Researchers will complete aging tests up to 10,000 hours for Alloy 617 and Alloy 230, obtaining aging effects on long-term microstructural evolution and mechanical behavior.

The team will perform a creep-fatigue-environment experiment to simulate the real material behavior in a VHTR (Figure 4). The tests will provide important experimental data to examine the correctness of existing design models for creep-fatigue behavior in high-temperature applications.

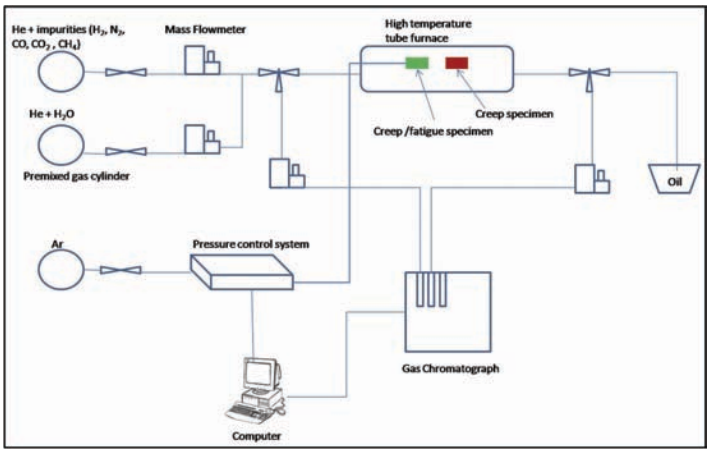

Figure 4. The set-up for a creep-fatigue-environment interaction experiment.

All test results with existing published data will be used as basic references to develop design guidelines for very high-temperature nuclear systems. The design guidelines will account for properties-based performance characteristics and support assessment of joint activities on high-temperature crack initiation and growth behavior.

The design approach will continue to expand the isochronous approach. Extensive literature already exists on isochronous curves and their application to practical elevated temperature design. In fact, this means of performing transient creep analyses is the oldest known method, going back to the 1940s. It has been rigorously proven to be an acceptable approximation to creep under sustained steady load, and it has been adopted by ASME Code Section III, subsection NH, for creep/fatigue evaluation in notch-like features. Relevant necessary work is related to variations in load and properties and is consistent with the range of experimental parameters that this project is examining. Some work has begun under another DOE-sponsored research program to explore alternative methods of characterizing and displaying mechanical property data, including isochronous curves. The work here will provide consistent design approaches with other ongoing code and design methodology programs.

NUCLEAR ENERGY RESEARCH INITIATIVE

Experimental and Computational Fluid Dynamics Analysis of Advanced Convective Cooling Systems

PI: Victor M. Ugaz and Yassin A. Hassan, Texas Engineering Experiment Station

Collaborators: None

Project Number: 07-058

Program Area: Gen IV

Project Start Date: June 2007

Project End Date: May 2010

Research Objectives

The objective of this project is to study the fundamental physical phenomena in the reactor cavity cooling system (RCCS) of very high-temperature reactors (VHTRs). One of the primary design objectives is to assure that the RCCS acts as an ultimate heat sink capable of maintaining thermal integrity of the fuel, vessel, and equipment within the reactor cavity for the entire spectrum of postulated accident scenarios. Since construction of full-scale experimental test facilities to study these phenomena is impractical, it is logical to expect that computational fluid dynamics (CFD) simulations will play a key role in the RCCS design process. An important question then arises: To what extent are conventional CFD codes able to accurately capture the most important flow phenomena, and how can the codes be modified to improve their quantitative predictions?

Researchers are working to tackle this problem in two ways. First, in the experimental phase, the research team plans to design and construct an innovative platform that will provide a standard test setting for validating CFD codes proposed for the RCCS design. This capability will significantly advance the state of knowledge in both liquid-cooled and gas-cooled (e.g., sodium fast reactor) reactor technology. This work will also extend flow measurements to micro-scale levels not obtainable in large-scale test facilities, thereby revealing previously undetectable phenomena that will complement the existing infrastructure. Second, in the computational phase, researchers will perform numerical simulation of the flow and temperature profiles using advanced turbulence models to simulate the complex conditions of flows in the cavity's critical zones. These models will be validated and verified so that they can be implemented into commercially available CFD codes. Ultimately, the results of these validation studies can be used to enable a more accurate design and safety evaluation of systems in actual nuclear power applications (both during normal operation and accident scenarios).

Research Progress

During this project period, the team has worked on parallel tracks of experiments and coordinated computational simulations. The experimental phase has consisted of performing a complete series of flow characterization studies in the RCCS test facility (Figure 1). The key features of the test facility include a copper vessel with integrated internal electrical heaters. The vessel incorporates a flange for connection of the upper and lower sections of the pressure vessel, just as in the full-scale system. An array of 20 thermocouples is positioned on the vessel for surface temperature measurements. The external enclosure (resembling the RCCS concrete walls) is constructed of glass to permit flow visualization, and stainless steel rising pipes (i.e., standpipes) were placed inside the cavity. A movable rack with 30 thermocouples is used to measure the axial temperature profile inside the cavity. This allows temperature measurements to be performed at various radial positions from the vessel wall. The air in the region

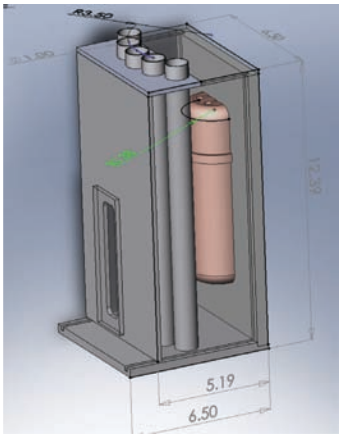

Figure 1. Overview of experiment facility design.

between the vessel and the standpipes is at ambient pressure. Each standpipe is connected to a different pump to permit independent flow control (either air or water can be used), and the hydraulic circuit incorporates a flow meter and a nozzle for tuning the flow.

In initial studies, the cavity is divided into four regions along the axial direction. A high-speed camera captures the flow in each zone at 200 frames per second, enabling visualization of the flow field inside the cavity using zinc stereate tracking particles (Figure 2). Researchers make measurements at steady state, and they have performed velocity field, vorticity field, and error analysis. The measurements show that heat is conducted from the reactor vessel to the cavity through radiative transfer and natural convection processes. Under the conditions probed in these experiments, the data suggest that 65 percent of the heat is carried by radiative transfer while 35 percent is carried by natural convection. The cooling pipes remove 30 percent of the heat inside the cavity. Results are obtained using grey surface approximation, cylindrical symmetry, and averaged fluid properties. The averaged Rayleigh number $Ra \sim 3.87 \times 10^5$ corresponds to fully turbulent flow. These results show the complexity of the heat transfer phenomenology in the RCCS and illustrate the coupling between the temperature profile and the vorticity field. Overall, the test facility provides a new advanced platform to study heat transfer in enclosed cavities with realistic boundary conditions.

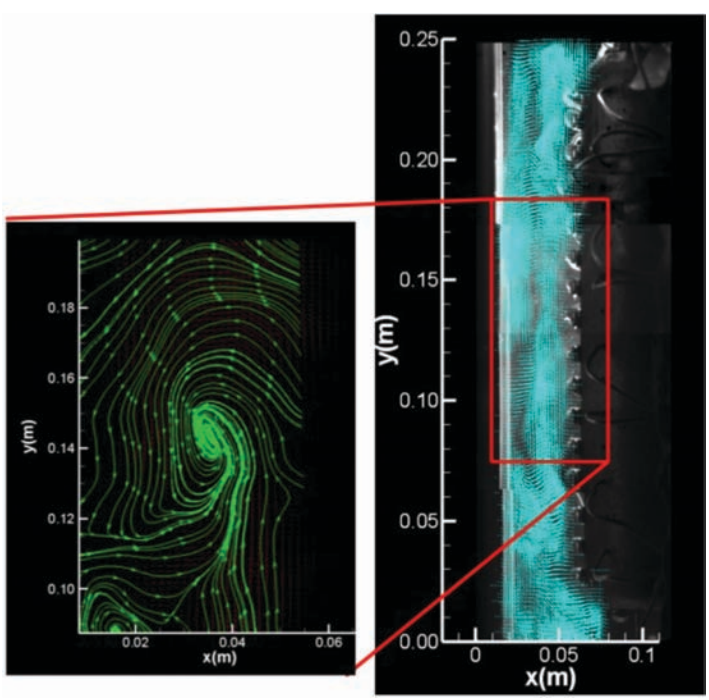

Figure 2. Experimental measurements of velocity field near the vessel sidewall.

The corresponding CFD calculations performed in the project's computational component show good agreement with the experimental data for the temperature distribution in the RCCS cavity region (Figure 3). Some differences are evident close to the cavity bottom wall because the mockup cavity bottom wall was partially realized in aluminum, while the CFD model cavity external box was assumed to be glass. The aluminum in the mockup introduces a back reflection inside the cavity region; the CFD model does not simulate this reflection. This discrepancy aside, the numerical results for the temperature distribution in the upper part of the RCCS cavity were in good agreement qualitatively and quantitatively with the experimental data. One strength of CFD codes is their ability to simulate radiation heat exchange phenomena in very complex geometries where the determination of view factors represents the main obstacle to analytical solution of the problem.

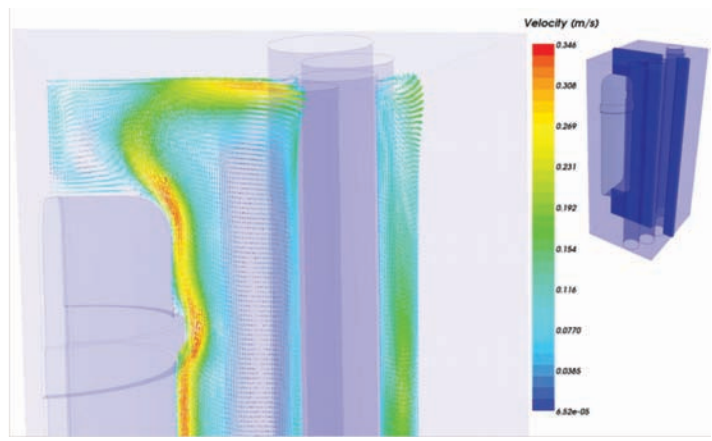

Figure 3. Velocity vector distribution in the RCCS cavity region on a plane normal to the vessel wall (water-cooled configuration shown).

The team performed numerical analyses on the RCCS with water-cooled and air-cooled configurations. Findings allowed researchers to address the better performance of the former versus the latter with respect to reducing stress on the cavity concrete walls. The sensitivity study performed over different vessel wall temperature distributions provides a general idea of the cavity wall temperatures during phases of a pressurized conduction cooldown accident scenario. The analyses showed that, in the critical stage of the transient, the cavity wall peak temperature might exceed design limits for the air-cooled configuration; meanwhile, the water-cooled configuration provides a more efficient cooling, with the cavity wall peak temperature below design limits, even if more arduous conditions are assumed throughout the transient evolution.

Finally, the team assumed that the real plant RCCS configuration would be somewhat distorted in the experimental facility and CFD model. Researchers performed a scaling analysis to address these distortions. The scaling analysis showed that both the experiment and CFD models accurately represent the physics inside the RCCS cavity for a wide range of operating conditions in both water-cooled and air-cooled configurations. In particular, the relative magnitude of buoyancy and inertia forces are properly represented. This implies the correct flow paths and recirculation regions are reproduced. Since the whole energy balance between the pressure vessel wall and the standpipes is due to radiation and convection heat exchange phenomena, a proper scaling of these two heat exchange mechanisms was necessary to address the real conditions of the RCCS safety system. The sensitivity over different standpipe mass flow rates, vessel wall temperature profiles, and vessel volumetric heat generation showed that the experimental facility and CFD model predict the correct proportion of energy transfer by radiation and convection in both water- and air-cooled configurations.

Planned Activities

The primary tasks associated with the project's experimental and computational phases are listed in this section. These tasks are in line with the proposed schedule status and milestones.

Experimental Phase:

- Continue to perform experiments for various flow and geometric conditions in the key convective zone areas.
- Continue to explore new seeding materials that can serve as local temperature indicators within the flow.

Computational Phase:

- Continue implementation and validation against experiment data under various conditions.
- Compare CFD calculations with any other available experimental data.
- Continue investigation of techniques to accurately model temporal and spatial flow structure. Large eddy simulation will provide the temporal and spatial flow regimes under turbulent, transitional, and laminar conditions. Researchers will identify turbulence phenomena of the turbulent coherent structure. These flow patterns will help in developing/refining turbulence models and global correlation for the RELAP system code.

NUCLEAR ENERGY RESEARCH INITIATIVE

Establishing a Scientific Basis for Optimizing Compositions, Processing Paths, and Fabrication Methods for Nanostructured Ferritic Alloys for Use in Advanced Fission Energy Systems

PI: G. R. Odette and Takuya Yamamoto, University of California-Santa Barbara

Collaborators: None

Project Number: 07-069

Program Area: Gen IV

Project Start Date: August 2007

Project End Date: July 2010

Research Objectives

The project team is developing high-performance alloys for advanced fission reactors. These materials will manifest a combination of properties that permit long-lifetime component operation at high temperatures to doses of 200 displacements per atom (dpa).

Achieving these ambitious objectives in a practical structural material requires a combination of innovative alloy design and optimization, including development of compatible processing, fabrication, and joining paths. This research focuses on nanostructured dispersion-strengthened ferritic alloys (NFAs). NFAs contain a high density of yttrium-titanium-oxygen (Y-Ti-O) nano-features (NFs) that result in superior high-temperature creep strength while manifesting remarkable thermal stability and unique irradiation damage resistance. NFAs are typically processed by mechanically alloying (MA) iron-titanium-chromium (Fe-Ti-Cr) powders by ball milling with yttrium oxide (Y_2O_3), followed by powder hot consolidation by isostatic pressing (HIPing) or extrusion. MA dissolves the Y_2O_3 constituents, which then precipitate, along with Ti, during high-temperature processing.

The program of research consists of the following five tasks:

- **Task 1: Developing a Deformation Processing Database.** The project team is characterizing deformation-annealing temperature re-crystallization regimes and other approaches to produce more isotropic properties in directionally deformed microstructurally anisotropic and textured NFAs.
- **Task 2: Solid-State Joining.** The team is developing diffusion bonding and friction stir welding (FSW) methods that preserve the NFs and produce outstanding joint properties.
- **Task 3: Alternative Alloys and Alloy Optimization.** The team is optimizing NFA compositions and processing paths to maximize a variety of NFA performance indices.
- **Task 4: Identification and Optimization of NFs.** The team is resolving critical issues related to the character of various NFs, as well as developing means to manipulate their character for NFA property optimization.
- **Task 5: Other Best Effort Studies and Target-of-Opportunity Irradiations.** The team is carrying out neutron irradiation studies of NFAs to characterize their behavior in severe nuclear irradiation environments.

Research Progress

Task 1: Deformation Processing Database. Team members had proposed a non-uniform straining-annealing mapping approach to efficiently establish a basic deformation-processing database for NFAs. Preliminary studies on MA957 provided a proof-in-principle demonstration of this approach. Researchers developed the finite element modeling simulations, constitutive laws (both static and creep) and experimental characterization methods that are the basis of this task. Specific methods include scanning electron microscopy (SEM), electron backscattering

diffraction, and transmission electron microscopy (TEM). However, the available supply of MA957 is too limited for more extensive studies. For this and other reasons, team members decided to delay Task 1 in order to take advantage of a recent collaborative funding opportunity announcement (CFOA) effort. The collaboration aims to produce much larger heats of best-processing practice 14CrYWT NFAs. The CFOA also involves a deformation-processing task that is highly complementary to this task's proposed research.

Task 2: Solid-State Joining. Standard fusion welds destroy the performance-sustaining NFs, thus severely degrading NFA joint properties. Thus the research team is pursuing solid-state approaches to joining. Researchers have demonstrated a successful NFA-NFA high-temperature diffusion-bonding procedure. They have recently carried out atom probe tomography studies, confirming previous characterization by TEM and small angle neutron scattering (SANS), showing that MA957 can be joined by FSW without extensive destruction of the NFs. The CFOA project team will produce and characterize an FSW alloy.

Task 3: Alternative Alloys and Alloy Optimization. Researchers have been characterizing the sequence of microstructural changes associated with atomizing, milling, and annealing or consolidating delete Cr rapidly solidified powders (RSPs) produced by ATI Powder Metals as part of the CFOA. One notable feature is that the as-atomized RSPs contain 0.2 weight percent (wt%) Y, along with 14 wt% Cr, 3 wt% tungsten (W), and 0.4 wt% Ti. This unusual processing path will help determine if pre-alloying an RSP with Y reduces the required milling time compared with milling Y-free powders with Y_2O_3. The Cr RSP included those with and without small weight-percent O additions atomized in argon (Ar), as well as those quenched in a helium (He) gas to increase the RSP solidification rate.

TEM and electron microprobe analysis studies have shown non-uniform distributions of phase-separated Y in all the as-atomized powders. The team performed high-energy milling (Spex milling) for 10 hours. The process resulted in a much more uniform distribution of Y dissolved in the ferrite matrix. Uniform distributions of Y were not observed after attritor milling for 1 and 5 hours, but good Y mixing was found after 20-hour and 40-hour milling times. Researchers examined 10-hour Spex-milled low-O powders, annealed with a process that mimics HIP with a temperature–time cycle of 1150°. Using a variety of techniques including SANS, atom probe tomography (APT) and TEM, the team determined that these powders contained NFs. This was also the case for two heats of 40-hour attritor-milled low-O powders HIPed at 1150°C. In one case, the powders were pre-annealed at 1000°C before HIPing. These results show that the milling both dissolves the Y and introduces sufficient O to produce NFs upon annealing or consolidation.

Both the powders and consolidated alloys contain a bimodal grain size distribution, with diameters of less than one and of several micrometers (μm), respectively. Notably and unexpectedly, however, both TEM and focused ion beam lift-out APT studies of the large grain regions show that they also contain a high density of NFs, as shown in Figure 1(a). More recently, the team examined attritor-milled powders that were HIP-mimic-annealed at 1150°C. SANS characterization of the alloy showed a minimal NF population for 1-hour and 5-hour mill times, with significant increases of NF scattering at 20 hours. Similar behavior was also observed in RSP with O with additional increases in the NF population between 20 and 40 hours, as shown in Figure 1(b). SANS studies of attritor-milled low-O powders that were consolidated at 850°C by extrusion also showed minimal NF scattering for 5-hour mills and increasing NF populations between 20- and 40-hour milling times.

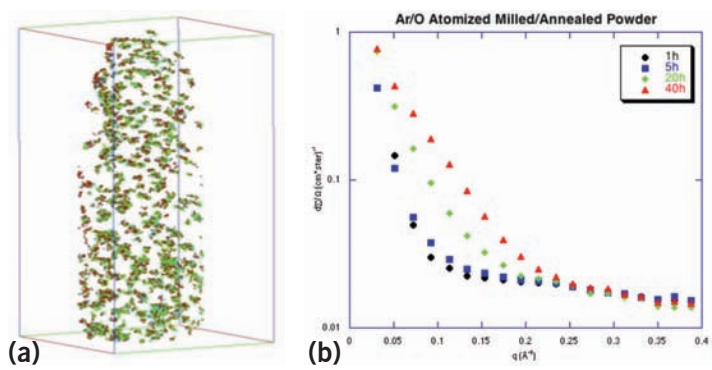

Figure 1. (a) An APT map showing a high density of Y-T-O-enriched clusters in a large grain region of a milled and annealed RSP; (b) SANS curves for annealed RSP after attritor milling for 1-, 5-, 20- and 40-hour milling times.

Task 4: Identification and Optimization of the NFs. Identities and characteristics of various NFs, and how they vary with NFA composition and processing, are not well established. Different characterization techniques result in varying views of the NFs.

To help resolve these NF "identity" issues, the project organized a multi-technique, multi-institution study on a single reference alloy, MA957 (14Cr-0.3Mo-0.9Ti-0.25Y_2O_3). This study showed that MA957 contains a wide range of sizes and types of precipitate features, like coarser TiO_2 and titanium-aluminum oxynitride phases. The team also found that different phases and sizes of precipitates are often co-associated with each other. The smaller NFs are not completely uniformly distributed in MA957, but researchers generally found good agreement on the NF population parameters both for the various

techniques and between different institutions. Individual measurements varied by factors of two around these nominal average values. Assuming the 40 to 80 percent Fe delete and Cr contents of the NF are artifacts (see below), the APT studies consistently evaluated NF Y-Ti-O compositions to be 15 to 20 percent Y, 35 to 45 percent Ti, and 40 to 50 percent O, in agreement with each other (but not SANS). Notably, the compositions of the larger particles found by APT are not known oxides.

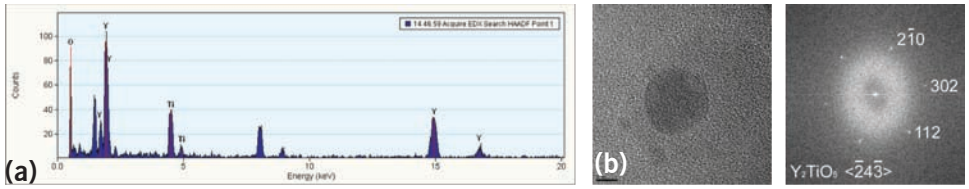

Figure 2. (a) A typical EDS spectra showing a composition of a precipitate in MA957 consistent with Y_2TiO_5; (b) a HRTEM image and corresponding FFT diffraction pattern that is consistent with indexing.

Since it is surprising that the larger APT features are similar to, or even more non-stoichiometric than, the smaller NFs, the project team has applied a variety of high-resolution analytical TEM techniques to characterizing features in MA957 in the size range of 5 to 30 nm. In particular, researchers developed a technique to extract features over a wide range of sizes from MA957 on deposited C foils. Electron dispersive x-ray spectroscopy (EDS) and high-resolution transmission electron microscopy (HRTEM) with fast Fourier transform (FFT) indexing on our FEI Titan was used to characterize these features. EDS (see example in Figure 2[a] finds the ratio of Y to Ti to average about 1.5 and that of O to Y+Ti to average 1.23. These ratios are inconsistent with APT values of these ratios as less than one. Notably, the EDS did not find any significant Fe or Cr in the oxide features. The HRTEM FFT indexing shows some precipitates are consistent with Y_2TiO_5, while the other precipitates remain unidentified. Delete indexing is mostly consistent with Y_2TiO_5 oxides (see example in Figure 2[b]). The project team has recently also applied electron energy loss spectroscopy and energy-filtering TEM techniques to the extracted features. However, results to date suggest that the most useful TEM methods are high-angle annular dark field (HAADF) for imaging, HRTEM FFT indexing for phase identification, and EDS for composition measurements. Figure 3 summarizes the size distribution of NFs and oxides (HAADF) in MA957, as well as the NF-oxide compositions observed with different techniques.

Finally, researchers recently carried out small angle x-ray scattering (SAXS) and anomalous small angle x-ray scattering (ASAXS) measurements on a series of NFA. The data are currently being analyzed.

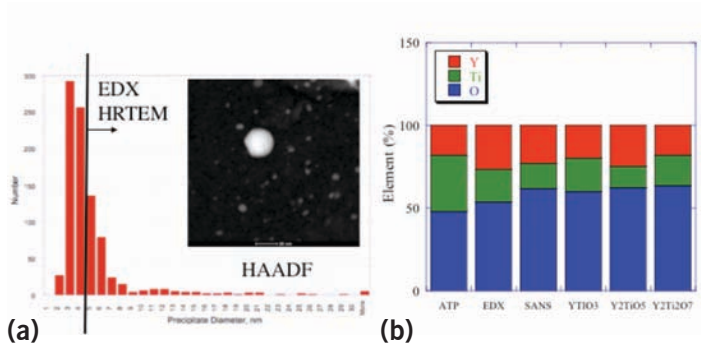

Figure 3. (a) The size distribution of NF in MA957 characterized by HAADF field emission scanning TEM imaging; (b) the average composition of the NF and oxides determined by various techniques along with those for stoichiometric oxides.

Task 5: Other Best Effort Studies and Target of Opportunity Irradiations. The team is involved in several other efforts related to this project. The researchers are working on an irradiation experiment in the Idaho National Laboratory Advanced Test Reactor (ATR) as part of the ATR National Scientific Users Facility. Researchers have completed the detailed design of the UCSB ATR-1 irradiation experiment and have prepared specimens. The ATR irradiations will be completed in 2010, when the team will move on to post-irradiation examination (PIE) experiments. Small and micro-machined specimens can be supplied to universities, including UCSB, as well as international institutions, to support a wide range of basic experiments and PIE characterization studies. In fact, the large number of specimens from UCSB ATR-1 is envisioned as constituting a specimen "lending library" that will support extensive collaboration and cutting-edge research on irradiation effects.

UCSB also has two capsules in the radiation experiment STIP-V (spallation proton irradiation at the Paul Scherrer Institute in Switzerland).

Planned Activities

Research on all five tasks will continue in 2010, with activities that include the following:

Task 1: Deformation Processing Database. Characterization of the basic tensile and viscoplastic properties of NFAs will continue. Deformation processing studies of the larger heat of best practice 14YWT NFAs will begin in the spring of 2010.

Task 2: Solid-State Joining. Diffusion bonding and FSW studies will continue, including mechanical property and microstructural characterization of the joints.

Task 3: Alternative Alloys and Alloy Optimization. In addition to continued studies of the CFOA larger heat alloys, the team will also explore a large matrix of processing variants (milling, annealing/consolidation time, and temperature histories) and compositional variants (Y, Ti, and O variations) based on small research heats of NFAs, including mechanical property and microstructural characterization.

Task 4: Identification and Optimization of the NFs. Advanced characterization studies will continue on MA957, along with a small subset of the alloys cited in Task 3, to clarify the NFs' composition and structure. Characterization techniques will include SANS, TEM, APT, XAS, x-ray diffraction (XRD), SAXS/ASAXS, and PAS. The team will carry out initial XRD studies on bulk extractions of the NFs and oxides.

Task 5: Other Best Effort Studies and Target-of-Opportunity Irradiations. A detailed PIE plan for the UCSB ATR-1 and STIP-V irradiation will be completed. Thermal aging studies will continue and will be expanded to include additional NFAs.

The project will request a one-year no-cost extension to continue this research beyond April 2010.

NUCLEAR ENERGY RESEARCH INITIATIVE

A Research Program on Very High-Temperature Reactors

PI: Sudarshan Loyalka, University of Missouri-Columbia

Collaborators: North Carolina State University, Washington University-St. Louis

Project Number: 08-043

Program Area: Gen IV

Project Start Date: September 2007

Project End Date: September 2010

Research Objectives

Prismatic and pebble-bed very high-temperature reactors (VHTRs) are very attractive both from a thermodynamic efficiency viewpoint and for their hydrogen-production capability. This project addresses numerous challenges associated with the fuel cycle, materials, and complex fluid dynamics and heat transfer associated with VHTR designs. Consortium members will perform the following tasks:

- Conduct physical experiments for fission product transport phenomena in the overcoating and compact structural graphite, as well as transport through tri-isotopic coating layers.
- Develop improved sorption measurement techniques to measure accumulation of condensable radionuclides ("plateout") in the VHTR primary coolant circuit, and obtain representative data.
- Develop advanced computations of charged radioactive dust (aerosol) transport in the VHTR coolant circuit and confinement by exploring direct simulation Monte Carlo (DSMC) techniques for deposition and resuspension; conduct experiments to verify computational predictions.
- Develop a program to measure emissivity for various VHTR component materials, both bare and oxidized, and obtain extensive data.
- Develop an experimental program to characterize gas, fission products, and particle flows in the complex geometries of pebble-bed modular reactors (PBMRs); help improve computational approaches and computer programs through experimental understandings.

Research Progress

To meet project objectives, the team must characterize and verify measurement techniques for silver diffused into a graphite matrix or silicon carbide (both spatial and quantitative). Therefore, researchers have focused on developing a simple test sample for diffusion of silver into graphite and, after exploring several designs, successfully developed a qualitative assessment technique. The technique utilizes a one-inch cylindrical cell containing a small cavity into which silver is placed. The initial design included a threaded plug on one end, although the team has also explored hermetically sealed designs using a compound of phenolic resin, isopropanol, and graphite (Graphi-bond) to prevent the escape of silver. This resulted in the successful development of a graphite cell with a silver kernel which has exhibited measurable diffusion.

Further experiments explored different interior configurations and core make-ups. In some experiments, the section of the cell was taken from above the dome, divided into halves, and analyzed via neutron activation analysis. One half was shaved on all sides to ensure that no powder material from the cell's center was present, while the other was left as-is. As expected, the shaved sample was found to have a silver concentration of 2 ppm, while the non-shaved sample had a concentration of 3 ppm. These numbers are consistent with those expected when diffusion occurs. That is, the shaving removed the region of highest silver concentration.

For the next experiments, researchers sectioned a cell with a flat interior and solid core, producing sections of 10 to 20 microns, which they will irradiate and count. Using these data, the team will be able to obtain a preliminary quantitative value of the diffusion coefficient.

The team has acquired initial data on helium (He) diffusion in air using a classical apparatus in which two bulbs separated by a capillary or porous media are maintained at different temperatures. This type of experiment can yield measurements of slip coefficients, which are useful in determining transport of He gas mixtures. Preliminary experiments were carried out for mixtures of He and air at different molar ratios and a constant system pressure. The team has modified the system to achieve a higher temperature gradient, approximately 300K over the capillary bundle length. As the resulting He-air data are substantially different from those obtained at room temperature, the team is redesigning the system again to allow for data acquisition at even higher temperatures—closer to VHTR operation (approximately 600K)—and replacing the capillary bundle with different types of porous media (such as a graphite plug). The project is also exploring constructing a glass system to test corrosive materials (such as iodine) in air.

Researchers investigated a thermo-gravimetric (TGA) technique to measure the accumulation of condensable radionuclides ("plateout") in the primary VHTR coolant circuits, but issues with stability and sensitivity led the team to pursue neutron activation analysis as a complementary method. The project decided to proceed with both methods simultaneously. Initial activation analysis data have been encouraging.

An experimental system for generating fission product vapors produces a certain vapor pressure of fission product in a furnace, then dilutes that vapor with another gas stream before flowing the diluted vapor to the TGA. Researchers vary fission product concentration by controlling the furnace temperature and the flow ratio through the furnace to the dilution flow. The fission product vapor pressure must be kept above the saturation pressure corresponding to the tube wall temperature to avoid plate-out.To address temperature limitations, the system was modified by replacing the TGA with a simple ceramic column packed with pieces of solid graphite. EDS analysis of graphite samples following testing with cesium-iodide (CsI) vapor showed no cesium or iodine quantities, within the detection limit of the instrument. Other samples from the same batch of graphite are being analyzed using activation analysis and inductively-coupled plasma (ICP). The team has also produced and begun to analyze samples of graphite powder exposed to cesium vapor. The next step is to examine cesium vapor adsorption on stainless steel and Hastelloy X.

Researchers have made significant progress regarding aerosol dynamics through both experimental and computational methods—specifically the DSMC and deterministic approaches to modeling particle resuspension. Progress has also been made using DSMC for computations concerning evolution of charged particles, particularly relevant with regard to radioactive aerosols or dust.

Further, using methods developed to model electric fields created by charged aerosol particles, researchers have investigated the problem of diffusion to and from small particles. An important phenomenon present in VHTRs is evaporation and condensation of volatile fission products from/onto the surfaces of aerosol particles (graphite dust). These small particles will often settle onto the surfaces of the VHTR primary coolant loop, hindering diffusion of volatile fission products. The team has examined the evaporation rate of a small sphere of iodine resting on a flat surface. Efforts are now being refocused back to the computation of electric fields produced by charged aerosols and the phenomenon of self-charging found in radioactive aerosols. Researchers are also investigating self-charging by means of a Monte Carlo code, incorporating previous work found in literature and expanding it to account for additional phenomena.

The team is investigating wear on graphite and pebbles in a PBMR resulting in graphite dust generation. To represent this phenomenon, researchers have focused on an experiment using a drill press test bed, using SEM to examine the particles after various treatments to break up clumping. The project has collected some initial size distributions for graphite dust and acquired some initial insights into the role of wear.

Researchers have made further progress generating carbon nanoparticles using a spark aerosol generator (Palas, GFG-1000). Particles were collected by both diffusive and thermophoretic deposition at different spark frequencies of 50 hertz (Hz), 100 Hz, and 400 Hz for two-minute intervals. The team has characterized sizes, shapes, and size distributions of collected particles.

The project designed and built two experiments for measuring thermophoretic deposition of graphite particles generated from the GFG-1000. Researchers have successfully used the first system for carbon nanoparticles generated at a spark frequency of 20 Hz and the second system to generate both carbon and gold particles (these will be useful for studies with respect to radioactive particle coagulation). They studied the role of different parameters on particle generation and made significant upgrades to the electrodynamic balance to measure the thermophorectic force on single graphite particles.

In addition, they have successfully modeled thermophoretic particle deposition in cylindrical tube geometries using the computational fluid dynamics code FLUENT. Results of preliminary computations agree well with the published experimental data.

Many applications in aerosol science, including nuclear aerosols, require knowledge of both size and charge distributions. Recent progress involves using two differential mobility analyzer (DMA) classifiers and a particle counter in a tandem arrangement. Having explored these ideas, the project has completed initial measurements of charge and size distributions of several types of nanoparticles (including carbon). Several instruments connected in series make up the apparatus used in this study, as shown in Figure 1.

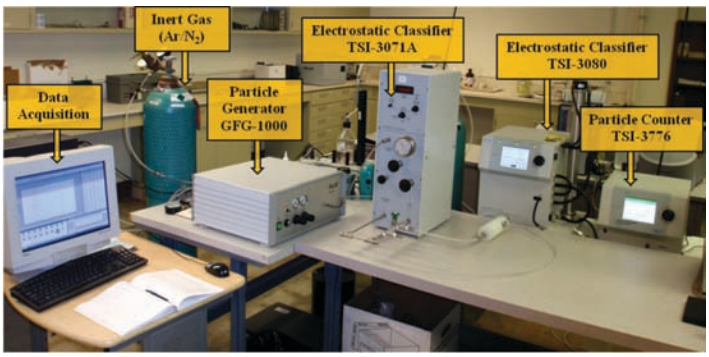

Figure 1. Experimental apparatus for measuring particle size and charge distribution.

The project has developed a program to measure emissivity for various VHTR component materials, both bare and oxidized, and has obtained a range of data. Researchers use resistive-heating of a sample in vacuum and measure power loss and temperature of the sample to calculate the emissivity. Figure 2(a) shows the apparatus, including the bell jar, two data acquisition units (temperature, voltage), turbo-pump, water cooling unit, roughing pump (floor), power switch, pressure indicators, turbo-pump controller, and power supply. Figure 2(b) shows a portion of the bell jar internals.

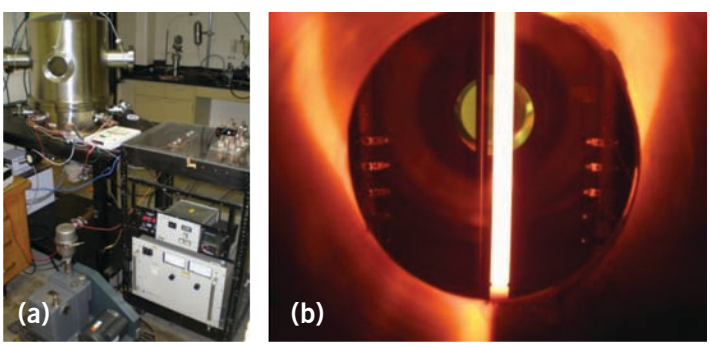

Figure 2. (a) Experimental setup for the emissivity experiments; (b) internal components of the bell jar with a stainless steel strip heated to about 770°C.

Emissivity measurements for pure nickel conducted in the temperature range of 350°C to 900°C followed the trend of values as found in the literature for partially oxidized nickel. Hastelloy X data taken over several runs in the temperature range of 334°C to 1025°C for bare, oxidized, and graphite-coated specimens show that graphite-coated Hastelloy has an emissivity twice as great as the bare specimen.

Further progress has been made on an experimental program to characterize gas, fission products, and particle flows as well as pebble motion in the complex geometries of PBMRs. The team has set up and begun testing a continuous pebble flow experimental loop and a separate loop, which characterize gaseous flow using a gas tracer technique. The team is assembling equipment (see Figures 3 and 4) for investigation of bed structure in terms of solids and voids distribution using gamma ray densitometry and gamma ray computed tomography, as well as a three-dimensional pebble flow field using an advanced non-invasive radioactive particle tracking technique. Researchers are using software for discrete element modeling to model the pebble bed dynamics.

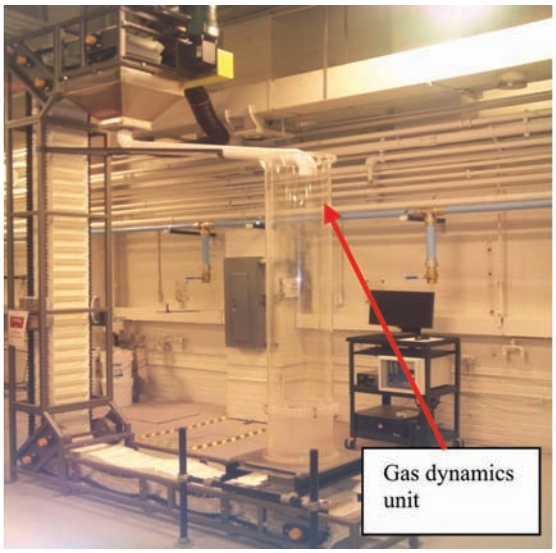

Figure 3. Continuous pebble flow experimental setup.

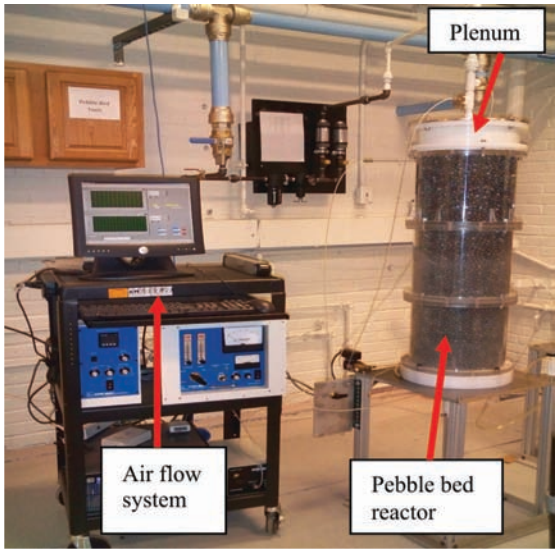

Figure 4. Advanced gas dynamics experimental setup.

Researchers have made further progress on a single particle tracking system that uses three collimated two-inch-square sodium iodide detectors, which search for the maximum counting rates for a single particle position. The Labview program is used for automatic control (see Figure 5). This method is for benchmarking purposes only. The project is proposing a new method of tracking radioactive particles, which was successfully tested (in both forward and inverse) with an array of six of the above-mentioned sodium iodide detectors.

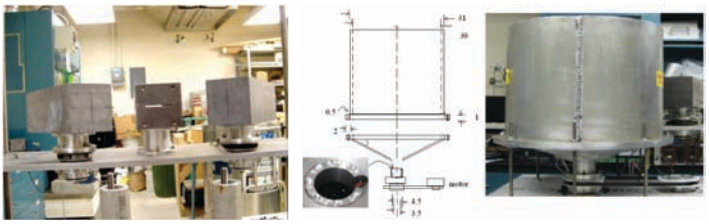

Figure 5. Single particle tracking system.

The team has also addressed the incompressible packing conditions in pebble bed reactors. Researchers have developed an analytic approximate solution with a new kinematic model including appropriate boundary conditions. The solution is based on the velocity description of the packing density in the hopper. The packing structure can be presented with a jamming phenomenon from flow types. The gravity-driven macroscopic motions are governed not only by the geometry and external boundary conditions of silos and hoppers, but also by flow properties of granular materials (such as friction, viscosity, and porosity). The team has also explored a molecular dynamics simulation technique to describe pebble motion in a gravitational field.

The project has resulted in several presentations and publications, and additional ones are currently in review. The team has identified the challenges toward meeting project objectives and has realized initial successes in all project areas.

Planned Activities

Researchers will continue to acquire additional data, improve experimental designs, and explore computational approaches in the areas discussed above. The project anticipates requesting a no-cost extension of the grant to realize all the proposed objectives.

NUCLEAR ENERGY RESEARCH INITIATIVE

Cladding and Structural Materials for Advanced Nuclear Energy Systems

PI: Gary S. Was, University of Michigan

Collaborators: Alabama A&M University, Pennsylvania State University, University of California-Berkeley, University of California-Santa Barbara, University of Wisconsin-Madison

Project Number: 08-055

Program Area: Gen IV

Project Start Date: September 2007

Project End Date: September 2010

Research Objectives

The goal of this consortium is to address key materials issues in the most promising advanced reactor concepts that have yet to be resolved or that are beyond the existing experience base of dose or burnup. The research program consists of three major thrusts: 1) high-dose-radiation stability of advanced fast reactor fuel cladding alloys, 2) irradiation creep at high temperatures, and 3) innovative cladding concepts embodying functionally graded barrier materials.

The objectives of this research are to:

- Develop an understanding of the high-dose-radiation stability of candidate sodium fast reactor (SFR) cladding and duct alloys under the expected range of temperatures and doses, using a closely integrated program that combines targeted charged-particle and neutron irradiation, *in situ* irradiation, and computer simulation of defect microstructures.
- Determine the stability of oxide dispersion-strengthened (ODS) steel and ultrafine, precipitation-strengthened (HT-UPS) austenitic steel.
- Characterize and understand the mechanisms for irradiation creep in silicon carbide (SiC) in tri-isotropic (TRISO) fuel, ferritic-martensitic (FM) alloys, and ODS and HT-UPS steels.
- Develop barrier layers for protection of FM alloys from fuel-clad chemical interaction and of Alloy 617 from attack by coolant impurities in the intermediate heat exchanger of the Very High-Temperature Reactor.
- Develop modeling tools to explain the behavior of FM steels under irradiation and predictive tools to extend the reach of understanding beyond the experimental database.

Beyond scientific achievements, this consortium is expected to provide substantial long-term benefits that will be crucial for success of the advanced reactor program, including establishing pathways for the incorporation of data into the ASME codes and standards.

Research Progress

Irradiated Microstructures: Experiment and Modeling. To extend the operational range of nuclear fuel cladding and structural materials in advanced nuclear energy and transmutation systems, scientists must understand the irradiation-induced evolution of the microstructure and associated changes in bulk properties at relevant temperatures and doses. To develop this understanding, the project team is taking a comprehensive approach including bulk irradiation, *in situ* irradiation, irradiated microstructure characterization, and computer simulations.

The team irradiated and analyzed alloys considered for fast reactor cladding and other structural applications. Alloys HT9, T91, HCM12A, NF616 and a 9CrODS steel were irradiated with protons at 400°C at doses ranging from 1 to 10 displacements per atom (dpa). Researchers then examined the irradiation-induced microstructures and grain boundary compositions using transmission electron microscopy (TEM) techniques. Varying lots of HT9 do not show significant differences in radiation response when irradiated to 1 dpa at 400°C. Significant radiation-induced enrichment of chromium (Cr) occurs at 400°C and

3 dpa, which then appears to decrease upon increasing dose. Researchers propose that changes in the irradiated microstructure may be responsible for the turn-around in Cr segregation. In fact, the behavior of dosed grain boundary precipitates mirrors that of radiation-induced segregation (RIS), as shown below. RIS and carbide size both increase up to 3 dpa. Above that dose, precipitate size changes little through 10 dpa, and grain boundary solutes redistribute. The similar trend of RIS and grain boundary coverage at the prior austenite grain boundaries (PAGBs) suggests that precipitate growth may be affecting grain boundary Cr content.

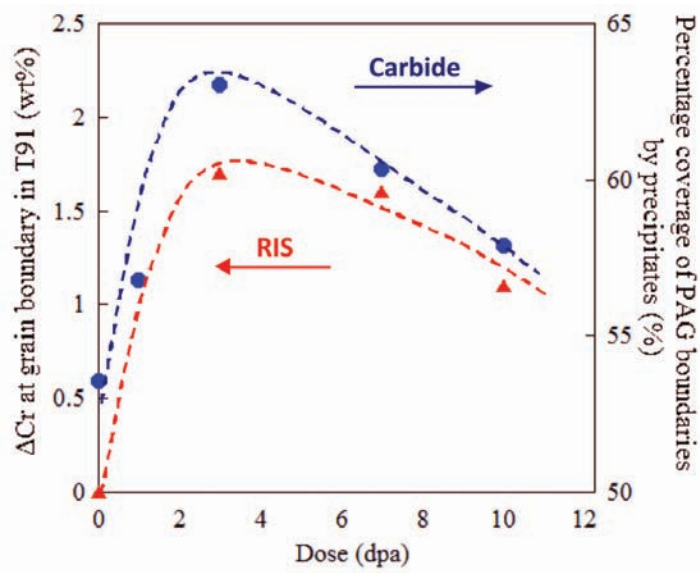

Figure 1. Comparison of RIS and carbides at grain boundaries.

Spatially dependent cluster dynamics modeling of vacancy and interstitial cluster evolution in FM iron-chromium (Fe-Cr) alloys has been used to predict the evolution of visible interstitial cluster loops. Researchers are comparing results directly to the data experimentally measured in proton irradiation studies between 3 and 10 dpa. The initial results indicate that the best agreement on the number density and mean size of the interstitial-type dislocation loops occurs when significantly decreasing the mobility of interstitial clusters below that typically observed in molecular dynamics simulations. The figure below shows the modeling predictions as a function of varying the diffusion pre-factor of the single self-interstitial, with the best agreement for values of between $5x10^9$ and 10^{10} nanometers $(nm)^2$ per second, with an activation energy of 0.36 electron volts (eV). Future experiments will be performed at both 1 and 100 dpa to provide additional experimental data to benchmark the interstitial mobility values used in the computer simulations.

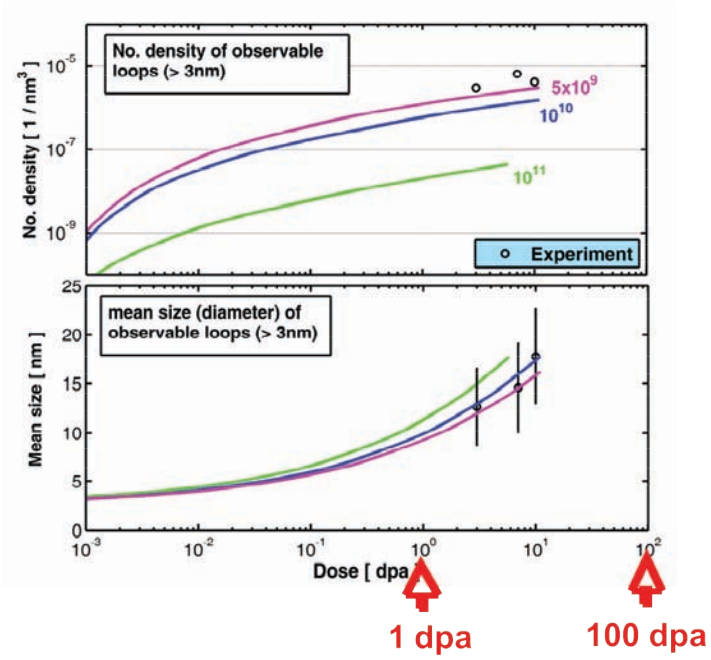

Figure 2. Cluster evolution as a function of dose for loops of size three nm or larger.

***In Situ* TEM of Irradiated FM Alloys.** Researchers irradiated the Fe-9Cr-0.1C model alloy at 25°C, 200°C, and 300°C at doses up to 10 dpa. This alloy is characterized by small-grained regions that are considered fully martensitic. One-mega-electron-volt (MeV) krypton (Kr^{2+}) ions were used with a count rate of 150 counts per second (equivalent to 9.4 $x10^{11}$ ions/cm^2-sec). At this energy, the ions completely transverse the foil. The irradiation temperatures were 25°C, 200°C, and 300°C. The evolution of the damage structure was followed closely by imaging using several different reflections at various doses. The irradiation results revealed much information about the microstructure's development under irradiation. The figure below shows that at higher doses, self-organization occurs—as alignment of irradiation-induced clusters develops between 5 and 10 dpa, as other researchers have seen.

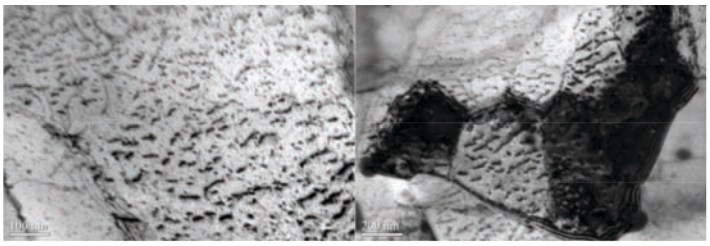

Figure 3. Fe9Cr0.1C irradiated at 25°C with 1-MeV Kr ions to 10 dpa, showing the development of large-scale alignment of radiation-induced defects after 10 dpa.

After studying the defect density, researchers measured loop size and number density *in situ* and compared the measurements to the results of cluster dynamics modeling of radiation-induced microstructure evolution. The figure below shows a comparison of the results for an Fe-12Cr model alloy irradiated at 200°C. The agreement is quite good and highlights the importance of detailed data obtained with *in situ* measurements of damage evolution to calibrate models.

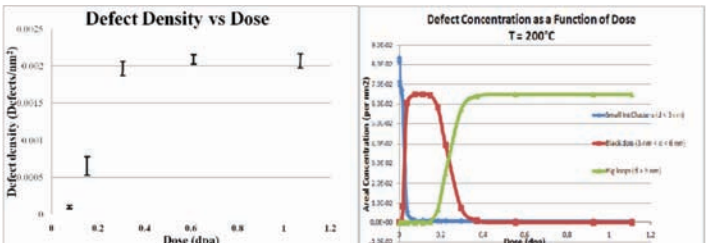

Figure 4. Visible defect density plotted versus dose in dpa for 200°C irradiation of an Fe-12Cr-0.1C model alloy as measured from experiment (left) and calculated density (green line) using a cluster dynamics model.

Barrier Layer Development. The project team is exploring and comparing two approaches to surface modification of IN617, a nickel-base superalloy: 1) aluminization of the surface by pack cementation and 2) aluminization followed by cladding with FeCrAlY/RE, a ferritic alloy known for its ability to readily form alpha alumina. The team has developed suitable low-temperature (approximately 650°C) aluminization procedure and identified conditions to achieve the desired characteristics of the modified surface layer. Cladding with commercial FeCrAlY foil (100 micrometers thick) is successfully accomplished by diffusion bonding on the previously aluminized IN617. The NiAl layer resulting from aluminization appears to be an effective diffusion barrier between the outer FeCrAlY coating and the substrate. Promotion of a thin alpha alumina layer with minimal prior growth of metastable phases is achieved by pre-oxidizing at 900°C–1000°C in flowing argon with an oxygen partial pressure of less than 0.1 parts per billion. Related interdiffusion and oxidation studies are in progress.

Researchers will test aluminized specimens with and without cladding in helium with various impurities. Exposure to a decarburizing environment resulted in very low weight gain in the aluminized sample, indicating a protective coating. The clad sample showed a higher linear oxidation rate comparable to that of the uncoated sample, but preliminary examination revealed this to be a result of damage at the sample edges during preparation for

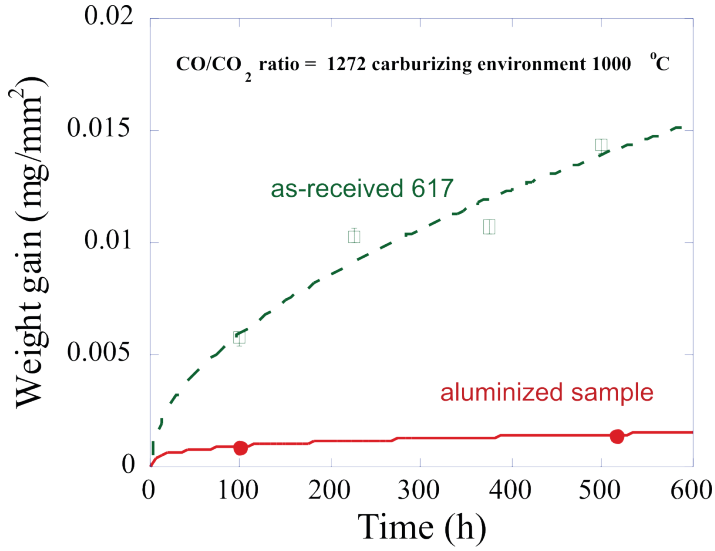

Figure 5. Weight gain in as-received versus aluminized 617 after exposure to a carburizing environment at 1000°C for 500 hours.

the environmental exposures. These experiments will be repeated under more favorable conditions.

Planned Activities

Continued studies on the effect of irradiation on microstructures will focus on proton and heavy ion irradiation of the multiple alloys in the project, which include a 9Cr model alloy, 12Cr model alloy, 9CrODS, 14CrODS, 18CrODS, HT-UPS, HCM12A, NF616, HT9, T91, and D9. Alloys will be irradiated from 300°C–700°C to doses of 10 dpa (protons) and 100 dpa (ions). Following radiation, researchers will characterize the materials to understand changes in microstructure and microchemistry. The team will perform irradiations on both bulk samples and on TEM disks. Modeling efforts will continue with a focus on spatially dependent microstructural development and the effect of compositions on diffusion under radiation; specifically, researchers will extend the atomic scale thermokinetic modeling to include interstitial energetics, and these will be combined with the vacancy energetics to yield a dilute model to defect diffusion and radiation-induced segregation. Atomistic simulations will also be used to better understand the structure, composition, and stability of precipitates in ODS steels. The program will link computational studies to the microstructural features that develop in the model alloys and link the radiation-induced changes in model alloys to the commercial alloys. Finally, the team will compare the microstructural changes in the ion-irradiated materials to the microstructural changes of neutron-irradiated materials from samples placed in the Advanced Test Reactor.

During the next year, the project team will conduct irradiation creep experiments of both silicon carbide (SiC) and T91, followed by TEM of the crept microstructures to gain insight into the mechanism of creep.

The success in forming barrier layers on Alloy 617 will be extended to the ferritic steels, including the assessment of diffusional compatibility with FeCrAlY layers and the behavior of aluminized layers. Researchers will also test samples for durability in relevant environments.

NUCLEAR ENERGY RESEARCH INITIATIVE

6.2 Fuel Cycle Research And Development

There are 28 NERI research projects currently being performed that closely relate to the research goals of the FCR&D program; 8 of these projects were awarded in FY 2006 and 20 projects (12 NERI and 8 NERI-C) were awarded in FY 2007.

During FY 2009, a number of research projects targeted the separation of actinides and lanthanides by several techniques (aqueous process with redox, aqueous process with soft donor atoms, and UREX+). Extensive work is taking place in the advanced fuel development area. Projects involve analytical studies and modeling techniques, developing and optimizing materials, developing fuel processing and fabrication techniques, and improving fuel coatings. Transmutation projects are targeting alloys for the advanced burner reactor, transuranic transmuters, and MA recycling in LWRs.

Systems analysis projects are developing and optimizing computer models for fuel cycle analysis, using those codes to evaluate different scenarios, and conducting economic evaluations. Two projects are improving SFR simulation methodology and measurement techniques. Research efforts under the NERI-C projects related to the FCR&D program focus on separations systems and analysis; fuel performance, measurements, and radiation effects; risk-informed analysis and computational tools; and small export reactors.

More information about FCR&D can be found on the following website: *http://www.nuclear.energy.gov/FuelCycle/neFuelCycle.html.*

An index of the research being performed under this program follows, along with a summary of each project.

NUCLEAR ENERGY RESEARCH INITIATIVE

Directory of Advanced Fuel Cycle Initiative Project Summaries and Abstracts

FY 2006 Project Summaries

06-007 Radiation Stability of Candidate Materials for Advanced Fuel Cycles 81

06-038 The Development and Production of a Functionally Graded Composite for Lead-Bismuth Service 85

06-047 Development and Utilization of Mathematical Optimization in Advanced Fuel Cycle Systems Analysis 87

06-058 Engineered Materials for Cesium and Strontium Storage....89

06-113 Accelerator-Based Study of Irradiation Creep of Pyrolytic Carbon Used in TRISO Fuel Particles for the Very High-Temperature Reactor 93

06-116 Development of Acetic Acid Removal Technology for the UREX+ Process 97

06-137 Design and Development of Selective Extractants for Actinide/Lanthanide Separations....99

06-141 Microwave Processing of Simulated Advanced Nuclear Fuel Pellets 101

FY 2007 Project Summaries

07-015 Radiation-Induced Segregation and Phase Stability in Candidate Alloys for the Advanced Burner Reactor....105

07-023 Chemistry of Transuranic Elements in Solvent Extraction Processes: Factors Controlling Redox Speciation of Plutonium and Neptunium in Extraction Separation Processes 107

07-027 New Fission Product Waste Forms: Development and Characterization 109

07-035 Computations for Advanced Nuclear Fuels....111

07-037 Experimental Development and Demonstration of Ultrasonic Measurement Diagnostics for Sodium Fast Reactor Thermohydraulics....113

07-046 Fundamental Processes of Coupled Radiation Damage and Mechanical Behavior in Nuclear Fuel Materials for High-Temperature Reactors 117

07-051 Economic, Repository, and Proliferation Impacts of Advanced Nuclear Fuel Cycles 119

07-059 Analysis of Advanced Fuel Assemblies and Core Designs for the Current and Next Generations of Light-Water Reactors 121

07-060 Powder Metallurgy of Uranium Alloy Fuels for Transuranic-Burning Fast Reactors....123

07-063 Neutronic and Thermal-Hydraulic Coupling Techniques for Sodium-Cooled Fast Reactor Simulations....125

07-064 Fundamental Studies of Irradiation-Induced Defect Formation and Fission Product Dynamics in Oxide Fuels....127

07-071 Identification and Analysis of Critical Gaps in Nuclear Fuel Cycle Codes Required by the SINEMA Program 129

NUCLEAR ENERGY RESEARCH INITIATIVE

FY 2007 NERI-C Project Abstracts

08-014 An Innovative Approach to Precision Fission Measurements Using a Time Projection Chamber 131

08-020 Risk-Informed Balancing of Safety, Non-Proliferation, and Economics for the Sodium-Cooled Fast Reactor 135

08-033 Deployment of a Suite of High-Performance Computational Tools for Multi-Scale Multi-Physics Simulation of Generation IV Reactors 137

08-039 Real-Time Detection of Actinide Compositions in the UREX+ Process 141

08-041 Performance of Actinide-Containing Fuel Matrices Under Extreme Radiation and Temperature Environments 145

08-051 Radiation Damage in Nuclear Fuel for Advanced Burner Reactors: Modeling and Experimental Validation 149

08-058 Advanced Instrumentation and Control Methods for Small and Medium Export Reactors with IRIS Demonstration 153

08-067 Advanced Aqueous Separation Systems for Actinide Partitioning 155

NUCLEAR ENERGY RESEARCH INITIATIVE

Radiation Stability of Candidate Materials for Advanced Fuel Cycles

PI: Todd Allen and James Blanchard, University of Wisconsin–Madison (UW)

Collaborators: None

Project Number: 06-007

Program Area: FCR&D

Project Start Date: March 2006

Project End Date: March 2009

Research Objectives

This project used proton irradiation to further understand the microstructural stability of those ceramics being considered as matrix material for advanced fuels. Following were the specific goals for this work:

- To determine the radiation stability of candidate materials in response to proton irradiation at temperatures of 600°C–900°C. Following irradiation, researchers examined samples using transmission electron microscopy (TEM) to understand the effect of radiation on lattice stability, phase change, void growth, and other microstructural features.
- To determine the effect of radiation on hardness and fracture toughness in response to proton irradiation at temperatures of 600°C–900°C. Researchers estimated the relative changes in fracture toughness as a function of radiation using crack length propagation following Vicker's indentation.
- To perform structural analysis using finite element analysis to determine the limiting performance of these ceramic fuel matrices, identify promising candidate materials for advanced reactors, and identify pressing data needs.

Researchers tested the following materials: titanium carbide (TiC), zirconium carbide (ZrC), titanium nitride (TiN), zirconium nitride (ZrN), magnesium oxide (MgO), and magnesium oxide–zirconium dioxide ($MgO\text{-}ZrO_2$).

Research Progress

Researchers irradiated ZrC, ZrN, TiC, and TiN with a 2.6 MeV proton beam at 600°C, 800°C, and 900°C up to 1.75 displacements per atom (dpa). Generally, the irradiated microstructures of the studied ceramics are dominated by a high density of dislocation loops, as shown in Figure 1. The nitride ceramics display slightly different radiation responses from their counterpart carbides. In irradiated ZrN, researchers observed Moiré fringes associated with the dislocation loops, while in the irradiated TiN, the presence of stacking fault tetrahedra (SFT) was clearly demonstrated along with the dislocation loops.

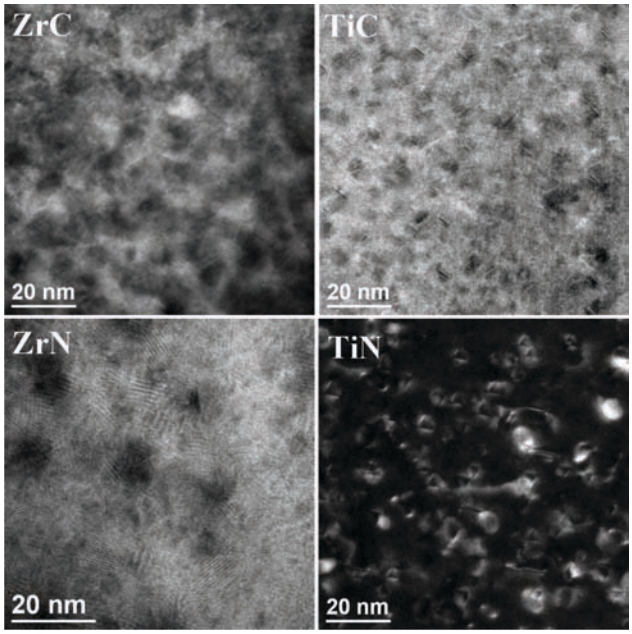

Figure 1. Microstructures of proton-irradiated ZrC, TiC, ZrN, and TiN at 800°C.

The radiation response of ZrC exhibited behavior consistent with its metallic electrical, magnetic, and optical properties. The microstructure of proton-irradiated ZrC primarily comprised a high density of nanometer-sized dislocation loops, while no irradiation-induced amorphization or voids were observed in the grains.

The average loop size increased with dose, while the density of dislocation loops decreased with irradiation temperature. The 600°C and 800°C irradiation produced lattice expansions with measured values that were in good agreement with the reported results from neutron irradiation studies. Irradiation at 1.75 dpa and 600°C produced an approximately 0.99 volume percent swelling. For the 900°C irradiation, the microstrutural evolution deviated from that developed in irradiations at the lower temperatures. Researchers observed a slight lattice contraction and a high population of grain boundaries decorated with nanometer-sized bubble clusters.

Regarding mechanical property changes, increases in hardness were found for all three irradiation temperatures; but as the temperature increased, the hardening effect became less pronounced. The team believes that hardening behavior is likely related to a high concentration of point defects. In addition, the fracture toughness of ZrC increased significantly after irradiation at 800°C for 1.75 dpa.

Proton irradiation of ZrN at various temperatures did not induce any voids or bubbles for a dose up to 1.75 dpa. However, researchers observed delaminating lines and aligned bubbles in the vicinity of the irradiation damage peak, which occurred at a much higher dose level and concentration of stopped hydrogen. The irradiated microstructures were dominated by a high density of dislocation loops associated with Moiré fringes and unresolvable point defects. Lattice resolution TEM images showed some of the loops were vacancy-type in nature. Although the density of dislocation loops increased with dose, the average size remained nearly constant. The irradiated sample showed only a very slight lattice expansion, and as the irradiation temperature decreased, the increment of the lattice parameter increased for a certain dose. Specimens irradiated at 600°C, 800°C, and 900°C exhibited radiation hardening, with the hardening effects relatively more pronounced at low irradiation temperature. The research team attributes radiation hardening in ZrN to the formation of point defects. However, further annealing experiments on the irradiated sample are required to form definite conclusions about the hardening mechanism of irradiated ZrN.

The research team studied the irradiated microstructures of TiC. For irradiated TiC, they conducted a detailed investigation of the microstructure evolution with bright field, dark field, and high-resolution TEM. These techniques have provided clear evidence that the most prominent defects present are Frank-type dislocation loops. The team also studied lattice changes versus different irradiation conditions and found very clear trends: as the dose increased, the lattice expansion became larger; while for a fixed dose, the lattice increment decreased with increasing temperature. Knoop hardness measurement on TiC irradiated at 800°C showed a consistent radiation hardening effect with other ceramics, indicating a similar defect microstructure. To achieve reliable fracture toughness data for the irradiated TiC, researchers developed a new method involving fabrication of micro-cantilever beams using a focused ion beam in the irradiated surface layer and then fracturing the cantilever beams using a nanoindentation instrument. This new method can directly incorporate the microstructural data for developing a further understanding of the radiation effect on the crack propagation resistance of ceramics.

The team confirmed the presence of stacking fault tetrahedra (SFT) in titanium nitride irradiated at 600°C and 800°C. These SFTs occur with a much higher density than do the loops. Researchers found features in TiN similar to the Frank-type dislocation loops seen in irradiated TiC. The densities of SFT were very similar for each of the examined conditions (temperature and dose). The similarity indicates these SFT are likely created quite early after the irradiation starts, that their presence inhibits the nucleation of additional SFT, and that the continued irradiation and creation of point defects serves to grow the existing SFT. In irradiated TiN, Frank loop density showed a monotonic increase from low- to high-dose conditions achieved at 600°C. This increase indicates that, unlike the SFT, the Frank loop defects continue to nucleate throughout the irradiation. At higher temperatures, interstitials are able to migrate faster and are more likely to be emitted from less stable smaller dislocation loops. For an equivalent dose, these mechanisms are expressed by a smaller average loop size and a higher loop density for a lower temperature. The lattice parameter showed a monotonic increase with increasing doses between 0 dpa and 1.25 dpa at 600°C, while at 800°C, the lattice expanded at 0.25 dpa but contracted at 0.5 dpa.

The project team investigated dual phase MgO-ZrO_2 ceramics as potential candidates for inert matrix fuels, initially performing two irradiations on samples of MgO and MgO-40 wt% ZrO_2 prepared at the Idaho National Laboratory. For the first irradiation, a 300 keV neon ion beam irradiated the specimen to a fluence of 1.0×10^{16} ions/cm^2 (1 dpa) at 800°C. The second irradiation used a 150-keV helium ion beam to irradiate the specimen to a fluence of 1.7×10^{16} ions/cm^2 (10 dpa). Following each irradiation, researchers used x-ray diffraction and nanoindentation to characterize the specimens. The lattice parameter of MgO remained unchanged even at the higher dose of 10 dpa, while for the dual phase MgO-ZrO_2, the monoclinic phase disappeared at 1 dpa and reappeared at 10 dpa. This result indicates that prolonged irradiation might transform the higher-order cubic or tetragonal phase

back to monoclinic. The nanoindentation results indicate that irradiation caused both an increase in hardness and a reduction in the Young's modulus.

Researchers also successfully synthesized additional $MgO\text{-}ZrO_2$ samples.

Planned Activities

The project has been completed.

NUCLEAR ENERGY RESEARCH INITIATIVE

The Development and Production of a Functionally Graded Composite for Lead-Bismuth Service

PI: Ronald G. Ballinger, Massachusetts Institute of Technology

Collaborators: None

Project Number: 06-038

Program Area: FCR&D

Project Start Date: April 2006

Project End Date: May 2010

Research Objectives

The purpose of this project is to develop a functionally graded composite product that will be both corrosion-resistant in lead (Pb) and lead-bismuth (Pb-Bi) alloys and structurally adequate at temperatures up to 700°C. The project is applying the results of a previous collaborative development program to the production of prototypic cladding and piping geometry products. The MIT team developed specifications for the cladding and tubing products under the Advanced Fuel Cycle Initiative (now FCR&D) and is now supervising manufacture and initial testing and analysis. At each step in the fabrication process, detailed characterization is being performed; the process includes detailed microstructural characterization, corrosion testing, and modeling. The project will produce a minimum of ten meters each of two product forms: fuel cladding and coolant piping. The research team will evaluate the products produced for corrosion resistance and structural properties. Mechanical properties testing includes tensile and creep behavior of samples from each product form at temperatures up to 700°C.

Research Progress

During the past year, significant progress has been made in a number of areas:

- Production of weld wire for the overlay process.
- Completion of the weld overlay step in the overall process.
- Completion of diffusion studies to verify that the corrosion-resistant layer will not dilute to the point where protection is lost during a component's life.

Weld Wire Production. The researchers produced approximately 225 kg (500 pounds) of weld wire during FY 2009 by melting a material comprising an alloy of iron, chromium, and silicon (Fe-12Cr-2Si), which they processed into weld wire with a diameter of 0.089 mm (0.035 inches). The wire was then shipped, along with the T91 steel alloy extrusion billets, to Arc Applications, Inc., for the weld overlay process. Figure 1 shows photographs of the various processing steps.

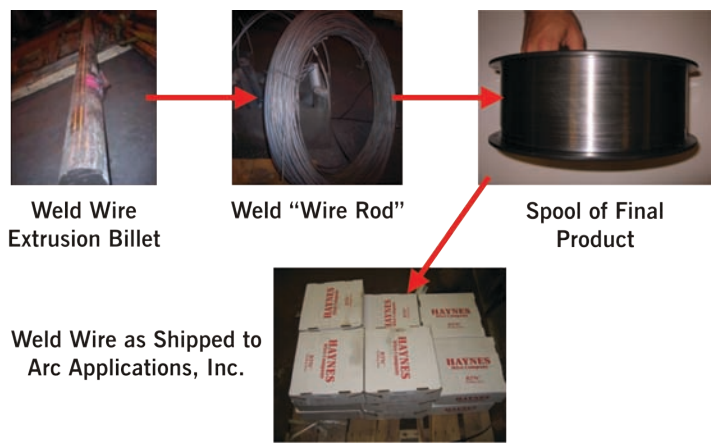

Figure 1. Photographs showing the various steps in the weld wire production process.

Weld Overlay Process. The extrusion billets were weld-overlaid on the inside diameter for the eventual piping form and the outside diameter for the eventual cladding form. Figure 2 shows photographs of the actual overlay process.

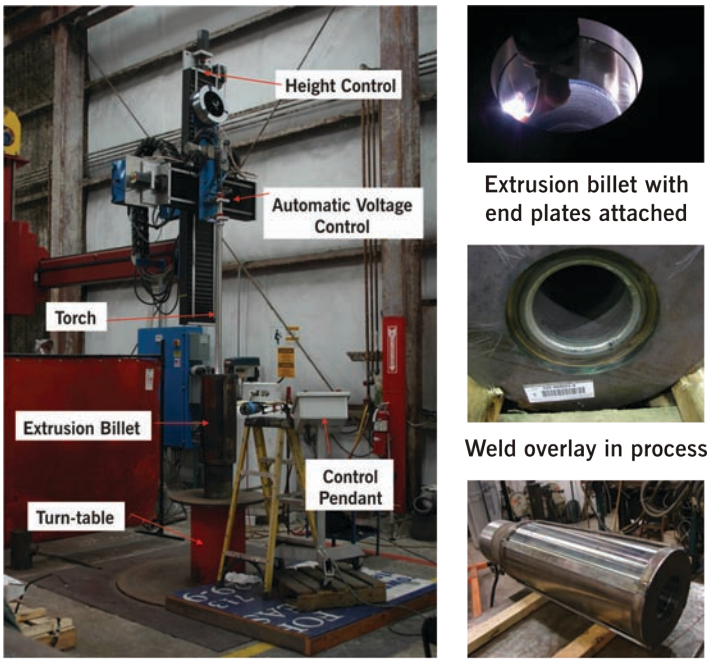

Figure 2. Photographs showing the weld overlay process.

Diffusion Studies. Since the cladding layer has a different chemistry than the underlying structural material—in particular the Si and carbon content—sufficient Si must remain in the cladding layer over the life of a component to ensure protection. Additionally, weld dilution will occur during fabrication, which may translate to uncertainty in the protective layer thickness. However, weld dilution studies conducted this past year indicate that this phenomenon will not be a problem, although depletion of the Si in the protective layer required verification. Researchers studied the potential for dilution during operation by performing a series of diffusion experiments in which bi-layers of T91/weld overlay were first fabricated and then exposed to temperatures from 700°C–800°C for up to 1,200 hours. Figure 3 shows the microstructures of diffusion couples exposed at 800°C. Migration of Si occurs into the T91 substrate, stabilizing the ferrite phase, and migration of carbon occurs into the Fe-Cr-Si layer. Figures 4 and 5 show the data and modeling predictions for material exposed at 800°C. These results indicate that dilution of the Si layer to below the protective limit of 1.25 percent will not occur for either the fuel cladding form or the piping form over their expected lives.

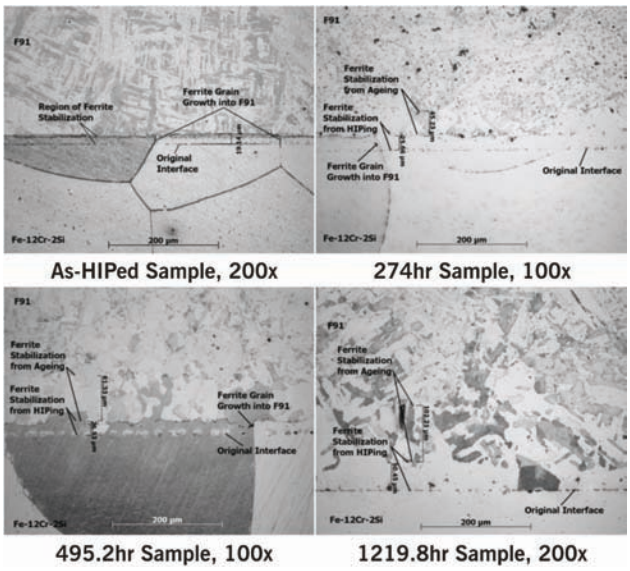

Figure 3. Microstructures of diffusion couples exposed at 800°C.

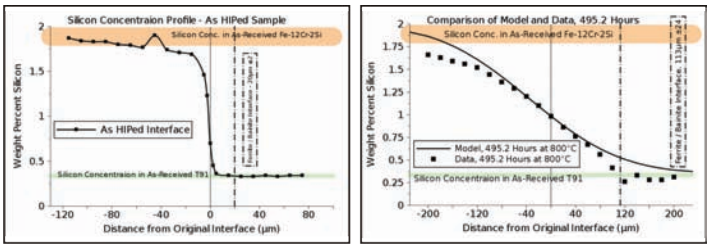

Figure 4. Data and model results for diffusion couples exposed at 800°C.

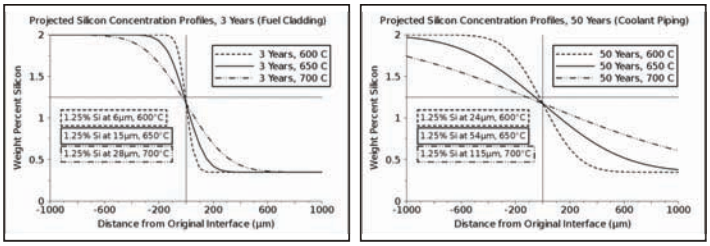

Figure 5. Modeling results for expected dilution of corrosion-resistant layer for the fuel cladding form and the piping form of the functionally graded composite.

Planned Activities

The research team will complete the project in FY 2010. The billets with weld overlay will be first processed into tube reduced extrusions with approximate dimensions of 50.8 mm outside diameter (2 inches). At this point, the piping product form will be in final condition. The project team will use pilgering to process the fuel cladding product form to fuel cladding dimensions. The team will analyze the product forms to determine if the process has been successful from a mechanical point of view. The final product forms will also be corrosion-tested in Pb-Bi at temperatures up to 700°C to verify success.

NUCLEAR ENERGY RESEARCH INITIATIVE

Development and Utilization of Mathematical Optimization in Advanced Fuel Cycle Systems Analysis

PI: Paul J. Turinsky, North Carolina State University

Collaborators: Argonne National Laboratory, Idaho National Laboratory

Project Number: 06-047

Program Area: FCR&D

Project Start Date: March 2006

Project End Date: March 2010

Research Objectives

The objective of this project is to develop mathematical techniques to optimize deployment strategies for advanced nuclear fuel cycle/reactor/fuel facilities. Researchers will employ a stochastic optimization approach, which will determine the tradeoff surface of this multi-objective optimization problem. The optimization will consider economic, energy, environmental, and nonproliferation resistance metrics of the fuel cycle, which will be modeled using the verifiable fuel cycle simulation (VISION) code.

This project will accomplish several goals:

- The capabilities developed will assure that optimum deployment strategies are determined with reduced scientist/engineering effort, providing higher confidence in utilizing the results in policy decision making.
- The automated capability should make it possible for less technically sophisticated individuals to utilize fuel-cycle simulation capability.
- The multi-objective mathematical optimization will determine the tradeoff surface, resulting in different optimization deployment strategies as one moves across the surface, which will provide quantitative data on such items as the relationship of repository capacity to energy costs.

Decision makers could use resulting data to establish policies concerning incentives and requirements to encourage the preferred evolution of the commercial nuclear power enterprise.

Research Progress

Idaho National Laboratory (INL) has been developing the simulation capability to evaluate the performance of different closed nuclear fuel cycles. Metrics of interest that are being evaluated include decay heat generation rate with regard to the waste geological repository, proliferation resistance, natural resource utilization, and economics. The VISION code continues to be developed as the associated simulation tool. It utilizes a system dynamics model of advanced nuclear fuel cycles using PowerSim software. VISION indicates when there is a need to build reactors and their support facilities based upon satisfying a projected U.S. energy growth rate and the nuclear market share.

The VISION code has the capability of modeling several different reactor types and separation processes, such as uranium recovery by extraction (UREX), co-extraction (COEX), and electrochemical processes. VISION can run several different combinations of reactor and reprocessing options. The two main options VISION has analyzed are the one-tier and two-tier cases. In the one-tier case, all light-water reactor (LWR) used fuel is sent directly to fast recycle reactors (FRRs); in the two-tier case, the used fuel will be recycled as MOX (a blend of plutonium and uranium oxides) in the LWR before it is sent to the FRR.

This project previously added a forecasting methodology to determine when various facilities of the fuel cycle should be built to meet energy demands. This methodology required the program to look ahead for a specified number of years, determining the maximum number of FRRs that could be operated without a fuel shortage over each FRR's lifetime.

Over this past reporting cycle, the project acquired new PowerSim SDK software and integrated it into the VISION optimization driver that is being developed. This new version incorporates many features previously hand-coded into the optimization driver. Researchers continue to improve the simulated annealing (SA) optimization engine, enhancing it to allow the concurrent evaluation of multiple simulations on multi-core and multi-processor machines. This enhancement has enabled the parallel SA algorithm to reduce computer runtimes, allowing increased optimization search coverage. PowerSim has also recently been enhanced to utilize multi-core architectures. Through an alternate source of funding, the team has purchased a six-processor computer, each process having quad-cores, and used the computer as the test bed for the VISION parallel SA optimization wrapper. Testing indicates total CPU utilization exceeding 95 percent on a dual-core machine and 60 percent on a quad-core machine. The built-in multi-core capability in the latest PowerSim feature pack release is expected to further augment this technique, giving multi-level parallelism and even greater CPU utilization and throughput.

Work has been completed on evaluating objective functions. The team accounted for the fact that decisions made over the planning horizon, i.e., a finite time period, influence the fuel cycle's behavior beyond the planning horizon. This follows since the behavior beyond the planning horizon impacts the values of objective functions, e.g. repository heat load and radio-toxicity burden, which are being minimized via optimization of the decision variables. So what is needed is a clear, justifiable demarcation between costs and benefits assigned to the current planning scenario and those deemed to fall outside of the planning horizon. The breakdown pursued is as follows: economic costs for facilities and materials will be tracked through the so-called planning horizon. At the end of the planning horizon (currently the year 2100), the simulation will continue to run without further inputs of uranium ore or construction of new facilities. The simulation ends when the system shuts down for lack of fuel, all facilities shut down, or an upper limit on simulation time is reached. This simulation enables continued tracking of virgin fissile material first introduced in the planning horizon until final disposition in a repository. In that way, scientists can determine this material's energy extracted, proliferation resistance, heat load, and radiotoxicity burden, using this data to evaluate associated objective function values. With regard to the objective function value associated with capital expenditures, the cost of each facility with a useful lifetime that extends beyond the planning horizon is being proportioned by the fraction of total facility useful lifetime that is within the planning horizon. At INL, scientists have created a new version of the VISION simulation that runs 200-year simulations by default; however, its increased complexity renders it unsuitable for optimization work. This new version may be utilized for comparison and benchmarking purposes, however.

Testing of the SA algorithm is using, as the objective function, minimization of decay heat generation after shutdown over a given number of years. The decision variable is the fraction of total FRR reactors that come online as a function of time. The project team chose this test problem since the optimum answer is known: build as many FRRs as possible, limited by the availability of LWR spent fuel required to ultimately fabricate the FRR fuel. To determine the minimum and maximum values of decay heat generation (useful in debugging the SA algorithm driver version of VISION), the team analyzed two fuel cycle scenarios without utilization of the optimization wrapper. One scenario does not utilize FRRs at all, which will maximize the decay heat generation after shutdown. The other scenario utilizes FRRs to the maximum extent, which will minimize the decay heat generation after shutdown and hence equates with the optimum solution. Given these lower and upper bounds on decay heat generation after shutdown, continued testing of the SA algorithm driver version of VISION is progressing.

Planned Activities

In the near future, the project will completely implement the parallel SA mathematical optimization algorithm for different objective functions. Having completed the algorithm, the team will implement a multi-objective implementation of SA (MOSA). Given this capability, researchers will assess various fuel cycle scenarios both to verify that the simulation tool is working correctly and to gain insights into optimum decisions for various fuel cycle scenarios. The project will request a no-cost extension to September 30, 2010, to complete the planned work, which coincides with the remaining research required for the doctorate student on this project to satisfy all degree requirements.

NUCLEAR ENERGY RESEARCH INITIATIVE

Engineered Materials for Cesium and Strontium Storage

PI: Sean McDeavitt, Texas A&M University

Collaborators: Purdue University

Project Number: 06-058

Program Area: FCR&D

Project Start Date: April 2006

Project End Date: March 2009

Research Objectives

Next-generation spent fuel reprocessing methods being developed under FCR&D include solvent extraction schemes to isolate cesium (Cs) and strontium (Sr) from spent nuclear fuel.[1–3] Isolating these isotopes for short-term decay storage eases the design requirements for long-term repository disposal; a significant amount of the radiation and decay heat in fission product waste comes from Cs-137 and Sr-90. For the purposes of this project, the fission product extraction (FPEX) process is considered the baseline extraction method.

The final-year objectives for this project were to synthesize and characterize a series of bentonite ceramics (an aluminosilicate structure) with up to 40 weight-percent simulated fission products. This project began as a complementary effort to the engineering development of a fluidized bed steam reformer at Idaho National Laboratory (INL). However, both INL and Texas A&M results indicated that steam reforming is too vigorous for efficient immobilization. Therefore, this project expanded its focus to examine alternate fabrication options and to develop and characterize a new ceramic form for the Cs and Sr isotopes.

Research Progress

The team prepared a simulated waste stream by dissolving nitrate salts containing non-radioactive Cs and Sr into a dilute nitric acid solution. Rubidium (Rb) and barium (Ba) were also added because their similar chemical behavior makes them likely components of the waste stream. The simulated waste solution was mixed with the natural mineral bentonite, which had previously been proposed as a nuclear waste immobilization matrix.[4] Bentonite clay was loaded with waste ions in concentrations ranging from approximately 16 mass percent to 32 mass percent total waste ions. The simulated liquid waste was added to the clay to the desired concentration, and the slurry was dried to a powder. The powder was pressed into a pellet and sintered at temperatures ranging from 700°C to 1400°C. Because of the known behavior of aluminosilicates, the anticipated products were alkaline earth feldspars and pollucites of Cs and Rb. Pollucite, an aluminosilicate, has been considered as a Cs-137 waste form material.[5]

When preparing the simulated waste solution, researchers chose the metal ion ratios (Cs, Sr, Ba, and Rb) to mimic DOE's proposed FPEX process stream.[6] The nitrate concentration was increased to the point of saturation to minimize the volume of liquid required to load the clay. The molar amounts in solution were 0.054M Ba, 0.061M Cs, 0.033M Sr, and 0.015M Rb, which corresponds to a solution concentration approximately 2.5 times higher than the expected FPEX product stream. The team chose to add the ions in aqueous form to simulate a wet clay loading process. Liquid simulated waste addition and drying was repeated until the desired waste ion concentration was reached. The dry powders were then crushed, homogenized, pressed to approximately 45 megapascals (MPa), and sintered with a heating rate of 5°C per minute and a 12-hour hold at the sintering temperature.

Differential Scanning Calorimetry (DSC) Data. To observe mass changes and heat evolution, the team heated samples of the loaded-but-unsintered bentonite clay up to 1450°C with a Netzsch STA 409. The instrument performs simultaneous thermogravimetric analysis (TGA) and DSC. Samples masses of 20 to 40 milligrams (mg) were loaded into a weighed alumina crucible, placed on the sensitive TGA balance (±40μg), and subjected to a controlled heating program under an argon cover gas. Figure 1 shows an example of the DSC/TGA data revealing transitions

during heating. For each change in the rate of mass loss, an endothermic/exothermic transition was visible in the DSC curve.

The initial endothermic peak in Figure 1 coincides with the vaporization of loosely bound water, which corresponds to a steep drop in mass (as is consistent with previously reported data[7]). The second endothermic reaction began at approximately 525°C. This coincides with the dehydroxylation mass loss (or the removal of structural water from the crystalline system), which was also previously observed in cation-loaded bentonite.[8] After this, a gradual exothermic transition is notable until the DSC trace peaks between 800°C and 875°C. The final endothermic trend continued as the temperature increased (except in samples where bloating occurred) until melting.

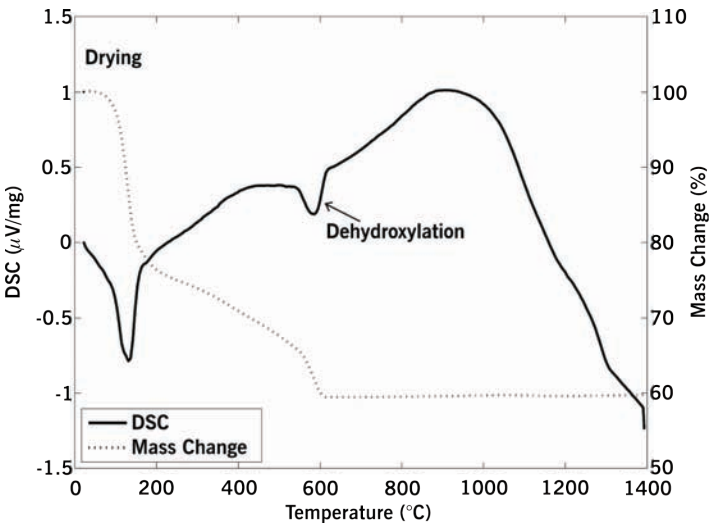

Figure 1. Percent mass change and heat flux vs. temperature for bentonite clay loaded with 22 weight-percent total waste ions (Cs, Sr, Ba, and Rb).

The mass loss traces quantified by the TGA data elucidate the meaning of the two DSC endotherms: the major changes in mass loss rates are clearly related to the consumption of energy (such as a phase change). This relationship is consistent with the data seen for pure bentonite clay.[7, 9] To some degree, each significant mass loss corresponds to the liberation of water bound within the structure (dashed line, Figure 1). The final mass loss occurred during dehydroxylation, at approximately 525°C. Balek found that after dehydroxylation the clay becomes an amorphous material, known as meta-montmorillonite.[8] Kaminski *et al* found the final release of nitrates also coincided with the release of dehydroxylation water.[10]

X-Ray Diffraction (XRD) Data. The team prepared crushed samples of the sintered ceramic products for XRD analysis. The powder size and morphology was certified using a calibrated Hirox optical microscope (Model KH 1300). The XRD equipment used was a Bruker-AXS Advanced Bragg Brentano X-Ray Powder Diffractometer, with a D8 Goniometer (Texas A&M University Chemistry Department). Samples were analyzed with copper radiation at 40 kV and 40 mA, with a step size of 0.015 degrees (2θ) and a scan speed of 0.1 seconds per step. Figure 2 shows representative data from samples containing 32 weight-percent total waste ions and sintered at 700°C, 800°C, 1000°C, and 1200°C.

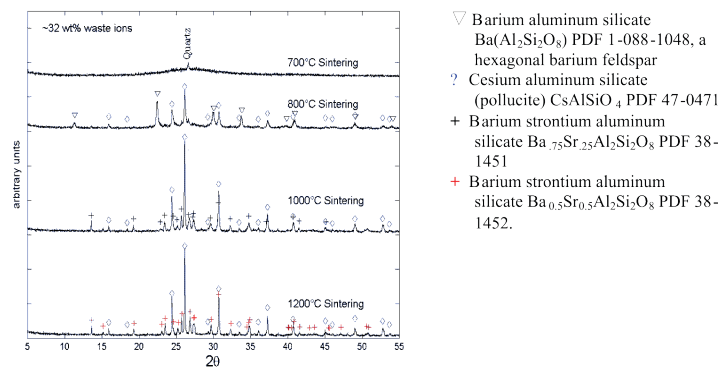

Figure 2. X-ray diffraction patterns from waste-loaded sintered bentonite at various temperatures (32 weight-percent total waste ions).

The data in Figure 2 at 700°C show an amorphous hump from 20 to 30 2θ with only the quartz impurity peak visible (Figure 1), consistent with the observations above. The data in Figure 2 at 800°C confirm formation of the cesium aluminum silicate pollucite ($CsAlSiO_4$) and a hexagonal Ba feldspar ($Ba(Al_2Si_2O_8)$). The data at temperatures at or above 1000°C no longer display the hexagonal feldspars, but the monoclinic forms were clearly evident. The transformation from a hexagonal layered structure to the monoclinic three-dimensional configuration required higher energy to enable restructuring, hence the higher sintering temperatures were necessary to develop those phases. The XRD pattern attributed to pollucite increased in intensity with higher sintering temperature (Figure 2). At 1000°C, a high silica cesium aluminum silicate ($Cs_4Al_4Si_{20}O_{48}$) was detected but only in the sample with the lower, 22 weight-percent waste concentration (not shown). Monoclinic feldspars of Ba and Sr were observed in samples sintered at 1000°C ($Ba_{.75}Sr_{.25}Al_2Si_2O_8$ and $Ba_{0.5}Sr_{0.5}Al_2Si_2O_8$). The data at 1200°C displayed only two obvious crystallization spectrums, pollucite and a 50:50 Ba-to-Sr atom ratio monoclinic feldspar (Figure 2).

Processing and Structural Observations. Sintering loaded bentonite powders at 700°C and 800°C created brick-like samples with open porosity and a multicolored brown-red appearance. These samples were brittle and easily pulverized. This is in contrast to samples generated at 1000°C and higher, where the product samples had less porosity and a uniform coloration and exhibited high toughness akin to glass and other solid ceramics. Sample

densities were approximately 2 g/cm^3 when sintered at 1000°C and reached a maximum level of approximately 3 g/cm^3 at 1100°C. The endothermic heat flux above 1000°C seen in Figure 1 connotes an energy-consuming reaction; this is consistent with viscous sintering, as are the higher density and reduced porosity. At 1200°C, sintering caused the samples with lower waste loadings to slump and crack. When sintered at 1200°C, the Cs formed pollucite crystals, and the Ba and Sr formed lath-shaped crystals up to 10 micrometers long (Figure 3). The lowest loading, 15 weight-percent waste ions, swelled and became a pumice-like foam material. At the 32 weight-percent ion loading, the pellets were hard, smooth, and a uniform grey color. At the highest sintering temperature tested, 1400°C, the samples completely melted.

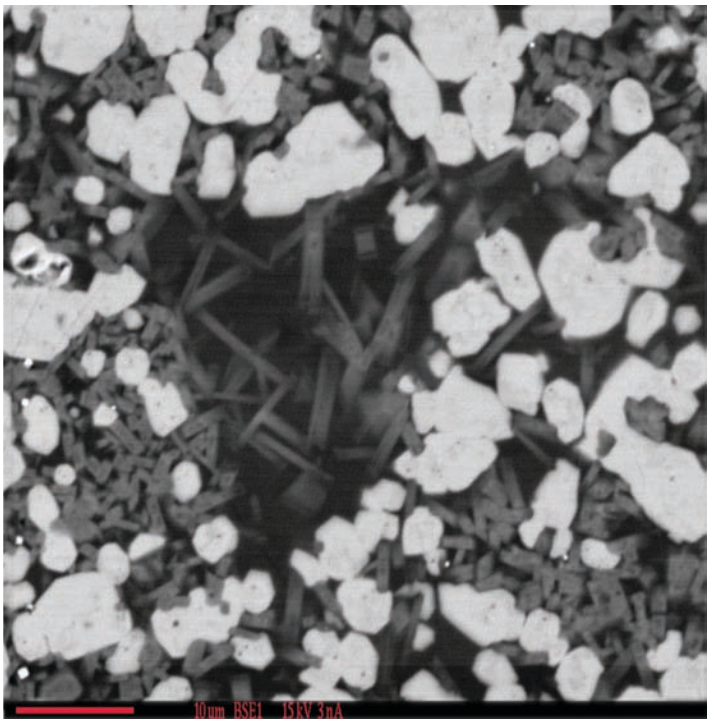

Figure 3. Backscattered electron image of bentonite sintered at 1200°C displaying three phases (the bar indicates 10 micrometers).

Planned Activities

The information reported here highlights selected results of the project's final year. The team is completing the final report, which will contain a more complete presentation of the processing methods developed and the behavior of this new waste form material. This NERI project is complete, but the development of bentonite as a waste host may continue under future research funding.

References

[1] T.A. Todd, T.A. Batcheller, J.D. Law, R.S. Herbst, *Cesium and Strontium Separation Technologies Literature Review*, in Idaho National Engineering and Environmental Laboratory, 2004.

[2] C.W. Forsberg, "Rethinking High-Level Waste Disposal: Separate Disposal of High-Heat Radionuclides (90Sr and 137Cs)," *Nuclear Technology*, 131 (2000) 252–268.

[3] C. Pereira, G.F. Vandegrift, M.C. Regalbuto, A. Bakel, D. Bowers, A.V. Gelis, A.S. Hebden, L.E. Maggos, D. Stepinski, Y. Tsai, "Lab-Scale Demonstration of the UREX+1a Process Using Spent Fuel," *Waste Management*, 7.

[4] L.P. Hatch, "Ultimate Disposal of Radioactive Wastes," in BNL-1345, Brookhaven National Laboratory, 1953.

[5] D.M. Strachan, W.W. Schulz, "Glass and Ceramic Materials for the Immobilization of Megacurie-Amounts of Pure Cesium-137," 1976.

[6] C.L. Riddle, J.D. Baker, J.D. Law, C.A. McGrath, D.H. Meikrantz, B.J. Mincher, D.R. Peterman, T.A. Todd, "Fission Product Extraction (FPEX): Development of a Novel Solvent for the Simultaneous Separation of Strontium and Cesium From Acidic Solutions," *Solvent Extraction and Ion Exchange*, 23 (2005) 449–461.

[7] M. Onal, Y. Sarikaya, "Thermal Behavior of a Bentonite," *Journal of Thermal Analysis and Calorimetry*, 90 (2007) 167–172.

[8] V. Balek, Z. Malek, S. Yariv, G. Matuschek, "Characterization of Montmorillonite Saturated With Various Cations," *Journal of Thermal Analysis and Calorimetry*, 56 (1999) 67–76.

[9] R.E. Grim, W.F. Bradley, "Investigation of the Effect of Heat on the Clay Minerals Illite and Montmorillonite," *Journal of the American Ceramic Society*, 23 (1940) 242–248.

[10] M.D. Kaminski, C.J. Mertz, M. Ferrandon, N.L. Dietz, G. Sandi, "Physical Properties of an Alumino-Silicate Waste Form for Cesium and Strontium," *Journal of Nuclear Materials*, 392 (2009) 510–518.

NUCLEAR ENERGY RESEARCH INITIATIVE

Accelerator-Based Study of Irradiation Creep of Pyrolytic Carbon Used in TRISO Fuel Particles for the Very High-Temperature Reactor

PI: Lumin Wang and Gary S. Was, University of Michigan

Collaborators: Oak Ridge National Laboratory, Idaho National Laboratory

Project Number: 06-113

Program Area: FCR&D

Project Start Date: March 2006

Project End Date: March 2010

Research Objectives

Pyrolytic carbon (PyC) is one of the important structural materials in the tri-structural isotropic (TRISO) fuel particles that will be used in the next generation of gas-cooled very high-temperature reactors (VHTRs). When the TRISO particles are under irradiation at high temperatures, creep of the PyC layers may cause radial cracking, leading to catastrophic particle failure. Therefore, a fundamental understanding of PyC creep behavior during irradiation is required to predict overall fuel performance.

The primary objective of this project is to characterize PyC creep behavior through a systematic program of accelerator-based proton irradiation and *in situ* measurements under stress at various temperatures between 400°C and 1200°C. The research team will analyze test data to determine creep coefficients, which will then be correlated to existing coefficients measured under neutron irradiation.

Research Progress

During the last year, researchers focused on three major tasks:

- Modifying the stage design to decrease the frequency of sample breakage during stage loading and unloading.
- Conducting an irradiation creep experiment on PyC.
- Reducing anisotropy of PyC produced with chemical vapor deposition.

The following is a description of the accomplishments on these tasks.

Modification of the Irradiation Creep Test Facility. The primary modifications to the creep stage affect how the samples are clamped and suspended from the stage. Figure 1a is a schematic of the initial creep stage set-up, and Figure 1b shows the modified set-up. In the revised stage, samples are individually clamped at the top and bottom. The clamps are also narrower in the new design, allowing samples to be mounted closer to one another. In addition, each sample is suspended from the stage with a bolt through the top clamp rather than with a static clamp (as in the former stage set-up).

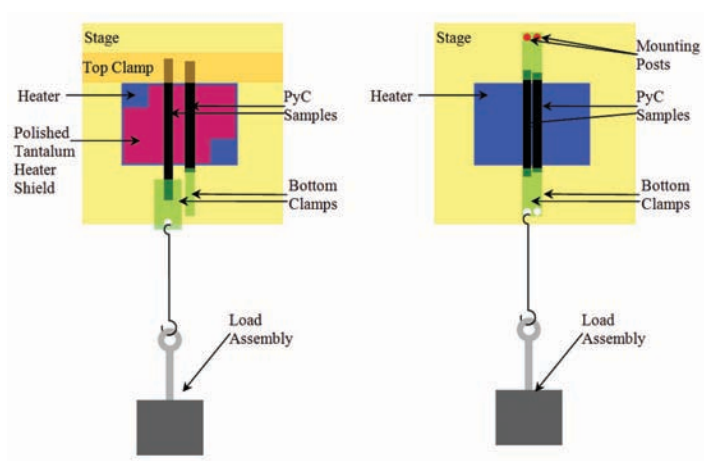

Figure 1. Schematic drawings of irradiation creep stage: (a) initial stage set-up and (b) modified stage set-up.

These modifications provide two positive changes to the irradiation creep system: First, the narrower clamps allow for the samples to be mounted closer together, which reduces the amount of heater that is visible to the LSE from between the PyC samples. Reducing the spacing between samples decreases the chance of the LSE's becoming saturated. (During the irradiation creep experiment, the visible parts of the heater shield scattered extra laser light, saturating the LSE.) The second change is the utilization of individual top clamps and mounting posts, which reduces the probability that any sample misalignment would result in the sample's breaking. The majority of sample breaks occurred where the sample extends from the top clamp, which is where misalignment produces a lateral bending stress that causes the sample to break. Using individual clamps and mounting posts allows the samples to have a small range of angular freedom, so the dead weight aligns with the sample's center line.

Irradiation Creep Experiment. During the last year, researchers utilized the new stage design to perform three PyC irradiation creep experiments. One experiment used a PyC sample 40 ± 2 micrometers (μm) in thickness with two million electron volt (2 MeV) protons at 800°C. The beam current density was kept constant at 17.4 microamperes per square centimeter (μA/cm^2), which resulted in a damage rate of 1.96x10^{-6} displacements per atom per second (dpa/s). The applied stress of 25.48 megapascals (MPa) was applied to the sample throughout irradiation.

Researchers measured sample elongation using a laser speckle extensometer with the master speckle pattern located on the heater shield and the slave speckle pattern located on the stressed sample. They used a two-dimensional infrared thermal image of the gauge section to find the sample temperature, and they measured the beam current density with a charge integrator that measures the total deposited charge per second. The current density is converted into dose in units of dpa using the damage profile generated by Monte Carlo simulation code SRIM.[1]

The team performed two proton-irradiation creep experiments with similar conditions to show that the PyC creep experiments are reproducible (see Table 1). Figure 2 contains plots of the elongation versus time data from the two experiments. Data in Figure 2(b) are smoothed with a 1,000 point moving average.

Table 1: Comparison of data from two irradiation creep experiments of PyC.

	4-15-09	4-27-09
Sample Width (mm)	3.16	3.3
Sample Thickness (μm)	36	35
Load Mass (g)	300	300
Applied Stress (MPa)	25.87	25.48
Temperature (°C)	800	800
Irradiation Ion	p^+	p^+
Ion Energy (MeV)	2	2
Ion Current (μA)	20	20
Ion Flux (p^+/cm^2*s) *	1.134x10^{14}	1.134x10^{14}
Dose Rate (dpa/day)	0.208	0.208

*particles per square centimeter per second

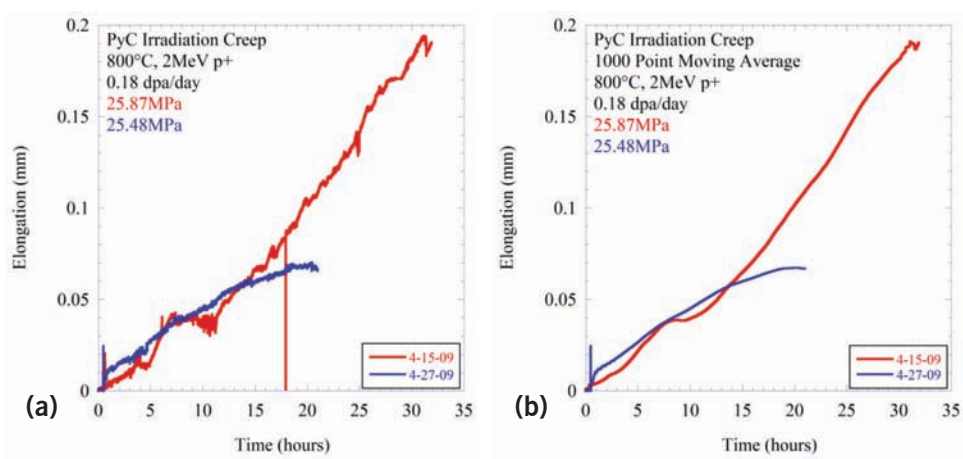

Figure 2. Plots of (a) raw elongation data and (b) smoothed elongation data with a 1,000 point moving average.

From the linear curve fit of the 4-15-09 data, the team determined the value of the steady state elongation constant (k) to be 0.804 mm/dpa, which can be converted into a creep constant by dividing by the gauge length (9 mm) resulting in a rate of 0.089 dpa^{-1}.

Anisotropy Reduction in PyC Samples. As confirmed through optical anisotropy measurements, the previously produced PyC samples are highly anisotropic—so much so that the experimental results cannot indicate the IPyC and OPyC (inner and outer) layers in the TRISO particles. Therefore, the team acted on two suggestions for decreasing the PyC anisotropy: the addition of acetylene gas to the deposition gases and depositions at atmospheric pressure.

Acetylene gas break-down, also referred to as cracking, is an exothermic reaction. Cracking of propylene is endothermic. Therefore, adding acetylene to the hydrocarbon gas offsets the endothermic nature of the propylene cracking. The deposition gas composition recommendation is 70 percent argon, 25.5 percent propylene, and 4.5 percent acetylene. The volume flow rate for the gases is 100 standard cubic centimeters per minute (sccm) argon, 36.3 sccm propylene, and 6.4 sccm acetylene.

The other suggestion was to perform the deposition at atmospheric pressure. The previous method deposited PyC in a pressure range of 100-150 torricellis (torr). Working at these low pressures limits formation of carbon clusters in the gas phase. The probability of interaction between gas particles is low, so the majority of the deposition process results from direct deposition of small particles onto the substrate. Direct deposition of small particles onto the substrate increases the anisotropy of the PyC. Increasing the deposition pressure increases the number and size of carbon clusters that form in the gas phase, which decreases anisotropy.

The research team implemented both suggestions within the tube-furnace system that is being used for PyC production. The team has conducted 31 depositions at various conditions and identified promising deposition conditions for better-quality samples.

Planned Activities

Future work will focus primarily on the continuation of the systematic process of changing deposition parameters to produce a more suitable, high-density, low-anisotropy PyC. This process will require density and anisotropy measurements to find the best deposition conditions. Once researchers have succeeded in this task, they will resume proton irradiation-induced creep experiments. The experiments will be performed with 3.2 MeV protons at various temperatures, stresses, and dose rates.

References

[1] *http://www.srim.org/*

NUCLEAR ENERGY RESEARCH INITIATIVE

Development of Acetic Acid Removal Technology for the UREX+ Process

PI: R. M. Counce and J. S. Watson, University of Tennessee

Collaborators: Oak Ridge National Laboratory

Project Number: 06-116

Program Area: FCR&D

Project Start Date: March 2006

Project End Date: May 2009

Research Objectives

The overall goal of this project was the selection and experimental verification of the most appropriate technology to separate or destroy acetic acid produced from decomposition of acetohydroxamic acid in the UREX+ process. Acetic acid accumulation would hamper reuse of nitric acid and increase waste volume. Specific goals entailed 1) evaluation of the chemistry of selected systems, 2) flow sheet studies of the most promising approach, and 3) selective engineering tests. The objective of this project, then, is to provide reference studies sufficient for incorporating an acetate removal step into the UREX+ process conceptual flow sheet when needed.

Research Progress

Acetic acid arises from acetohydroxamic acid (AHA), used to suppress plutonium in the first step of the UREX+ process. AHA is later hydrolyzed into hydroxyl amine nitrate and acetic acid. Acetic acid needs to be purged from the UREX+ process in order to recycle nitric acid with more confidence and avoid possible interference with downstream steps.

The project team screened leading technologies for this purging on the basis of somewhat rudimentary estimates of economics, safety, development time, health, and environmental metrics, and developed flow sheets for the two most promising technologies. These two technologies were then subjected to more rigorous comparison based on the above metrics. A bench-scale evaluation of the most appropriate technology was performed to demonstrate process viability. Researchers determined that solvent extraction was the best choice under process conditions.

Researchers then tested solvents already used in the UREX+ process to determine if they would be sufficient for the removal of acetic acid. The tributyl phosphate (TBP) dodecane diluent, used in both UREX and NPEX, gave sufficient distribution coefficients for acetic acid in addition to a high separation factor from nitric acid. This solvent system was tested under various TBP concentrations in the dodecane to create a concentration plot that can be used for further flow sheet development.

Researchers examined each step in the UREX+ process to determine if acetic acid interfered with performance, which would make it necessary to remove the acetic acid prior to that step. The team found no such interferences. Therefore, the acetic acid removal step can be placed anywhere in the process. For simplicity, the team proposes to place the removal step at the end of the process, after TALSPEAK, where all desirable metals have already been extracted and the nitric acid waste stream is prepared for recycle.

Other studies performed have focused on contactor operation for expected flow sheet conditions. Researchers conducted the remaining hydraulic tests on a 1:2 organic-to-aqueous (O/A) ratio to complete the preliminary data reported previously. However, the 0.95-inch weir did not provide a single non-contaminated point regardless of the throughput/rpm combination. Therefore, researchers adjusted the weir size to one inch and performed the hydraulic tests again. While ranges were found where the system would effectively separate the two phases, the project team did not locate a single fail point. Therefore they modified the procedure for the extraction tests at the 1:2 O/A ratio, choosing a point within the range of successful operation.

The results of the 1:2 extraction tests are given below. The equilibrium distribution ratios for acetic and nitric acid are given in Table 1. Tables 2 and 3 provide the results of two extraction tests conducted at varied total throughput but an organic to aqueous phase ratio of 1:2.

Table 1. Average equilibrium distribution ratios for organic to aqueous ratio of 1:2 (STDev = standard deviation).

Equilibrium Averages		STDev
Acetic Molarity in Aqueous	0.03530	0.00052
Nitric Molarity in Aqueous	0.44648	0.00026
Acetic in Organic	0.01515	0.00052
Acetic Fraction Extracted	0.30037	0.01036
Nitric in Organic	0.04805	0.00026
Nitric Fraction Extracted	0.09716	0.00053
Acetic Distribution	0.42948	0.02117
Nitric Distribution	0.10762	0.00065

Table 2. Results of 1:2 extraction test at 270 ml organic and 540 ml aqueous per minute at 4800 RPM.

270/540 Averages		STDev
Acetic Molarity in Aqueous	0.03678	0.00052
Nitric Molarity in Aqueous	0.44251	0.00091
Acetic in Organic	0.01368	0.00052
Acetic Fraction Extracted	0.27106	0.01036
Nitric in Organic	0.05202	0.00091
Nitric Fraction Extracted	0.10519	0.00185
Acetic Distribution	0.37200	0.01950
Nitric Distribution	0.11756	0.00231

Table 3. Results of 1:2 extraction test at 300 ml organic and 600 ml aqueous per minute at 5400 RPM.

300/600Averages		STDev
Acetic Molarity in Aqueous	0.03862	0.00000
Nitric Molarity in Aqueous	0.44223	0.00026
Acetic in Organic	0.01183	0.00000
Acetic Fraction Extracted	0.23443	0.00000
Nitric in Organic	0.05230	0.00026
Nitric Fraction Extracted	0.10575	0.00053
Acetic Distribution	0.30622	0.00000
Nitric Distribution	0.11826	0.00066

These tests provided efficiency numbers for both sets of throughput conditions. At both total throughput conditions at an O:A ratio of 1:2, the nitric efficiency resembled the other O/A ratios tested; it was within an experimental error of 100%. However, the acetic efficiency dropped significantly at a 1:2 O/A ratio. At an O/A volumetric flow ratio of 270/540, the average efficiency was 86.62%; at a ratio of 300/600, efficiency decreased to 71.30%. These two results differ drastically from the average percentages (mid 90s) at other O/A ratios.

To explain the differences in acetic acid removal efficiency, the researchers ran batch time shake tests while looking specifically at which phase remained continuous. As expected, the organic phase remained continuous at O/A ratios of 2:1 and 1:1. At the 1:2 ratio, however, continuity switched, and the aqueous phase became continuous. This change in continuity helps to explain the differences in extraction efficiency and is also in agreement with results that Ralph Leonard obtained in a similar system.

Planned Activities

This project has concluded, and the project team submitted a final report on the full results of the activity.

NUCLEAR ENERGY RESEARCH INITIATIVE

Design and Development of Selective Extractants for Actinide/Lanthanide Separations

PI: Robert T. Paine, University of New Mexico

Collaborators: Washington State University, Idaho National Laboratory

Project Number: 06-137

Program Area: FCR&D

Project Start Date: April 2006

Project End Date: September 2009

Research Objectives

This project was designed to remove transuranic elements from used nuclear fuel destined for either storage or reuse in transmutation processes. In particular, the investigators sought to develop an efficient solvent extraction-based separation scheme to recover americium (Am) and curium (Cm) from the acidic liquid remaining after UREX+2 processing to remove uranium (U), plutonium (Pu), neptunium (Np), cesium (Cs), and strontium (Sr). The team also sought to separate trivalent actinides from fission product lanthanide ions. The project focused on the continued development and optimization of "NOPOPO ligands," which the researchers previously demonstrated are effective extractants under laboratory-scale conditions and show promise as part of a large-scale process add-on to UREX+2.

The primary objectives of this project included 1) the design, synthesis, and extraction performance characterization of 2,6-bis(phosphinomethyl)pyridine N,P,P´-trioxides (NOPOPO) as potential reagents for separating Am, Cm, and fission product lanthanides from other transuranics and fission products, and 2) the development of a separations "platform" for the mutual separation of Am/Cm from the lanthanides. Preliminary analyses indicated that one member of the family of ligands, $(EtHx)_4$NOPOPO, offered improved separation of Am^{3+} ions from acidic aqueous solutions compared to the octyl-N,N-diisobutylcarbonoylmethyl-phosphine oxide (CMPO) ligand used in the transuranic extraction (TRUEX) process. Initial research produced a best-case extractant platform, which was then subjected to a complete round of synthesis optimization and performance characterization with a realistic raffinate stimulant component representative of the uranium extraction (UREX+) process. Specific project tasks included the following:

- Optimize the NOPOPO synthesis.
- Conduct further extraction testing of $(EtHx)_4$NOPOPO.
- Study extractant phase compatibility as well as hydrolysis and radiolytic stability.
- Design and synthesize new NOPOPO derivatives with improved solubility, phase compatibility, and stability characteristics.
- Conduct extractive testing of the new platform derivatives to determine their relative efficacy.
- Conduct focused testing on the best-case platform derivative to optimize synthesis and characterize performance with realistic waste solutions.
- Perform a cost analysis for the new process.

Research Progress

Over the three-year project lifetime, the project team developed a general scheme for the efficient synthesis of NOPOPO extractants. In general the scheme has permitted synthesis scale-up activities to the 25 g scale, which is the nominal limit for academic laboratory operations. Further scale-up is feasible but would need to be accomplished in a custom synthesis laboratory setting. The project has specifically accomplished syntheses for derivatives with NOPOPO R group substituents: R = 2-EtHx, Oct, Dodecyl, 2-$CF_3C_6H_4$, and 3,5-$(CF_3)_2C_6H_3$. Using standard spectroscopic methods, researchers have fully characterized each new extractant. They have also prepared and characterized a dithiophosphinic acid NOPO ligand, and selected coordination chemistry was examined.

The team completed extensive studies of the chemical stability of the 2-EtHx NOPOPO derivative toward nitric acid. This ligand was found to be stable for more than one year in contact with nitric acid up to at least 3M HNO_3. In addition, researchers completed survey radiation stability testing of 2-EtHx NOPOPO and found the ligand to have satisfactory performance.

The original focus of the project was 2-EtHx NOPOPO extraction performance. Early samples of the ligand displayed very favorable performance for selective extraction of trivalent lanthanide and actinide ions in concentrated HNO_3 solutions. However, during the course of the studies, researchers noted that extraction performance of some samples had degraded. After extensive study, they discovered that a low-level impurity had begun to appear in the extractant and was forming water-soluble lanthanide/actinide complexes. Upon further investigation, they traced the source to the presence of an impurity in the commercial starting material for the NOPOPO synthesis. The team addressed this problem and, in the process, developed several new NOPOPO derivatives for alternative solvent system applications.

At the close of the project, collaborators at Washington State University continued to characterize the extraction of NOPOPO ligands. Overall performance of this family of extractants remains very promising, and the project team encourages continued development.

Planned Activities

The lifetime of the current project has come to an end. Researchers are seeking funding for further development.

NUCLEAR ENERGY RESEARCH INITIATIVE

Microwave Processing of Simulated Advanced Nuclear Fuel Pellets

PI: D. Clark and D. Folz, Virginia Polytechnic Institute and State University

Collaborators: University of Tennessee

Project Number: 06-141

Program Area: FCR&D

Project Start Date: March 2006

Project End Date: June 2009

Research Objectives

The objective of this project was to sinter simulated (non-radioactive) oxide and nitride inert matrix fuel (IMF) pellets using microwave energy. Researchers on the Virginia Tech (VT) team used microwave hybrid heating (multi-mode and single mode) to sinter the pellets, while the University of Tennessee (UT) researchers used direct microwave sintering (no microwave susceptor). The teams characterized the sintered pellets with respect to density and grain morphology. Following are the primary tasks of this project:

- Prepare green pellets.
- Demonstrate direct microwave heating (DMH) to achieve sintering.
- Demonstrate microwave hybrid heating (MHH) to achieve sintering.
- Characterize pellets before and after microwave processing.
- Evaluate microwave processes.

Research Progress

Work completed in the past year consisted of the following tasks:

- Grain size determination on 8 mole-percent yttria-zirconia (8YZ) sintered samples.
- Master sintering curve (MSC) construction from conventional sintering of 8YZ.
- Microwave dilatometer design.
- Inert atmosphere setup inside multimode microwave furnace.
- Green pellet fabrication.

Grain Size Determination on 8YZ Sintered Samples. During the last two years, researchers sintered 8YZ samples in a conventional furnace and two different microwave furnaces and monitored sample density and grain size. The microwave processing achieved a full sintering (approximately 97 percent density) in 8YZ at temperatures 300°C lower than with a conventional method.

To study grain size, the project team used a diamond saw to section right cylindrical samples from sintered pellets, which they mounted, ground, and polished. In order to reveal the grain structure, researchers thermally etched polished samples at temperatures 150°C below the sintering temperature. Scanning electron microscopy (SEM) was used to observe the grain structure.

The team used the mean lineal intercept method to estimate grain size values according to American Society for Testing and Materials (ASTM) Standard E-112. Figure 1 shows the variation in grain size with temperature for different processing methods.

For conventional and multimode microwave-sintered samples, the grain size increased slightly as the sintering temperature increased. These samples also exhibited smaller grain size than single-mode microwave-sintered samples. The single-mode samples' enhancement in grain size could be caused by the diffusion mechanisms responsible for grain growth acceleration during microwave sintering.

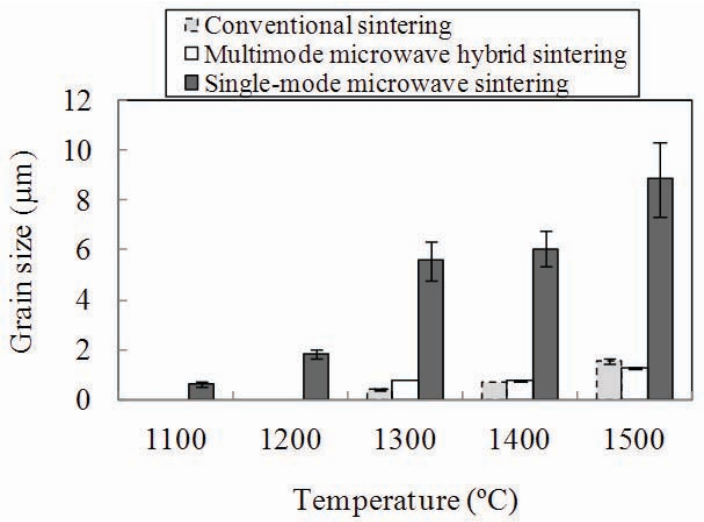

Figure 1. Change in grain size with temperature in a single-mode microwave, a multimode microwave, and a conventional furnace.

Figure 2 shows representative micrographs of 97 percent dense 8YZ samples processed in a single-mode microwave and a conventional furnace. The conventionally sintered sample and the multi-mode microwave-sintered sample are quite similar to each other and significantly different from the single-mode microwave-sintered sample. With a difference of 300°C in processing temperatures, the conventional and single-mode samples show similar grain size (0.7 μm) and hardness, as depicted in Figure 2. Since the 8YZ samples reached full densification at 1100°C, further increase in temperature to 1400°C resulted in significant grain growth, as shown in Figure 2 (far right).

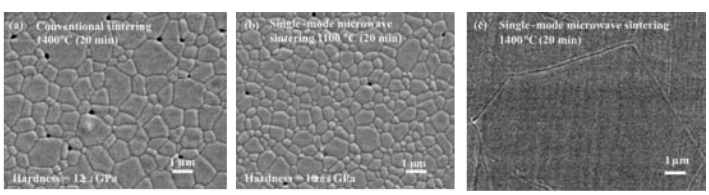

Figure 2. SEM images of 97 percent dense 8YZ.

In many applications, smaller grain-sized ceramics are preferred, as they exhibit better properties.[1] However, large grain sizes are preferable for fuel pellets, as such pellets decrease the fission gas release rate during irradiation,[2] which essentially reduces the rate of swelling. Studies on conventional sintering methods have shown that larger grain sizes are obtained only at high sintering temperatures (greater than 1500°C). This work has shown that, by adopting single-mode microwave sintering, larger grain sizes can be obtained at lower temperatures.

MSCs for Conventional Sintering of 8YZ. The very high activation energy reported during the last year for sintering 8YZ (1,000 kJ/mol) was erroneous due to an equipment problem. New data, as shown in Figure 3, indicates that the best convergence of the density-versus-theta curves occurs at an activation energy of 600 kJ/mol.

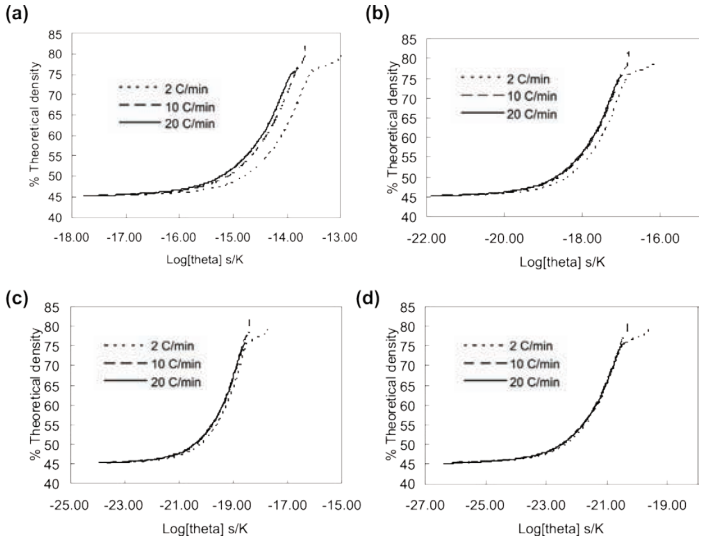

Figure 3. Percent theoretical density (% TD) versus log [theta] temperature curves for different activation energies: (a) Q = 300 kJ/mol; (b) Q = 400 kJ/mol; (c) Q = 500 kJ/mol; (d) Q = 600 kJ/mol.

Microwave Dilatometer Design Setup. Constructing the MSC requires a continuous record of linear shrinkage data, which is readily obtained by performing experiments in a dilatometer. However, most commercially available dilatometers do not utilize microwave energy as a heat source, so MSC models have not been applied to a microwave sintering process. The project team has developed a design (Figure 4) for a microwave dilatometer

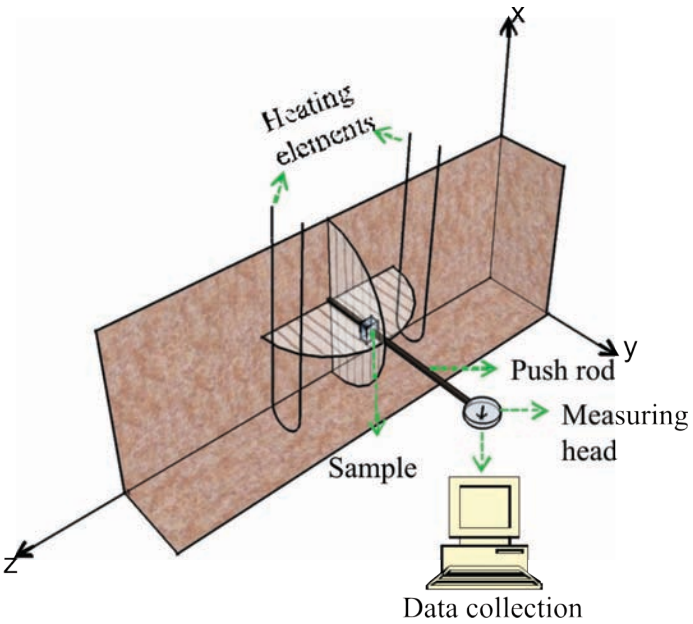

Figure 4. Schematic sketch of a microwave dilatometer inside a single-mode microwave cavity.

to make measurements under microwave irradiation. The design includes a set of heating elements for calibrating the push rod and for studying the change in activation energy for sintering with a change in conventional-to-microwave heating ratio. Understanding these changes is essential to understanding the fundamental reasoning behind enhancement in sintering during a microwave process.

Figure 5(a) shows a complete view of the single-mode microwave furnace. In this setup, the sintering experiments are done in a TE103 cavity which has been machined for incorporating the standard push rod, along with slots for inserting two $MoSi_2$ heating elements. The cavity has a well-defined electromagnetic field distribution at 2.45 GHz frequency. To prevent perturbing the microwave field during a sintering experiment, the push rod is inserted into the cavity only along the vertical direction. This design criterion required that the cavity be shifted by 90°, accomplished by attaching a standard flexible twistable waveguide (Figure 5[b]) that can rotate the cavity. Figure 5(c) shows the modified design of the system with the cavity in a vertical direction. In order to control these elements, a specially designed circuit was developed (Figure 6).

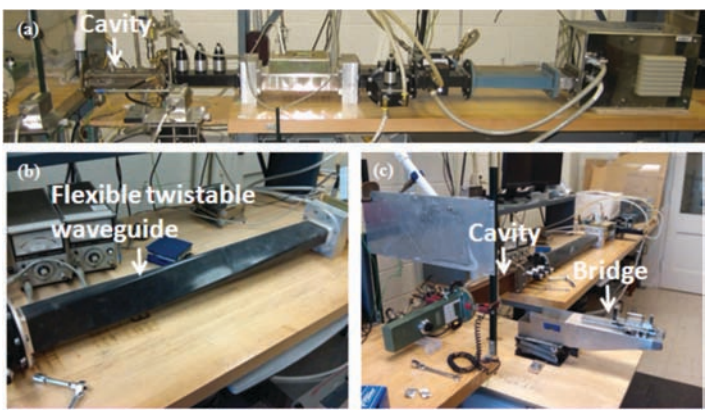

Figure 5. (a) A pictorial view of the standard TE103 single-mode microwave cavity; (b) flexible twistable waveguide; (c) a modified version of TE103 with necessary changes for a dilatometer setup.

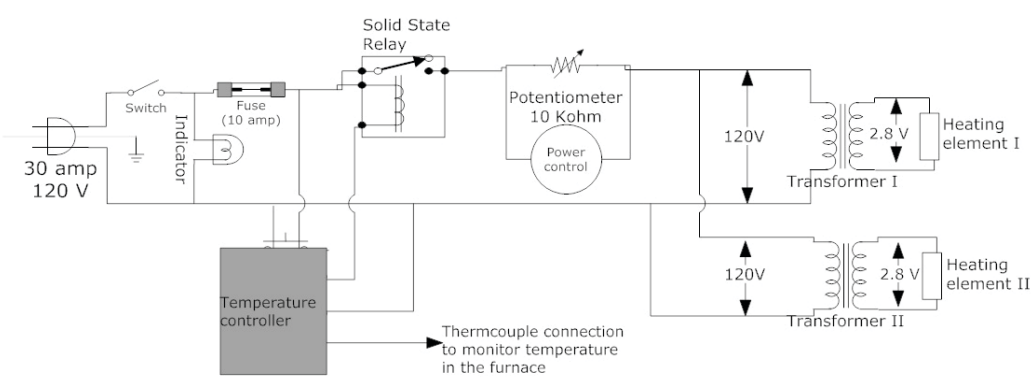

Figure 6. Electrical circuit layout for controlling the heating elements.

In order to record the data from the digital meter, the project team developed microwave controller software. This software not only allows one to control the microwave source but also to continuously record the data from the temperature monitors and the digital readouts. It can collect data at the precise interval of time for constructing the MSC.

After testing the current design, the team determined a need for a design-specific standard calibration technique to obtain precise and accurate measurements. Researchers are in the process of developing a procedure.

Inert Atmosphere Setup Inside the Multimode Microwave Applicator. The team designed a setup to study effects of an inert atmosphere on 8YZ's sintering behavior inside a microwave furnace. This design underwent major changes and is still being modified; researchers resolved issues with microwave interference with the temperature-measuring device, but they are still working to address remaining issues.

Green Pellet Fabrication. Team members have been working to fabricate high-density green pellets of zirconium oxide (ZrO) and zirconium nitride (ZrN). Researchers used several methods to process pellets of zirconium dioxide (ZrO_2): spec milling, ball milling, uniaxial pressing, isostatic pressing, and resonant acoustic mixing. The team also fabricated various powder blends, which have anywhere from one to five components and particle sizes ranging from 100 nm to 90 μm. The densities obtained using resonant acoustic mixing ranged from 67 to 74 percent TD, while the highest density obtained by conventional processing was 77 percent TD. Table 1 shows the composition of the traditionally processed powders; Table 2 shows the density range for the four- and five-component blends.

Table 1. Composition of traditional ZrO2 powder blends.

	NOAH (4μ-90μ)	TOSOH (45μ soft aggolermates)	ZTECH (45μ soft aggolermates)	Aldrich (5μ)	Aldrich (100μ)
Group I	73 wt%	10 wt%	—	14 wt%	3 wt%
Group II	73 wt%	—	10 wt%	14 wt%	3 wt%
Group III	73 wt%	10 wt%	3 wt%	14 wt%	—
Group IV	73 wt%	3 wt%	10 wt%	14 wt%	—
Group V	60.5 wt%	9.7 wt%	7 wt%	18.5 wt%	4.3 wt%

Table 2: Density range for four- and five-component ZrO2 blends.

Group	Average (%ρt)	High (%ρt)
Group I	75	77
Group II	69	70
Group III	72	73
Group IV	70	70
Group V	72	73

The small ZrN powder (1 μm to 2 μm average particle size) was blended with large ZrN powder (44 μm) to form a bimodal distribution. Powders were blended either by ball milling for 4 hours to 36 hours using 2-millimeter media or in a Spex mill for 1 minute to 10 minutes in hexane, then dried and reblended. All powders were uniaxially pressed at 45 ksi and held at this pressure for 30 seconds, then isostatically and/or uniaxially pressed at various pressure combinations for 30 seconds.

Fractional densities were determined for each sample. The maximum density increase (72 percent TD) was seen for only one isopress operation after the initial uniaxial pressing at 45 ksi. The ball-milled powder blends showed the maximum fractional densities, which might be explained by the presence of agglomerates in the powder (noted through SEM).

Researchers initially varied the small ZrN powder from 1 weight percent to 27 weight percent. Two blends showed the highest fractional densities: 15 weight percent small with 85 weight percent large and 23 weight percent small with 77 weight percent large. The team obtained 75 percent TD by using ball milling to blend 10 μm with 44 μm ZrN powder. The powder was then uniaxially pressed at 45 ksi and isopressed at 32.5 ksi. Ball milling produced higher fractional densities because it breaks up the large agglomerates (see Figure 7).

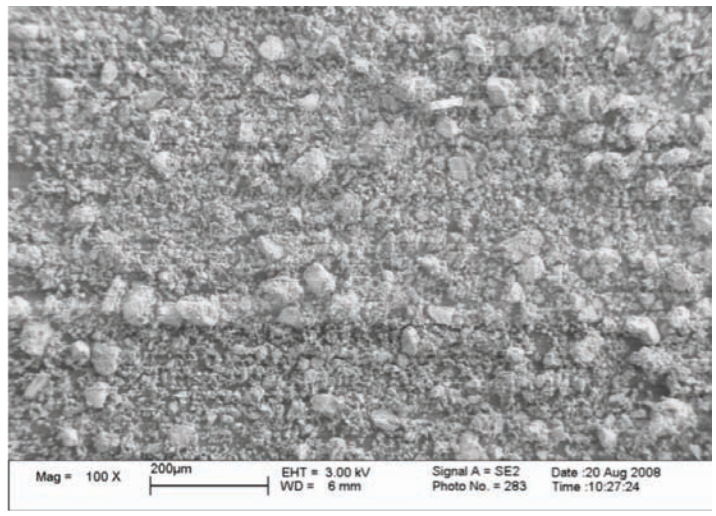

Figure 7. SEM photomicrograph of 44 μm ZrN powder after ball milling, which shows a large amount of powder measuring less than 44 μm.

Planned Activities

The project is continuing in a no-cost extension until June 2010. The team will continue to develop the microwave dilatometer and to conduct experiments that will lead to a MSC for microwave-processed inert matrix candidate 8YZ.

References

[1] C. B. Carter and M. G. Norton, *Ceramic Materials Science and Engineering*, Springer, New York, 2007, p. 315.

[2] *Journal of Nuclear Materials*, 278 (2000) 54–63.

NUCLEAR ENERGY RESEARCH INITIATIVE

Radiation-Induced Segregation and Phase Stability in Candidate Alloys for the Advanced Burner Reactor

PI: Gary S. Was, University of Michigan and Brian Wirth, University of California-Berkeley

Collaborators: Los Alamos National Laboratory, Oak Ridge National Laboratory

Project Number: 07-015

Program Area: FCR&D

Project Start Date: September 2007

Project End Date: August 2010

Research Objectives

The project objective is to determine the effect of radiation on segregation and phase stability of candidate alloys that may be used as structural materials for the advanced burner reactor (ABR). This project will focus on ferritic-martensitic (F-M) alloys T91 and HT9; an experimental oxide dispersion-strengthened (ODS) alloy; and an advanced austenitic alloy, D9. Researchers will investigate the electronic-magnetic-elastic interactions between chromium and radiation-induced defects. The project seeks to provide an understanding of radiation-induced segregation (RIS) and phase stability that can be used to develop predictive irradiation performance models.

Investigators will conduct experiments by proton and heavy ion irradiation over the dose range of 1-100 dpa and the temperature range of 400°C–600°C. Analysis of RIS, phase microstructure, dislocation microstructure, and hardening will be conducted under all conditions. Researchers will also use *ab initio* electronic structure calculations to investigate the configuration-dependent binding and migration energies of chromium (Cr) with vacancy and interstitial defects. This will enable the development of atomistic-based kinetic Monte Carlo models to investigate the Cr diffusivity and segregation behavior by interstitial and vacancy mechanisms.

Research Progress

The project team irradiated alloys T91, HT9, and D9 with 2.0 MeV protons to doses of 3, 7, and 10 dpa at temperatures of 400°C and 500°C. Alloys were also irradiated to 1 and 100 dpa at 400°C, with the 100 dpa irradiation conducted using iron (Fe) ions. T91 and HT9 are ferritic-martensitic alloys and are viable candidates for ABR structural materials. The austenitic alloy D9 is also a leading candidate, yet it can suffer from RIS of silicon.

Following irradiation, researchers performed RIS measurements by scanning transmission electron microscopy and energy dispersive x-ray spectroscopy. None of the three alloys displayed pre-existing segregation in any of their grain boundaries.

Thus far, the research team has analyzed the T91 and HT9 specimens irradiated at 400°C and 500°C. Only prior austenite grain boundaries aligned edge-on to the electron probe are considered in the RIS analysis. Alloy T91 exhibits Cr enrichment and Fe depletion at all three doses at 400°C, as Figure 1 shows. The magnitude of the Cr enrichment is less than or equal to 1.5 weight percent at all boundaries studied. The point-to-point change in Cr concentration is inversely related to the change in Fe concentration in a nearly one-to-one ratio. At all three doses at 400°C, T91 exhibits silicon, nickel, and copper enrichment. However, alloy HT9 exhibits Cr enrichment at 3 dpa but Cr depletion at 7 dpa and 10 dpa. The magnitudes of all observed Cr concentration changes, though, are less than 1.0 weight percent—below the inherent measurement uncertainty. Nickel enrichment of approximately 1.0 weight percent is observed at all three doses in HT9 at 400°C. At 500°C, the amount of Cr segregation is considerably less, falling within the noise of the measurements. However, nickel and silicon enrichment is still evident at all doses.

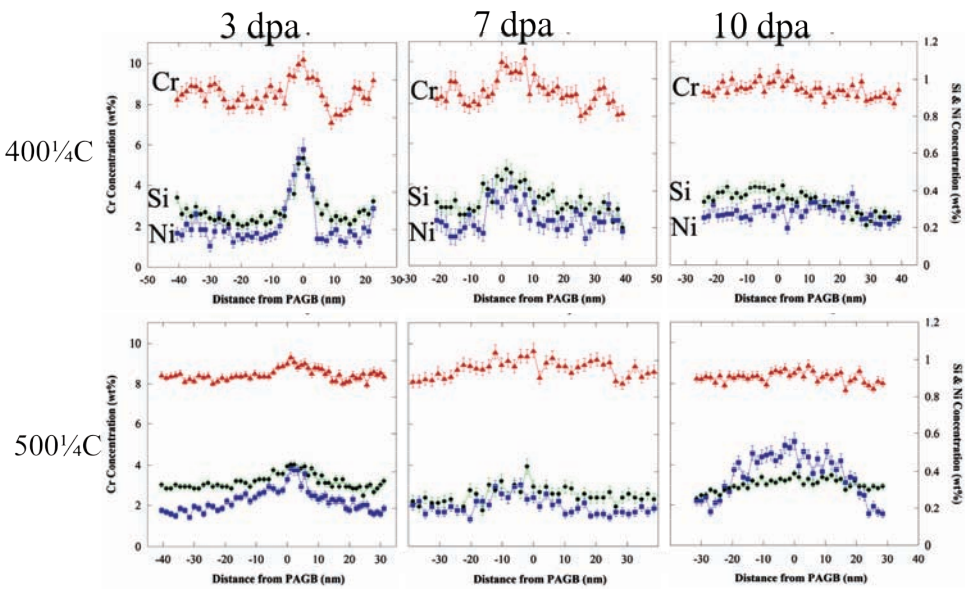

Figure 1. Grain boundary composition profiles in alloy T91 following proton irradiation at 400°C and 500°C to 3, 7 and 10 dpa.

The team performed hardness measurements on all alloys before and after irradiation. Irradiation-induced hardening is greater at 400°C than at 500°C, as expected. Hardening saturates around 7 dpa, and the values compare well to those found in literature.

The team developed a lattice-based kinetic Monte Carlo (KLMC) model to simulate vacancy-mediated Cr transport and segregation to grain boundaries in concentrated Fe-Cr alloys. The team has recently extended the model to interstitial-mediated transport. The model has been informed by *ab initio* electronic structure calculations and validated by comparing to Cr diffusivity data. The initial simulations involve calculating the radiation-induced segregation of Cr in an Fe-10%Cr alloy to a grain boundary sink. The electron irradiation was 10^{-6} dpa/second, and temperatures ranged from 300°C to 700°C. The team utilized a semi-empirical Fe-Cr alloy potential that provides faster Fe than Cr diffusion. Initial KLMC results indicate Cr enrichment at the grain boundary located at the 0th atomic plane, and the findings indicate that Cr enrichment is increasing with fluence. Future simulations will verify these results. In addition, researchers will evaluate the effect of interatomic potential on the ratio of Cr-to-Fe diffusivity; they will also extend the method to simulating ion and neutron irradiation conditions.

Planned Activities

During the third year of the project, the team will conduct analyses of irradiations at 1 and 100 dpa to determine RIS behavior over a dose range of 1–100 dpa and to determine the agreement in behavior between proton and heavy ion irradiation. Team members will also focus on RIS in alloys HT9, ODS, and D9. Local electrode atom probe (LEAP) will also be used to analyze the alloys' grain boundary segregation.

The KLMC code for vacancy-mediated Cr transport has recently been extended to incorporate interstitial-based diffusion. The KLMC simulations will be used to predict Cr segregation tendencies as a function of irradiation temperature, irradiating particle (ion or neutron), and dose. In addition, the team will continue a second modeling task focusing on the dislocation loop evolution in F-M alloys. In particular, the modeling will use atomistic molecular dynamics simulations, atomic-scale kinetic Monte Carlo, and rate theory methods. Using these tools, researchers will help evaluate the formation mechanism of interstitial loops with Burger's vector of a<100>, and will predict the size and density of evolution of both a/2<111> and a<100> loop populations. The predictions will be benchmarked against the experimental database generated by the proton and heavy ion irradiations, in addition to available neutron irradiation data.

NUCLEAR ENERGY RESEARCH INITIATIVE

Chemistry of Transuranic Elements in Solvent Extraction Processes: Factors Controlling Redox Speciation of Plutonium and Neptunium in Extraction Separation Processes

PI: Alena Paulenova, Oregon State University

Collaborators: Argonne National Laboratory

Project Number: 07-023

Program Area: FCR&D

Project Start Date: April 2007

Project End Date: March 2010

Research Objectives

The objective of the project is to examine the factors controlling redox speciation of plutonium (Pu) and neptunium (Np) in the uranium recovery by extraction (UREX+) process in terms of redox potentials, redox mechanisms, kinetics, and thermodynamics. Researchers will employ radiochemical redox-speciation extraction schemes in parallel to the redox experiment. The resulting distribution of redox species will be studied using spectroscopic, electrochemical, and spectro-electrochemistry methods, in addition to other methods, such as x-ray absorption spectroscopy and laser spectroscopy that are available at Argonne National Laboratory (ANL). This work will result in creation of a database on redox stability and distribution of redox couples in the nitric acid/nitrate electrolyte, as well as development of redox buffers to stabilize the desired oxidation state of separated radionuclides. Researchers will evaluate effects of temperature and concentrations of acid and salt on actinide nitrate's redox potential, considering a range of chemical matrix conditions. The database generated from the experimental work will be integrated into a selected existing actinide speciation code.[1]

Research Progress

Reaction Between Np(VI) and Nitrous Acid (HNO_2). It is difficult to predict and control the redox speciation of neptunium, which is very important for its successful separation by solvent extractions with tributyl phosphate (TBP) from aqueous nitric acid (HNO_3). Both Np(VI) and Np(V) redox states are simultaneously present in significant amounts, and their extractability into TBP is very different. Initially, after leaching of spent fuel, Np(VI) is predominantly present. However, leaching of fuel elements and radiolysis of HNO_3 in both aqueous and organic phase produces HNO_2, hence, a significant amount of Np(V) is also produced.

$$2NpO_2^{2+} + HNO_2 + H_2O \rightarrow 2NpO_2^{+} + 3H^{+} + NO_3^{-}$$

The team examined the kinetics of the forward reaction in nitric acid. The order of the reaction with respect to HNO_2 and Np(VI) was studied in HNO_3 of molarity 4M at 20°C. Researchers varied one reactant's initial concentration and maintained the other's concentration constant. The study showed that both reacting orders are close to, but not exactly equal to, the first order. The reduction of Np(VI) was strongly dependent on the environment's acidity. The team performed a series of experiments, varying the solutions' concentrations of nitric acid while using lithium nitrate ($LiNO_3$) to maintain ionic strength constant. Results indicate that the reaction rate slows with increasing acidity. The reaction order with respect to HNO_3 concentration was in the vicinity of –0.85.

Nitrous Acid Scavengers. The research team studied methylurea (MU) and acetamide (AcA) as possible scavengers for nitrous acid due to their reactivity towards HNO_2. Researchers performed ultraviolet–visible–near-infrared (UV–Vis–NIr) spectroscopy to determine Np speciation and to identify and quantify HNO_2 and its interaction with MU and AcA before and after irradiation. In low quantities and at concentrations of 1 to 15 millimolar (mM), AcA has not proven itself efficient in preventing the formation of nitrous acid. The team also attempted to inhibit reduction of Np to Np(V) by adding small concentrations (1 to 10 mM) of MU and 1 to 10 mM vanadium as a holding oxidizer, but the experiment

was unsuccessful. To analyze MU performance, researchers used an easily identifiable spectral change by nitrosation of methylurea by HNO_2, which leads to the formation of nitrosomethylurea (NMU), as shown in Figure 1. The team experimented with higher concentrations (over 100 mM) of MU to inhibit the radiolytic production of nitrous acid, which was successful at an overall dose of 40.5 kGy (Figure 2).

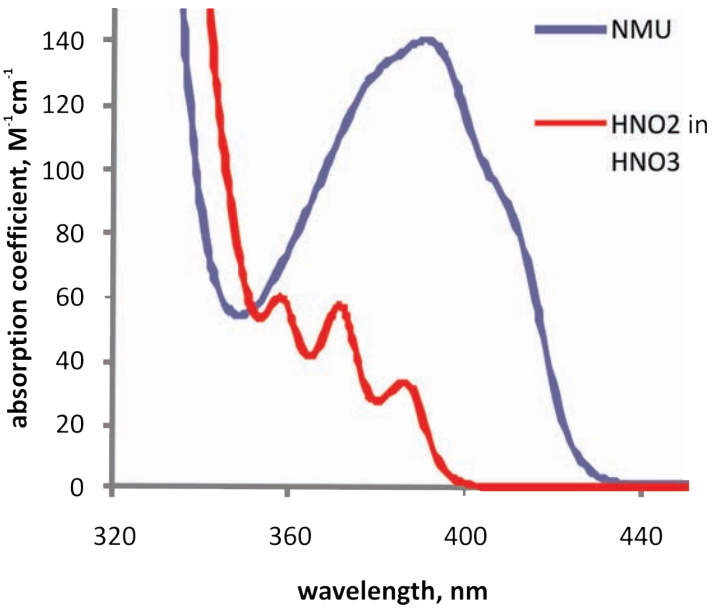

Figure 1. Change of UV absorption spectrum of HNO_2 in HNO_3 by addition of MU. The new characteristic spectrum of NMU can be easily distinguished from the spectrum of HNO_2 in HNO_3. The MU itself does not have any absorption spectrum in the UV-Vis region.

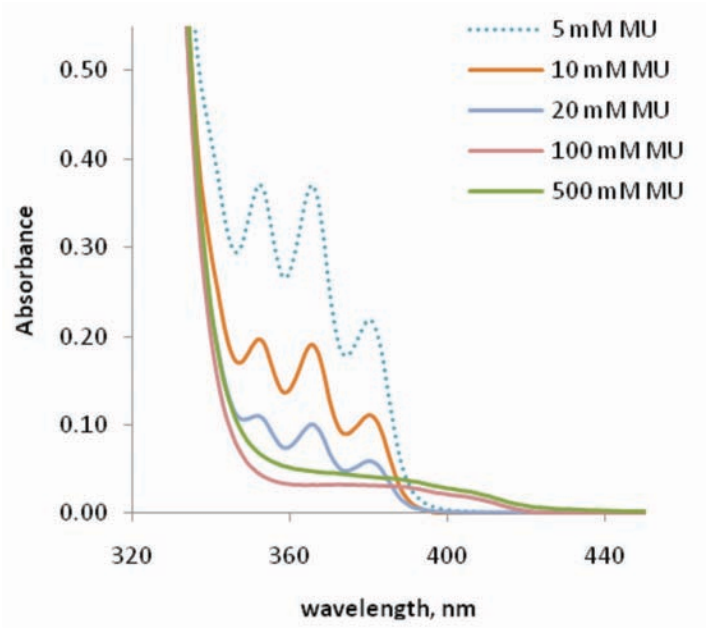

Figure 2. Changes in absorbance spectrum of solutions of 4M HNO_3 with initial additions of 10 mM $NaNO_2$ and 5-500 mM of MU after irradiation by a dose of 40.5 kGy.

Planned Activities

The research team plans to conduct the following tasks in the upcoming year:

- Conduct experiments to analyze the effect of radiolytical production of HNO_2 from HNO_3 in organic extractants; assess the kinetics of reduction of Np(VI) in the organic phase.
- Examine the effectiveness of various novel amides as HNO_2 scavengers in both aqueous and organic phases; test their performance under radiolysis.

NUCLEAR ENERGY RESEARCH INITIATIVE

New Fission Product Waste Forms: Development and Characterization

PI: Alexandra Navrotsky, University of California-Davis

Collaborators: Brigham Young University, Eltron Research, Inc., Sandia National Laboratories

Project Number: 07-027

Program Area: FCR&D

Project Start Date: June 2007

Project End Date: May 2010

Research Objectives

This project will identify advanced methods for chemical partitioning of spent nuclear fuel into cesium (Cs), strontium (Sr), and minor actinide (MA) constituents that can be stored for future disposition. Researchers will study new waste forms and disposal strategies for the steam reforming process to produce a storage form that incorporates Sr and Cs, their decay products, and rare earth fission products. The project team will conduct a broad characterization study of inorganic ceramic waste form phases and the thermochemistry of these phases; this study will provide a comprehensive data set from which to select the appropriate waste form. Emphasis will be on perovskite phases as a major constituent of the final waste form. Project goals are to reduce costs of the guanidinium carbonate steam reforming waste process, to minimize risk of environmental contamination during waste processing, and to provide technical solutions to various issues related to Cs, Sr, and MA disposal.

Project objectives include the following:

- Establish ceramic waste forms for disposing of Cs, Sr, and MAs. The process uses transition metal oxides loaded *in situ* with minimal additional processing steps, minimizing waste volume and producing durable waste forms for all cations and their decay products.
- Fully characterize phase relationships, structures, and thermodynamic and kinetic stabilities of promising waste forms.
- Establish a sound technical basis for understanding key waste-form properties, such as melting temperatures and aqueous durability, based on an in-depth understanding of waste form structures and thermochemistry.
- Establish synthesis, testing, scaleup, and commercialization routes for waste-form implementation.

The proposed work will provide information on the waste forms' durability and stability, supporting evaluation of their potential for viable storage or disposal scenarios. Since Cs and Sr form new elements by radioactive decay over several hundred years, researchers will study the behavior and thermodynamics of these waste forms using non-radioactive analogues.

Research Progress

Phases of Titanite Glasses (MTiSiO5, where M=Ca, Sr, or Ba). The team is analyzing enthalpy of formation ($\Delta H^{\circ}_{f,ox}$) of the titanite glasses (-38.8 ± 3.4 ($CaTiSiO_5$), -162.9 ± 2.4 ($SrTiSiO_5$), and -127.6 ± 3.0 ($BaTiSiO_5$) $kJmol^{-1}$. Researchers crystallized $SrTiSiO_5$ and $BaTiSiO_5$ glass at 880°C for 30 hrs and correlated the results with crystallization behavior measured by thermogravimetry (TG) and differential scanning calorimetry (DSC). For $MTiSiO_5$ (M = Sr, Ba), the major exothermic peak was due to crystallization to $M_2TiSi_2O_8$, confirmed by x-ray diffraction (XRD). In addition, a weak exothermic peak was observed at higher temperatures, suggesting an additional phase formed. Assuming the higher-temperature peaks are due to the crystallization of rutile (TiO_2), the reaction can be written:

$$2MTiSiO_5 \text{ (glass)} \rightarrow M_2TiSi_2O_8 + TiO_2.$$

The ΔH_{cryst} values measured from DSC curves for $SrTiSiO_5$ and $BaTiSiO_5$ are -34.7 and -39.3 kJ/mol, respectively. These values are comparable to half of the above reaction enthalpies (M = Sr (-70.6 ± 2.4 kJ/mol) and Ba (-87.1 ± 4.6 kJ/mol). This result indicates that there might be only a narrow temperature window for synthesis of the crystalline M-analogue of titanite; outside of this window, the energetically more stable fresnoite phase would form and leave non-stoichiometric residues prior to the crystallization of $MTiSiO_5$.

Heat Capacity Measurements. The team measured the heat capacities (C_p) of the fresnoites ($Ba_2TiSi_2O_8$ and $Sr_2TiSi_2O_8$) using the Quantum Design Physical Property Measurement System (PPMS)®. Researchers are analyzing and comparing thermodynamic functions (e.g., C_p and entropy) for the Ba- and Sr-fresnoites.

Fresnoite, Titanite, and Pollucite Phases: The team completed calorimetric studies and published three papers in FY 2009. The results show that all those materials are stable and possible waste ceramics having high durability. However, substitution of decay products increases the tendency for glass formation (rather than crystallization) in these systems.

Planned Activities

During the coming fiscal year, the research team plans to complete calorimetry on new samples from Sandia National Laboratories, as well as on perovskites.

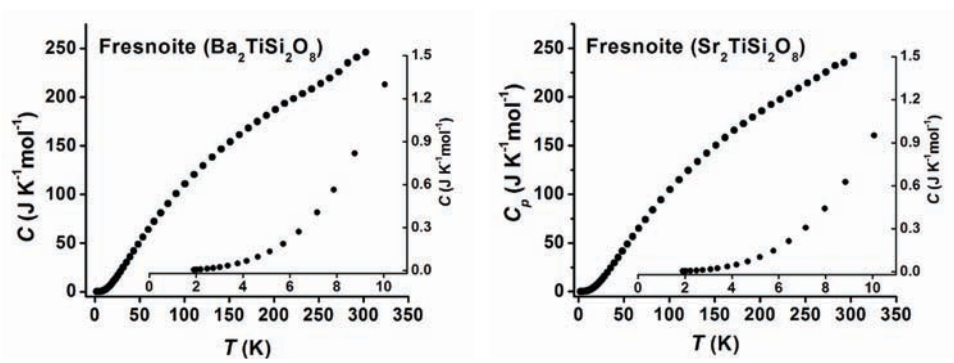

Figure 1. Experimental molar heat capacities for $Ba_2TiSi_2O_8$ and $Sr_2TiSi_2O_8$ are shown. The inset displays the low-temperature data on an expanded scale.

NUCLEAR ENERGY RESEARCH INITIATIVE

Computations for Advanced Nuclear Fuels

PI: Sudarshan K. Loyalka

Collaborators: None

Project Number: 07-035

Program Area: FCR&D

Project Start Date: June 2007

Project End Date: June 2010

Research Objectives

The project objective is to develop advanced computational techniques to improve understanding of fission gas distribution and heat transfer in solid fuel under normal and accident conditions. To successfully implement an efficient and effective nuclear power strategy, new fuels must be developed to provide optimal performance over long periods of time. In this project, researchers will develop atomistic-scale to continuum-scale models to replace the empirical models used in existing fuel performance codes. The computational programs of fission product transport will apply to the pyrolytic carbon and silicon carbide coatings of tri-isotropic (TRISO) fuels as well. The programs will help provide estimates for the transport behavior of noble gases, iodine, tellurium, cesium, strontium, silver, palladium, and rare earth fission products in the layers of the TRISO-coated particle fuel. The process can provide data for both normal and accident conditions—where measurements are either impractical or cost-prohibitive. This work will also help reduce uncertainties and elucidate transport mechanisms.

Research Progress

The project team has continued to make progress on the construction of direct-simulation Monte Carlo (DSMC) programs for both fission product and phonon transport. In both areas, researchers have continued testing the programs and incorporating increasingly realistic models for intermolecular, phonon, and gas-surface interactions and geometries.

The project performed initial studies of gaseous flows in nano-pathways (that could be typical of cracking in TRISO and nuclear fuels and coatings). Researchers focused on free-molecular transport in fine capillaries of a range of shapes and explored geometry's effect on this transport. These computations have provided insights into geometry's role in molecular transport in nuclear materials with narrow flow pathways. The results will also be useful in guiding computations that include intermolecular collisions and more realistic gas-surface collision operators. Geometries considered by the project team include straight, conical, and helical tubes; Figure 1 depicts some helical geometries of different aspect ratios. The team published an article on this initial work in the *Journal of Nuclear Materials*.

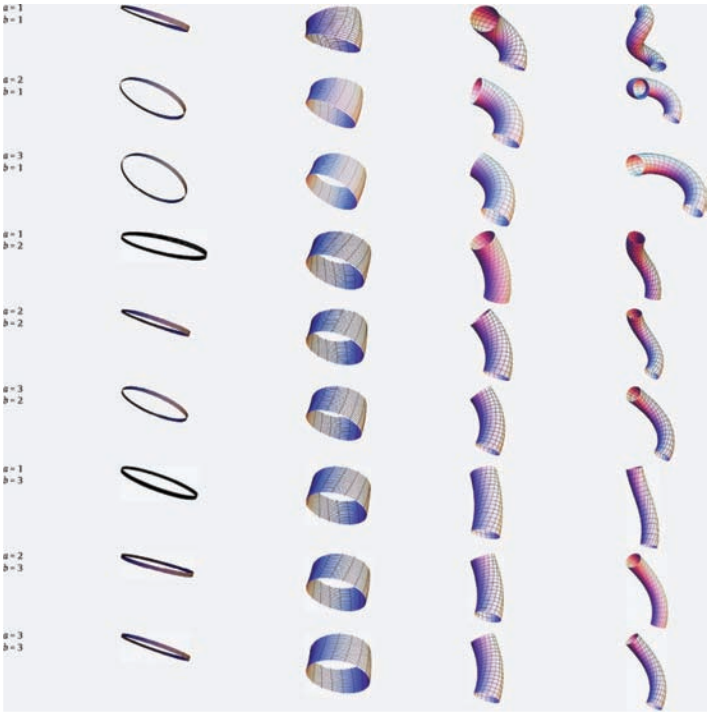

Figure 1. A sampling of helical geometries considered by the project team.

In addition to using the DSMC programs mentioned above, the research team has also explored using variational and analytical techniques for addressing phonon heat transfer. Phonons in a solid crystal are described by transport equation

$$\frac{\partial N}{\partial t} + \mathrm{u} \cdot \frac{\partial N}{\partial \mathrm{r}} = C(N)$$

where $\mathrm{u} = \partial\omega / \partial\mathbf{k}$ is the phonon velocity, C is the collision integral, and N denotes the distribution function for phonons of type g. The team's techniques compute solutions over the entire range of the ratio of the phonon mean free path, or the average distance it can travel unimpeded, to the system dimensions in slab geometry. Researchers have obtained simple results of general applicability. The team is preparing several manuscripts for publication on this and related work.

Planned Activities

The project team will continue construction and testing of the computer programs for both molecular and phonon transport. At this point, the primary challenges are improving both the computational times and fidelity to multi-physics descriptions. The team will continue preparing manuscripts for publication.

The project will be requesting a one-year no-cost extension for the project to June 2011.

NUCLEAR ENERGY RESEARCH INITIATIVE

Experimental Development and Demonstration of Ultrasonic Measurement Diagnostics for Sodium Fast Reactor Thermohydraulics

PI: Akira Tokuhiro, Kansas State University

Collaborators: Argonne National Laboratory

Project Number: 07-037

Program Area: FCR&D

Project Start Date: June 2007

Project End Date: May 2010

Research Objectives

This research project will address some of the principal technology issues related to sodium-cooled fast reactors (SFRs), primarily development and demonstration of ultrasonic measurement diagnostics linked to effective thermal convective sensing under normal and off-normal conditions. Sodium is well-suited as a heat-transfer medium for the SFR. However, because it is chemically reactive and optically opaque, sodium presents engineering accessibility constraints relative to operations and maintenance (O&M) and in-service inspection (ISI) technologies that are currently used for light water reactors. Thus, there are limited sensing options for conducting thermohydraulic measurements under normal conditions and during off-normal events (maintenance, unanticipated events). Acoustic methods, primarily ultrasonics, are a key measurement technology with applications in non-destructive testing, component imaging, thermometry, and velocimetry.

This project will yield a better quantitative and qualitative understanding of sodium's thermohydraulic condition under varied flow conditions. The work scope includes evaluating and demonstrating ultrasonic technologies and defining instrumentation options for the SFR.

The researchers will demonstrate ultrasonic technology through the following activities:

- Design, construct, and operate a small, simple, university-based sodium flow loop with an inventory of approximately five to six liters.
- Develop and demonstrate ultrasonic velocimetry and thermometry, with a focus toward improved SFR O&M (i.e., using velocimetry and thermometry as diagnostic tools during normal and off-normal operations).
- Test a compact sodium-to-supercritical carbon dioxide (CO_2) heat exchanger and generate convective heat-transfer data, correlations, and operational experience during normal and off-normal operations.

Research Progress

Activities in 2009. During this reporting period, the project team began to design a flow loop to accommodate the prototype test section and cold trap.

The project is awaiting access to Argonne National Laboratory's (ANL's) Sodium Plugging Experimental Facility, where the advanced burner reactor (ABR) concept employs a supercritical CO_2 Brayton-cycle power-conversion technology. As shown in Figure 1, the apparatus consists of a main sodium loop with three test sections, a bypass sodium loop including a cold trap/economizer assembly, and an auxiliary system comprising argon and vacuum lines. The main loop and bypass loop are constructed from stainless steel tubing. Other major components include electromagnetic (EM) flow controllers, EM pumps, EM flow meters, and expansion and dump tanks. The sodium loop system is about 1.8 meters tall and is heated by a number of ceramic band heaters. The loop's maximum operating temperature and pressure are

510°C and 207 kilopascals (kPa) (= 30 pounds-force per square inch gauge [psig]), respectively. At about 800 amperes (A), the nominal flow rate and pressure head are $4x10^{-5}$ cubic meters per second (m^3/s) (= 2.4 liters/minute) and 40 kPa, respectively; however, the EM pumps can operate at up to 1,000 A for higher flow rate and pressure-head operations.

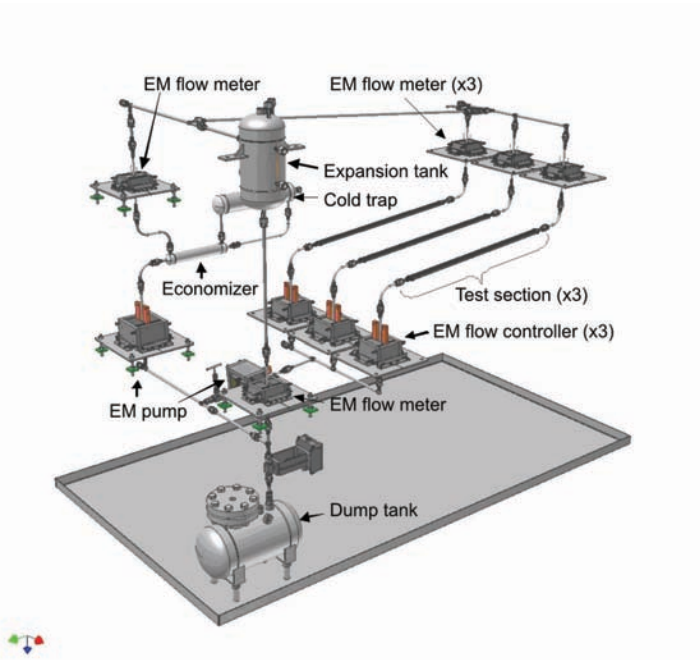

Figure 1. Schematic of a small sodium loop facility at ANL.

A key component for efficient power conversion is a compact heat exchanger known as the printed circuit heat exchanger (PCHE). In the ANL's ABR (or a similar SFR), this would be a sodium-to-CO_2 heat exchanger. Each PCHE is essentially a monolithic block of stainless steel containing embedded narrow flow channels. If the sodium should become supersaturated with impurities (e.g., oxides), the impurities could plug these flow channels. The project team needs experimental data to assess plugging characteristics. Researchers at ANL have shown that, for the PCHE flow-channel sizes being considered for the sodium-to-CO_2 heat exchanger, no plugging occurs if the sodium is maintained pure and the sodium temperature is well above the impurity saturation temperature. The team is acquiring additional plugging behavior data with measured levels of particulates flowing through the channels. With this data, researchers can determine the optimum design of the PCHE sodium-to-CO_2 heat exchanger.

Ultrasonic Doppler Velocimetry, Thermometry, and Sensor Design. Ultrasonic Doppler velocimetry (UDV) is a non-invasive, ultrasound-based method of measuring velocity as a function of both space and time. UDV can be used with gases; however, acoustic velocity in gas is roughly 300 meters per second, whereas acoustic velocity in liquids is 1,500 meters per second (or greater), allowing UDV to be used as a quasi-live velocimetric "tool" in liquids. It provides spatial velocity information (distribution) which is derived along the acoustic beamline by measuring and sufficiently sampling the Doppler shift (per channel) at the time of echo detection (thus requiring "seeding" of some sort). Temporal velocity information can be derived as the ultrasonic burst and echo reception (Doppler shift measurement) is rapidly (electronically) cycled. Thus, spatio-temporal velocimetric information is acquired much like a laser-based velocimetry method (laser Doppler, particle image, etc.). The principles of UDV are noted in a well-documented list of publications at *www.met-flow.com*.

The project has purchased and begun initial testing of a Met-Flow Ultrasonic Velocity Profile Model DUO, Krautkramer-Branson (analog) ultrasonic pulser/analyzer, and National Instruments data acquisition unit with software. In order to realize ultrasonic velocimetry and thermometry at SFR-relevant temperatures, the project requires transducers that can operate in excess of 500°C. The Curie temperature limits piezoelectric (Pz) elements commonly used in ultrasonics; the highest Curie temperature for commercially available piezoelectrics is 650°C for bismuth titanate. The Pz on hand is limited to 250°C. Although plans are under way to procure appropriate Pz elements, the project has initiated a design effort to integrate gas cooling of lower-temperature transducers. One current design is shown in Figure 2. The team is also considering a novel "acoustic well" of tightly wrapped metal sheets to thermally isolate the low-temperature Pz element.

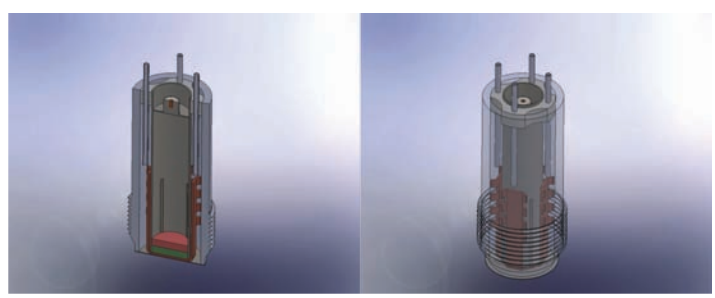

Figure 2. Current design of the cooled ultrasonic transducer.

Planned Activities

Based on the objective to develop and demonstrate ultrasonic technologies for the SFR, a scope of work was defined in terms of project tasks and associated metrics. Researchers plan to undertake the following:

- Finish design of the pipe flow test section for velocimetry and thermometry. A prototype is shown in Figure 3.
- Finish design of the active "economizer" (cold trap).
- Conclude and select a compact sodium-to-CO_2 heat exchanger and plan to integrate the delivered heat exchanger for testing.
- Complete testing of ultrasonic signal-processing instrumentation for thermometry in early 2010.
- Finish compact heat exchanger design analysis using computational fluid dynamics.

Figure 3. Schematic of flow test section with provisional location of ultrasonic transducer (top) and prototype test section with guard heater "tape."

- Construct the test loop or integrate components to the ANL loop (above) and conduct velocimetry, thermometry, and heat exchanger performance testing.

A subcontracting arrangement has been approved that transfers the project in its entirety from Kansas State University to the University of Idaho.

NUCLEAR ENERGY RESEARCH INITIATIVE

Fundamental Processes of Coupled Radiation Damage and Mechanical Behavior in Nuclear Fuel Materials for High-Temperature Reactors

PI: Simon Phillpot, University of Florida

Collaborators: Idaho National Laboratory, Los Alamos National Laboratory

Project Number: 07-046

Program Area: FCR&D

Project Start Date: June 2007

Project End Date: May 2010

Research Objectives

A longstanding issue for the nuclear industry is degradation of mechanical properties of nuclear fuels under irradiation, including both fissionable material and cladding. Developing fuel systems with improved resistance to radiation damage will allow longer burnups, improved usage efficiency, increased time between refueling, and decreased waste. The project objective is to elucidate the radiation-induced effects on microstructure and mechanical properties of nuclear fuel materials. This research will focus on developing an understanding of 1) the fundamental mechanisms of radiation damage in polycrystalline materials, 2) the effect this damage has on plastic deformation, and 3) the effect of mechanical deformation on radiation tolerance.

The research team will use uranium dioxide (UO_2) fuel material in hexagonal close-packed (HCP) titanium (Ti) clad (representing HCP Ti alloys for fast reactors and zircaloy for cladding in thermal reactors). To simulate radiation damage, researchers will apply state-of-the-art large-scale atomic-level simulation through a judicious combination of both conventional and accelerated molecular dynamics (MD) methods. They will elucidate mechanical behavior by applying large-scale MD simulations. This systematic program for simulating radiation's effects on structural and mechanical properties of polycrystalline Ti and UO_2 will identify radiation damage mechanisms and provide insights into the expected behavior of nanocrystalline microstructures and nanocomposites. This work will ultimately help researchers design microstructures that are less susceptible to radiation damage and thermomechanical degradation.

Research Progress

Mechanical Properties of a Polycrystalline HCP Metal. Figure 1 shows dislocation processes in a large grain-sized sample of HCP magnesium (Mg). The same initial structure, with a grain size of 60 nanometers (nm), underwent two different tensile stresses, 1.5 and 1.18 gigapascals (GPa). Basal <a> partial slip mainly occurs at approximately a five percent strain, as exhibited in Figure 1(a). An extended dislocation (marked "A" in Figure 1[a]) initiated from a grain boundary (GB) was also found in the strained system. Moreover, the number of extended dislocations increased markedly at the larger strain shown in Figure 1(b). Cores of full dislocations were observed, marked as "B" in Figure 1(b). During deformation tests of structures with grain sizes from 6 nm to 60 nm, the fraction of the total number of dislocations that were extended or full consistently increased as the grain size increased. Moreover, as shown by comparing Figures 1(b) and (c), a larger external stress gives rise to not only higher dislocation density but also a higher fraction of extended or full dislocations for a similar strain.

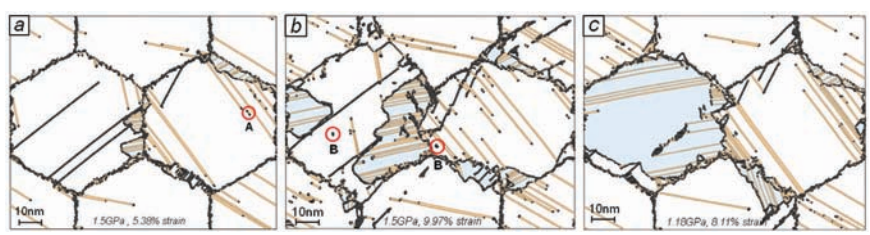

Figure 1. Snapshots of strained [11$\bar{2}$0]-textured HCP structures with a grain size of 60 nm at 1.5 and 1.18 GPa. In (a) and (b), total strains are 5.38 percent and 9.97 percent at 1.5 GPa, including elastic strain of approximately 3 percent. In (c), total and plastic strains are 8.11 percent and 5.43 percent at 1.18 GPa. Note microstructural features: A - extended dislocation, B - full dislocation. Cyan, brown, and black indicate a twinned region, stacking fault (face-centered cubic [FCC]), disordered (non-HCP or -FCC), respectively.

The interaction between slip and twinning can be viewed as processes of competition and cooperation. The first competition takes place between pyramidal <c+a> slip and $\{10\bar{1}2\}$ $<10\bar{1}1>$ twinning. As exhibited in Figures 1(a) and (b), the pyramidal <c+a> dislocation can physically block the growth of the twinning region. Moreover, increasing the stress accelerates this phenomenon by promoting slip rather than twinning. The same trend is also found between basal <a> slip and $\{10\bar{1}2\}$ $<10\bar{1}1>$ twinning. At low stress, the twinning process is more dominant than the basal slip. However, twinning activity decreases compared to the basal slip as the stress increases.

By contrast, there are also several cooperation processes between slip and twinning, with one deformation mechanism helping to activate the other. For example, a $\{10\bar{1}2\}$ $<10\bar{1}1>$ tensile twinning originated at GBs can initiate a basal <a> slip through an emissive dislocation. Conversely, a high density of dislocations leads to compressive twinning. A second cooperative process is observed in the slip behavior in a twinned area. When an I1-type stacking fault in a $\{10\bar{1}2\}$ $<10\bar{1}1>$ twinned area accommodates the propagation of twinning, the Schmid factor for slip increases, promoting a new slip process.

Radiation Damage in Ti. The team performed cascade simulations in Ti with the interatomic interactions described by two different modified embedded atom method (MEAM) potentials: MEAM_2006 and the higher-fidelity MEAM_2008. The cascade simulations have been performed at 100 kelvins (K) with a primary knock-on-atom (PKA) energy range from 0.1 kiloelectron volts (keV) to 50 keV. Researchers performed statistical calculations based on multiple cascade simulations including several different crystallographical directions. No significant direction dependence was observed using either potential.

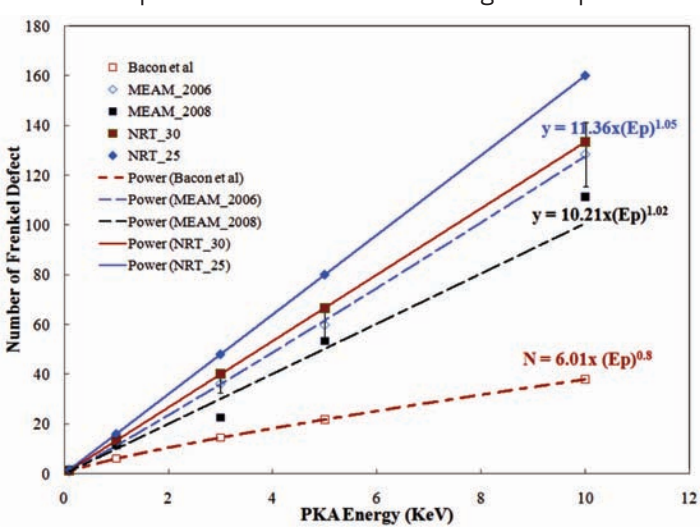

Figure 2. Number of Frenkel defects produced in a cascade in Ti for three different interatomic potentials, with comparison to the corresponding Norgett, Robinson, and Torrens (NRT) model values.

The research team has found that both MEAM potentials predict a higher number of surviving defects than an earlier potential by Finnis and Sinclair (FS). To investigate this difference, researchers evaluated the effects of time step and thermostat. Neither had any significant effect on the number of surviving defects. Further, to eliminate any impact of the analysis method, researchers analyzed the defects using both common neighbor analysis and the lattice matching approach. These two methods complement each other. When the appropriate cutoff was used for these methods, they yielded almost the same number of system defects.

The survival of Frenkel defects as a function of PKA energy is usually much lower than the NRT relationship, which depends on the threshold energy for cascade simulation. To account for this discrepancy, the team calculated the threshold energy using MEAM_2006. MEAM_2006 predicts a lower threshold energy than the FS potential, which leads to a higher number of surviving system defects. However, the relative ratio of surviving Frenkel defects with respect to the number predicted by NRT was still higher using the MEAM_2006 potential.

Planned Activities

Work is currently under way to:

- Simulate the interactions of radiation damage with the microstructure in nanocrystalline UO_2. Using the simulation findings, the research team can assess the relative importance of direct vacancy-interstitial recombination within the perfect-crystal regions and the recombination associated with the GBs.
- Simulate deformation processes in both textured and random polycrystalline HCP microstructures.
- Extend work on cascade simulations in single-crystal Ti to polycrystalline materials, thereby assessing cascade–GB interactions.
- Simulate deformations in irradiated Ti polycrystals, thereby elucidating the coupling of radiation damage and mechanical properties.

The project has requested a no-cost six-month extension.

NUCLEAR ENERGY RESEARCH INITIATIVE

Economic, Repository, and Proliferation Impacts of Advanced Nuclear Fuel Cycles

PI: Professor KB Cady, Cornell University

Collaborators: University of Texas at Austin

Project Number: 07-051

Program Area: FCR&D

Project Start Date: June 2007

Project End Date: May 2010

Research Objectives

The project objective is to compare the use of fast reactor (FR) advanced nuclear fuel cycles with that of inert matrix fuel (IMF) in light-water reactors (LWRs) as a means of reducing actinide inventory, focusing on economics and proliferation resistance. In addition to making use of the current LWR fleet, IMF can offer a four-fold increase in repository capacity when compared to direct disposal of an energy-equivalent quantity of spent LWR fuel, with over 98 percent destruction of plutonium (Pu)-239. Research also suggests that leaving IMF pins in the reactor after their reactivity has been depleted (effectively making them actinide targets) could offer a significant increase in actinide destruction. FRs can potentially increase repository capacity by more than an order of magnitude per kilowatt of electricity generated. However, FR spent fuel must be recycled many times in order to achieve this result, whereas the increase in repository capacity offered by IMF does not require reprocessing. Unlike previous studies that assumed the continuous recycling of spent FR fuel, this project will analyze the impact of IMF and FR transmutation strategies over the 100-year period from 2010 to 2110.

Research Progress

During FY 2009, the project team ran simulations for various IMF compositions (as laid out in the original proposal) for burnups from 650 to 850 megawatt-days per kilogram of initial heavy metal (MWd/kgIHM). The two IMF compositions comprised eight and twelve elements, respectively, and included neither Pu nor MA. Researchers performed reactivity calculations using codes VBUDS (visualization, burnup, depletion, and spectra) and MCNPX (Monte Carlo N-Particle eXtended), trying to determine whether a LWR could maintain criticality between refuelings while at the same time recycling actinides from its own spent fuel. The team produced decay profiles for the end-of-life byproducts using ORIGEN 2.2.

A probabilistic model for the lifecycle cost of IMF and FR fuel cycles is under development. Unit costs are being assembled through Organisation for Economic Co-operation and Development/Nuclear Energy Agency publications, published data from the Thermal Oxide Reprocessing Plant (or THORP), and the Advanced Fuel Cycle Cost Basis, which is being assembled by Idaho National Laboratory. The project team has undertaken an assessment of “best case” reprocessing costs, assuming a system of government-owned reprocessing plants, each with a 40-year service life that would reprocess spent nuclear fuel generated between 2010 and 2100. The team has also initiated a literature survey to review previous work on high burnup IMF and FR fuel cycles applicable to burn down of transuranics from LWR-based fuel cycles and disposition Pu from dismantled weapons.

Planned Activities

The project is in its final six months. Results from FY 2009 research were presented at the Global 2009 meeting in Paris and will be presented at the 2010 Physor meeting in Pittsburgh, Pennsylvania.

The team will continue to investigate the use of an IMF-based fuel cycle in LWRs for actinide transmutation and compare this cycle to continuous recycle in a fast breeder reactor. The coming year will focus on an optimization of both fuel cycles from a systems perspective, allowing the fuel cycles to be compared on an even footing. To this end, the team is in the process of developing a simulated annealing wrapper that can be put around both VBUDS and MCNPX so that reactor parameters can be varied. Results should help researchers find optimal reactor configurations that will maximize both actinide burndown over a 100-year time frame and economic viability.

NUCLEAR ENERGY RESEARCH INITIATIVE

Analysis of Advanced Fuel Assemblies and Core Designs for the Current and Next Generations of Light-Water Reactors

PI: Jean C. Ragusa, Texas A&M University

Collaborators: None

Project Number: 07-059

Program Area: FCR&D

Project Start Date: September 2007

Project End Date: May 2010

Research Objectives

Existing light-water reactor (LWR) advanced fuel assembly designs could reduce the plutonium (Pu) inventory of reprocessed fuel. Nevertheless, these designs are not effective in stabilizing or reducing the inventory of minor actinides (MAs). The project objective is to focus on developing LWR fuel assemblies that can efficiently transmute Pu and minimize the MA inventories. This project investigates and analyzes advanced LWR assembly designs with improved thermal transmutation capability regarding transuranic (TRU) elements, especially MAs. Researchers have studied various fuel types, namely high-burnup advanced mixed oxides (MOX) and inert matrix fuels (IMFs), in various geometrical designs that are compliant with the core internals of current and future LWRs. The team is analyzing several fuel pin and fuel assembly designs, as well as neutronics/thermal hydraulics effects. The best-performing designs will be used in three-dimensional core depletion methodology to determine overall transmutation performance in various fuel cycle scenarios. Transmutation efficiency and safety parameters are criteria for ranking the various designs.

Research Progress

The team has analyzed multiple recycling of TRU elements for various concepts of advanced MOX fuel and IMF designs. The in-core and long-term isotopic transmutation/depletion is customarily handled through lattice physics and depletion codes Dragon and Origen. Researchers used Perl to write an automated sequence to generate and study multiple cycles (generations) of the same concept. The sequence should seamlessly link the main computational engines for in-core irradiation and out-of-core decay.
Each fuel assembly (FA) concept is based on the energy equivalence principle between the standard uranium oxide (UOX) FA and the proposed FA. The energy equivalence principle was derived and verified based on public domain data regarding the French experience with UOX/MOX-loaded cores. The proposed FA designs are placed into two broad categories: "homogeneous" designs, which use one type of fuel element, and "heterogeneous" designs, which use two. The homogeneous FA concepts include multiple recycle of various MOX fuels: Pu only, Pu only with americium (Am) coating, Pu+neptunium(Np)+Am, TRU, TRU without curium. The heterogeneous designs are based on the DUPLEX concept: the inner FA zone contains oxide fuels whereas the outer zone contains IMF pins. For oxide fuels, the project team has employed standard UOX and MOX (Pu only) pins. When needed, oxide fuels are enriched in U-235, up to the legal constraint of five weight percent (w/o), to maintain cycle length. Some concepts rapidly violate the U-235 enrichment constraint or void coefficient safety limits as the number of cycles increases. To improve neutron moderation in such assemblies, the radius of oxide fuel pins is optimized. For instance, Figure 1 shows the U-235 enrichment required to maintain cycle length

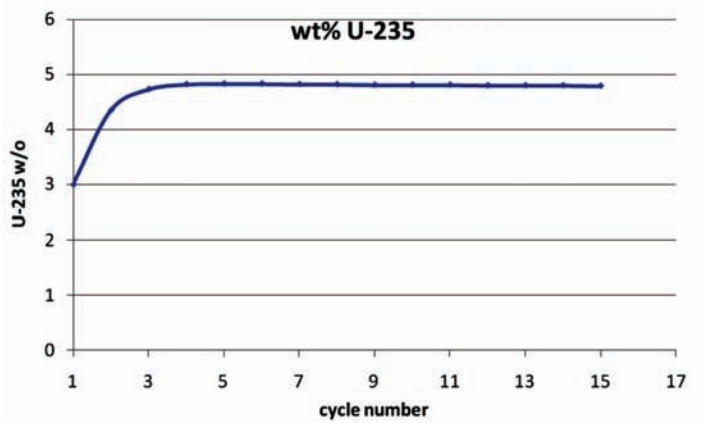

Figure 1. U-235 enrichment required to maintain cycle length for multiple recycling of MOX (TRU) fuel.

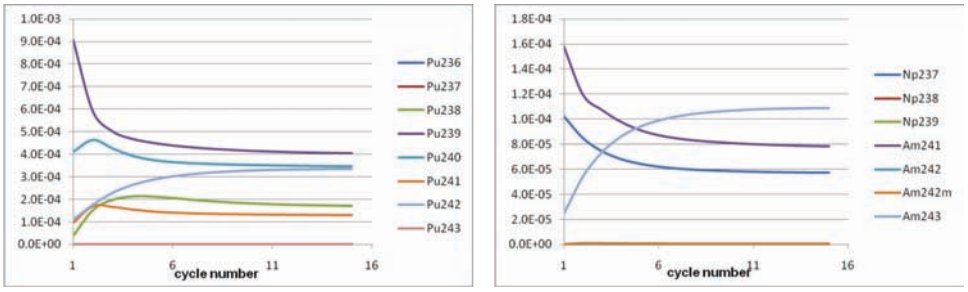

Figure 2. End-of-cycle concentrations of Pu, Np, and Am for recycled MOX (TRU) fuel.

for a FA based on MOX (all TRU) pin type as a function of the recycling number. Figure 2 shows the end-of-cycle concentrations of Pu, Np, and Am for recycled MOX (TRU) fuel.

Shown below (Figure 3) are the maximum fuel centerline temperatures in the core versus burnup for each of the following cases:

- Conventional 4.9 percent enriched uranium oxide (UO_2) (core power = 3,120 megawatts [MWt])
- 4 percent Pu, 3.7 percent U-235 MOX (core power = 4,012 MWt)
- 8 percent Pu, 2.3 percent U-235 MOX (core power = 4,012 MWt)
- 12 percent Pu, 0.3 percent U-235 MOX (core power = 4,012 MWt)

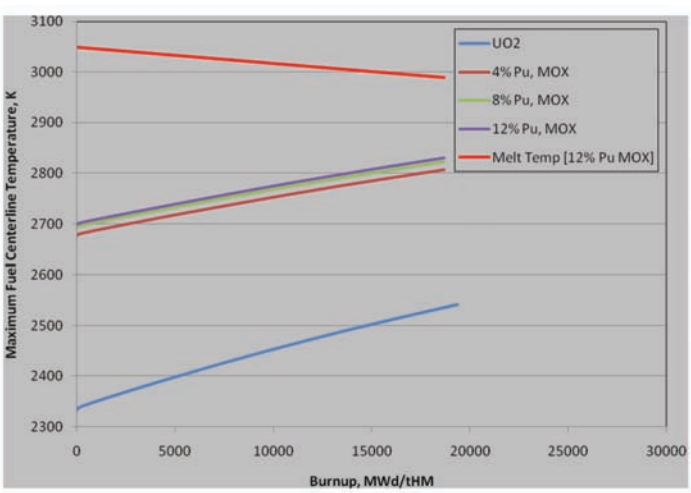

Figure 3. Maximum fuel centerline temperatures in the core versus burnup for four fuel mixes.

The substantial difference in fuel centerline temperatures between the UO_2 fuel and MOX fuels is due to the lower core thermal power for the UO_2 core. The melting temperature for 12 percent Pu MOX also illustrates the fuel melt thermal margin for these assembly designs. The plot covers the first cycle. During this cycle, the assembly has its highest content of fissile material and is located in the hottest section of the core. Therefore, the plot shows the minimum thermal margin during the core lifetime.

Planned Activities

Following is a list of planned activities to be accomplished over the next year (during a no-cost extension):

- Pursue development of advanced MOX (TRU-based) fuel with an optimized pin radius.
- Develop advanced IMF fuel concepts for multiple recyclings.
- Continue modeling fuel pins and assembly concepts.
- Enhance the iterative exchange of information between neutronics and subchannel codes.
- Develop LWR-based fuel cycle scenarios (multiple recycles versus one recycle).
- Assess quantifiable metrics for fuel assembly designs (e.g., long-term radiotoxicity per TWe.h/yr, MA inventories per TWe.h/yr, safety parameters, etc.).
- Pursue evaluation of fuel assembly and core design safety margins.

NUCLEAR ENERGY RESEARCH INITIATIVE

Powder Metallurgy of Uranium Alloy Fuels for Transuranics-Burning Fast Reactors

PI: Sean M. McDeavitt, Texas Engineering Experiment Station

Collaborators: None

Project Number: 07-060

Program Area: FCR&D

Project Start Date: April 2007

Project End Date: March 2010

Research Objectives

Fast reactors are being evaluated as a means of enabling transmutation of transuranic (TRU) isotopes generated by nuclear energy systems. TRU isotopes have high radiotoxicity and relatively long half-lives, making them unattractive for disposal in a long-term geologic repository. Fast reactors are able to utilize transuranic elements as fuel, thereby destroying them while releasing their valuable residual energy content. An enabling technology is the fabrication of metallic fuel containing TRU isotopes using powder metallurgy methods.

The performance of uranium (U) alloy fuels was demonstrated at the Experimental Breeder Reactor-II between 1964 and 1994. One of these alloys, U-10 weight percent zirconium (Zr), was fabricated by injection casting rods from a molten pool of U-Zr alloy. Even though this method is proven and effective, it was accompanied by high material losses due to chemical interactions with quartz casting molds. For the newer TRU-bearing fuel designs, direct melt casting is less practical since americium and, to a lesser extent, neptunium have especially high vapor pressures and cannot be contained in a molten alloy pool at 1200°C to 1500°C. Casting at elevated temperatures under high pressure has been shown to alleviate volatility losses, but this method has not been demonstrated beyond the bench scale, and casting mold losses are still a challenge.[1]

This project is developing powder metallurgical fabrication technologies to produce U-Zr-TRU alloys at relatively low processing temperatures (500°C to 600°C) using a combination of hot extrusion and/or "alpha-phase" sintering. The project team will quantify fundamental aspects of both processing methods. Surrogate metals will be used to simulate the TRU elements. For example, magnesium (Mg) will be used since it has a melting point similar to plutonium's and vapor pressure properties comparable to americium's. If successful, this process will produce novel solutions to some of the nagging issues related to metallic fuels, such as fuel-cladding chemical interactions and fuel swelling, volatility losses during casting, and casting mold material losses.

Research Progress

Two candidate processing pathways are being investigated: 1) hot extrusion between 500°C and 650°C and 2) sintering of alpha uranium with liquid phase enhancements at approximately 650°C. These activities required the design and implementation of a depleted uranium (DU) powder production system. Metallic uranium metal powder is pyrophoric in air and readily oxidizes in relatively inert atmospheres. Therefore, the research team generated an in-house method to prepare uranium metal powder. The powder production system utilized the uranium hydrogen interaction to break down larger pieces of uranium into fine powder. After several iterations, the team built a successful reusable system. The product's nominal size was on the order of one to three microns (μm); a representative image of the powder is shown in Figure 1.

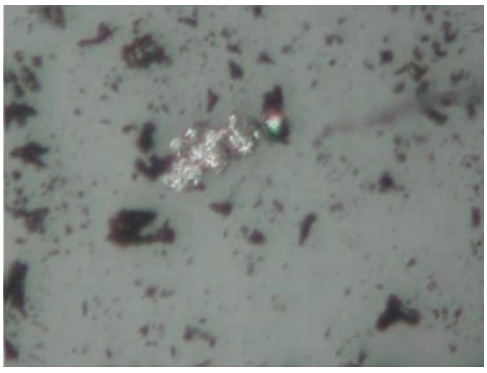

Figure 1. Uranium metal powder; fine particles are approximately 1 μm, and larger particles are 10 to 50 μm.

The uranium powder was pressed into pellets of various compositions: pure U, U-10Zr, U-1Mg, U-10Zr-2.4Mg (all compositions in weight percent). The pellets were heated to 650°C, just below U's alpha-beta phase transition. The Mg compositions represent the equivalent atom fractions representative of 10 and 20 weight percent Pu, respectively. The pellet dimensions were measured before and after heating; *in situ* dimension changes were measured using a linear variable differential transducer (LVDT). Figure 2 shows representative micrographs from the various alloys.

Post-experiment measurement of the pellets proved to be an unreliable indicator of sintering because the pellets cracked during cool-down. The cracking increased the samples' diameters and heights. The cracks occurred in greater frequency along the pellet edges. With the exception of the U-10Zr-2.4Mg pellet, the pellets were slightly conical in shape. The team believes this result to be an artifact of the powder pressing procedure. A greater density occurs on one end of the pellet during pressing and thus leads to gradient in the pellet's sinter rate. The LVDT measurements proved to be extremely sensitive to outside vibration, making a subset of the data inappropriate for analysis.

All pellets showed signs of sintering and an increase in density. The pellets with the greatest densification and lowest porosity were the DU-1Mg and DU-10Zr-2.4Mg. The U-1Mg pellet had a porosity of 14 ± 2 percent. The DU-10Zr-2.4Mg porosity could not be conclusively determined, as the image lacked clearly visible pores. However, the pellet had very few pores, indicating a high degree of sintering. In the DU-10Zr-2.4Mg alloy, large grains of U were surrounded by Zr. This phenomenon was not present in the DU-10Zr pellet; the Zr and DU stayed segregated, indicating that Mg's liquid-phase sintering effects are significant. This implies that the Mg's surrogate nature may be suspect since the binary behavior of Zr-Mg and Zr-Pu are dissimilar.

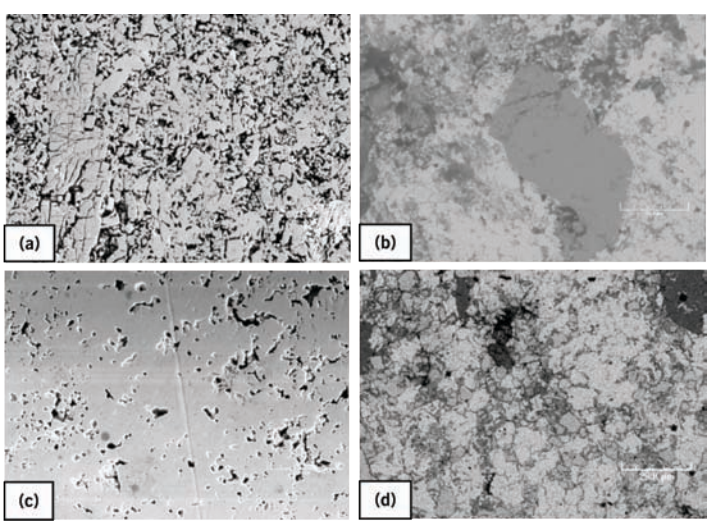

Figure 2. Micrographs of U and U alloys sintered at 650°C for 20 to 24 hours: (a) U metal, (b) U-10Zr, (c) U-1Mg, and (d) U-10Zr-2.4Mg.

The team has established hot extrusion tooling for engineering fabrication of pins. Figure 3 shows the apparatus that will be used to extrude U-10Zr and U-10Zr-2.4Mg alloy pins. Figure 3(a) shows the disassembled apparatus. All of the pieces are made of H13 tool steel, which has high hardness, toughness, and good heat-checking properties at extrusion temperatures (above 600°C). The apparatus is designed such that the die piece is modular and different reductions can be tested. Figure 3(b) shows the apparatus after assembly. The canister with the powder is loaded into the top piece, followed by the ram. A 100-ton press then forces the loaded canister through the die, resulting in the powders fusing into a dense alloy.

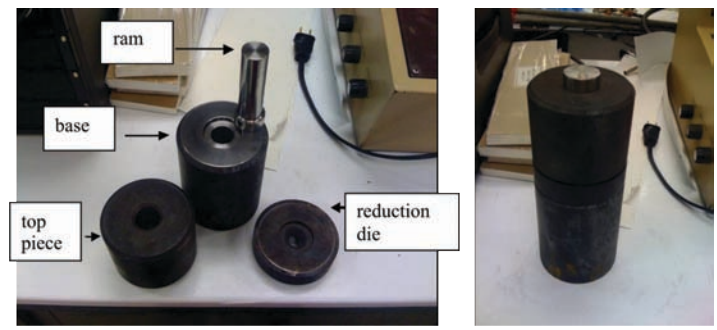

Figure 3. Extrusion punch and die assembly for U-Zr alloy extrusion.

Planned Activities

The team will complete the extrusion described above in spring of 2010. The project will request a no-cost extension to complete this research.

References

[1] D. E. Burkes, R.S. Fielding, and D.L. Porter, "Metallic Fast Reactor Fuel Fabrication for the Global Nuclear Energy Partnership", *Journal of Nuclear Materials 392 (2009)*, 158-163.

NUCLEAR ENERGY RESEARCH INITIATIVE

Neutronic and Thermal-Hydraulic Coupling Techniques for Sodium-Cooled Fast Reactor Simulations

PI: Jean C. Ragusa, Texas A&M University

Collaborators: Argonne National Laboratory, Commissariat à l'Energie Atomique, University of Chicago

Project Number: 07-063

Program Area: FCR&D

Project Start Date: September 2007

Project End Date: May 2010

Research Objectives

The project objective is to develop and implement efficient neutronic-thermal-hydraulic coupling algorithms with application to sodium-cooled fast reactors. This project involves prototyping the following two methodologies: 1) multiphysics coupling paradigms using an operator-split technique that can preserve the accuracy of each physics component and 2) multiphysics coupling paradigms based on Jacobian-free formulations with physics-based preconditioners. The researchers will address the different spatial and time scales found in sodium-cooled fast reactor applications and will apply their methodology to typical anticipated transients without scram.

Research Progress

To assess the inconsistencies of traditional coupling strategies, researchers are developing a test-bed code based on reduced physical models that includes the following physics components: multigroup neutron diffusion, monophasic conservation laws (mass, momentum, energy) for the coolant, and nonlinear heat conduction. This code is used for the following purposes:

- To demonstrate loss of accuracy order due to traditional operator-split techniques used in conventional coupling schemes.
- To implement Jacobian-free full resolution coupling schemes.
- To develop adaptive preconditioning techniques.
- To investigate high-order time discretizations and adaptive time-stepping strategies.

The team plans to implement the best-performing techniques in SHARP (Simulation-based High-efficiency Advanced Reactor Prototyping), the new neutronics/thermal-hydraulics code package for advanced fast reactor analyses. SHARP is based on the UNIC code (neutronics) and the Nek-5000 code (computational fluid dynamics) developed at Argonne National Laboratory (ANL).

A fully implicit coupling paradigm based on the Jacobian-free Newton-Kylov (JFNK) has been set up for nonlinear physics multiphysics applications. The computer code developed serves as a test bed code for methods development and contains the following features:

- State-of-the-art computer science toolbox and libraries for efficient spatial discretizations, handling and interfacing of the various physics components, fast and robust linear algebra for parallel computing platforms. Some of the supporting libraries include PETSc (linear and nonlinear algebra), LibMesh (finite element spatial discretization), SLEPc and Arpack (eigensolvers), Gmsh (mesh generation), ParMetis (mesh partitioning), and VisIt (results visualization).
- Coarse grain physics models for rapid testing and verification; finer grain models can replace the existing ones in a straightforward fashion through the common C++ interface.

Nonlinearly coupled neutron diffusion and heat conduction were solved in the JFNK framework. Researchers obtained results using third-order methods in space and time, yielding the theoretically expected convergence rates of three in space *and* time, demonstrating that fully implicit multiphysics coupling schemes can preserve the theoretical

convergence order. These results open the way for more efficient multiphysics simulations in reactor analysis and design. Code verification for large-scale nonlinearly coupled multiphysics simulations has also become a major focus of this research. Through extensive use of the method of manufactured solutions (MMS), the team has successfully verified accuracy of various multiphysics simulations. Figures 1 and 2 present sample results for a specific situation. Figure 1 shows the spatial discretization and the thermal flux. Figure 2(a) presents the reference power level and core average temperature. Figure 2(b) shows a zoomed plot at the local of the power peak; the resolution entailed various operator-split (OS) schemes and various tightly coupled schemes (JFNK-based). Time-step sizes forty times smaller were required to avoid divergence of the OS-based schemes, demonstrating that tightly coupled schemes can be effective in obtaining high-fidelity answers for multiphysics simulations.

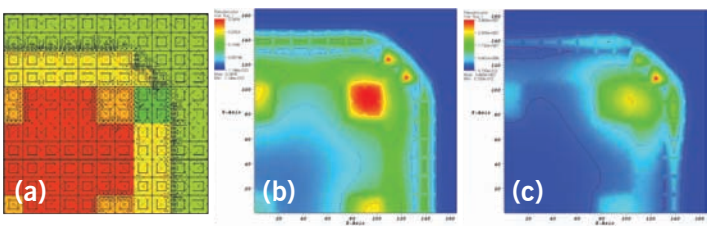

Figure 1. "Two-dimensional super-prompt-critical transient benchmark" (ANL Benchmark Problem Book ANL-7416): (a) spatial mesh, (b) thermal flux at t = 0 seconds and (c) t = 3 seconds.

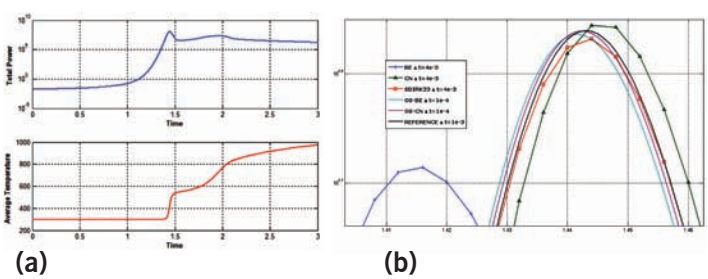

Figure 2. "Two-dimensional super-prompt-critical transient benchmark" (ANL Benchmark Problem Book ANL-7416): (a) reference power level and core average temperature versus time and (b) peak power levels with various coupling schemes.

Planned Activities

Following is a list of the anticipated tasks for the upcoming year:

- Complete development of the following: 1) the test-bed code for technique testing, which will include a flexible implementation to model both OS coupling and full-resolution coupling techniques; 2) Jacobian-free techniques with adaptive preconditioners (i.e., a mechanism to switch between various degrees of representation for off-diagonal terms by recognizing that not all instants in a transient simulation need highly accurate preconditioners for the nonlinear terms); and 3) adaptive time-stepping algorithms.
- Develop a few transient scenarios representative of a sodium-cooled fast reactor (excluding the effect of moving meshes).
- Analyze the effect of multi-mesh coupled simulations on overall accuracy; such situations are typical of coupled simulations, in which each physic component is solved on a specific mesh and can introduce inaccuracy. Address the effect of moving meshes.
- Perform a critical analysis of various techniques: 1) OS versus Jacobian-free, 2) preconditioners, and 3) time-stepping strategies based on several transient runs.
- Down-select and recommend methods to be implemented in the interface code of SHARP; these methods will drive the coupled neutronic/thermal-hydraulic simulations using UNIC/Nek.

NUCLEAR ENERGY RESEARCH INITIATIVE

Fundamental Studies of Irradiation-Induced Defect Formation and Fission Product Dynamics in Oxide Fuels

PI: James Stubbins, University of Illinois

Collaborators: Argonne National Laboratory, Los Alamos National Laboratory, Oak Ridge National Laboratory

Project Number: 07-064

Program Area: FCR&D

Project Start Date: May 2007

Project End Date: April 2010

Research Objectives

This project will address performance issues of oxide-type nuclear fuels in proposed fast-spectrum reactors. Studying radiation effects and fission product transport processes in oxide-type nuclear fuels will establish a fundamental understanding of fuel performance. Researchers will model irradiation effects in cerium and uranium oxide (CeO_{2+x}, UO_{2+x}, and $[CeU]O_{2+x}$) surrogate fuels, comparing their performance with mixed oxide (MOX) fuels. The irradiation effects will be induced by ion implantation over a range of energies and doses to simulate the effects of fission product damage. The project team will also examine transport and trapping of simulated fission products. Researchers will use inert gas ions such as krypton (Kr) and xenon (Xe) for ion implantation experiments to cause irradiation damage; the ions will also be used for dynamic transport studies to understand trapping and defect mobility processes in these fuel forms. The team will also examine ions that simulate fission products and can substitute for U or Ce atoms in the oxide structure.

The experimental studies will be complemented by modeling using molecular dynamics (MD) simulations of damage cascades in the oxide lattice and kinetic Monte Carlo (kMC) to study defect dynamics. The MD approach is useful in understanding the early stages of damage during energetic displacement cascades under irradiation; kMC is useful for using the defect configuration energies from MD to examine defect and fission product transport mechanisms.

Research Progress

The research effort during the second full year focused on both gathering experimental data to benchmark the models and further developing the modeling capabilities.

Researchers have studied defect evolution (formation and agglomeration) under ion irradiation. Both *in situ* and *ex situ* xenon (Xe)/krypton (Kr) ion irradiations were carried out on pure CeO_2, as well as lanthanum (La)-doped CeO_2 thin films grown on strontium titanate (STO) substrates. The team has investigated the growth of void and bubble structures by the mechanisms of both thermally activated migration and irradiation-induced point defect mobility. A thorough exploration of parameter space is now being carried out. Current results are demonstrated in the graphs on the following page.

The team used a simulated radar image modeling (SRIM) simulation package to calculate projected ion ranges. Researchers employed a range of ion energies so that they could control the peak damage region and level of Kr/Xe implantation. Energy dispersive spectroscopy (EDS) analyses were done to measure the presence of Xe and Kr in the irradiated thin film. Figure 1 shows some results for the CeO_2 irradiated/implanted with 150-kilo-electron-volt (keV) Kr ions at 600°C.

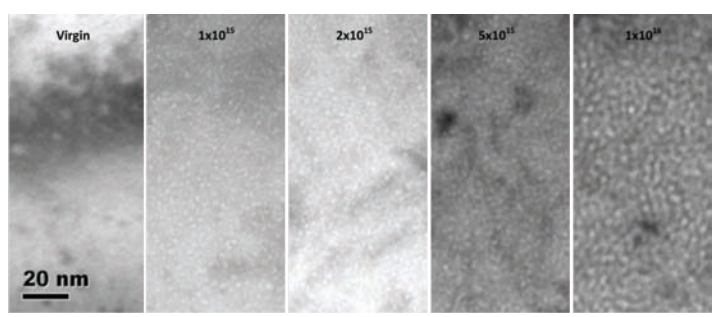

Figure 1. Bright-field images show the sequential change of Kr bubbles with the increase of dose (ions/square centimeter) at 600°C. These micrographs are taken by underfocusing the objective lens.

At higher implantation energies, the team used a combination of EDS and transmission electron microscopy (TEM) techniques. Some structures registered with either inverse contrast with the under/overfocusing techniques or z-contrast with the scanning tunneling electron microscopy (STEM) techniques. These structures were shown to be voids in the case of 1-mega-electron-volt (MeV) Kr irradiations and Xe bubbles in the case of 700-keV Xe irradiations (see Figure 2). There is clear evidence that Xe bubbles have a certain level of mobility allowing them to agglomerate, becoming bigger bubbles. These experiments show a resulting decrease in density. The *in situ* irradiations have generated consistently higher density than *ex situ* irradiations. This may be explained by the much larger free surface area when the specimens were irradiated. These results provide significant benchmarking data to validate either kMC simulations or rate theory-based meso-scale models.

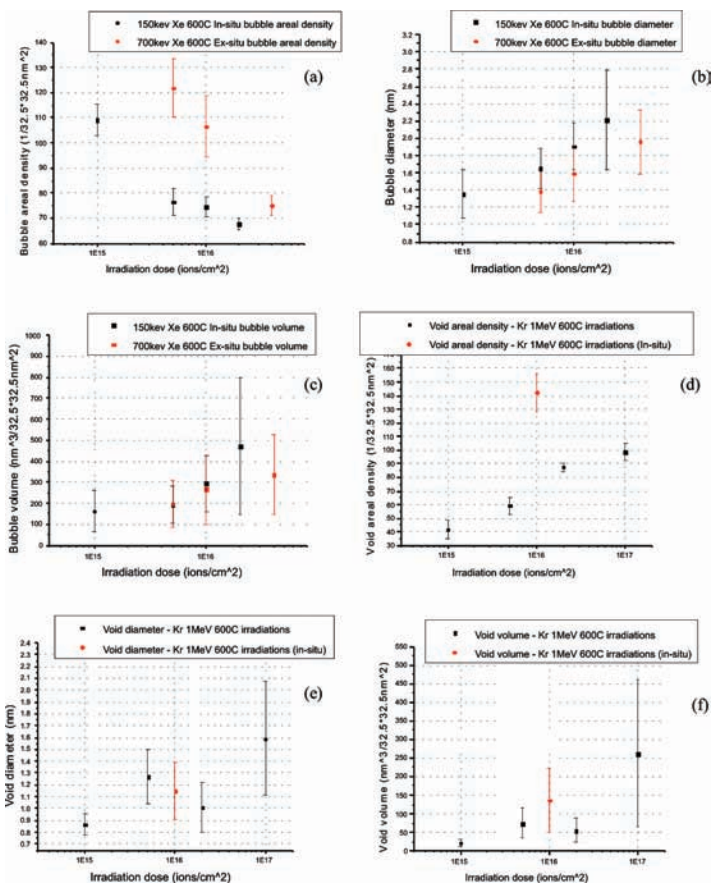

Figure 2. Ion irradiation effects in the growth of bubble/void structures in 5-percent La-doped CeO_2 thin film irradiated with 700 keV Xe (a, b, and c) and 1MeV Kr (d, e, and f) ions at 600°C. Areal density is shown in (a) and (d), bubble/void diameter in (b) and (e), and bubble/void volume in (c) and (f). The statistical survey of bubble/void density and diameter of each data set contains measurements of 5 different areas of 32.5 by 32.5 nanometers (for density) and 100 bubble/void structures (for diameter) to yield statistically meaningful results.

The kMC code has been further developed to include modeling capabilities of the La-doped CeO_2 materials system. The research team is constructing point defect interactions and defect clustering models, which they will test in the near future.

Planned Activities

This project will be extended into a fourth year because of a funding delay. During the next year, the team will use experimental data generated to date to benchmark the kMC modeling work. Researchers will continue to explore the parameter space of bubble/void growth under irradiation. They will run experiments on 25-percent La-doped CeO_2 and compare results to those of pure CeO_2 and 5-percent La-doped CeO_2. This comparison will provide information about the interaction of defects and bubble/void structures with impurity species. As La is one of the fission fragments, the experimental results will provide valuable data from an engineering perspective. The team will fabricate UO_2 films and examine them for radiation effects in ion beam irradiations, comparing the results with CeO_2 system models. Modeling impurity species in the nuclear oxide fuel systems will be the next step in developing modeling capabilities.

Researchers will carry out ion irradiations at the lower end of irradiation doses. The results will provide information about the fundamental defect chemistry, formation, and growth of dislocation loops and dislocation networks. To model evolution of extended defect structures accurately, knowledge of the basic defect chemistry is crucial. This understanding will provide significant insights to the model being constructed with the kMC transport code.

NUCLEAR ENERGY RESEARCH INITIATIVE

Identification and Analysis of Critical Gaps in Nuclear Fuel Cycle Codes Required by the SINEMA Program

PI: Adrian Miron, University of Cincinnati

Collaborators: Idaho State University

Project Number: 07-071

Program Area: FCR&D

Project Start Date: July 2007

Project End Date: September 2009

Research Objectives

The research objectives of the project are to 1) carry out a detailed review of the existing codes describing aspects of the nuclear fuel cycle (NFC) and 2) identify the research and development (R&D) needs required to develop a comprehensive model of a global nuclear energy infrastructure and associated NFCs. Researchers will also recommend appropriate computer codes for integrating into the Simulation Institute for Nuclear Enterprise Modeling and Analysis (SINEMA), the simulation network that will model the global nuclear energy infrastructure, associated fuel cycles, and components. SINEMA will provide an integrated toolbox to support the global and domestic assessment, development, and deployment of nuclear energy systems at various levels of detail. The plan is to implement SINEMA using interconnected and interactive pyramid architecture.

The project will accomplish the following three primary tasks:

- Develop a detailed review of NFC codes:
  - Develop appropriate questionnaires and typical letters to be submitted to code developers and their organizations.
  - Conduct a systematic and detailed review of domestic and international NFC codes.
  - Develop a relational database.
- Identify R&D needs and gaps in NFC computer codes.
- Identify the best code packages to be linked within the SINEMA framework.

Research Progress

University of Cincinnati, in collaboration with Idaho State University, carried out this research in support of advanced fuel cycle systems analyses. This research provides deliverables that are of complementary value to larger and more global efforts of this type, such as the SINEMA program, formerly managed at Idaho National Laboratory. The project successfully accomplished all its initially identified objectives.

First, the project team carried out a detailed review of the existing codes describing various aspects of the NFC. The review covered both domestic and international nuclear engineering codes, from top-level, nuclear enterprise models down to system, component, and micro-scale models. The codes were assessed through a systematic approach that focused on their input/output (I/O) parameters but covered other aspects such as functional and design requirements, method of solution, strengths and weaknesses, computer language and platform, capability to link with other codes, etc.

Two main avenues were established for achieving the NFC code review: internet research and literature research. Researchers also had intensive correspondence with code authors or contact points.

The internet research included all U.S. national laboratories; appropriate domestic, international, or foreign organizations; and universities with nuclear engineering programs. The team identified important internet resources on NFC codes and procedures for obtaining them, along with their documentations. This avenue produced the most results in terms of identifying codes of interest for this research.

Among other resources, researchers utilized the Radiation Safety Information Computational Center (RSICC), maintained by the Oak Ridge National Laboratory, to obtain information on nuclear industry codes. This search led to intensive correspondence with code authors or contact points, which resulted in most of the relevant data. This avenue also produced expected results for some codes developed by national laboratories or found in the literature.

While literature review revealed only a few new NFC codes of interest for this research, this activity showed that most of these codes focused on very specific applications and are thus limited in scope. Combinations of codes are usually used and reported in literature to broaden the scope of research. This review also showed the researchers' preferences for several codes or code combinations for NFC studies.

Universities developed several NFC codes pertinent to this research, and pertinent information on these codes was readily obtained. Obtaining relevant information, in particular codes' I/O parameters, was more challenging within the nuclear industry, potentially triggering issues of intellectual property and proprietary information.

Finally, the NFC code review resulted in 76 codes of interest, of which the team obtained complete or partial information for 52 NFC codes. This research confirmed the existence of 22 other NFC codes for which no I/O information was obtained for various reasons. In addition, two codes are obsolete versions of other codes and are represented in the database only by name. Per the project work scope, the database includes no thermal hydraulics codes except for several that are widely used by the nuclear engineering community.

The project compiled the NFC code information in a flexible and easy-to-update relational database. The database allows for various searches on various codes' properties, including I/O parameters, which were the project's focus. This database represents the first and only modern organization of information on existing NFC codes.

The relational database made possible the design of queries to identify R&D needs for a comprehensive model of the global nuclear energy infrastructure and the associated NFCs. This investigation represented the second research objective. The following statements are general conclusions on the team's findings:

- Most of the codes found were initially developed 20 or 30 years ago, and just a few are undergoing periodic updates. The tremendous progress in computing power should enable creation of a framework to comprehensively model the NFC at a level of detail established by the potential user. This R&D aligns perfectly with SINEMA's vision.
- With the exception of the current top-level NFC codes, very few codes are concerned with the front or back end of the cycle. Most codes found deal with in-core fuel management and reactor design. While the NFC's front end may be easily modeled, a reprocessing code is critical for NFC studies of a closed cycle. A reprocessing code is/was under development at INL. However, detailed information on this code may be hard to obtain because of proprietary and/or security concerns.
- Very few codes may be used for fast reactor design or to accommodate other advanced NFCs, such as a thorium cycle. Again, such codes are key to studies of advanced and closed NFCs.

The third project objective was to identify and recommend codes to be linked within the SINEMA framework architecture. The research showed that linking codes from one NFC category to another was not possible because not enough codes exist in each category.

Researchers also developed several questionnaires and template letters that were submitted to code developers and their organizations. One of the questionnaires included the required information on the NFC codes, while the other was created to gather information about the all NFC codes researchers worldwide have ever used, along with the relevant problem. The second questionnaire was to serve as a check that all pertinent NFC codes were considered.

The project team designed and developed a website for this project. The site has the capability to fill in the questionnaires online and includes other information about this project, such as the project description contact information for the project team, progress reports, and useful links. The website helped us achieve the required consistency for the NFC code review and provided a professional, formal, secure, and fast means of communication with potential collaborators. Finally, links to the database and various pre-programmed queries on its NFC codes were embedded in the web page.

In addition, partial results of this research were presented at the 2009 American Nuclear Society Conference in Atlanta, Georgia, as well as in front of nuclear engineering students and faculty at several universities.

Planned Activities

The project was successfully completed, after a three-month no-cost extension, on September 31, 2009.

NUCLEAR ENERGY RESEARCH INITIATIVE

Fission Time Projection Chamber Project

PI: Dr. Nolan E. Hertel, Georgia Institute of Technology

Collaborators: Abilene Christian University, California Polytechnic State University, Colorado School of Mines, Idaho National Laboratory, Lawrence Livermore National Laboratory, Los Alamos National Laboratory, Ohio University, Oregon State University

Project Number: 08-014

Program Area: FCR&D

Project Start Date: October 2008

Project End Date: October 2010

Research Objectives

The Neutron Induced Fission Fragment Tracking Experiment (NIFFTE) program has been under way for nearly two years. The program's mission is to measure fission cross sections of the primary fissile materials (uranium and plutonium isotopes: ^{235}U, ^{239}Pu, ^{238}U) and, eventually, the minor actinides across energies from approximately 50 kilo-electron volts (keV) up to 20 mega-electron volts (MeV). The program aims for an absolute uncertainty of less than one percent while investigating energy ranges from below 1 eV to 600 MeV. Fast, resolved, and unresolved resonance regions in plutonium and other transuranic elements bear large uncertainties, and these dominate power plant safety margins.[1]

These basic nuclear physics data are being reinvestigated to support next-generation power plants and a fast burner reactor program. This data will support all aspects of the projected nuclear renaissance by providing improved nuclear cross-section data. Reducing uncertainties in these fission cross sections will reduce uncertainties in power peaking, transmutation rates, criticality levels, neutron lifetimes, and many other reactor parameters in modeling efforts. Such efforts are key, as the nuclear community will assess future reactor designs' performance largely through simulations. Therefore, reducing uncertainties in fundamental properties will, in turn, reduce the safety margins currently built into reactor designs.

The measurement program utilizes a time projection chamber (TPC) to measure these cross sections with improved accuracy. Traditional fission cross-section measurements are typically relative to the cross sections of ^{235}U. The TPC project, on the other hand, uses the hydrogen cross section as its reference, and time-of-flight techniques are used to determine neutron energies. The hydrogen cross section is smoothly varying and is well known at the energies of principal interest in fission reactor design.

Research Progress

A number of different components combine to produce this fission cross-section measurement device.

Mechanical System. The mechanical system consists of the pad plane readout system, a micromegas gas amplification system, the pressure vessel, and the shroud that covers the TPC. In the project's first year, conceptual ideas were turned into computer-aided design (CAD) drawings, which were later improved. During FY 2009, the project team constructed and bench-tested these pieces. Figure 1 provides a photograph of the shroud, a field-programmable gate array (FPGA) card, an analog preamp card, the completed field cage micromegas, and the cathode pad plane.

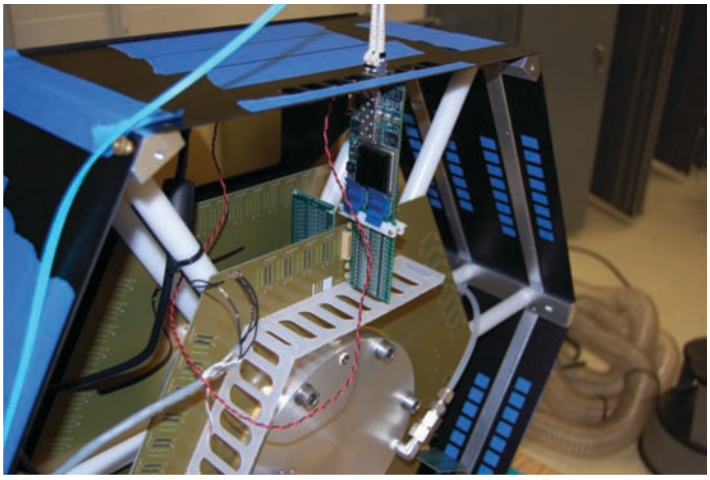

Figure 1. The TPC with the electronics used for the first data gathering. The preamp card attaches to the gold cathode pad plane. The EtherDAQ (data acquisition) card attaches to the top of the preamplifier card. An optical cable connects the EtherDAQ card to a computer for read-out. The black shroud is part of the electromagnetic shield and cooling system (the face is removed for viewing). The openings in the shrouds for cabling are covered with blue tape to prevent direct access to high-voltage components during testing.

Simulations and Mock Data Challenge. To guide the TPC's operating parameters, the team designed a mock data challenge to test the analysis tools. The team simulated a complete data set, beginning with neutron creation in the spallation target and ending with ionization tracks due to neutron-induced fission fragments in the fill gas. Researchers then converted the ionization tracks to the digitized signals that will be TPC output. These signals were then saved and analyzed by the track reconstruction software. The team used this mock data challenge and its associated simulations to further optimize the TPC operating parameters and to improve the pointing resolution of the track fitting algorithms. Figure 2 shows a comparison between these simulated data and real data taken with the TPC.

Analog/Digital Card Readout. An integral part of the TPC is the high-density channel readout system. The team designed and fabricated two unique system components: the analog preamplifier and the digital boards. The analog preamplifier board collects 32 channels of analog data, routes them through an independent preamplifier with a 9,000-to-1 signal-to-noise ratio, and sends them to the digital board. The digital board consists of 32 analog-to-digital converters, a FPGA, memory banks, and a fiber optic 1-gigabyte-per-second Ethernet controller.

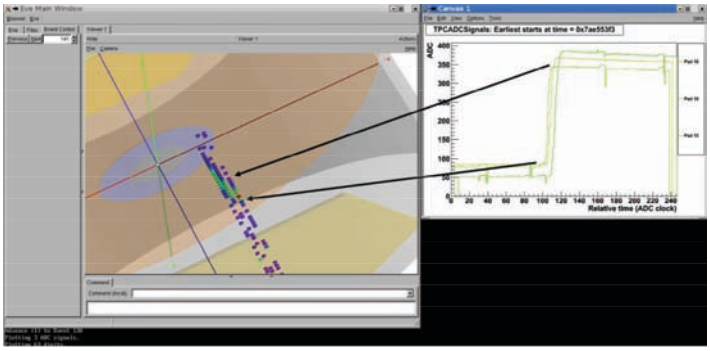

Figure 2. Event display showing the raw TPC waveforms along with their corresponding differentiated digits from run 100000001 (December 10, 2009, 09:26).

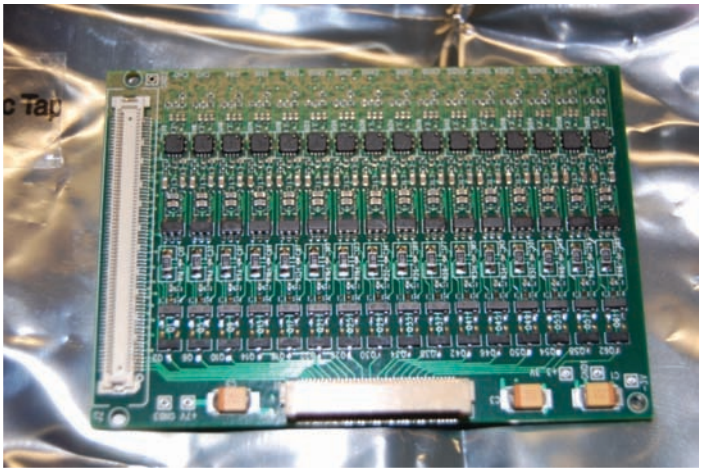

Figure 3. A fully loaded 32-channel preamp for the fission TPC.

Target Preparation. TPC targets differ from standard fission foils in the quality, purity, and uniformity of the necessary deposited material. In addition, an ultra-thin carbon backing is deposited on the targets. The project has prepared such targets in a number of configurations, including segmented targets containing different actinides and a californium-252 (^{252}Cf) spotted target for TPC calibration. Figure 4 provides pictures of a target.

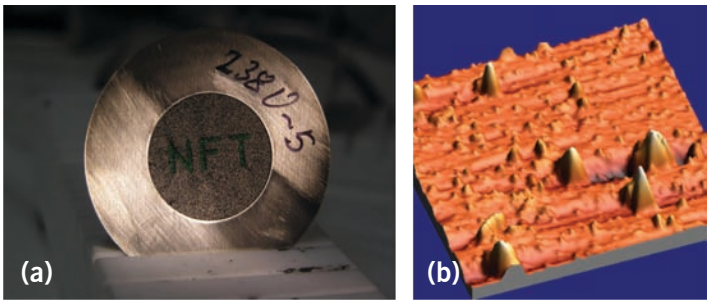

Figure 4. (a) A target with the letters NFT created from uranium. Such targets are used to check the detector's pointing resolution. (b) An atomic force microcroscopy (AFM) image of the foil surface shows very high uniformity.

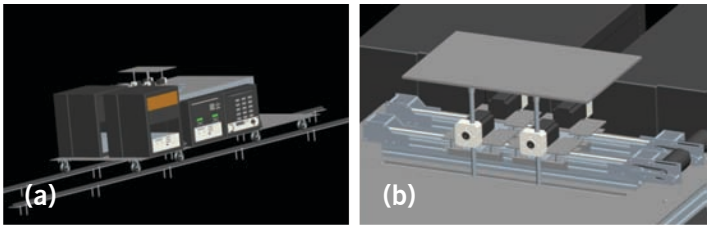

Figure 5. (a) A CAD drawing of the TPC stand. The stand rolls along the beam axis using casters on a rail system. (b) A close-up of the stand's (x,y) positioning table, which holds the TPC.

Beam Line Infastructure. To obtain high-quality measurements, researchers have devoted much time to optimizing the flight path and beam line infrastructure. This effort includes quantification and minimization of room-returned and air-scattered neutrons, as well as collimator design. The team also designed the TPC stand, which includes a three-axis positioning system and the electronics required to operate the TPC (Figure 5).

Planned Activities

The TPC will begin acquiring data in the upcoming year; one sector of one sextant is already populated. The first fission measurements, using a ^{252}Cf source, are scheduled for early in the year. The hydrogen standard work will be used to calibrate the TPC for cross-section ratio measurements. Researchers will quantify the scattered and direct radiation fields with the new collimation and final TPC configuration. The project plans to complete ^{235}U-to-^{238}U fission cross-section ratio measurements by the end of the fiscal year. Data analysis will continue after the project's end date. A no-cost extension will be sought to finish the data analysis and additional measurements.

NUCLEAR ENERGY RESEARCH INITIATIVE

Risk-Informed Balancing of Safety, Non-Proliferation, and Economics for the Sodium-Cooled Fast Reactor

PI: George Apostolakis, Massachusetts Institute of Technology

Collaborators: Idaho State University, Ohio State University

Project Number: 08-020

Program Area: FCR&D

Project Start Date: October 2007

Project End Date: October 2010

Research Objectives

The project objective is to develop risk-informed design and evaluation tools for the sodium-cooled fast reactor (SFR) that take into account safety, economics, licensability, and proliferation resistance. The research team will apply these tools to a number of design alternatives, identifying opportunities to reduce the SFR's cost while maintaining its high level of safety and proliferation resistance. Examples of proposed design variations include increasing the core outlet temperature and employing alternative thermodynamic cycles.

The resulting risk-informed methodology will help develop technical requirements for industrial design organizations, identify research needs, assess the technology risk of alternatives, and assist with planning. Industrial groups can use this methodology to perform design tradeoffs that would make the SFR economically competitive and licensable, yet still safe and proliferation-resistant.

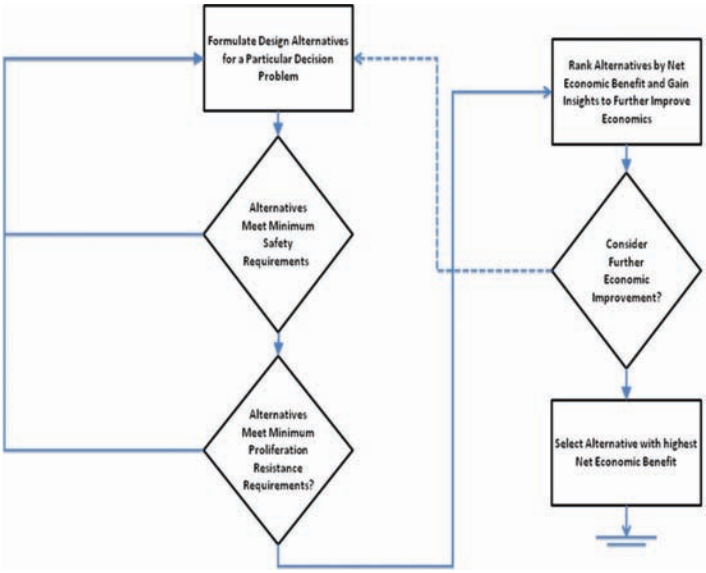

Figure 1. Decision-making methodology.

Research Progress

Methodology Overview. Figure 1 shows the overall methodology. The project team determines whether a design alternative satisfies the safety and non-proliferation requirements. Project researchers are not attempting to optimize these; the focus is on each alternative's economic benefit.

The Technology-Neutral Framework. Safety requirements are determined by the Nuclear Regulatory Commission's (NRC's) Technology-Neutral Framework (TNF), described in NRC regulation NUREG-1860. The TNF proposes a risk-limit curve (frequency-consequence [F-C] curve, with C as dose) that must envelop risk for the complete spectrum of conceivable accidents. Using this concept of acceptable risk, the designer's objective function would be to develop the minimum-cost system that satisfies the F-C curve.

The TNF requires that event sequences called licensing basis events (LBEs) be used to determine whether the F-C curve is satisfied. The project team has developed functional event trees to identify generic LBEs. The safety functions that serve as top events in the trees are (in order of appearance) shutdown, fuel heat removal, primary heat removal, and late shutdown. The accident initiators modeled are small reactivity insertion, medium reactivity insertion, large reactivity insertion, local flow blockage, loss of offsite power, loss of flow, shutdown transients, large steam generator leak, small seismic, medium seismic, and large seismic.

The last major element of furthering the use of the functional event trees is assigning consequences to each sequence according to the damage expected from each LBE. Each release category from PRISM (composite

application guidance software) has been assigned to a generic release category, and each advanced liquid metal reactor (ALMR) damage category has been assigned to a generic release category.

Unprotected Transient Overpower. Researchers created a SFR model in accordance with RELAP (government codes) to calculate the conditional clad failure probability for various accident sequences. Even though the unprotected transient overpower (UTOP) initiating frequency falls below the F-C curve cutoff, SFR analysis focuses on this unprotected transient. The UTOP study indicated that assumptions on mission termination time significantly affect the likelihood of clad failure in a metal-fueled SFR, but those assumptions are irrelevant under the TNF as all UTOPs' initiating frequencies are less than the F-C cutoff (10^{-7} per reactor year). Thus, UTOPs do not impose any design constraints. However, the techniques outlined here may be useful in determining design limits for other accident scenarios.

Safety Analysis. The project team will perform integrated analysis of severe accident sequences with a combination of computer codes SAS4A and MELCOR. RCS, a routine that is currently under development, provides an interface between the two codes. The team is performing detailed uncertainty with the coupled computer codes to demonstrate an improved approach to performing uncertainty analyses for transient safety analyses.

The conceptual design stage does not warrant detailed transient analyses for every design alternative for a broad spectrum of accident scenarios. For this reason, researchers have developed a set of generic consequence categories with associated ranges of accident consequences. These generic results can be used in design tradeoff studies to assess a design alternative's ability to satisfy the TNF limit curve.

Economic Assessment. Several design alternatives were suggested using risk-based methods, and the team is determining the designs' potential economic benefits. The main focus is on the containment issue, determining how rugged a structure must be to meet TNF standards and other regulatory guidelines. Extensive work has been done to show that energetic events will always fall below the threshold for consideration under the TNF (10^{-7} per reactor year). As a result, the traditional dome-like containment structure may not be required as a pressure-retaining structure. Instead, the design can be focused on radionuclide containment at lower pressures, maybe as low as five pounds per square inch, gauge (psig). This smaller and less rugged containment would lead to considerable savings in construction costs—as much as five percent of the reactor's total direct capital costs in the ALMR reference model.

The project team also reviewed applicability of NRC guidelines on aircraft impacts to determine possible implications on containment design requirements. The actual standards and requirements are not clearly defined, but further study may help to clarify relevant requirements.

Non-Proliferation Activities. The purpose of this year's work has been to identify realistic scenarios, subject to current safeguards efforts, to be used in evaluating the probability of proliferator success at various facilities of interest. The following list shows activities in this area:

- Devising scenarios for diversion of weapons-usable materials, misuse of the nuclear energy system's facilities, and abrogation scenarios.
- Positioning of the tree scenarios of interest within the probability-consequence criterion curve used to describe the acceptable limits, in terms of proliferation resistance, for the selected designs.
- Selecting design alternatives within the SFR fuel cycle and adding selected safeguards to decrease the fuel cycle's vulnerability.
- Determining the basic event probabilities involving proliferator tactics via expert opinion.

Planned Activities

For the remaining period of performance, the project team will do the following:

- Evaluate seismic risk.
- Perform containment transport analyses for released radionuclides with the RCS and MELCOR codes.
- Perform containment load analyses for different magnitudes of spray fire with MELCOR and user functions developed from CONTAIN-LMR models.
- Determine the effect on overall SFR efficiency of raising core outlet temperatures and using supercritical carbon dioxide instead of water in the power conversion system.
- Demonstrate the practicality and value of the success tree-based method in proliferation risk assessment.
- Evaluate the basic event probabilities in the success trees via expert opinion.
- Create consensus acceptance criteria for proliferation risks.

NUCLEAR ENERGY RESEARCH INITIATIVE

Deployment of a Suite of High-Performance Computational Tools for Multiscale Multiphysics Simulation of Generation IV Reactors

PI: Michael Z. Podowski, Rensselaer Polytechnic Institute

Collaborators: Brookhaven National Laboratory, Columbia University, State University of New York at Stony Brook

Project Number: 08-033

Program Area: FCR&D

Project Start Date: September 2007

Project End Date: September 2010

Research Objectives

The overall project objective is to deploy advanced simulation capabilities for next-generation reactor systems utilizing newly available, high-performance computing facilities. The approach includes the following major components:

- Development of new simulation capabilities for state-of-the-art computer codes (FronTier, PHASTA, and NPHASE) coupled with molecular dynamics (MD)-type analysis.
- Development of advanced numerical solvers for massive parallel computing.
- Deployment of a multiple-code computational platform for Blue Gene supercomputer simulations of sodium fast reactor (SFR) fuel performance during accidents.

Planned project deliverables are:

- Deployment of high-performance computing tools for coupled thermal-hydraulic, neutronic, and materials multi-scale simulations of the SFR.
- Application of the new computational methodology to study reactor fuel and core transient response under beyond-design and accident conditions.

Research Progress

Work progress on the major tasks of the project is summarized below.

Development of a MD-Based Model of Reactor Fuel Properties. Testing of the LAMMPS and MOLDY MD simulation models continued. Both models use the neutron flux and primary knock-on-atom (PKA) method as input. The main objective has been to extend the range of processes which can be analyzed using the combined models.

Another important issue concerned using MD model output as input to micro- and macro-scale simulations based on the continuum approach to fluid mechanics used by FronTier, PHASTA, and NPHASE-CMFD codes.

Model Development for Fuel Rod Heatup and Failure. Work continued on the development of various finite element models implemented in the FronTier code. Three major parts of the overall model are fuel material heatup and melting, cladding failure, and fission gas ejection through breached cladding. Researchers have investigated several modeling issues, such as anticipated modes of cladding failure and different time scales of individual phenomena and their associated time step in FronTier simulations. Figure 1 shows a typical result of the FronTier simulation of fuel material heatup.

Other issues included fission gas transport into the failure zone and evaluation of pressure at the FronTier model's outflow boundary. The latter issue, combined with the evaluation of gas outflow, is a part of the FronTier/PHASTA coupling. Work will continue on both issues.

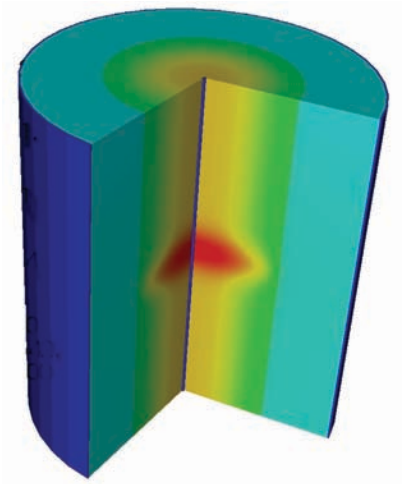

Figure 1. FronTier simulation of a local fuel heatup during a hypothetical loss-of-flow accident in an SFR.

Development of a Model for Fission Gas Injection From a Failed Fuel Element Into the Reactor Coolant Channel. Direct numerical simulation (DNS) model development continued for fission gas injection into reactor coolant channels. The team has investigated several numerical issues associated with modeling high-velocity jet injection through a small opening in breached cladding. In particular, researchers have been studying grid size's effect on accuracy of predicting instantaneous positions of gas/liquid interfaces. Furthermore, the team has investigated the possibility of using adaptive grids to improve computational efficiency. Figure 2 is an illustration, showing PHASTA prediction results.

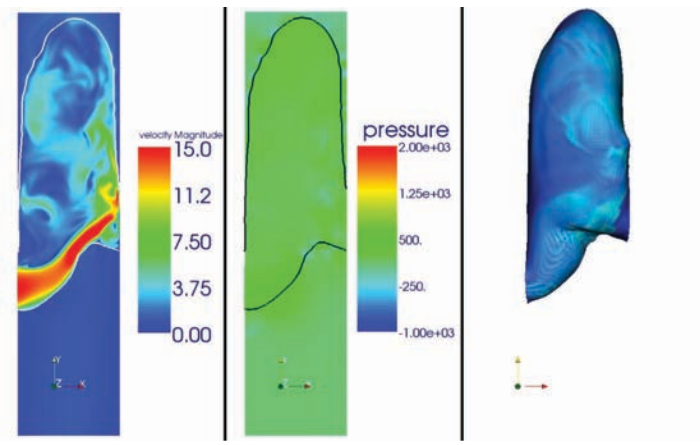

Figure 2. PHASTA simulation of a fission gas jet inside SFR coolant channels.

Another issue concerned development of a PHASTA-based model of bubbly two-phase flows. The main objective has been to develop a methodology allowing one to convert the instantaneous DNS simulations into time-averaged velocity and void fraction distributions, which could be used as references in developing and verifying a multifield model.

Development of a Two-Fluid Model of Gas/Liquid Sodium Interaction in the Reactor Coolant Channel. The project team worked on developing and testing a multifield of fission gas/liquid sodium flow in reactor channels following cladding failure. Figure 3 depicts a typical result of the NPHASE-CMFD simulation of gas/sodium two-phase flow. The initial model has been extended to account for a multi-rod section of a typical SFR coolant channel. The new computational domain has been implemented in the NPHASE-CMFD code.

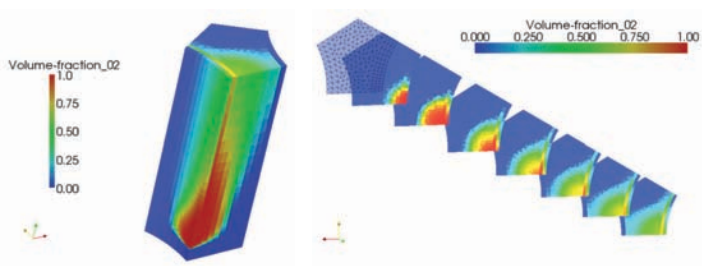

Figure 3. NPHASE simulation of fission gas transport along the failed fuel element of an SFR.

An important aspect of the multifield model development concerns the coupling between the NPHASE-CMFD and PHASTA DNS/Level-Set models. The objectives here are twofold. First, the PHASTA results have been converted into a format which allows them to be used as an input to the NPHASE-CMFD code. Secondly, the team has been working on the formulation of a direct two-way coupling between PHASTA and NPHASE-CMFD.

To accompany work on the last three tasks discussed above, the team continued efforts to develop improved computational algorithms for NPHASE, PHASTA, and FronTier codes. The main thrust is converting the existing algorithms into a fully coupled nonlinearly implicit formulation, which will provide a low-cost means of avoiding operator splitting errors and instabilities.

Selected results of the project work were presented at the 2009 ANS Student Conference in Gainesville, Florida. More recent results were published in the Proceedings of the 13th International Topical Meeting on Nuclear Reactor Thermal-Hydraulics (NURETH-13) and presented at the NURETH-13 conference in Kanazawa, Japan. The project submitted abstracts of three new papers to international conferences to be held in 2010.

Planned Activities

The planned activities for 2010 include the following tasks:

- Complete development of the MD-based model of reactor fuel properties and implement the model on the Blue Gene computer.
- Complete development of the FronTier-based models of fuel rod heatup and failure.
- Formulate a complete model of fission gas injection into a reactor coolant channel following a cladding breach.
- Complete development and numerical testing of the DNS/Level-Set model of fission gas jet dynamics inside reactor coolant channels.
- Complete development and testing of the interface between FronTier and PHASTA.
- Complete development of a parallel-processing version of the NPHASE-CMFD code and implement it on the Blue Gene computer.

- Complete development of an interface between PHASTA and NPHASE-CMFD.
- Implement improved computational algorithms for FronTier, PHASTA, and NPHASE-CMFD to enhance overall computational platform performance.
- Perform multi-scale multiple-code simulations of the progression of a hypothetical fuel-channel-blockage accident in an SFR.
- Present the new results at conferences, and publish the results in conference proceedings and archival journals.

The project expects to request a no-cost extension once the necessary time for the project completion can be properly estimated. In addition to a late start, the project confronted associated difficulties with finding qualified PhD students as research assistants, as well as unforeseen scientific and computational complications associated with solving some of the technical tasks.

NUCLEAR ENERGY RESEARCH INITIATIVE

Real-Time Detection Methods to Monitor Transuranic Compositions in UREX+ Process Streams

PI: Sean M. McDeavitt, Texas Engineering Experiment Station

Collaborators: Argonne National Laboratory, Purdue University, University of Illinois-Chicago

Project Number: 08-039

Program Area: FCR&D

Project Start Date: October 2008

Project End Date: September 2011

Research Objectives

A priority in the nuclear community is developing advanced methods for reprocessing used nuclear fuel. The most prominent method under development is uranium recovery by extraction, or the UREX+ family of processes, which recover uranium, selected fission products, and transuranic (TRU) isotopes for recycle or storage. As the implementation of UREX+ on a real scale (i.e., more than 1,000 tons of fuel per day) approaches over the next 20 years, safeguards strategies, materials control, and accountability methods must be considered.

The objective of this consortium is to develop real-time detection methods to monitor the UREX+ process and to safeguard the separated TRUs against diversion from within a processing facility. The consortium team's comprehensive development strategy incorporates an array of traditional detectors and advanced metastable fluid detectors into a novel assembly designed specifically for application in conjunction with a UREX+ centrifugal contactor array. The development experiments range from laboratory benchmarks to hot-cell demonstrations with real UREX+ spent fuel experiments. Team members will also perform supporting research to develop safeguards strategies for the UREX+ process and to evaluate corrosion behavior of critical component materials in the UREX+ system.

Research Progress

Assembly Design Experiments. The project's major focus is to determine how flow rate and flow geometry affect detector response for real-time detection in a UREX+ process stream. A simple test apparatus has been completed to enable flow-rate sensitivity studies. In this apparatus, dissolved species of selected radioisotopes are circulated at various flow rates and tube-fill levels to generate gamma spectra using isotopes with half-lives ranging from three to sixty days. Stainless steel coils in three different geometries are being studied in the system. The gamma spectra measurements are being made using a three-inch-diameter by three-inch-tall sodium iodide (NaI) detector. The research team chose five radioactive test isotopes to simulate the process flow streams. These are isotopes of chromium (^{51}Cr), rubidium (^{86}Rb), cerium (^{141}Ce), ytterbium (^{175}Yb), and gold (^{198}Au). These isotopes were selected based on their half-lives, gamma energies, and availability in soluble nitrate chemicals. The team produces these isotopes using neutron irradiation of the nitrate salts of the natural elements. Initial tests are nearly complete.

Detector Strategy Development. Project collaborators delivered nine different UREX+3a samples (microcurie [μCi] activities). These samples originate from each interim separation step in the UREX+3a process flowsheet (excluding the TALSPEAK process, in which the lanthanides are separated from americium and curium). The samples were characterized for 10 seconds and 600 seconds with four different gamma detector types: NaI, LaBr, high-purity germanium (HPGe) P-type, and HPGe N-type. In the case of the HPGe N-type detector, researchers also took measurements at 3,600 seconds because it is most likely to be used in a reprocessing facility. This detector has higher neutron resistance and good energy resolution. Figure 1 shows a complete representative 3,600-second spectrum.

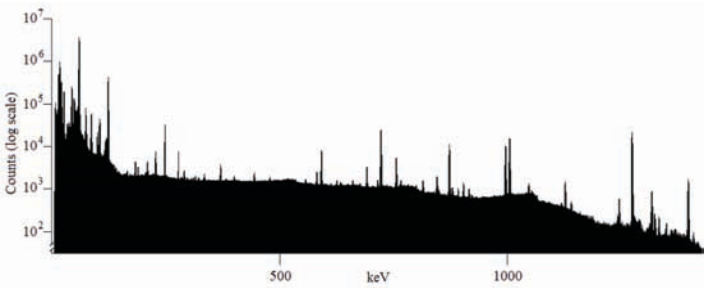

Figure 1. A 3,600-second HPGe N-type gamma spectrum from a UREX+3a sample of spent fuel after extracting strontium, technetium, cesium, and uranium.

The diluted and dried UREX+3a samples used in this study represent most of the processing stages. Several of the actual and simulated gamma ray spectra of the UREX+3a samples were very similar. Based on these results, researchers developed a simple detection strategy (see Figure 2).

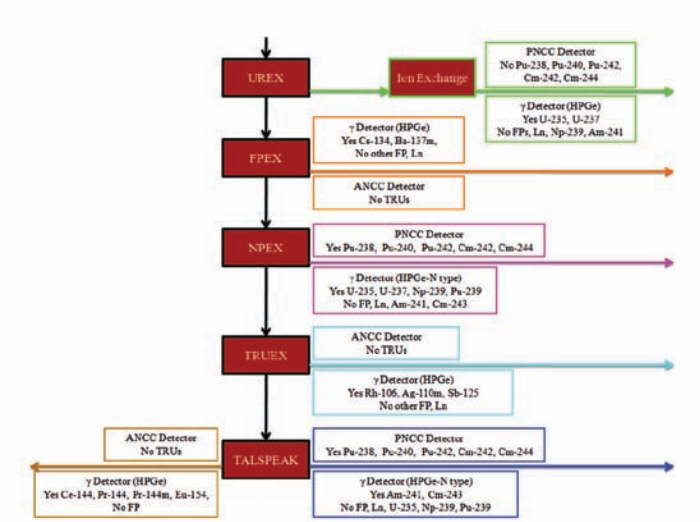

Figure 2. A detection scheme for the UREX+3a process to prevent significant amounts of TRUs from leaving the system through undesired paths.

Safeguards Strategy Development. The team has developed a detailed safeguards approach for a UREX+1a reprocessing facility. The approach includes use of nuclear material accountancy, containment and surveillance, and solution monitoring. Facility information was developed for a hypothesized UREX+1a plant with a throughput of 1,000 metric tons of heavy metal per year. Team members established safeguard goals and measures. Diversion and acquisition pathways were considered; however, the analysis focuses mainly on diversion paths. The detection systems can provide near real-time measurement of special fissionable material in feed, process, and product streams. The team also considered advanced front-end techniques for quantification of fissile material in spent nuclear fuel. If a significant quantity of nuclear material was diverted from the UREX+1a reprocessing facility, these techniques would significantly improve the safeguards system's timely detection of the diversion. Early detection would deter such an occurrence.

Tension Metastable Fluid Detectors. Tension metastable fluid states offer unique potential for radical transformation in radiation-detection capabilities. States of tension metastability may be obtained in tailored resonant acoustic systems, such as the acoustic tension metastable fluid detector (ATMFD) system, or via centrifugal force-based systems, such as the centrifugal tension metastable fluid detector (CTMFD) system. Both these systems are under development. Tension metastable fluid detector (TMFD) systems take advantage of the weakened intermolecular bonds of liquids in sub-vacuum states.

Nuclear particles incident onto sufficiently tensioned fluids can nucleate critical-size vapor bubbles. These bubbles grow from nanoscales and then can be seen, heard, and recorded with unprecedented efficiency and capability. Previous work has shown that TMFD systems can detect neutrons with energies spanning eight orders of magnitude with at least 95 percent intrinsic efficiency; these systems remain insensitive to gamma photons and also provide directional information on the radiation source. Researchers are testing the CTMFD system's ability to detect key actinide isotopes constituting special nuclear materials in spent fuel. The system can detect alpha activity (at nearly 100 percent efficiency) of U isotopes at concentrations of approximately 100 parts per billion. This result is unprecedented and 100 to 1,000 times more sensitive than conventional liquid scintillation spectroscopy. TMFD systems have an inherent capability concerning on-demand tailoring of fluid tension levels allowing for energy discrimination and spectroscopy. This ability appears especially useful in detecting the key U isotopes and other TRU isotopes of plutonium, neptunium, americium, and curium that arise at different stages of nuclear fuel reprocessing (i.e. UREX+).

Corrosion of UREX+ Process Materials. During the past year, the team worked on immersion corrosion tests, static potentiodynamic corrosion, and dynamic electrochemical test set-up. A portion of the results are presented here, highlighting the impact of hydrodynamic effects that may induce erosion corrosion in the UREX+ centrifugal contactors.

In a system where a metal alloy is moving through a corrosive fluid, the leading edge is likely to experience the greatest effect of erosion corrosion. The team is performing light optical microscopy on the leading edges of dynamic corrosion samples. Researchers examine surface irregularities that indicate some form of erosion effect. Researchers exposed coupons to solution of 5M HNO_3

+ 0.1M HF at 1,000 rotations per minute (rpm) for 48 and 96 hours. They then compared the sample surfaces to those of coupons before exposure. Preliminary results are shown in Figure 3. The as-received sample's edges do not show any major disturbances or roughness, while the other micrographs do show edge damage or increased roughness.

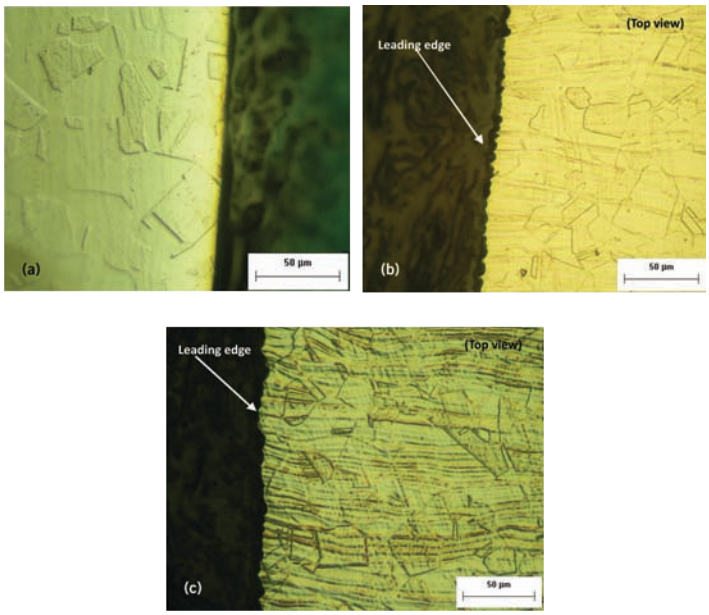

Figure 3. Light optical microscopy of leading edges of coupons, viewed from the top: (a) as-received material, (b) after 48 hours at 1,000 rpm in 5M HNO_3 + 0.1M HF, and (c) after 96 hours at 1,000 rpm in 5M HNO_3 + 0.1M HF. All samples have been electroetched.

The samples in Figures 3(b) and (c) were cross sections obtained from the middle of the corroded samples. Surface topography clearly differs between the corroded and uncorroded samples. Comparing the two corroded samples (48 and 96 hours) shows some significant topographic differences, corresponding to differences in mass losses.

Planned Activities

By the end of the third project year, the proposed detector assembly and detector arrays will be completed, benchmarked, and ready for full-scale application. Activities will include bench-scale testing with simulated and real UREX+ process fluids. In addition, a complete safeguards strategy will be in place to take advantage of the information stream enabled by this new detector system. A corrosion database will be available to enable material selection for superior detector performance. During the coming year, the project team will continue the activities described above to advance this detector concept and demonstrate the safeguards methodologies.

NUCLEAR ENERGY RESEARCH INITIATIVE

Performance of Actinide-Containing Fuel Matrices Under Extreme Radiation and Temperature Environments

PI: Brent J. Heuser, University of Illinois at Urbana-Champaign

Collaborators: Georgia Institute of Technology, South Carolina State University, University of Michigan

Project Number: 08-041

Program Area: FCR&D

Project Start Date: January 2008

Project End Date: September 2010

Research Objectives

The specific objectives of the second year were:

- Commissioning a dedicated growth facility to grow uranium oxide (UO_2) compound thin films.
- Investigating, through experiment, consequences of radiation damage in UO_2 surrogate thin film samples with and without actinide surrogates.
- Implementing first-principle computational algorithms to study radiation damage processes in UO_2.
- Implementing accelerated Monte Carlo computational algorithms to study fission gas bubble behavior in UO_2.

These research objectives encompass the fabrication, modification via ion bombardment, and subsequent characterization of impurity (actinide surrogate/fission gas) segregation/precipitation in thin film fuel matrices. The project seeks to understand radiation's effects on actinide and fission gas transport in nuclear fuel matrices containing actinides within a closed fuel cycle.

Research Progress

Thin-Film Growth Facility. Construction of a dedicated thin-film growth facility is complete (see Figure 1). This facility uses three magnetron sputter guns to co-deposit one or two actinide surrogates (cerium [Ce] and neodymium [Nd] are currently loaded) simultaneously with UO_2, U_3O_8, or U_4O_9 via reactive gas sputtering onto a heated substrate. One radio frequency (RF) and three direct current power supplies drive the sputter guns. Two mass flow control valves regulate a high-purity argon (Ar) plus oxygen (O_2) mixture. System pressure is maintained by a gate valve, which in turn is controlled via a feedback loop with a Baratron capacitance manometer. Figure 2 shows a close-up of the sputter guns during operation. The plasma above the sputter target is visible.

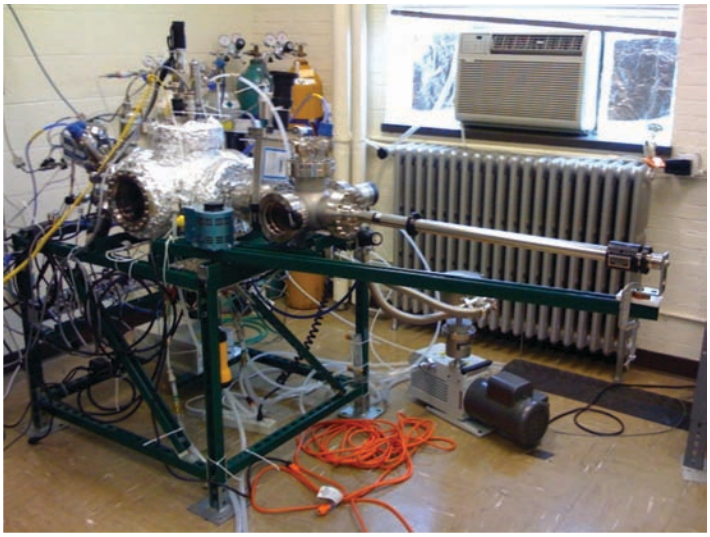

Figure 1. Dedicated thin-film growth facility. The main processing chamber is to the left, load-lock (without transfer mechanism) to the right. The sample stage (not shown) mounts to the top of the main chamber.

Figure 2. Close-up view of the three magnetron sputter guns with one gun in operation.

The team has successfully used this system to grow UO_x uranium oxide compounds spanning the range from x=2 to x=2.7, as shown in Figure 3. Samples in Figure 3 were grown at elevated temperatures and are single-crystal. Many UO_x samples have been fabricated for FY 2010 studies.

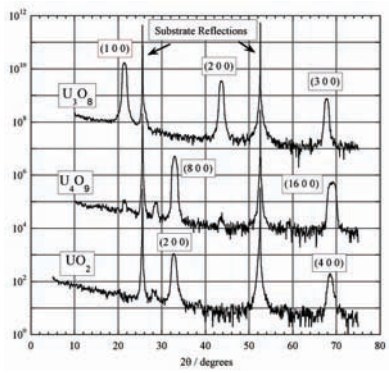

Figure 3. Specular scans of three single-crystal UO_x films showing the progression of oxygen stoichiometry from x=2 to x=2.7. The distinction between UO_2 and U_4O_9 is subtle; the peak shift of the primary (l00) reflections is approximately 0.2 degrees.

Radiation Damage Processes in CeO_2 Surrogate Matrices. Researchers characterized radiation damage processes in single-crystal CeO_2 thin films and studied radiation-enhanced diffusion (RED) of actinide surrogates such as lanthanum (La). Using films with 0.05 [La]/[CeO_2] on strontium titanate ($SrTiO_3$) substrate, researchers subjected them to both heavy ion bombardment and elevated temperatures. The team used secondary ion mass spectrometry (SIMS) to measure the La RED. Figures 4 and 5 provide the respective La depth profiles.

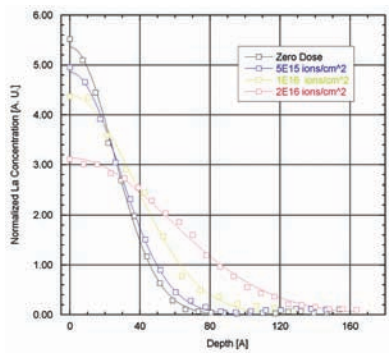

Figure 4. La depth profile as a function of dose measured with SIMS (test conducted at room temperature). Heavy ion bombardment was performed using 1.8 megavolt (MeV) krypton (Kr^+) ions. The solid lines are best-fit Gaussian profiles. The total sample thickness was 370 Å.

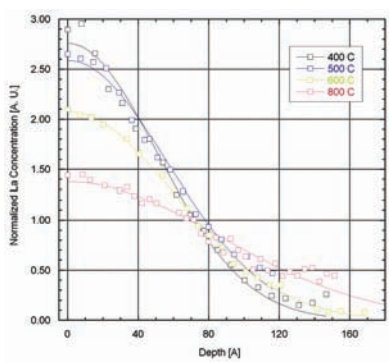

Figure 5. La depth profile as a function of temperature. Dose was consistent at $1x10^{16}$ ions per square centimeter (cm^2).

The team performed *ex situ* transmission electron microscopy (TEM) analysis of the irradiated thin films, as well as un-irradiated ones. An example of the un-irradiated film is shown in Figure 6, which indicates a low-angle tilt boundary. Figure 7 shows a high-resolution TEM image of the irradiated sample. Irradiation-induced features indicate dislocation loops. However, no precipitation of the La actinide surrogate was observed. Selected area diffraction patterns show that the CeO_2 thin film remains single-crystalline, $SrTiO_3$ near the thin film becomes nano-sized polycrystalline (multiple rings in diffraction pattern), $SrTiO_3$ substrate in a deeper region becomes nearly amorphous (the outer rings in the diffraction pattern disappeared), and $SrTiO_3$ substrate beyond a depth of 780 nanometers (nm) is undamaged (780 nm is believed to be the range of ion irradiation). However, there are elliptical deformations of the diffraction spots of the CeO_2 thin film. This could indicate a small distortion of the lattice led by irradiation-induced strain.

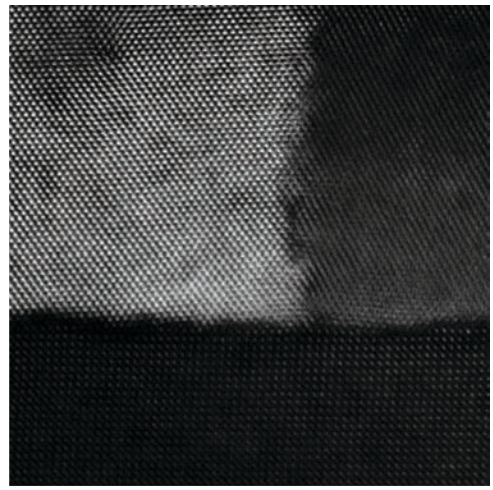

Figure 6. TEM image of single-crystal CeO_2 thin film (upper portion) on $SrTiO_3$ substrate. A low-angle tilt boundary bisects the CeO_2 film. Boundaries such as this one are responsible for the 0.2 degree mosaic width observed in x-ray diffraction measurements of the (002) rocking curve (not shown).

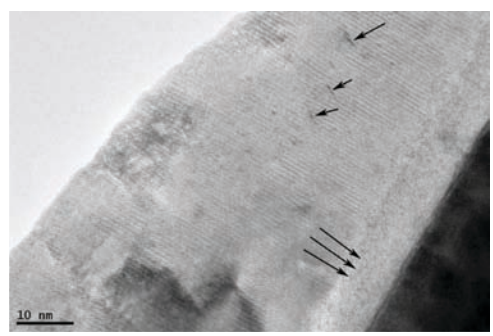

Figure 7. High-resolution TEM image of Kr-irradiated CeO_2 thin films. The three individual arrows in the upper portion of the image indicate dislocation loops. The set of three arrows in the lower portion of the image indicate a radiation-induced mixing zone at the film-substrate interface.

The team continued their investigations of CeO_2 with 5 percent La, irradiating the sample at 600°C to a dose of 0.1 ions per square angstrom ($Å^2$). The most significant features identified in these images are dislocation loops and black dot structures. The number density of both features is seen to increase with sample thickness.

Computational Activities. The team has completed a proof-of-concept implementation of a variable charge potential for UO_2. Work is in progress to integrate this potential into the molecular dynamics (MD) software LAMMPS.

Figure 8 provides results of MD simulations of the heterogeneous dissolution mechanism (bubble re-solution induced by localized heating from the passage of energetic heavy ions). Researchers used the temperature profiles obtained from two temperature calculations. To test the parameters, the team simulated electronic sputtering events for which quantitative experimental data exists. The team also developed a first-passage-based fast Monte Carlo software, which has been applied to study fission gas bubble population evolution under different scenarios, such as various dissolution mechanisms and diffusivities.

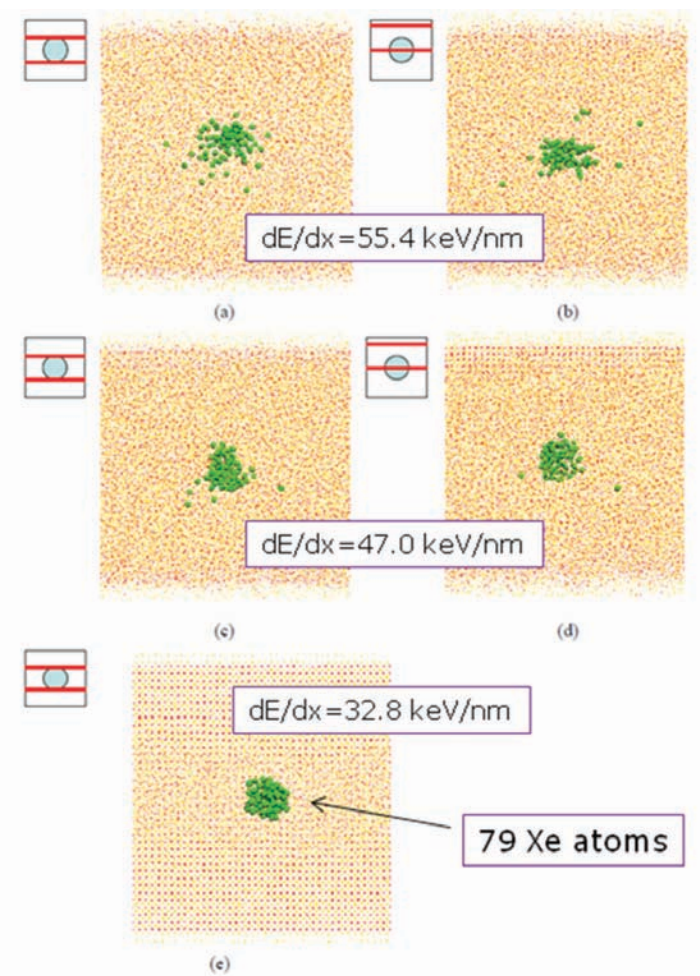

Figure 8. MD simulation of heterogeneous xenon (Xe) bubble re-solution in UO_2. The effect of the energy deposition differential (dE/dx) on re-solution is shown. Greater deposition differential values result in the dispersion of Xe atoms from a bubble. However, complete bubble destruction is never observed.

The team has also performed kinetic Monte Carlo simulations of oxygen transport in UO_{2+x}, including migration of di-interstitial clusters. The code now includes three models of oxygen migration based on literature and first-principles calculation: mono-interstitials only (Murch model), mono- plus di-interstitials, and second mono- plus di-interstitials.

The team is constructing atomic potentials for UO_2 and other related actinides. Researchers are using *ab initio* calculations to obtain the needed energetics and electron densities and related structural properties, in conjunction with using elasticity theory to calculate elastic interaction energies. The team will input these data into a potential fitting process to get the actual interatomic potentials for U-U, U-O and O-O.

Atomistic MD simulations were also a tool to investigate how the presence of grain boundaries affects phase stability and damage processes. To study grain boundaries' effects, researchers built the so-called digital microstructures that mimic the realistic microstructural properties in topological properties (grain boundary area, triple junction length, vertices) and statistical properties (distributions and various moments of grain boundary area, triple junction length, vertices). Using a newly developed inverse Monte Carlo method, researchers successfully created the first digital microstructure model. They also developed methods to put atomic-level information in the model. The next step is to use those models to simulate various problems, including the irradiation damage process, transport process (diffusion and thermal conductivity), and phase transition (helium diffusion and bubble formation).

The project is also working on void formation and growth based on a free energy formulation. Researchers are first taking into account the elastic or strain energy, surface energy, and helium gas pressure. The next step is to consider the flux of atoms and energetic particles.

Planned Activities

The project plans the following activities for the next fiscal year:

- Experimental studies of RED and radiation-induced precipitation of the actinide surrogate Nd in UO_x compounds with SIMS, TEM, Rutherford backscattering spectrometry (RBS), x-ray photoelectron spectroscopy (XPS), extended x-ray absorption fine structure (EXAFS), and x-ray absorption near edge spectra (XANES). Of interest is the effect of oxygen stoichiometry on the transport process. In addition, researchers will map an extensive temperature-dose parameter space with regard to the RED and radiation-induced precipitation processes.
- Experimental studies of Xe bubble behavior under energetic heavy ion bombardment in UO_x compounds with TEM, RBS, and SIMS. Of interest is the bubble re-solution behavior under different dose-temperature regimes.
- Continued computational analogs of actinide transport and Xe bubble stability and migration using the accelerated kinetic Monte Carlo algorithm.
- Continued first-principles modeling of diffusivity within UO_x and modeling microstructure's (grain boundary area) effect on diffusivity and precipitation processes.

NUCLEAR ENERGY RESEARCH INITIATIVE

Radiation Damage in Nuclear Fuel for Advanced Burner Reactors: Modeling and Experimental Validation

PI: Niels Gronbech-Jensen, University of California-Davis

Collaborators: California Institute of Technology, Los Alamos National Laboratory, Northwestern University, University of California-Los Angeles

Project Number: 08-051

Program Area: FCR&D

Project Start Date: October 2007

Project End Date: September 2010

Research Objectives

This project team, a collaboration of scientists at four universities, studies radiation damage of nuclear fuels through modeling, simulation, and experimental characterization. Team questions focus on describing the behavior, structure, and properties of fuel materials relevant for advanced burner reactor service. The consortium addresses specific relevant issues, including:

- Fission product and ion range distributions modeled through simplified molecular dynamics (MD) methods.
- Understanding of interatomic force fields through first-principles calculations.
- Crystal defect and noble gas diffusion and aggregation through kinetic Monte Carlo (kMC) simulations.
- Crystal damage evolution through molecular modeling and empirical relationships between energy deposition and defects.
- Experimental characterization aimed at validating the multi-scale models.

Research Progress

In FY 2009, computational research activities involved development of new methods and models in five main areas:

- New first-principles formalisms for calculating cohesive and defect energies in actinide oxides
- Kinetic modeling of bubble formation induced by noble-gas fission products in uranium dioxide (UO_2)
- Energetics of mixed-oxide fuel materials
- Interatomic potentials for radiation-damage simulations
- New algorithms for simulations of radiation damage in oxides, including dissipative processes

Coupled with the computational work were activities aimed at experimental validation.

First-Principles Electronic-Structure Methods. The electronic structure of lanthanide and actinide compounds is often characterized by orbital ordering of localized *f* electrons. Current methods for density-functional theory studies of such systems include local density approximation (LDA)$+U$ (where U corrects for electron-electron repulsion). However, calculations using LDA$+U$ are plagued by significant orbital-dependent self-interaction, leading to erroneous orbital ground states. Researchers have developed an alternative scheme that modifies the exchange energy (not Hartree energy). This new approach reproduces the expected degeneracy of f^1 and certain f^2 states in free ions and the correct ground states in solid praseodymium oxide (PrO_2). In parallel with this effort, the research team has been exploring efficient methods to identify the lowest-energy self-consistent solutions within density functional theory (DFT)$+U$, through adiabatic switching from DFT to DFT$+U$.

Kinetic Modeling of Noble Gas Fission Products. Researchers have calculated defect energies for various defect types (e.g., Schottky defect clusters and interstitials) and noble gas atoms (helium, neon, argon, krypton, xenon) in UO_2 using DFT. The team has also developed a method to address the known problem associated with multiple self-consistent solutions in a $+U$ approach for UO_2. While the DFT$+U$ formalism helps in reproducing UO_2 correctly

as an insulator, however, it can also converge the system to metastable minima thereby resulting in wrong defect energy values. The team has found that low symmetry of the UO_2 crystal with Jahn-Teller distortions in the oxygen sublattice drastically reduces the uncertainty due to DFT+*U* metastable minima.

Grimes and Catlow's previous classical potential static-simulation work proved that a bound Schottky defect is an energetically favorable site for xenon (Xe). However, using MD simulations and a classical potential, the project team has found that Xe prefers to occupy a U vacancy by displacing a U atom to a nearby interstitial (octahedral) site (see Figure 1). The team has also found that U and Xe atoms are bound together by 2.6 eV.

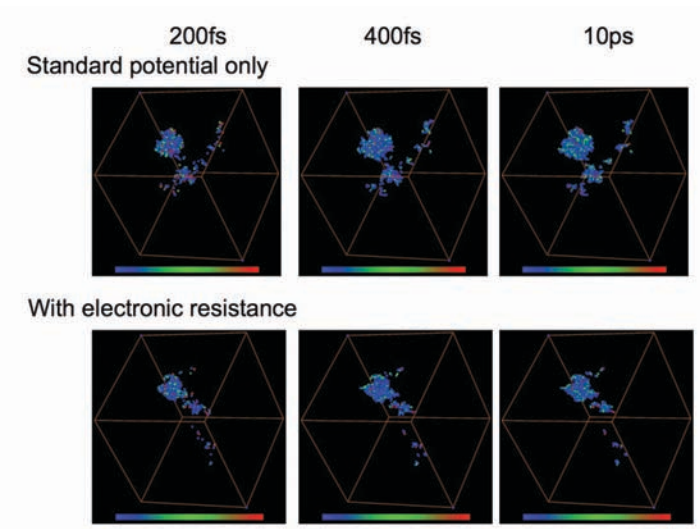

Figure 1. MD results of 20 kiloelectron volt (keV) uranium knock-on in the 111 direction (UO_2). Displaced atoms shown at different times. Top: traditional simulations with thermostat applied to the boundary layer. Bottom: results of bulk electronic coupling.

Mixed Oxides. This effort has focused on the study of $(U_xCe_{1-x})O_{2+/-y}$ mixed oxides. This surrogate for the urania-plutonia system is appropriate for university-based experimental studies and thus offers unique opportunities for direct experimental validation of the computational models. FY 2009 research activities included the calculation of prototypical ordered structures to probe the mixing and defect energies of $(U_xCe_{1-x})O_2$ solid solutions by DFT+*U* methods. The calculations demonstrated that mixing U(IV) and Ce(IV) ions in the fluorite structure leads to very small excess mixing energies, consistent with ideal-solution behavior at experimentally relevant temperatures. However, charge transfer between U and Ce, leading to the formation of U(V) and Ce(III) ions, gives rise to large excess enthalpies and entropies of mixing, with important consequences for phase-stability and defect energetics. In collaboration with Los Alamos National Laboratory, the project team tested the applicability of classical oxide potential models that were previously developed for U(IV), U(V), Ce(III), and Ce(IV) cations. These polarizable-shell-model potentials were found capable of accurately reproducing the first-principles calculated mixing energies, provided that literature estimates of the uranium fifth-ionization potential are refined slightly. The resulting potential models provide the framework for the development of Monte Carlo models that can be used to generate finite-temperature energies for direct comparison with calorimetric measurements, as well as input structures for radiation damage simulations. In parallel with the computational efforts, experimental activities involved the synthesis of a second set of urania-ceria samples. These samples were characterized by x-ray diffraction and found to be single-phase. They will be used for calorimetric measurements and further electron-microscopy studies.

Interatomic Potentials for Radiation-Damage Simulations. The project team has developed a methodology for generating interatomic potentials for use in classical MD simulations of atomistic phenomena occurring at energy scales ranging from lattice vibrations to crystal defects to high-energy collisions, thus covering all regimes relevant to the simulation of collision cascades and subsequent annealing. Building upon a charged-ion generalization of the well-known Ziegler-Biersack-Littmark (ZBL) universal potential, the team has obtained potentials that smoothly converge to the correct short- and long-range asymptotic behaviors, thus eliminating the need for arbitrary user-specified cutoffs. This method has been applied to the construction of potentials between the species plutonium (Pu), U, O, and Xe, in close collaboration with the other research groups involved in this project. In parallel, researchers are also working on Bayesian approaches to potential fitting, which enables the team to incorporate physics into the fitting process.

New Algorithms for Radiation Damage Simulations. Team scientists have adapted and further developed the Rare Event Enhanced Domain following Molecular Dynamics algorithm, or REED-MD. They use REED-MD in studies of energetic ion tracks in oxide fuels. The algorithm and its parameterization now allow for statistically meaningful simulations of, for example, range density profiles of relevant atomic species with initial energies up to 100 mega-electron volts (MeV), which may yield ranges up to 10 microns. Researchers have compared available experimental data on ion implantation into UO_2, and findings indicate that critical components to the motion of swift ions include the effective dissipation mechanisms associated with the atomic interactions with the electronic degrees of freedom in the system. Thus, these mechanisms are included in full MD simulations of damage cascades and damage production due to primary knock-on atoms; the results show significant differences from previously

published work in the literature (see Figure 1), where no bulk dissipation mechanisms have been considered. This work provides the key tool for estimating radiation damage in the fuel, and the research connects closely with the work on interatomic potentials described above.

Experimental Validation. Scientists are resolving the electronic and atomic structures for a variety of fluorite and solid-solution oxides using atomically resolved scanning transmission electron microscopy (STEM) and energy spectroscopy (EELS). In FY 2009 the team used atomic-scale imaging and spectroscopy to directly compare the probed partial density of states with a variety of first-principles-based calculations for urania, ceria, and zirconia. With the coupling of experiment and theory, the team has been able to validate first-principles-based modeling approaches based on the DFT+*U* formalism. The calculations have also elucidated key features in the electronic structure associated with defects and solid solutions; these features provide a framework for characterizing local defect structures in the relevant oxide materials by atomic-resolution EELS measurements.

Planned Activities

- The new first-principles methodology for calculating cohesive energies of actinide oxides will be generalized to the treatment of cations with multiple *f* electrons, including urania and plutonia. This work will also be adapted to modeling relevant urania solid solutions.
- Supporting the work on the diffusion and aggregation of fission products, researchers will study Xe diffusion using the newly developed Xe-UO_2 potential. The team will also calculate migration barriers of defects for use in kMC simulations.
- The team will develop MC models as a step in characterizing mixed-oxide materials. Researchers will use the models to calculate finite-temperature thermodynamic properties that can be compared to calorimetric measurements, as well as to perform atomic and chemical characterization studies based on electron microscopy. These activities are expected to lead to a validated procedure for developing mixed oxide potential models that accurately describe equilibrium and defect properties, a prerequisite for modeling radiation damage in realistic fuel materials.
- Potentials and algorithms for radiation-damage simulations will be advanced with the development of new potentials for mixed oxide fuels and a new approach for variable charge potentials for the actinides. This set of potentials will be the first comprehensive MD approach to high-energy ion collisions and radiation damage in oxide fuels, and the research team will use the MD results to characterize the evolving damage cascade from relevant fission and decay processes.
- A no-cost extension is requested through FY 2011. Development of computational methods should be complete in FY 2010, and a no-cost extension will facilitate their validation and integration to advance the accuracy of radiation-damage modeling in mixed-oxide fuels.

NUCLEAR ENERGY RESEARCH INITIATIVE

Advanced Instrumentation and Control Methods for Small and Medium Reactors with IRIS Demonstration

PI: J. Wesley Hines, University of Tennessee

Collaborators: North Carolina State University, Penn State University, South Carolina State University, Westinghouse Science & Technology Center

Project Number: 08-058

Program Area: FCR&D

Project Start Date: October 2007

Project End Date: September 2010

Research Objectives

The objectives of this NERI consortium research project are to investigate, develop, and validate advanced methods for sensing, controlling, monitoring, and diagnosing the proposed small and medium reactors (SMRs) and apply the methods to one of the integral pressurized water reactors. The reactor unit used in this research and development project is the International Reactor Innovative & Secure (IRIS) system. The IRIS design was developed by Westinghouse Nuclear Science & Technology Center, Pittsburgh. The research focuses on three major areas with the following objectives:

Objective 1: Develop and apply simulation capabilities and sensitivity/uncertainty analysis methodologies to address sensor deployment analysis.

Objective 2: Develop and test an autonomous/hierarchical control architecture and apply it to the IRIS system.

Objective 3: Develop and test an integrated monitoring, diagnostic, and prognostic system for SMRs using the IRIS as a test platform.

Research Progress

During this reporting period, the project team completed a high-fidelity FORTRAN model of the IRIS system, which is being used for simulation of operational transients under normal and degradation conditions. Plant monitoring and prognostic models will be developed using these data. The model includes both the primary system and the balance-of-plant. Researchers completed the sensitivity analysis using the simulation model to determine linearity of responses to input data.

The research team also developed a multivariate optimal controller design using adaptive control, robust control, and resilient control algorithms. Robust H-infinity controller and resilient controller designs were developed to achieve control under uncertainty and device degradation for the IRIS system. Control work included development of a multivariate model predictive controller (MPC) for the IRIS primary system (primary + helical coil steam generator). The task includes developing reconfigurable and fault-tolerant control strategy as part of the autonomous control structure. Researchers consider both internal faults and sensor faults. This task has used Simulink models of the various IRIS systems and the integrated model. The team completed preliminary measurements on the flow control loop and demonstrated the on-line implementation of fault detection algorithms for sensors and devices, along with developing a Simulink physics model of the single-tank control loop system and validating this system using loop measurements. Optimal sensor placement techniques were developed using fault diagnostic observability and sensor reliability criteria.

Researchers demonstrated the application of a new optimal sensor placement algorithm for the IRIS steam generator system. This approach is being extended to a nuclear desalination plant. The extension entails the development of a dynamic model of a multi-stage flash (MSF) desalination system with process heat being supplied from a nuclear reactor. The team completed the adaptive non-parametric model for process monitoring and application to a heat exchanger and an experimental flow control loop, including the development of the algorithms and demonstration of the integrated monitoring, diagnostic, and prognostic tools.

In the research described above, the research team has developed and applied fault detection, identification, and prognostic methodologies and control strategies. Those control and diagnosis systems not only can perform individually but also can be integrated as a comprehensive autonomous control system, where the individual systems cooperate with each other to perform overall management, decision making, and diagnosis of the nuclear power plant. The structure of the system is three-tier—execution level, coordination level, and management level—and is presented in the figure below.

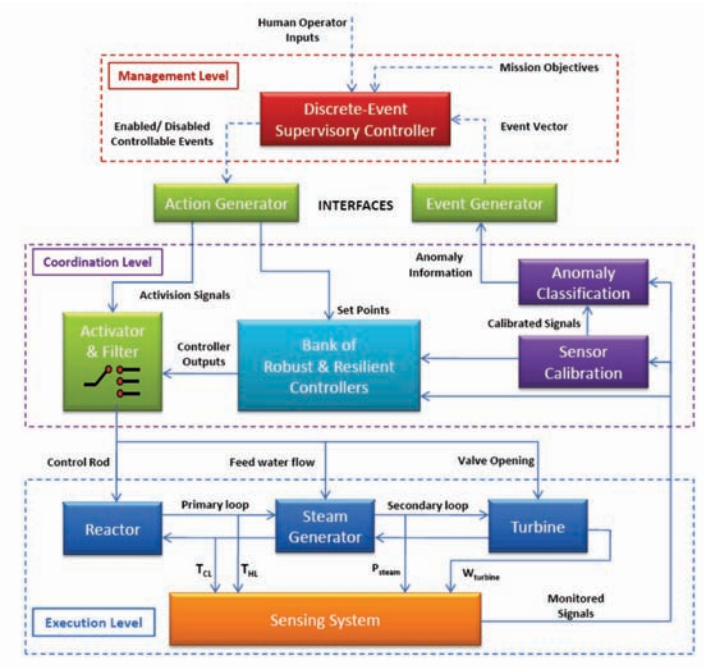

Figure 1. Three-tier structure of the integrated autonomous control system including execution level, coordination level, and management level.

Research experiences were provided for undergraduate students from South Carolina State University (a Historically Black Colleges and Universities [HBCU] institution). Their summer internship program included three students at the University of Tennessee and one student at North Carolina State University.

Additionally, several graduate students presented papers at the American Nuclear Society (ANS) annual and winter meetings. Nine papers were presented at the ANS Topical Meeting on Nuclear Plant Instrumentation, Controls & Human Machine Interface Technology (NPIC & HMIT 2009), which was held in April 2009 in Knoxville, Tennessee. Other conference presentations included the International Conference on Prognostics and Health Management 2009 in San Diego, California; ICONE 17 in Brussels, Belgium; and the 2009 Integrated Systems Health Management Conference in Covington, Kentucky. Two journal articles have been published: one in the *International Journal of Performability Engineering* (special issue on prognostics and health management) and one in the *Journal of Intelligent Manufacturing* (special issue on machinery health monitoring, diagnostics and prognostics).

Planned Activities

The plan for the path forward is to complete the remaining project tasks in each of the three topic areas and prepare a final project report. During this final phase, several papers are planned for presentation at national and international meetings, and additional manuscripts are being prepared for publication in scientific journals.

Current efforts are focused on modeling the rest of the IRIS nuclear steam supply system including the feedwater heaters, allowing the turbine taps to be dynamic and including more advanced electrical side behavior. These efforts will allow researchers to use detailed transient information to test plant control logic for dynamic stability aids, and the team will systematically evaluate and improve the MPC.

The team will develop a full-scope plant model to study both steady-state and dynamic behaviors of the desalination process. The dynamic MSF model will be coupled with the existing Simulink models of an IRIS plant. The proposed sensor network design framework will be applied to the modeled nuclear desalination process for fault detection, identification, and reconstruction.

The previously proposed sensor placement design will add the use of other optimization criteria, such as the process controllability constraint, as well as residual precision, data reconciliation, and gross error robustness goals used for monitoring normal operations and treatment of this problem as a multi-objective case. The goal of this task is to seamlessly incorporate various criteria for sensor placement design so that the resulting sensor location is optimal in a much broader sense and not just from a fault diagnosis perspective. The research team will extend the sensor placement technique and apply it to a water desalination plant, coupled to the IRIS as a heat source. Researchers will also apply developed methods to the previously instrumented laboratory two-tank loop to demonstrate the feasibility of the optimal sensor placement strategy being developed.

NUCLEAR ENERGY RESEARCH INITIATIVE

Advanced Aqueous Separation Systems for Actinide Partitioning

PI: Ken Nash, Washington State University

Collaborators: Hunter College, Idaho National Laboratory, Lawrence Berkeley National Laboratory, Pacific Northwest National Laboratory, Tennessee Technological University, University of New Mexico, University of North Carolina-Wilmington

Project Number: 08-067

Program Area: FCR&D

Project Start Date: October 2007

Project End Date: September 2010

Research Objectives

The project objective is to expand upon results of earlier studies of partitioning americium (Am) from fission product lanthanides. These continuing studies rely on synthesis of new separations materials integrated with radiochemical characterization of the complexes and separations systems. Multiple academic and national laboratory investigators contribute to this effort.

In the predominant trivalent oxidation state, the chemistries of lanthanides and actinides overlap substantially. As a result, their mutual separation is challenging. One fruitful approach is the application of complexing agents containing ligand donor atoms that are softer than oxygen (e.g., nitrogen [N], sulfur [S], and chloride [Cl^-]). The fundamental limitation of softer-donor systems is that their interactions with the target metal ions are systematically weaker than those of hard-donor oxygen systems. The investigators thus seek to increase the strength of actinide soft-donor interactions through subtle manipulation of conditions.

Research Progress

The team continues to evaluate the separation potential of samples synthesized by collaborators. The project has also sought out the expertise of a world-renowned expert in extraction chromatography to investigate some aspects of this chemistry's application. Characterization activities include homogeneous, single-phase solution chemistry investigations, liquid-liquid extraction studies, studies of metal ion uptake onto resinous materials, and application of various types of spectroscopic techniques. Separation studies are guiding improvements of new materials' separation potential.

During this fiscal year, the project has succeeded in preparing new pyridine and bipyridine derivatives of polyaza complexants. Triazole rings are mated to the central core of 2,6-pyridyl or 2,9-bipyridyl core groups, creating tetraaza complexants. The latest derivatives have incorporated normal alkane functional groups to improve lipophilicity of the moderately hydrophilic polyaza complexants. Metal ion uptake studies of these ligands' separation potential are also under way.

The project has also completed metal complexation studies of many classes of metal ions with phenanthroline-2,9-dicarboxylic acid (PDA). Researchers have completed spectrophotometric titrations of complexes of PDA with trivalent neodymium (Nd) and Am(III). Figure 1 shows a spectrum comparing the relative stability of Am^{3+}

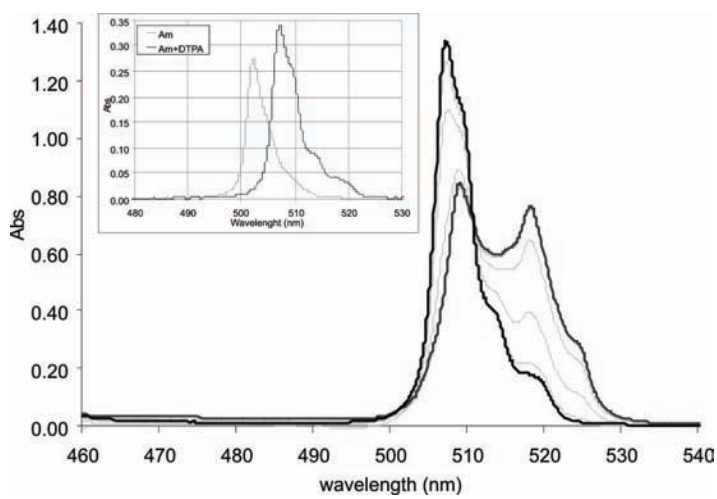

Figure 1. Spectra of the Am^{3+} ($6.34X10^{-6}$ M) PDA ($7.0X10^{-5}$ M) and DTPA ($1.0X10^{-4}$ M) competition as a function of pH (pH 3.18 to 8.21) using a liquid waveguide capillary cell (500 centimeters [cm]). The thick black line is the end point (pH 8.21), and the thick dark grey line is the start point (pH 3.18). The insert is the spectra of free Am^{3+} ($8.00X10^{-4}$ M, pH 4.13, grey line) in solution and Am^{3+} ($8.00X10^{-4}$ M) bound by DTPA ($1.00X10^{-3}$ M, pH 2.93, black line) using 1-cm cuvette.

complexes with PDA and DTPA (the actinide holdback reagent in the TALSPEAK process). A manuscript describing the enhanced binding of Am(III) is nearly ready for publication. To complement the single-phase studies, the team has begun characterization of the separation potential of PDA, phenanthroline, and the alcoholic derivative PDALC. Amide derivatives (PDAM) have recently been prepared and are being characterized. The limited solubility of these compounds in typical solvent extraction media must be overcome for more complete assessment; PDAM has shown improved solubility.

Researchers evaluated samples of tetraethylhexyl-NOPOPO extractant. The team found these molecules too difficult to purify and so have shifted focus to the tetraoctyl analog TO(NOPOPO) for characterization of actinide/lanthanide extraction potential. As these ligands are seen as potential substitutes/replacements for CMPO in TRUEX, the focus is on their ability to extract all actinide and lanthanide metal ions from nitric acid media. The team has completed studies of the extraction of thorium (Th^{4+}), plutonium (Pu^{4+}), neptunium oxide (NpO_2^{+}), uranium oxide (UO_2^{2+}), europium (Eu^{3+}), and Am^{3+} in this system. Extraction chromatographic studies are under way on samples of the tetraphenyl–NOPOPO derivative.

The project produced several two-to-three-gram samples of resin-immobilized ligands. The first examples of these materials were functionalized with one to three neutral phosphate esters bound to the polystyrene-divinylbenzene matrix via amine or amine/alcohol linkages. These carefully prepared metal-binding “environments” combine phosphoric acid or phosphate ester functional groups with a polyalcohol or polyamine microenvironment, enhancing the kinetics and potential selectivity of the metal ion binding site. Studies of uranium and actinide uptake onto these materials from nitric acid and nitrate salt media have yielded evidence for degradation of the phosphate esters. Continuing discussions have established the desirability of creating functionalized polymers containing phosphonate esters and malonamide functional groups, both of which should be more resistant to degradation. Initial observations of cation uptake of the phosphonate reveal improved stability relative to the phosphate esters, but there is strong competition from HNO_3. Researchers see the malonamide system even more positively, and they are preparing a 30-gram batch of material for in-depth studies.

Planned Activities

During the final year of this project, the project team will focus on expanding supplies of selected materials identified as most useful and continuing characterization of separations systems based on in-hand ligand supplies. Studies of the TO(NOPOPO) solvent extraction system are nearing completion; the team plans to follow with biphasic calorimetry investigations. Derivatives of phenanthroline containing alkylated amide functional groups soluble in organic solvents have recently come available, so investigations of this system can proceed to solvent extraction demonstrations. Studies of the potentially tetradentate pyridine triazole ligands have focused on the creation of several gram lots of selected lipophilic bi-, tri- and tetra-dentate aza extractant molecules. Characterization of these compounds will focus on their utility in synergistic systems, an approach designed to overcome the inherently limited strength of their interactions with lanthanide and actinide cations. The team is also working on improvements of the ^{234}Th isotope generator that was developed during the last year.

NUCLEAR ENERGY RESEARCH INITIATIVE

6.3 Nuclear Hydrogen Initiative

Nine NERI research projects are currently being performed that closely relate to the goals of NHI; six of these projects were awarded in FY 2006 and three projects (two NERI and one NERI-C) were awarded in FY 2007. Although post-FY 2009 hydrogen production research will fall under the Gen IV umbrella, the ongoing projects discussed in this section are still funded as NHI studies.

In FY 2009, NHI research projects focused on developing an efficient flowsheet for the sulfur-iodine (S-I) cycle, developing simulation tools, and conducting design/analysis of the S-I cycle. Research in high-temperature electrolysis is enhancing electrolyzer performance, developing improved cell materials, and creating new seal designs. Reactor/hydrogen support system research is creating new alloys and ceramics for heat exchangers and optimizing heat exchanger design/performance. The NERI-C NHI project is developing and modeling alternative thermochemical cycles for nuclear hydrogen production.

This section provides an index of the research being performed under NHI and a summary of the ongoing projects.

NUCLEAR ENERGY RESEARCH INITIATIVE

Directory of Nuclear Hydrogen Initiative Project Summaries and Abstracts

FY 2006 Project Summaries

06-024 Nickel-Silicon Alloys for the Sulfur-Iodine Reactor–Hydrogen Production Process Interface 159

06-027 Microstructure Sensitive Design and Processing in Solid Oxide Electrolyzer Cell 161

06-041 Dynamic Simulation and Optimization of Nuclear Hydrogen Production Systems.....165

06-054 High-Performance Electrolyzers for Hybrid Thermochemical Cycles 169

06-060 Development of Efficient Flow Sheet and Transient Modeling for Nuclear Heat Coupled Sulfur Iodine Cycle for Hydrogen Production 171

06-140 Gradient Meshed and Toughened Solid Oxide Electrolyzer Cell Composite Seal With Self-Healing Capabilities.....173

FY 2007 Project Summaries

07-030 Liquid Salts as Media for Process Heat Transfer from Very High-Temperature Reactors: Forced Convective Channel Flow Thermal Hydraulics, Materials, and Coatings 177

07-057 Optimization of Heat Exchangers.....179

FY 2007 NERI-C Project Abstracts

08-047 NERI Consortium - Advanced Electrochemical Technologies for Hydrogen Production by Alternative Thermochemical Cycles 181

NUCLEAR ENERGY RESEARCH INITIATIVE

Nickel-Silicon Alloys for the Sulfur-Iodine Reactor-Hydrogen Production Process Interface

PI: Joseph W. Newkirk, University of Missouri-Rolla

Collaborators: Idaho National Laboratory

Project Number: 06-024

Program Area: NHI

Project Start Date: March 2006

Project End Date: September 2009

Research Objectives

The goal of this project is to develop materials suitable for use in the sulfuric acid decomposition loop of the sulfur-iodine (S-I) thermochemical cycle for nuclear hydrogen production. Materials must have both acceptable corrosion resistance and sufficient ductility for component fabrication and avoidance of catastrophic failure. Nickel-silicon (Ni-Si) intermetallics show promise for such critical applications as the sulfuric acid vaporizer, vapor superheater, and decomposer. Past work indicates that adding minor alloying elements to nickel silicide (Ni_3Si) provides significant ductility at room temperature (7 to 10 percent elongation at failure), a unique property for normally brittle high-silicon materials. Ni_3Si can also be easily joined by traditional methods such as welding, and preliminary studies show this compound has excellent corrosion resistance.

In this work, the team will further develop Ni_3Si to maximize its ductility and corrosion resistance while reducing cost. Researchers will analyze the effects of adding elements such as niobium (Nb), boron, and iron. Microalloying may be used to improve resistance to corrosive impurities in the sulfuric acid-processing stream, such as iodine. Finally, the team will study the extent to which iron can be substituted for nickel in Ni_3Si without adversely affecting ductility or corrosion resistance.

Researchers will document mechanical properties of these new materials over a range of temperatures and strain rates. The team can then utilize these results to improve material properties and microstructure. As a final test, corrosion-resistant materials will be subjected to flowing sulfuric acid (H_2SO_4) at temperatures and pressures comparable to the actual sulfuric acid processing loop (120°C to 400°C at less then 10,000 psi) in order to measure corrosion rates.

Research Progress

As the project reaches its conclusion, efforts for the year focused on finishing the work to determine the corrosion protection mechanism, evaluating the behavior in various solution strengths and in conditions closer to those in the decomposition loop.

A summary of some of the results of testing on several compositions of Ni-Si alloys are shown in Table 1. All

Table 1. Results of Ni-Si alloy testing.

Alloy		Si content (at%)	Slope on passivation	mpy at passivation	Time for passivation (mins)
2BM1	HT	20.8	0.005	0.9	320
2BM1 (10% setting)	10 pass	20.8	0.005	1.2	300
2B0-M1B	HT	20.4	0.02	4	450
2B0-M1B (20% setting)	10 pass	20.4	0.02	2	80
2B-B	HT	19.7	0.004	2.6	1500
MM1C	HT	19.7	0	0	320
2B2 (7% setting)	10 pass	18	0.07	22.4	700
2B2	HT	18	0.14	64.5	370

alloys with Si compositions above 18 percent showed corrosion rates of less than 5 mils per year (mpy) in both the homogenized and rolled conditions.

The team carried out intermittent corrosion testing in 70 and 80 percent sulfuric acid. Comparisons of results are shown in Figure 1 below. The protective film formed is effective at both concentrations; the only thing that changes is the time to achieve the protective film. The 80-percent tests are faster, either because of the higher concentration or because the boiling temperature is higher. Tests carried out at 80 percent on samples that were then immersed in 70 percent show the protective nature of this film, as they lost almost no mass after reimmersion.

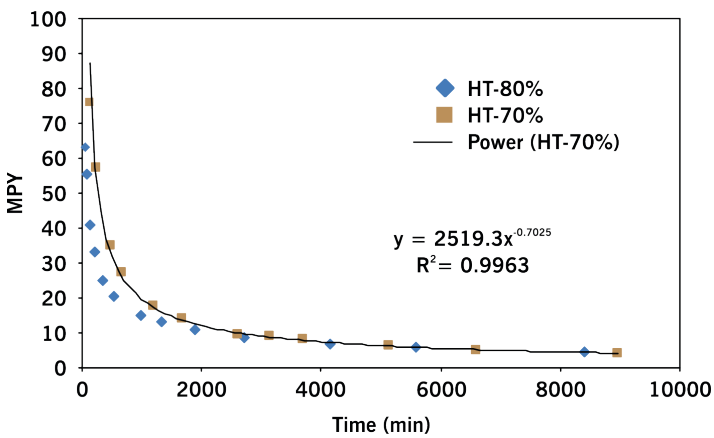

Figure 1. Results of intermittent corrosion testing in 70 and 80 percent sulfuric acid.

Researchers performed testing at INL under conditions closer to those potentially seen in the decomposition loop. Results show that the protective film is equally effective at higher temperatures and pressures. Figure 2 shows a comparison of tests at 300°C and 37.4 atm pressure in 70 percent sulfuric acid with those carried out at the boiling point and atmospheric pressure. The samples exhibited the same corrosion behavior, only faster. Both Nb-containing alloys (2B and MM1C) rapidly reached 5 mpy—at the higher pressures and temperatures. The alloy containing titanium (E) did not reach 5 mpy, but the corrosion rate still dropped off faster in the more aggressive environment. These results promise excellent and robust performance in the S-I decomposition loop.

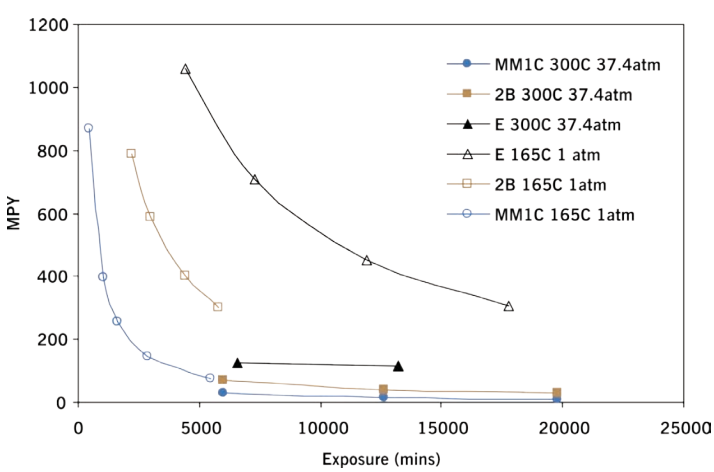

Figure 2. Results of tests conducted at 300°C and 37.4 atm in 70 percent sulfuric acid versus results of tests conducted at boiling point and atmospheric pressure.

A corrosion mechanism has been proposed to explain the linear corrosion region prior to passivation. Early corrosion results in the formation of a two-phase film with silicon dioxide (SiO_2) and nickel sulfate ($NiSO_4$). The $NiSO_4$ leads to porosity in the film as well as spalling. This continues until the dissolution of Ni has caused a concomitant increase in Si within the metal. At the higher Si content, the film changes to single-phase SiO_2. Analytical work shows the Si increase confirming that portion of the theory. The spalled material formed matches the rate of mass loss during corrosion for the linear region, but none occurs after passivation. This theory also explains the critical Si level necessary for full protection of the alloys. Thermodynamic calculations made with ThermoCalc software support this mechanism.

Planned Activities

The project was scheduled to end in early 2009 but was continued until September on a no-cost extension. A proposal for continued alloy development was submitted but not funded. The project team has supplied samples to several other DOE project areas and will supply more where applicable, but the project has been completed.

NUCLEAR ENERGY RESEARCH INITIATIVE

Microstructure Sensitive Design and Processing in Solid Oxide Electrolyzer Cell

PI: Hamid Garmestani, Georgia Institute of Technology

Collaborators: Pacific Northwest National Laboratory

Project Number: 06-027

Program Area: NHI

Project Start Date: March 2006

Project End Date: March 2009

Research Objectives

This project sought to optimize intermediate-temperature solid oxide fuel cells (IT-SOFCs), which would allow using far less expensive materials in cell construction. The specific aim of this study was to develop an inexpensive manufacturing process for deposition of functionally graded thin films of strontium-doped lanthanum manganite (LSM), specifically $La_{\chi}Sr_{1-\chi}MnO_{3\pm\delta}$, for use as IT-SOFC cathodes. LSM with porosity graded microstructures is regarded as one of the most promising cathode materials for SOFCs because of its high thermal and chemical stability, particularly with yttrium stabilized zirconia (YSZ), the most widely used electrolyte for SOFCs.

The search for alternative high-efficiency energy technologies has led to extensive research and development of electrochemical energy storage and converter systems such as capacitors, batteries, and fuel cells. Among these systems, fuel cells are a promising alternative resource in efficient and low-emission power generation. SOFCs are solid electrolyte types of fuel cells that are economically competitive, thanks to their high power density, fuel versatility, and variety of cell configurations. In addition, SOFCs do not utilize expensive metal catalysts. These advantages are associated with the high operating temperatures (700°C to 1000°C) of the SOFC and the ceramic nature of all components.

However, commercialization of SOFC technology faces some major problems. Cost and durability are the main challenges in designing optimized structures of SOFCs for the entire range of possible applications in stationary, transport, and portable power generation. One possible solution is lowering the operating temperature of the SOFC to intermediate temperature (500°C to 750°C). However, moving to lower operating temperatures can create critical problems in functionality of the cell components.

Research Progress

The project team conducted a literature review and determined that, of the five types of fuel cells currently being investigated, proton-exchange membrane (PEM) and SOFCs with all-solid components are currently the most attractive technologies for automotive and stationary applications. These two types have the potential to achieve higher power and energy densities. SOFCs are solid-state electrochemical devices that convert electrochemical energy directly to electrical energy with 45 to 50 percent electrical efficiency. SOFC cell components are constructed from ceramic materials that can tolerate operating temperatures in the range of 800°C to 1000°C. In fact, high operating temperatures facilitate utilizing the by-product heat in a bottoming cycle (such as fuel reforming) for electric power generation, which leads to a further improvement in the overall efficiency up to more than 80 percent. It also improves tolerance to impurities in the fuel. Figure 1 provides a schematic of a SOFC.

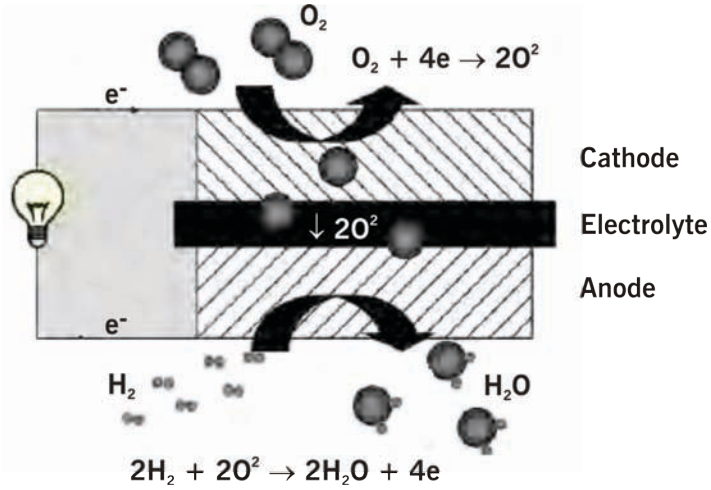

Figure 1. Schematic of an SOFC.

Appropriate materials for SOFC cell components depend on the functions of those components. In SOFCs, the cathode is the component at which the electrochemical reduction of the oxygen gas occurs. The cathode material and microstructure should be designed to provide sufficient porosity to enhance oxygen transport and demonstrate sufficient catalytic activity for oxygen reduction, stability at fabrication and operating temperatures, and good electronic conductivity at operating conditions. Among perovskite oxides, LSM is the best candidate for SOFC cathode material, as it has thermal properties matching the YSZ electrolyte and demonstrates high electrical conductivity.

Figure 2 shows the schematic of the proposed functionally graded porous LSM cathode. Large spheres represent large particles creating a large columnar pore structure in the outer layer to allow gas transport. Spheres gradually get smaller along the inner layers to maintain the structural integrity. Small spheres and small pores close to the electrolyte maximize the number of triple phase boundaries in the active nanostructured interlayer.

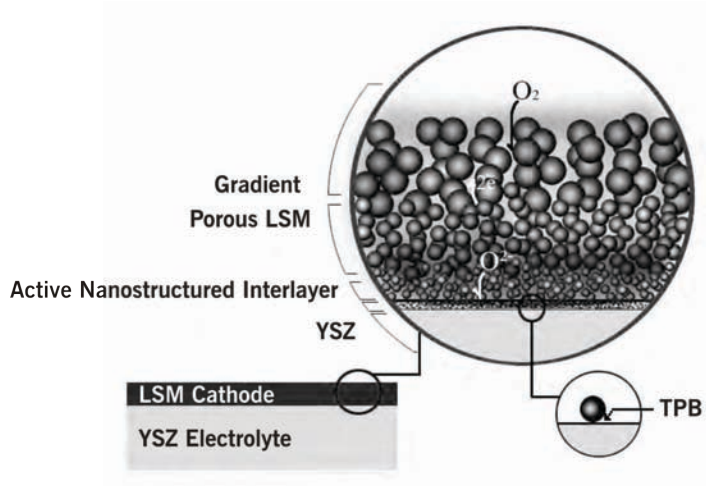

Figure 2. Schematic of a functionally graded porous LSM cathode on YSZ substrate.

Spray Pyrolysis System. SOFC components are fabricated using a wide range of methods. Thin film deposition techniques, such as physical and chemical deposition processes, have the potential of providing control over processing parameters. The project team chose the spray pyrolysis method as a low-temperature processing technique for deposition of porous LSM films onto dense YSZ substrates. Spray pyrolysis is a cost-effective technique with simple apparatus for deposition of uniform thin films of large surface areas under atmospheric conditions. It is performed at a relatively low temperature and at a high deposition rate. This process allows scientists to easily control the shape, size, composition, and phase homogeneity of the particles.

The project team developed a novel horizontal spray pyrolysis setup, shown in Figure 3. It consists mainly of a spraying unit, liquid feeding unit, and temperature control unit. The type of spray pyrolysis method used in this work is a spray pyrolysis in a tubular reactor. The solution is prepared by dissolving the stoichiometric ratios of the desired precursors into solvent using a magnetic stirring. The solvent is pumped to a 100 kHz ultrasonic atomizer toward the heated substrate held inside a tubular quartz reactor. The substrate was mounted on the graphite sample holder and heated by quartz heating bulbs located on top and below the tube. The substrate temperature was monitored by a type K thermocouple connected to the temperature controller monitor. Once the temperature controller showed the desired temperature, the solution was pumped into the atomizer, and the atomized droplets of the precursor were sprayed and transported toward the substrate to the reaction chamber using nitrogen (N_2) and oxygen (O_2) as the carrier gases. Upon reaching the hot surface of the YSZ substrate, the aerosol droplets were decomposed and converted to very small particles of the oxide compounds.

The novelty of this system relies on modifying the commonly used vertical system to a horizontal system in which the deposition process takes place similarly to liquid delivery chemical vapor deposition (LD-CVD). This setup provides advantages of both techniques. One benefit is the use of quartz lamps as heating sources that heat the YSZ substrate from both the top and bottom of the substrate, providing more consistent and accurate temperature measurements.

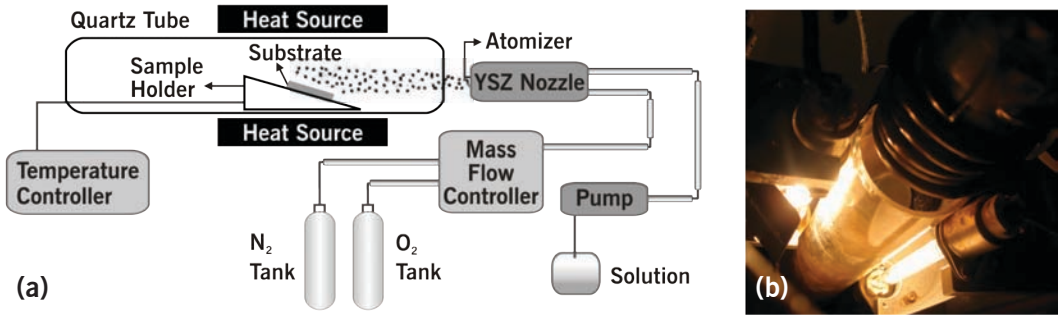

Figure 3. (a) Schematic of the spray pyrolysis setup; (b) photograph of the spray pyrolysis setup.

Table 1. Spray conditions for three experimental stages.

Stage	Condition / Solvent	Precursors (mg)			Solvent (ml)	Temperature (°C)	Solution flow rate (ml/min)	Pyrolysis composition	LSM film composition	YSZ electrolyte
A	Aqueous	Lauthanum acetate	Strontium acetate	Manganese acetate	Water	480	0.73	Endothermic (vaporization)	Inhomogeneous	Crack growth/ YSZ failure
		110.6	30	86	25					
	Organic	Tris Lanthanum	Bis Strontium	Tris Manganese	Ethylene glycol dimethyl ether	480	0.73	Exothermic	Homogeneous	No cracks
		80.3	22.7	100.7	25					
B	Organic	80.3	22.7	100.7	25	520, 540, 560, 580	0.73, 1.13, 1.58	Exothermic	Homogeneous	No cracks
C	Organic	Tris Lanthanum	Bis Strontium	Tris Manganese	1-2 Dimethoxyethane					
		180	60	160	100	520	0.73	Exothermic	Nanocrystalline fine interlayer	No cracks
		360	120	320	50	540	1.13		Gradient porous coarse layers	
		360	120	320	50	540	1.13			
		360	120	320	50	540	1.13			

Through a first round of experiments, researchers determined the range of initial spray conditions such as precursor and solvent type, solution concentration, nozzle-to-substrate distance, carrier gas flow rate, deposition temperature, and solution flow rate, over which the LSM film could be reproducibly deposited in the stoichiometric ratios on the YSZ substrate.

A second set of experiments used these results as a baseline and moved on to identify conditions for processing a multi-layered gradient porous LSM on the YSZ substrate. Researchers examined the effects of deposition parameters such as temperature and solution flow rate on the microstructure of LSM films. They achieved a gradient porous microstructure by applying a multiple-step spray deposition consisting of changes to the precursor solution concentration, deposition temperature, and solution flow rate. The overall results are summarized in Table 1.

To achieve optimal properties in a cathode, researchers sought to create a fine layer close to the electrolyte surface with gradually coarser outer layers. The experimental process described above provided the data depicted in Figure 4, the plot of electrode thickness as a function of deposition time at each deposition step. The rate of deposition increases as a function of solution flow rate and deposition temperature. The team determined thicknesses from scanning electron microscopy (SEM) cross-section micrographs.

Results of optimization studies of spray parameters revealed that the substrate surface temperature is the most critical parameter influencing the roughness and morphology, porosity, cracking, and crystallinity of the film. However, all conditions played a crucial role in the final product. Different solvents and concentrations of the solution, nozzle-to-substrate distance, and oxygen and solution flow rates all affected film quality.

As mentioned above, researchers utilized SEM to characterize and test the LSM films, determining the particle morphology, pore microstructure surface, and cross-sectional structure. Other characterization methods included an adhesion test (the Scotch tape test), energy dispersive spectroscopy (EDS) for the elemental analysis and chemical characterization, and x-ray diffraction (XRD) to identify the crystalline phases of the materials. The surface area and the pore volume of the graded porous LSM film were determined by the Bruanuer-Emmett-Teller (BET) method using a SA 3100 surface area and pore size

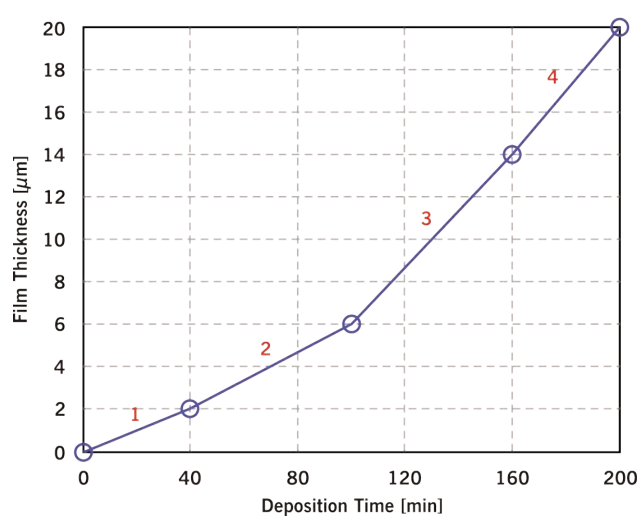

Figure 4. The plot of the first gradient cathode film thickness as a function of deposition time.

analyzer, based on adsorption of the monolayer of gas molecules on the solid surface. The temperature-dependent electrical conductivity of the LSM cathode films was measured using a four-point probe setup combined with a micro-heater to bring the sample to its operating temperature, i.e., 700°C.

The gradient porous LSM cathode was successfully deposited on YSZ. Optimal cathode properties consist of a fine layer close to the electrolyte's surface, with gradually coarser outer layers, which was the case with the final product. Overall, the LSM film is compositionally homogeneous and crack-free with a semi-columnar porous structure. Test results showed high cohesive strength.

In order to study the reproducibility of the gradient porous film via the spray pyrolysis technique, the project team repeated the same set of experiments, successfully producing a functionally gradient porous LSM cathode on top of a YSZ substrate. Therefore, spray pyrolysis can be utilized as a low-temperature processing technique to produce highly crystalline functionally graded LSM cathodes.

Planned Activities

This project is complete.

NUCLEAR ENERGY RESEARCH INITIATIVE

Dynamic Simulation and Optimization of Nuclear Hydrogen Production Systems

PI: Paul Barton and Mujid Kazimi, Massachusetts Institute of Technology

Collaborators: None

Project Number: 06-041

Program Area: NHI

Project Start Date: March 2006

Project End Date: February 2009

Research Objectives

This project was part of a research effort to design a hydrogen plant interfaced with a nuclear reactor—a promising alternative to fossil-fuel-generated hydrogen. The objective of this research was to build models for dynamic simulation and optimization of hydrogen production options using nuclear energy. There is a natural interdependence between design and operational decisions for integrated nuclear hydrogen production systems. This interdependence requires a modeling and simulation environment that can capture the physical and chemical design descriptions and map these into steady-state and dynamic predictions of the hypothesized system's behavior.

This project dealt mostly with dynamic modeling of the interface between the nuclear reactor and the hydrogen production plant, as well as the thermodynamics of the sulfur-iodine (SI) thermochemical cycle. A hybrid discrete/continuous model captures the continuous dynamics of the nuclear plant, the hydrogen plant, and their interface, along with discrete events such as major upsets. Use of detailed thermodynamic models allows researchers to examine the process in detail, study plant operations and accident scenarios, and conduct parameter estimation studies to identify possible improvements in materials, mechanical design, and safety issues.

Research Progress

The research team performed the following tasks:

- Developed detailed simulations of heat-transfer loops using hyperbolic equations.
- Developed and validated a novel simplification of the gas dynamics equations.
- Created and validated a simplified model for the heat-transfer loop.
- Simulated start-up of the two-loop system.
- Validated the simplified system of equations representing the heat-transfer loop using RELAP software.
- Developed a new formulation for the electrolyte-non-random two-liquids (electrolyte-NRTL) thermodynamic model; applied it to an extensive database of electrolytes to validate its performance.
- Studied the implications that exist in fitting binary parameters of excess Gibbs free energy models, such as the NRTL model, using experimental measurements of liquid-liquid, vapor-liquid, and vapor-liquid-liquid phase splits.
- Developed a new formulation based on a bilevel optimization strategy for accurately and thermodynamically consistently fitting binary parameters to experimentally measured phase equilibrium data.
- Developed a thermodynamic data reduction optimization framework to develop a self-consistent database of sulfuric acid's and hydrogen iodide's thermodynamic properties.

Modeling of the Heat-Transfer Interface and Nuclear Reactor. Since suitable models must be in place before simulation studies can begin, the majority of the effort was devoted to building dynamic models of the nuclear hydrogen production system. The overall system model involves models of the nuclear reactor, the interface, the hydrogen production plant, and the power conversion

unit. Hydrogen production in this model occurs as follows: heat exchangers produce high-temperature steam from water; the steam moves to an electrolysis cell where it is reacted into oxygen and hydrogen; the oxygen is recuperated; and the hydrogen/water stream moves to a steam separator to be concentrated.

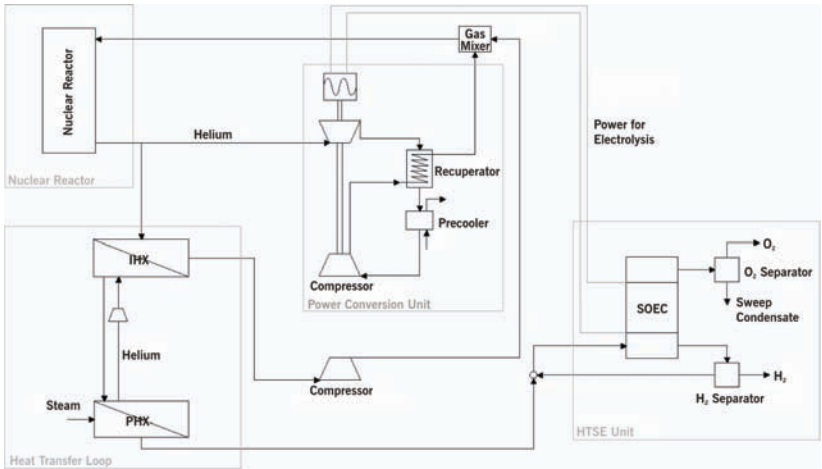

Figure 1. High-temperature steam electrolysis flow diagram.

Figure 1 shows the flowsheet for the system configuration. The main components of the process are highlighted: the nuclear reactor, gas turbine, heat-transfer loop, and high-temperature electrolysis cell. The nuclear reactor provides high-temperature heat for the gas turbine and the electrolysis cell; the gas turbine produces electricity for electrochemical reactions in the electrolysis cell; and the heat-transfer loop conducts heat from the reactor to the electrolysis cell. This intermediate heat-transfer loop guarantees safety and operability as it physically separates the nuclear reactor from the hydrogen production plant and decouples their operation by introducing auxiliary heat sources/sinks (not shown in the figure).

The project team used two loops for the heat-transfer loop model and chose helium as the heat-transfer fluid to provide safe and reliable operation. Each loop consists of a compressor and a pipe with sections at different external temperatures. The two heat-transfer loops are coupled through an intermediate heat exchanger. One loop transfers 50 megawatts of heat from the nuclear reactor to the second loop via an intermediate heat exchanger similar to the compact heat exchangers designed by Heatric. The second loop uses helium to transfer that heat to the hydrogen plant via the process tube-in-shell heat exchanger.

Researchers were able to simplify the model equations involved by taking into account only the relevant time scales for the simulated phenomena. In this case, simulation of fast time scales is often not necessary because discrete disruptions in the gas flow are rare. As changes in pressure propagate with the speed of sound, the research team can make a quasi-steady-state approximation (singular perturbation) for the equations related to fast dynamics. They validated predictions from their simplified system of equations by comparing results with simulation results from RELAP. Hence, the team is now able to use the simplified equations to represent gas dynamics. This simplification allows the use of implicit integrators; therefore, the team can implement larger models and achieve faster simulation speeds.

The next step was to implement a nuclear reactor model as the system's heat source. The project team adapted a model developed by Chunyun Wang at of the Massachusetts Institute of Technology based on a pebble bed modular reactor (PBMR) using helium as the coolant. This model was a collection of submodels representing phenomena inside the core: convective heat transfer between the core and the helium; conductive and radiative heat transfer in the core and reflectors; reactivity as a function of temperature, control rods, and poison; and fission power generated (point kinetics).

Researchers incorporated the adapted model into the heat transfer system described above. Figure 2 shows the desired configuration, which allows studying the effects of transients on the nuclear reactor.

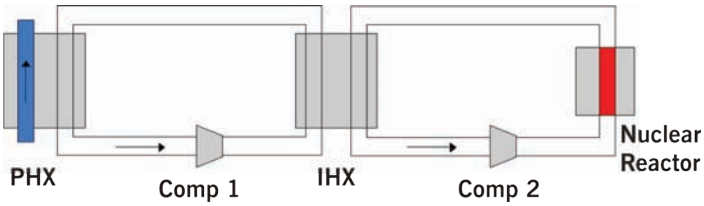

Figure 2. Heat transfer system with two loops.

The team then simulated a four-stage system start-up. The first was to stabilize the system at a low power level, which was achieved by running the compressors and nuclear reactor at one percent of the design power level and waiting until the system reached a steady state. Second, the heat removal system was started by increasing compressor power in both loops and gas flow on the cold side of the primary heat exchanger (PHX). Third, the heat generated in the nuclear reactor was boosted until it reached the design point. Finally, the temperature in the cold side of the PHX was raised, representing start-up of the chemical plant.

Modeling of the Sulfur-Iodine Thermochemical Cycle. Thermochemical water splitting is an energy-efficient, low-cost process for hydrogen production. The SI thermochemical cycle appears to be one of the most promising production processes. In this cycle, iodine and sulfur dioxide are combined with water, forming hydrogen iodide (HI) and sulfuric acid (H_2SO_4), which are immiscible and can be readily separated. Then the sulfuric acid is decomposed at about 850°C, releasing the oxygen and recycling the sulfur dioxide. Finally, the hydrogen iodide is decomposed at about 400°C, releasing the hydrogen and recycling the iodine.

Modeling uncertainty arises from the complex formation of H_2SO_4 and H_2O at high temperatures and/or concentrations. Difficulties include the extraction of HI from the HI_x mixture because of the presence of an azeotrope in the mixture, the possibility of iodine precipitating as a solid, and the strong immiscibility of the H_2O-HI-I_2 mixture. Modeling the chemical equilibria in the major unit operations presents a challenge to simulating the SI process. The model for calculating the chemical equilibria has to be valid for temperatures up to 800°C. Furthermore, the prediction of speciation in the process sections, which is not among the traditional virtues of electrolyte thermodynamic models, is important for the simulation of thermochemical cycles.

Hence, the project team focused on developing thermodynamic models at the conditions in question, as well as advanced optimization techniques for parameter estimation in phase equilibrium problems and thermodynamic data reduction. After a literature study, the team chose the electrolyte-NRTL model as the basis for the simulation of the SI thermochemical cycle's thermodynamics. The electrolyte-NRTL model has the ability to predict reaction and phase (vapor-liquid and liquid-liquid) equilibria, includes the effect of temperature, and can handle multiple-electrolyte solutions.

The team refined the electrolyte-NRTL model for application to multi-electrolyte, mixed-solvent systems. The changes can be summarized as the substitution of the Pitzer-Debye-Hückel equation with a detailed form of the original Debye-Hückel model, the inclusion of hydration chemistry in a way that reflects hydration's effect on the solution's structure, and re-derivation of the NRTL term to extend the model to multi-electrolyte solutions. The team applied the models with considerable success to an extensive database of univalent, bivalent, and trivalent electrolytes, aqueous solutions of acids and bases, and multi-electrolyte solutions. The refined activity coefficient formulations are considerably more complex than those of the original electrolyte-NRTL model. Their advantage is thermodynamic consistency. Moreover, the refined formulation provides stronger predictive capability for multi-electrolyte solutions.

Researchers also developed a novel approach for parameter estimation, which they cast as a bilevel program with multiple lower-level programs corresponding to semi-infinite constraints given by requirements for 1) stabilizing the predicted phase split, 2) excluding additional spurious phase splits, 3) predicting the correct number of phases in each phase split, and 4) predicting the correct number of azeotropes. Global optimization techniques are necessary for the lower-level program; otherwise, the model predictions might correspond to unstable phase splits. Additionally, global solution of the upper-level program gives a certificate of optimality, which is useful in the case of model-experiment mismatch. The formulation developed is independent of the thermodynamic model used for predicting phase equilibria.

One major difficulty with modeling the SI cycle is inconsistency of experimental data at the conditions of interest. Hence, the team needed a comprehensive framework that deals with all aspects of SI cycle thermodynamics. This framework starts with development of a self-consistent database of thermodynamic properties for the SI thermochemical cycle's various sections. For this objective, the team constructed a database of published thermodynamic data for the aqueous solutions of sulfuric acid and hydrogen iodide. The team then evaluated the data critically for self-consistency.

Planned Activities

The project is complete.

NUCLEAR ENERGY RESEARCH INITIATIVE

High-Performance Electrolyzers for Hybrid Thermochemical Cycles

PI: John W. Weidner, University of South Carolina

Collaborators: Argonne National Laboratory, Sandia National Laboratory, Savannah River National Laboratory

Project Number: 06-054

Program Area: NHI

Program Start Date: March 2006

Program End Date: March 2009

Research Objectives

The objective of this project was to provide the scientific basis for developing high-performance electrolyzers for use in two candidate thermochemical cycles for producing hydrogen from nuclear power: the hybrid sulfur process and the modified calcium-bromine cycle. A number of challenges currently prevent commercial viability of these thermochemical cycles, including 1) reducing the high cost of platinum and ruthenium catalysts, 2) minimizing sulfur dioxide (SO_2) crossover (a serious lifetime-limiting phenomenon), and 3) finding suitable operating conditions for optimal electrolyzer performance and cycle efficiency. This work built on the successful application of the proton exchange membrane (PEM) electrolyzer for producing hydrogen through the conversion of water and sulfur dioxide ($2H_2O + SO_2 \rightarrow H_2SO_4 + H_2$) and the dissociation of hydrogen bromide ($2HBr \rightarrow Br_2 + H_2$).

Researchers explored methods for improving utilization of platinum and ruthenium in the cathodes and anodes, along with replacing these elements with other materials such as metal alloys, silicides, mixed metal oxides, or a combination. The project team developed new membranes with low gas crossover and high conductivity, mechanical stability, and temperature resistance, enabling operation at higher temperatures and pressures. The team will evaluate the most promising catalysts and membranes in the PEM electrolyzer over a range of conditions (i.e., 30°C to 120°C, 1 to 10 atm, and 50 to 80 percent conversions) and will apply mathematical models to optimize cell and process performance.

Research Progress

The hybrid sulfur electrolyzer has been investigated as a means to produce clean hydrogen efficiently on a large scale by first decomposing concentrated sulfuric acid to SO_2 and O_2, and then electrochemically oxidizing SO_2 to sulfuric acid (H_2SO_4) with the co-generation of H_2. Project researchers have shown the importance of water transport in the cell to overall electrolyzer performance. Water is required at the anode to participate in the oxidation of SO_2 to H_2SO_4 and to hydrate the membrane. In addition, water transport to the anode influences the concentration of the sulfuric acid produced. The resulting sulfuric acid concentration at the anode influences the equilibrium potential of and the reaction kinetics for SO_2 oxidation and the average conductivity of the membrane. In this report, researchers extend their understanding of water transport to predict the individual potential contributions to the cell potential.

Figure 1 shows the specific-area resistance predicted from the project model[1] for three different thicknesses of Nafion® membrane as a function of sulfuric acid concentration. As the sulfuric acid concentration at the anode increases, the membrane water content decreases. Because the conductivity of Nafion is dependent on membrane water content, a decrease in the water content leads to a decrease in the membrane conductivity. The membrane conductivity as a function of sulfuric acid concentration was measured with a four-point measurement technique. Researchers combined this data with their water uptake data to find the conductivity as a function of water content. Thus, operating the Nafion-based electrolyzer at high current densities, where a high concentration of sulfuric acid at the anode results in high membrane specific-area resistance, will result in significant operating overpotentials. For example, Figure 2 shows the potential contributions to an N212 electrolyzer operating at $\Delta P = 600$ kPa and $T = 80°C$. The cathodic overpotential is due to the hydrogen evolution reaction and was measured by subtracting the membrane resistance from the membrane electrode assembly (MEA) resistance (measured by hydrogen pump).

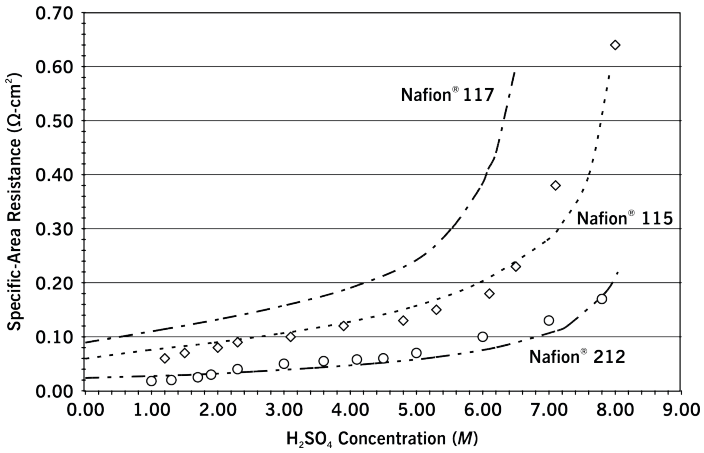

Figure 1. Membrane specific-area resistance as a function of sulfuric acid concentration at the anode at 80°C. The N212 (○) and N115 (◊) current interrupt points are experimental data.

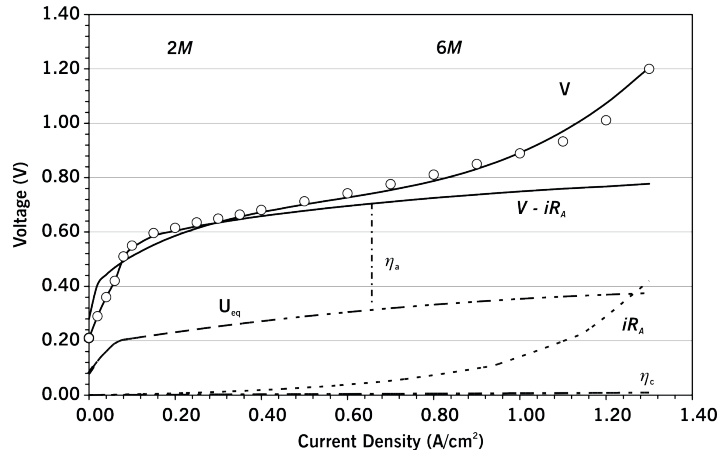

Figure 2. Contributions of the cell potential for N212 at 80°C. The points (○) are experimental data and the lines are model predictions. The total cell potential was predicted as the sum of the individual potential contributions.

The catalyst layer ohmic resistance was found to be very small and was the same for the anode and cathode. The team calculated overpotentials that were due to the electrode resistance and found them to be consistent with those reported previously in the literature. Thus, the catalyst layer ohmic resistance is a negligible component of the cell voltage and is not an important part of the anodic overpotential. The reversible cell potential, U_{eq}, was determined previously as a function of sulfuric acid concentration at the anode and P_{H2} at the cathode.[2] Because sulfuric acid concentration at the anode can be correlated with current density for each electrolzyer, this information has been plotted as a function of current density (see Figure 2). The contribution to the reversible cell potential by producing hydrogen at P_{H2} = 700 kPa is about 0.030 volts (V). The iR_A contribution is obtained by multiplying the membrane specific-area resistance by the current density. The V - iR_A lines in Figure 2 were determined by subtracting the iR_A contribution from the measured cell potential at each current density, again assuming that the resistance of the cell hardware is negligible. The anodic overpotential, then, is the difference between the V - iR_A curve and the contribution of the reversible cell potential, U_{eq}, and the cathodic overpotential, η_c. The model was used to predict the operating cell potential by summing the individual contributions. As Figure 2 clearly shows, the model closely predicts the experimental data for electrolyzer operating potential as a function of current density. Because the largest contribution to cell potential at high current density comes from the membrane specific-area resistance, Nafion is probably not a suitable choice for the membrane used in the hybrid sulfur process.

In conclusion, the project team has investigated the contributions of reversible cell potential, losses due to membrane specific-area resistance, and anodic overpotential for the hybrid sulfur electrolyzer. Results show that the membrane specific-area resistance increases with the concentration of sulfuric acid at the anode due to the decrease in membrane water content. Researchers have discussed the need for a novel proton exchange membrane, one in which the conductivity is not adversely affected by concentrated sulfuric acid. This membrane will allow operation at higher current densities (i.e., higher sulfuric acid concentration at the anode), which will reduce capital cost and improve efficiency. Finally, the team has used the model to predict the overall operating cell potential and shown the importance of water transport in determining the operating cell potential. Water flux to the anode influences the sulfuric acid concentration, which determines the reversible cell potential, the membrane specific-area resistance, and the electrode kinetics. Thus, careful control of the membrane water transport is essential for optimized electrolyzer operation.

Planned Activities

The project has been completed.

References

[1] J. A. Staser, M. B. Gorensek, and J. W. Weidner, "Quantifying Individual Voltage Contributions to the Hybrid Sulfur Electrolyzer," submitted, *J. Electrochim. Soc.*, November 2009.

[2] M. B. Gorensek, J. A. Staser, T. G. Stanford, and J. W. Weidner, "A Thermodynamic Analysis of the SO_2/H_2SO_4 System in SO_2 – Depolarized Electrolysis," *Int. J. Hydr. Energy*, 34 6089-6095 (2009).

NUCLEAR ENERGY RESEARCH INITIATIVE

Development of Efficient Flow Sheet and Transient Modeling for Nuclear Heat Coupled Sulfur Iodine Cycle for Hydrogen Production

PI: Shripad T. Revankar, Purdue University

Collaborators: None

Project Number: 06-060

Program Area: NHI

Project Start Date: April 2006

Project End Date: March 2010

Research Objectives

The main goal of this project is to develop a flow sheet for the closed-loop sulfur iodine (SI) cycle for nuclear hydrogen production. This flow sheet will use current advances in acid decomposition and product gas separation to achieve high thermal efficiency. It will result in the development of transient analysis methods for the SI cycle. Although the closed-loop SI cycle has recently been demonstrated on a bench scale, several challenges remain, such as maintaining stable operation, enhancing efficiency, obtaining thermodynamic data for the reactions, coupling to a high-temperature nuclear reactor, and determining transient behavior of the coupled system. This project will develop models to study transient performance of the closed-loop SI cycle. In addition, this research will explore several proposed alternatives to SI cycles.

Specific objectives of the project are to:

- Perform benchmark flow sheet analysis of the baseline SI cycle.
- Investigate membrane techniques for hydrogen iodide (HI) and sulfuric acid (H_2SO_4) decomposition and separation processes.
- Perform comparative flow sheet analyses of the modified cycles.
- Develop component-wise SI cycle models for application to the transient analysis.
- Perform preliminary analysis of transient behavior of the closed-loop SI cycle.

Research Progress

The SI cycle consists of three chemical reactions expressed as the following equations:

Section I - Bunsen reaction:
$I_2 + SO_2 + 2H_2O \rightarrow 2HI + H_2SO_4$

Section II - sulfuric acid decomposition:
$H_2SO_4 \rightarrow H_2O + SO_2 + \frac{1}{2}O_2$

Section III - hydrogen iodide decomposition:
$2HI \rightarrow H_2 + I_2$

For the current work, the flow sheet that General Atomics (GA) previously developed for the SI cycle was considered as a baseline. During the first year, efforts focused on developing and benchmarking a simulation model for the GA SI cycle flow sheet. This analysis was carried out to establish the simulation capability and check the GA flow sheet model's repeatability. The project team achieved the Section II convergence.

During the second year, the team simulated the SI thermochemical cycle using the chemical process simulation code ASPEN PLUS Version 12. Researchers studied the GA flow sheet and developed ASPEN models for Sections I and III. They performed a step-by-step simulation starting from the single component simulation to the whole sections simulation.

During the third year, researchers developed a simplified model for the SI cycle with chemical kinetics models of the three main SI reactions: the Bunsen reaction, sulfuric acid decomposition, and hydriodic acid decomposition. Each reaction was modeled with a single-control volume reaction chamber. The simplified model uses basic heat and mass balance for each of the three main reactions. For sulfuric

acid decomposition and hydriodic acid decomposition, researchers considered reaction heat, latent heat, and sensible heat. Since the Bunsen reaction is exothermic and its overall energy contribution is small, its heat energy is neglected. However, the input and output streams from the Bunsen reaction are accounted for in balancing the total stream mass flow rates from the SI cycle. The heat transfer between the reactor coolant (in this case helium) and the chemical reaction chamber was modeled with transient energy balance equations. Researchers used the model to study steady-state and transient behavior of the coupled system. The study showed that the rate-limiting step of the entire SI cycle is hydriodic acid decomposition.

In the model for the nuclear plant and its interfacing system, a simplified transient model of the SI cycle based on a control volume approach was coupled to a THERMIX thermal hydraulic model of the Pebble Bed Modular Reactor 268 (PBMR 268) and a point kinetics nuclear model. The researchers attained a steady-state solution of the SI cycle model and THERMIX model and carried out a transient analysis of the coupled system.

When unifying two dynamic systems that provide feedback to each other, the plant's relative time constants dictate the nature of the response. A PBMR is a thermal reactor; thus delayed neutrons are the important factor in reactor response, yielding a time constant of about 55 seconds. In the chemical plant, Section 2 and Section 3 have different response times (as Figure 1 illustrates). Section 2 has a response time of the order of 20 seconds; Section 3's response time is approximately 500 seconds. The limiting reaction rate in the chemical plant is that of Section 3. Since the chemical plant is composed of cyclic processes, the slowest reaction rate will occur in Section 3, the HI decomposition section. This rate provides at least a first-order approximation of the plant response.

HI decomposition requires a very large volume, which accounts for Section 3's long response time. This large volume is due to the reverse reaction rate of HI decomposition, which is on the same order as the forward reaction rate. In the simplified SI model, HI decomposition is the most challenging reaction in terms of chemical kinetics. In contrast, the chemical kinetics of the H_2SO_4 decomposition are straightforward, but high temperature and the solution's highly corrosive nature effect many material difficulties. The long response time of Section 3 slows chemical plant feedback to the nuclear reactor.

The project team studied a reactivity-induced transient in a PBMR reactor coupled to an SI cycle. Researchers considered a control rod ejection leading insertion of an unrealistically large amount of reactivity over a short time (0.1 seconds). This transient resulted in a large power excursion of short duration. Because of feedback of the negative fuel temperature coefficient, the reactor shut down. Figure 1 shows the relative reactor power and hydrogen generation rate for the first 500 seconds following the transient.

Planned Activities

The remaining tasks for the extended period are to:

- Perform further transient scenarios, including chemical plant driven transient in a coupled PBMR and SI plant system.
- Develop operational and process control strategies for the SI plant.
- Develop preliminary guidelines for the control logic in both plant sides.
- Identify research challenges for future work.

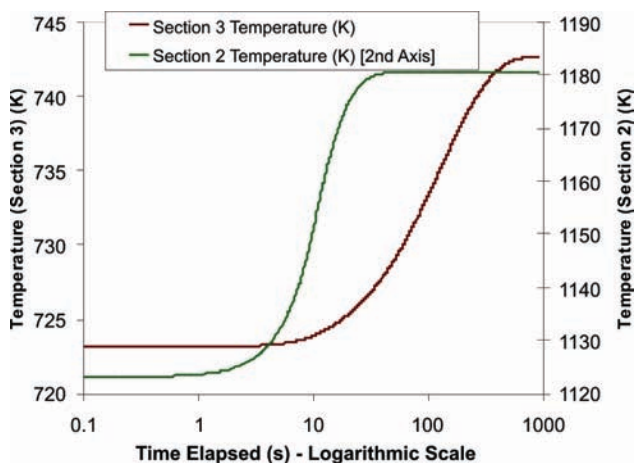

Figure 1. Response time of Section 2 and Section 3 decomposition reactions.

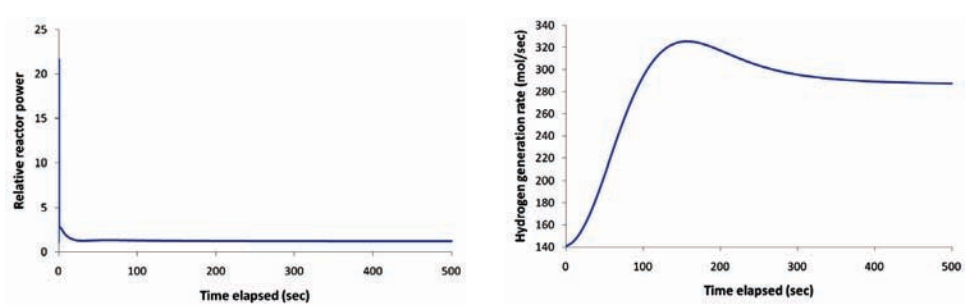

Figure 2. Relative reactor power and hydrogen generation rate following large reactivity insertion to the reactor.

NUCLEAR ENERGY RESEARCH INITIATIVE

Gradient Meshed and Toughened Solid Oxide Electrolyzer Cell Composite Seal With Self-Healing Capabilities

PI: Kathy Lu, Virginia Polytechnic Institute and State University

Collaborators: Idaho National Laboratory

Project Number: 06-140

Program Area: NHI

Project Start Date: June 2006

Project End Date: March 2010

Research Objectives

High-temperature electrolysis of water steam is a promising approach for hydrogen production. The potential becomes even more promising with the efficient utilization of abundant heat sources from nuclear power reactors. Hydrogen production through the above approach also allows for low electric consumption. Overall conversion efficiencies for high-temperature electrolysis are in the 45–50 percent range compared to approximately 30 percent for conventional electrolysis. However, current solid oxide electrolyzer cell (SOEC) seals hinder this promising technology because of a mismatch in thermal expansion coefficients that causes seal cracking and gas leakage.

This research focuses on designing a new glass seal system and increasing the operation time and high-temperature stability of SOECs used for splitting water into hydrogen. Specifically, the research team is focusing on improving SOEC seal thermal stability and performance by alleviating thermal stress and seal-cracking issues. The researchers are also trying to understand differences with the seal-interconnect interaction under different atmospheres for extended periods of time.

The team will conduct experiments to assess overall sealing glass stability, sealing performance, and interaction of the seal with other electrolyzer cell components.

Research Progress

In FY 2008, the research team systematically studied novel glasses of different compositions based on a SABS system (SrO-La_2O_3-Al_2O_3-B_2O_3-SiO_2). They examined Crofer 22 APU/SABS-0 glass, Ni substrate/SABS-0 glass, and shape memory alloy/SABS-0 glass interfacial diffusion at 800°C in an argon atmosphere for up to 200 hours.

This year, the team thermally treated both bulk and powder forms of SABS-0 glass in air and H_2/H_2O for 1,000 hours to study thermal stability and devitrification resistance. Weight measurements show negligible glass vaporization. Both the powder and bulk samples showed some surface devitrification, but the bulk glass remained amorphous under all thermal treatment conditions. Researchers observed needle-shaped crystals on the polished bulk SABS-0 surface for both the air and H_2/H_2O thermal treatment conditions. The team believes surface polishing to be the initiator of SABS-0 glass surface devitrification. The crystal phases, indentified as strontium and lanthanum silicates, increase with thermal treatment time. However, the crystalline phases are limited to the outermost surface of the polished SABS-0 glass for both air and H_2/H_2O atmosphere treatment conditions.

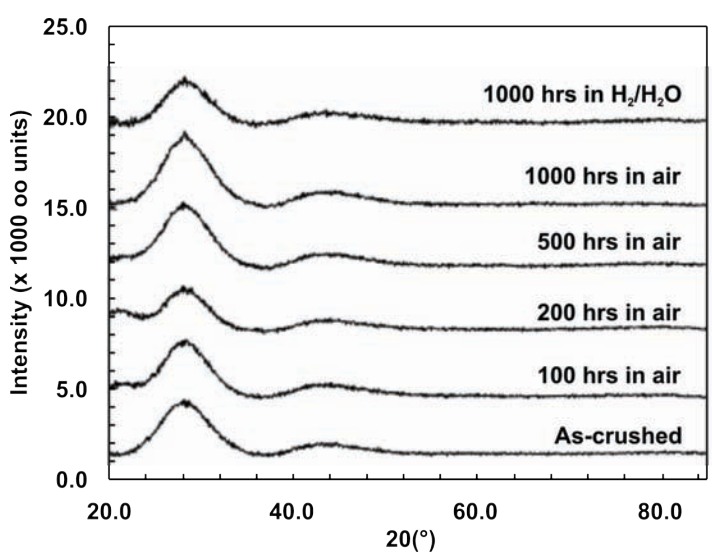

Figure 1. X-ray diffraction patterns of SABS-0 glass powders thermally treated at 800°C in air for different times and H_2/H_2O atmosphere for 1,000 hours.

The team investigated interfacial compatibility of Crofer 22 APU alloy/SABS-0 glass, $(Mn,Co)_3O_4$-coated Crofer 22 APU/SABS-0 glass, bare T441/SABS-0 glass, and $(Mn,Co)_3O_4$-coated T441/SABS-0 glass at conditions up to 1,000 hours at 800°C in both air and H_2/H_2O atmosphere. In air, all the studied samples showed pore- and crack-free interfaces. Energy dispersive spectroscopy (EDS) line-mapping results show that the interdiffusion zone is less than 5.0 microns (μm) after 1,000 hours of thermal treatment. There was an accumulation of lanthanum (La), aluminum (Al), chromium (Cr), titanium (Ti), manganese (Mn), and cobalt (Co) species at the diffusion couple interface. Chromium evaporation from the T441 alloy poses potential cracking problems for long-term use.

The study in a H_2/H_2O atmosphere also showed an accumulation of La, Al, Cr, Ti, Mn, and Co species at the diffusion couple interface. Interfacial cracking between the SABS-0 glass and the interconnects was more severe, and the $(Mn,Co)_3O_4$ coating was not very effective in preventing the cracking. All the elements present in the SABS-0 glass (oxygen [O], silicon [Si], strontium [Sr], La, and Al) diffuse 2–3 μm into the Crofer 22 APU alloy. Similarly, the primary elements present in Crofer 22 APU (iron [Fe] and Cr) also diffuse 2–3 μm into the SABS-0 glass, while the minor elements (Mn and Ti) accumulate at the interface. For the Crofer 22 APU alloy/SABS-0 glass sample, a distinct interfacial layer approximately 1–2 μm thick formed in the thermally treated samples. Surprisingly, the thickness of the interface layer *decreased* as thermal treatment time *increased* from 200 to 1,000 hours. For the $(Mn,Co)_3O_4$-coated Crofer 22 APU/SABS-0 glass sample, however, the thickness of the interface layer increased with thermal treatment time. The SABS-0 glass close to the interface devitrified after 200 hours and 500 hours of thermal treatment, although the extent of devitrification is limited to 5–7 μm. More oxides form on the SABS-0 glass side after 1,000 hours of thermal treatment.

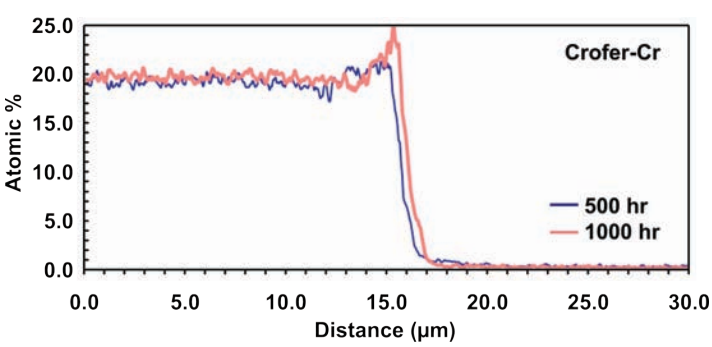

Figure 2. EDS spectra of the Cr element in the Crofer 22 APU/SABS-0 glass couple thermally treated at 800°C in air for 500 hours and 1,000 hours.

For both T441/SABS-0 samples (bare and coated), the thickness of the interface layer decreases with thermal treatment time from 200 hours to 500 hours. Appearance of pores and cracks along the interface (2–3 μm thick) suggests that the T441/SABS-0 sample has interfacial stability issues. The SABS-0 glass shows poor compatibility with the $(Mn,Co)_3O_4$ coating, and the bonding between the coated T441 alloy and the SABS-0 glass is weaker than that of uncoated T441/SABS-0 glass.

The research team thermally treated the Crofer 22 APU/SABS-0 and T441/SABS-0 glass samples at 800°C for 100 hours in air, argon, and wet hydrogen. With the Crofer 22 APU/SABS-0, the team identified two crystalline phases as $La_2Cr_2O_9$ and $Sr_7Al_{12}O_{25}$. Regardless of the thermal treatment atmospheres, these crystalline phases demonstrate good interfacial stability of the SABS-0 glass with the Crofer 22 APU alloy interconnect. With the T441/SABS-0, the team identified two crystalline phases as $La_2Si_2O_7$ and $Sr_7Al_{12}O_{25}$. Regardless of the thermal treatment atmospheres, these crystalline phases demonstrate good interfacial stability of the SABS-0 glass with the T441 alloy.

Of the four different seal glasses researchers have produced for extensive interfacial study with the T441 interconnect material (YSO-4, G18, SABS-0, and SCAN2), the SABS-0 glass shows the best performance, with no pores or cracks observed at the T441/SABS-0 interface. The other three glasses showed some closed pores on the metal side for the as-bonded and the thermally treated samples. On the glass side, the glass partially devitrified after bonding and also formed cracks.

Using a gas leakage test, the team evaluated the SABS-0 glass's sealing performance. For the T441-SABS-0-YSZ sealing test, researchers detected no gas leakage for up to 60 thermal cycles and 960 hours at 800°C. The gas tightness and the thermal cycling stability of the SABS-0 glass demonstrate the feasibility of the SABS-0 glass as a suitable SOEC seal.

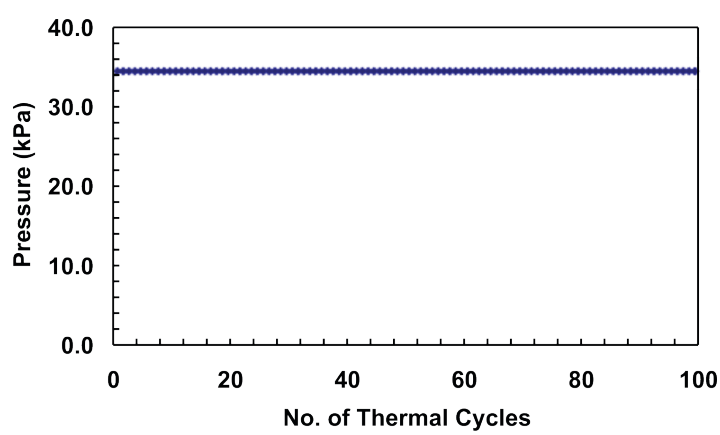

Figure 3. Sealing performance of the SABS-0 glass in the T441/SABS-0/YSZ assembly as a function of number of thermal cycles.

Planned Activities

Researchers plan to perform the following tasks over the next fiscal year:

- Continue to study SABS glass seal systems and tailor their compositions to produce complementary thermal behaviors during SOEC operation.
- Conduct comprehensive seal testing to demonstrate smooth thermal expansion coefficient transition, cracking resistance, and crack self-healing capabilities of the new composite seal.
- Make seals using actual SOEC seal configurations, and continue to optimize seal performances.

The research team has requested and received a no-cost extension. During this project, researchers discovered a promising SABS-0 glass system for which they have filed a provisional patent. In the long run, the new SABS-0 glass sealing system will have simpler design, lower cost, and higher performance than the composite seal. This new research area, which was not included in the initial plan, requires more research efforts but will also offer much more impact than the initial plan. The research team is further testing this new seal glass based on the high moisture condition recommended by Idaho National Laboratory. The new completion date is March 2010.

NUCLEAR ENERGY RESEARCH INITIATIVE

Liquid Salts as Media for Process Heat Transfer from Very High-Temperature Reactors: Forced Convective Channel Flow Thermal Hydraulics, Materials, and Coatings

PI: Kumar Sridharan, University of Wisconsin-Madison

Collaborators: None

Project Number: 07-030

Program Area: NHI

Project Start Date: June 2007

Project End Date: May 2010

Research Objectives

This project investigates the use of liquid salts as heat transfer fluids to utilize process heat from very high-temperature reactors (VHTRs) and other Generation IV reactors for hydrogen production. Favorable thermal properties of liquid salts (such as their lower melting point, high boiling point, high heat capacity, chemical stability, and low pumping power requirements) allow for efficient transport of high-temperature thermal energy. To successfully implement a liquid salt reactor/hydrogen production process interface, scientists require an accurate assessment of the thermal hydraulics in small-diameter channel, high-efficiency compact heat exchangers. Thermal hydraulics and materials are both key operational issues in these small channels, which operate under high flow velocity and high temperatures. In particular, information on corrosion/erosion resistance of materials and coatings is needed for the construction of intermediate heat exchanger systems, along with operational experience to determine minimum channel sizes to avoid clogging and to optimize heat transfer.

Specific project objectives are to 1) investigate material and coating corrosion performance by performing static corrosion tests in two liquid salts—FLiNaK and 32%$MgCl_2$-68%KCl—at 850°C for 500 hours, 2) fabricate a forced convection loop to study thermal hydraulics (including clogging effects) in small channels and particle transport and deposition issues, and 3) evaluate materials and coatings under prototypic velocity liquid salt flow conditions. Materials to be investigated include Inconel alloys 800H, 600, 617, 625, and 718, Haynes 230, 316 stainless steel, and carbon-carbon and silicon-carbide (SiC) composites. Coatings to be studied include optimized electroplated nickel (Ni) as well as hard carbon and pyrolytic carbon coatings.

Research Progress

Molten Salt Loop Construction and Testing. The research team has designed and constructed the forced convection molten salt test loop to examine effects of molten salt flow through small diameter channels, similar to channels for the intermediate heat exchanger (IHX). The loop is made entirely out of 316 stainless steel, which exhibits less corrosion than Inconel 600 in both fluoride- and chloride-based salts. Because of the high temperatures and the salt's corrosive nature, researchers had to develop a specialty pump, flow meter, and pressure sensor for the loop. The test section is approximately 0.6 meters long, and IHX channels have diameters that range from 1 to 10 millimeters (mm). These tests are intended to produce experimental pressure drop and heat transfer data for small channel flow of liquid salts in heating and cooling conditions. Researchers will initiate experiments with

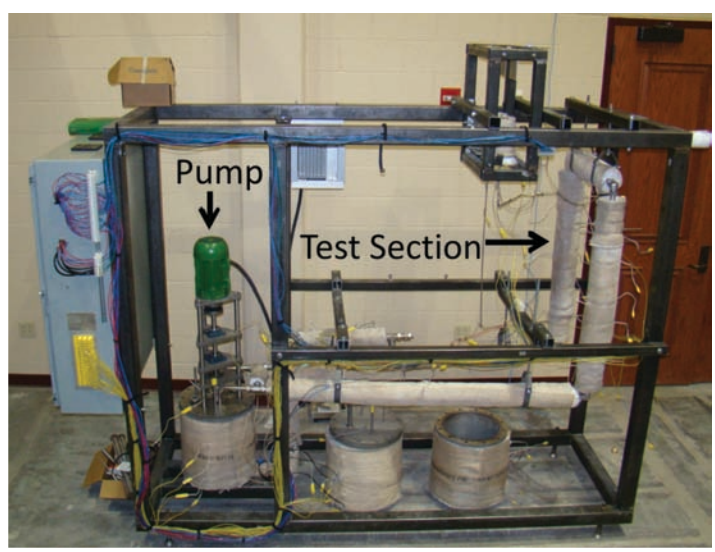

Figure 1. Forced convection molten salt materials test loop.

prototypical IHX flow (a Reynolds flow of approximately 150) but will investigate a wide range of Reynolds flows. These tests will also help the team study the transfer of corrosion products from the hot to cold sections of the loop.

Static Corrosion Testing in Liquid Chloride Salts. Researchers exposed several candidate alloys to molten KCl-$MgCl_2$ eutectic salt at 850°C: Inconel alloys 800H, 600, 617, 625, and 718; Haynes 230; 316 stainless steel; silicon-carbide (SiC) composite; and coated SiC composite. Figure 2 shows a static corrosion test in which alloys were sealed in quartz ampoules with KCl-$MgCl_2$. The team analyzed the salt and corrosion test specimens using neutron activation analysis, scanning electron microscopy, and energy dispersive spectroscopy. Results indicate that the primary mode of corrosion in molten chloride salts is selective dissolution and dealloying of chromium (Cr) from the base alloy.

Figure 2. Photograph of quartz ampoules encapsulating alloy samples and molten KCl-$MgCl_2$ salt after corrosion tests at 850°C.

The team investigated several coatings and post-processing techniques for the economic application of common high-temperature alloys and ceramics in molten salts. For iron (Fe)- and Ni-based alloys, the team studied Ni electroplating, molybdenum thermal spray, and diamond-like coatings. Ni electroplating greatly reduced the rate of corrosion caused by Cr dealloying from the base alloy. Additionally, the team used a chemical vapor deposition (CVD) process to deposit a SiC/pyrolytic carbon coating on C/SiSiC composite substrates, then exposed the samples to molten KCl-$MgCl_2$ at 850°C for 500 hours. Figure 3 shows SEM cross-sectional images of the uncoated and coated composites. The coated composite was remarkably more resistant to corrosion.

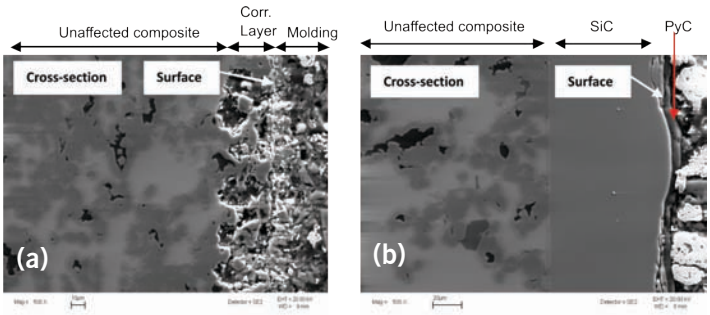

Figure 3. Cross-sectional SEM images of C/SiSiC composite samples after corrosion tests in molten KCl-$MgCl_2$ at 850°C for 500 hours: (a) uncoated composite and (b) composite with SiC/pyrolytic carbon coating.

Using Incoloy-800H, researchers studied microstructural modification by grain boundary engineering (GBE) as a possible method to mitigate corrosion in molten chloride salts. GBE greatly decreased the rate of Cr dealloying. Figure 4 shows Cr x-ray maps of Incoloy-800H, unmodified and post-GBE, after exposure to KCl-$MgCl_2$ at 850°C. The grain boundary engineered specimens lost much less Cr than the unmodified alloy, indicating longer service life for the modified alloy.

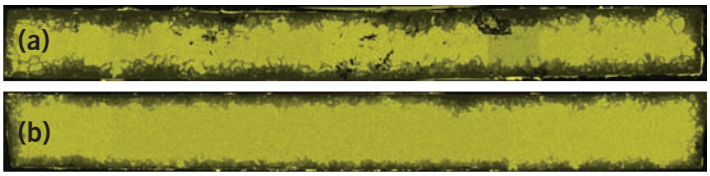

Figure 4. SEM-EDS-Cr maps of cross-sections of Incoloy 800H after corrosion tests in molten KCl-$MgCl_2$ at 850°C: (a) as-received and (b) after GBE.

Planned Activities

In the immediate future, the research team will measure heat transfer properties of molten salt in the forced convection loop and will evaluate viability of small channel heat exchanger designs. The team will also study materials corrosion in the forced convection loop. Because GBE proved to greatly reduce Cr dealloying along specific Cr pathways, researchers will investigate this approach for other alloys, such as 316 stainless steel.

NUCLEAR ENERGY RESEARCH INITIATIVE

Optimization of Heat Exchangers

PI: Ivan Catton, University of California-Los Angeles

Collaborators: None

Project Number: 07-057

Program Area: NHI

Project Start Date: June 2007

Project End Date: June 2010

Research Objectives

The primary goal of this project is to optimize heat exchangers (HEs), mostly to support Gen-IV nuclear reactor concepts. Project objectives can be split into six steps, as follows:

- Develop a surface morphology for a heat exchanger that increases surface heat removal effectiveness by as much as a factor of four.
- To validate this new morphology, develop a new type of mathematical model capable of predicting flow and heat transfer in two- and three-dimensional (2D and 3D) spatial structures of HEs and compact heat exchangers (CHEs) at different length scales. This task entails solving for flow variables (pressure, velocity, temperature) in two fluids that are exchanging energy and a solid interface.
- Use the model as a basis for an optimizing method enabling full exploitation of the possible operating design parameter variations that are known to be beneficial. This model must be fast-running (much faster than current computational fluid dynamics [CFD] programs)–many runs in a short time allows for optimization.
- To verify this model, design and carry out experiments to 1) measure heat transfer dependency on surface augmentation, 2) validate the ability of CFD to predict results, and 3) validate HE and CHE models that can be used for optimization.
- Once the model and augmented surfaces are perfected and optimized, optimize several HEs or CHEs meeting the stated needs.
- To take the last task one step further, design and test a printed circuit heat exchanger (PCHE) applicable to the high-temperature inert-gas Brayton cycle.

Research Progress

The research was split into three different tasks, corresponding to the project's three-year duration.

The first project task was to develop a model for predicting friction and heat transfer from an augmented surface and demonstrate the model's fidelity by comparison with experimental data. The project team created a fast-running CHE optimization design tool. It could treat the full conjugate process using volume averaging theory (VAT) to simplify discrete energy and momentum equations. The tool's function incorporates the multilevel heterogeneous process of the heat exchanger, where conjugate effects are very important. To utilize VAT, the effects convection and conduction must be separate in the energy equations—an achievement that could be approached several ways. One could use modern CFD to achieve direct numerical simulation. However, this process is very time-consuming. One could use existing methods and/or models to approach the problem as if working with a porous medium. This method can be simplified by using an approach based on VAT. If VAT was applied to the whole HE, however, the results would be inaccurate.

To retain accuracy down to the surface augmentation, the project team wrote a VAT-based computer program that separates the HE into three levels. The lowest level is the interfacial surface between fluid and solid. The mid level is the HE's specific geometry, such as fin and tube. The upper level treats the conjugate problem, applying results of the lower level as the closure (see next page). This

program creates a model with the maximum number of parameters available for optimization, and the model can be optimized using an available commercial optimizing program (such as DOE Fusion Pro from the S-Matrix Corporation).

To use this model, researchers constructed a database for augmented surfaces (an effort that will continue throughout the grant period). The team used only data from experiments that measure the actual interface heat transfer coefficient. So far this database includes ribs (rectangular, triangular, hemispherical), fins (plane, augmented), 3D (hemispheres, dimples, scales), and pins (rectangular, circular, oval).

With this process, closure is necessary to model CHEs. For momentum equations, this closure takes the form of the friction factor or drag coefficient. For energy equations, this closure takes the form of the interface heat transfer coefficient. VAT-based equations use a representative elementary volume (REV) (the control volume); the friction factor and heat transfer coefficient must be known for each REV. Energy equation closure allows for substantial gains only when the connection is maintained between porous medium morphology and the rigorous formulation of mathematical equations for transport. Scientists can develop and solve numerically a VAT-based equation set to determine the heat transfer coefficient from the experimental gas phase temperature response. Only the measured temperature response, flow condition, and physical properties of the system are needed. This data can be found for a specific REV using commercial CFD programs as well as through experiment.

The second project task was to complete development and validation of an augmented surface model. The project team conducted experiments and CFD studies to complete the data sets needed for the augmented surface model and began optimization studies of selected surfaces. Researchers have developed and begun to implement an experimental procedure for measuring internal heat transfer coefficients. In addition, the team has demonstrated the use of CFD to determine the heat transfer coefficient and friction factor for one morphology.

The team addressed CHE optimization in four steps. First, researchers had to employ the two temperature VAT equations to determine the parameters needed for optimization, such as overall dimensions of the heat exchanger and required effectiveness. Second, the team used DOE Fusion Pro to perform statistical design of experiments for the many optimization parameters. Next, the team chose specific cases for numerical simulations, suggested by statistical analyses of optimization parameters. Researchers used the fast-running model, developed in the first task, to perform these numerical simulations. The fourth step was to statistically analyze the numerical results to obtain an optimization response surface.

Following this process, the project has optimized a plane fin heat sink of specific size with augmented fins. The parameters for this problem were changing fin height, width, pitch, and Reynolds number. Figure 1 shows the effect of varying fin height and width for a set pitch/fin width and Reynolds number. The lines on the figures represent optimization goals: 1) minimizing thermal resistance and midpoint temperatures (goals are met to the left of these lines), and 2) maximizing effectiveness (goal is met to the right of this line). In Figure 1(a), a plane fin heat sink, the areas cross, indicating that all three goals cannot be met. However, augmenting the surface of the fin (Figure 1[b]) produces an area that meets all desired goals.

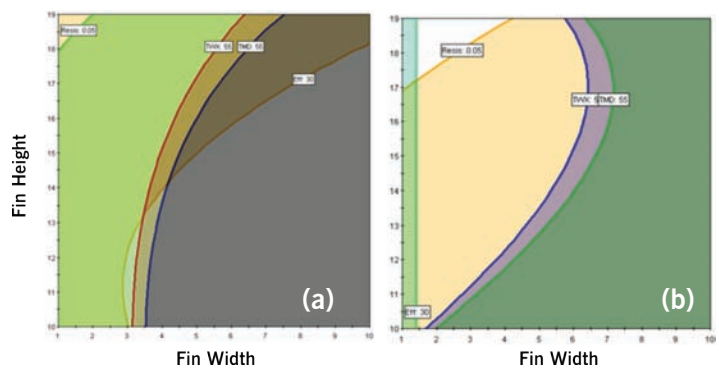

Figure 1. (a) Plane fin; (b) plane fin with augmented fins.

Planned Activities

The project will use the VAT-based model to complete optimization of several different types of augmented surfaces. The VAT-based CHE optimization model can be used to produce several optimum PCHE or flat plate HE recuperator designs that meet the requirements of the supercritical carbon dioxide Brayton cycle. Using these designs, the team will fabricate the optimized augmented surfaces and test them, validating the computational tools. The project will also propose high-temperature conditions, materials, and PCHE candidates for further study.

NUCLEAR ENERGY RESEARCH INITIATIVE

NERI Consortium - Advanced Electrochemical Technologies for Hydrogen Production by Alternative Thermochemical Cycles

PI: Serguei N. Lvov, The Pennsylvania State University

Collaborators: Argonne National Laboratory, Tulane University, University of South Carolina

Project Number: 08-047

Program Area: NHI

Project Start Date: October 2007

Project End Date: September 2010

Research Objectives

The consortium's main objective is to establish the most efficient technologies for hydrogen production that can be combined with nuclear reactor or solar heat sources. The medium-temperature thermochemical cycles, which convert water to hydrogen and oxygen, represent such technologies, and their potential should be thoroughly investigated. Based on outcomes from the first-year studies, the project identified the copper-chlorine (Cu-Cl) alternative thermochemical cycle as the most promising system to be addressed during the second year. During this reporting period, the consortium groups carried out experimental and theoretical studies specifically related to the Cu-Cl thermochemical cycle. The primary focus was development of the CuCl-hydrochloride (HCl) electrolyzer and exploration of avenues for increasing cycle efficiency.

Research Progress

Development of CuCl Electrolyzer. The team developed a laboratory-scale CuCl electrolyzer for testing different types of cation-exchange and anion-exchange membranes. Researchers varied reagent flow rates, concentrations, and temperature, then collected and measured the hydrogen produced. Figure 1 provides a schematic diagram of the system. Researchers used the data to estimate the current and voltage efficiency of the electrolysis processes and optimize process parameters and electrolytic cell design. From the Cu-Cl electrolysis experiments performed with a proton-exchange membrane, the team found that 1) the decomposition potential was around 0.4 volts (V), (2) the current efficiency was 98 percent, and 3) the voltage efficiency was 80 percent at 0.5 V and 0.1 amperes per square centimeter (A/cm^2), 50 percent at 0.8 V and 0.35 A/cm^2, and 40 percent at 1.0 V and 0.55 A/cm^2.

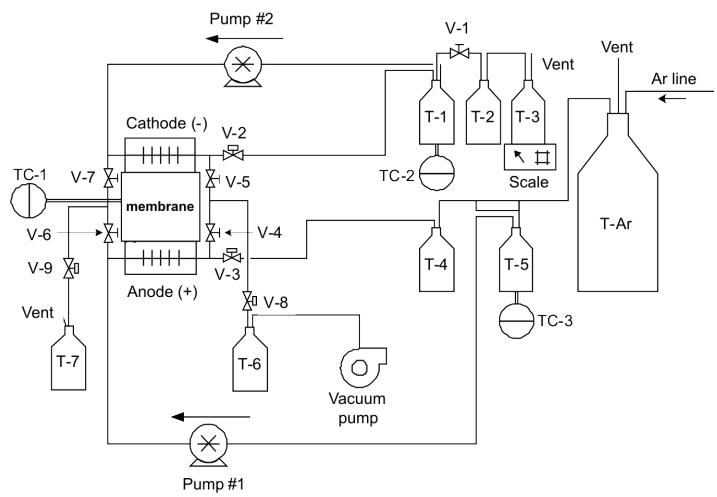

Figure 1. Schematic diagram of the CuCl electrolyzer: T-1 – Deionized water recirculation tank; T-2 – hydrogen (H_2) gas collection tank; T-3 – water displacement tank; T-4 – CuCl/HCl waste tank; T-5 – CuCl/HCl supply tank; T-6 – vacuum catch tank; T-7 – D.I. water supply tank (vacuum line); TC-1, 2, and 3 – measuring thermocouples; V-1 through V-9 – shut-off valves.

Thermodynamic Model of CuCl Electrolyzer Anolyte. The team has finalized development of the electrolyzer anolyte model represented by the Cu(I,II)-HCl-H_2O system. The model is based on a representative set of data on CuCl(s) solubility in aqueous solutions of HCl in the concentration range of one to seven moles per kilogram (mol kg^{-1}) HCl and a temperature range of 25°C to 100°C. The model considers a number of aqueous Cu(I) species (Cu^+, $CuOH^o$, $Cu(OH)_2^-$, $CuCl^o$, $CuCl_2^-$, $HCuCl_2^o$), aqueous Cu(II) species (Cu^{2+}, $CuOH^+$, CuO^o, $HCuO_2^-$, CuO_2^{2-}, $CuCl^+$, $CuCl_2^o$, $CuCl_3^-$, $CuCl_4^{2-}$), and a mixed Cu(I)/Cu(II) chloride aqueous complex, $Cu_2Cl_3^o$. The modelling approach is based on the minimization of the total Gibbs energy using a set of self-consistent thermodynamic properties and incorporates an adequate model for calculating the activity

coefficients. Using the model, researchers could calculate the decomposition potential similar to the experimentally observed value and theoretically predict the maximum possible current density of 2 A cm^{-2} at 0.8 V of the applied voltage when anolyte [0.2 mol kg^{-1} CuCl + 2 mol kg^{-1} HCl] (aq) is flowing at a rate of 30 cm^3 min^{-1}.

Synthesis and Characterization of New Ion Exchange Membranes. The team developed a new polyolefin-based Cl^- anion-conducting membrane that shows very desirable properties, such as high Cl^- ion conductivity (up to 100 or more microsiemens per centimeter [mS/cm]) and low Cu^+ and Cu^{+2} ions diffusion. The new membrane exhibits significantly better properties than commercial membranes in both 2 molar (M) HCl and 2 M HCl-0.2 M CuCl solutions. One example is a polyethylene copolymer containing many pending $NR_3^+Cl^-$ groups located at the end of side chains. The co-continuous hydrophobic and hydrophilic domains in the resulting PE-$NR_3^+Cl^-$ membrane allow a very high ion exchange capacity (IEC) without significantly weakening its stability by excess water-swelling. The combination of high IEC and good mobility of side chain results in high conductivity.

New Catalysts for Electrolyzer Anode. The low-cost high surface area active carbon black (VC 72R) was found to have an activity towards CuCl oxidation comparable to that of precious metal catalysts (platinum [Pt] and ruthenium oxide [RuO_2]). Electrochemical oxidation of Cu(I) in the CuCl-HCl-H_2O system was studied by cyclic voltammetry (CV) on the electrocatalysts made from VC 72R, Pt, Pt/C, and RuO_2. The four materials investigated had redox peaks with similar peak current density, indicating that the redox peak of Cu(I)/Cu(II) is not dependent on the catalysts. The kinetic currents in Tafel plots corrected for mass transfer showed that VC 72R has comparable activity to conventional catalysts made from Pt, Pt/C, and RuO_2. Mass transfer was identified as a significant source of impedance.

Electrolyzer Modeling. Researchers developed a mathematical model for the electrolyzer system to predict the change in concentration of copper chloride versus time as a function of design and operating parameters. The design parameters used were the volume of the system and the electrode surface area; the operating parameters were the concentration of copper chloride and current density. The experimental results were found to be in close agreement with the model developed. The next step would be to integrate this model into the Aspen Plus model for the complete Cu-Cl cycle.

Electrodialysis of Electrolyzer Catholyte and Anolyte. Using the electrodialysis cell that project researchers built and improved, they showed that it is possible to separate an HCl solution (typically 0.5 M HCl) into a stream of almost pure water (typically 0.01 M HCl) and a stream with a higher concentration of HCl (typically 2.2 M HCl), which could be concentrated even further if needed. Three combinations of anion-exchange and cation-exchange membranes were tested (AMX/CMS, ACM/CMS, and AAVC/CHV). The team also performed several sets of electrodialysis experiments with an ACS/CMX stack using a solution of 0.25 M CuCl, 0.75 M $CuCl_2$, and 4.5 M HCl in deionized water as the initial diluate stream. This solution simulates the stream that would be leaving the anode side of the electrolyzer in the Cu-Cl cycle. The electrodialysis cell was able to preferentially remove Cu(I) and H^+ from the diluate stream. Some of the CuCl and HCl were transferred from the diluate to the concentrate; the $CuCl_2$ remained in the diluate. Analysis of these experiments is still in progress.

Aspen Plus Modeling of the CuCl Electrolyzer. The team has simulated two major variants of the cycle. One assumes an anion-exchange membrane electrolyzer, and the other assumes a cation-exchange membrane electrolyzer. In either case, the power requirement is the same (voltage x current = charge transferred = H_2 produced), so the efficiencies of the different process schemes depend on how other parts of the cycle are managed. Hence, the cycle efficiencies are comparable. The team's current goal is to improve process efficiencies to better than 35 percent.

Aspen Plus Modeling of the Cu-Cl Thermochemical Cycle.

Electrolyzer: In the CuCl electrolyzer, Cl^- ions are transferred from cathode to anode, while electrons flow in the opposite direction, from the anode to the cathode. Three second-order equations for cell voltage, ohmic losses, and activation overpotential are incorporated in the electrolyzer model to solve for the overall cell potential.

Efficiency improvement: The team achieved efficiency improvement by first identifying the process units that had the highest heat duty. Subsequently, researchers added a series of pre-heaters and heat exchangers to conserve maximum energy and thus reduce the overall process load. The team changed the flowsheet model to produce an estimated efficiency of about 32 percent.

Heat pump cycles: The team carried out an extensive study on the heat pump cycle and associated working fluids to generate electricity from low-temperature heat available in the flowsheet. Researchers developed an Aspen Plus simulation to evaluate the effect of various working fluids on the net heat pump efficiency. They examined a wide range of turbine inlet temperatures between 50°C and 250°C. One hundred and eight (108) refrigerants with boiling points between -88.65°C and 110.65°C were investigated as working fluids. Recovery of some low-temperature waste heat increased overall efficiency by two percent (a small but potentially significant increase).

Solubility data regression: The team used the Aspen Plus process simulator to simulate phase diagrams of H_2O-$CuCl_2$ (43 data points), HCl-H_2O-$CuCl_2$ (30 data points), HCl-H_2O-CuCl (60 data points), and HCl-H_2O-CuCl-$CuCl_2$ (112 data points) systems. Researchers thus found the activity coefficients of electrolyte species over a wide temperature and concentration range using the NRTL model and electrolyte NRTL model. Around 250 data points from the literature were used to obtain the model parameters. Then the solubility isotherms in the H_2O-$CuCl_2$, HCl-H_2O-$CuCl_2$, HCl-H_2O-CuCl, and HCl-H_2O-CuCl-$CuCl_2$ systems were predicted and compared with the available literature data. The electrolyte NRTL model accurately predicted system solubility over the concentration and temperature ranges of interest.

Azeotropic separation of HCl-H_2O system: The HCl-H_2O mixture exhibits a negative azeotrope at a boiling temperature of 110°C for a system pressure of one bar at a hydrogen chloride concentration of 20.2 percent (by weight) and water concentration of 79.8 percent (by weight). The predicted phase diagram proves to be trustworthy and reliable for the process design of the azeotrope's separation into its components. The azeotropic distillation process for the separation of the HCl-H_2O mixture is simulated with the Aspen Plus. The simulation studies help confirm that the complete separation of the HCl-H_2O azeotropic mixture into its components is possible using the electrolyte $CuCl_2$.

High-Temperature Hydrolysis and Decomposition Reactions. The team is researching the hydrolysis reaction $2CuCl_2(s) + H_2O(g) \rightarrow Cu_2OCl_2(s) + 2HCl(g)$. The goals are to identify 1) a reactor design that provides the needed mass and heat transfer and 2) an engineering method to reduce the amount of steam required to obtain full conversion to the oxychloride. Researchers successfully tested a spray reactor, and results indicate sufficient mass and heat transfer. Also, the results of a sensitivity study show that a reduction in pressure from 1 bar to 0.5 bar reduces the steam-to-$CuCl_2$ molar ratio from about 17 to 12 while maintaining the yield of Cu_2OCl_2 near 100 percent. Some experiments were conducted in the spray reactor/ultrasonic nozzle apparatus to which an aspirator pump was added at the exit of the bubbler. It was found that the steam-to-$CuCl_2$ ratio was 11, less than half of the ratio of 23 used in the experiments with the ultrasonic nozzle. Analysis of the data indicated that smaller amounts of CuCl were formed at subatmospheric pressure than at atmospheric pressure. The XRD patterns also show evidence of $CuCl_2$, which indicates that conversion was not complete. Further optimization of the operating variables is needed. The oxygen evolution reaction, $Cu_2OCl_2(s) \rightarrow \frac{1}{2} O_2(g) + 2CuCl(s)$, is a relatively simple thermal decomposition process. The most recent work involved heating an in-house product from the hydrolysis reactor from room temperature to 700°C and following the evolution of the gaseous products with a mass spectrometer. The team found that evolution of oxygen starts at about 400°C and is essentially complete at around 525°C.

Planned Activities

This project is in the no-cost extension stage. The project will complete studies on the Cu-Cl thermochemical cycle with preparation and submission of papers, presentations at professional meetings, and preparation of the final report.

Index of NERI Projects

FY 2006 Projects

06-006 *Ab Initio*-Based Modeling of Radiation Effects in Multi-Component Alloys 23

06-007 Radiation Stability of Candidate Materials for Advanced Fuel Cycles 81

06-024 Nickel-Silicon Alloys for the Sulfur-Iodine Reactor-Hydrogen Production Process Interface 159

06-027 Microstructure Sensitive Design and Processing in Solid Oxide Electrolyzer Cell 161

06-038 The Development and Production of a Functionally Graded Composite for Lead-Bismuth Service 85

06-041 Dynamic Simulation and Optimization of Nuclear Hydrogen Production Systems....165

06-046 Managing Model Data Uncertainties in Simulator Predictions for Generation IV Systems via Optimum Experimental Design 25

06-047 Development and Utilization of Mathematical Optimization in Advanced Fuel Cycle Systems Analysis 87

06-054 High-Performance Electrolyzers for Hybrid Thermochemical Cycles 169

06-057 Uncertainty Quantification in the Reliability and Risk Assessment of Generation IV Reactors 29

06-058 Engineered Materials for Cesium and Strontium Storage....89

06-060 Development of Efficient Flow Sheet and Transient Modeling for Nuclear Heat Coupled Sulfur Iodine Cycle for Hydrogen Production 171

06-068 An Advanced Neutronic Analysis Toolkit with In-Line Monte Carlo Capability for Very High-Temperature Reactor Analysis 33

06-100 Improving Corrosion Behavior in the Supercritical Water Reactor, Lead Fast Reactor, and Very High-Temperature Reactor Materials by Formation of a Stable Oxide....35

06-109 Multi-Scale Modeling of the Deformation of Advanced Ferritic Steels for Generation IV Nuclear Energy Systems....37

06-113 Accelerator-Based Study of Irradiation Creep of Pyrolytic Carbon Used in TRISO Fuel Particles for the Very High-Temperature Reactor....93

06-116 Development of Acetic Acid Removal Technology for the UREX+ Process 97

06-137 Design and Development of Selective Extractants for Actinide/Lanthanide Separations....99

06-140 Gradient Meshed and Toughened Solid Oxide Electrolyzer Cell Composite Seal With Self-Healing Capabilities....173

06-141 Microwave Processing of Simulated Advanced Nuclear Fuel Pellets 101

FY 2007 Projects

07-003 An Advanced Integrated Diffusion/Transport Method for the Design, Analysis, and Optimization of Very High-Temperature Reactors....41

07-011 Implications of Graphite Radiation Damage on the Neutronic, Operational, and Safety Aspects of Very High-Temperature Reactors....43

07-015 Radiation-Induced Segregation and Phase Stability in Candidate Alloys for the Advanced Burner Reactor....105

07-017 Advancing the Fundamental Understanding and Scale-Up of TRISO Fuel Coaters via Advanced Measurement and Computational Techniques 45

07-018 Fission Product Transport in TRISO-Coated Particle Fuels: Multi-Scale Modeling and Experiment 49

07-020 Emissivity of Candidate Materials for Very High-Temperature Reactor Applications: Role of Oxidation and Surface Modification Treatments 53

07-023 Chemistry of Transuranic Elements in Solvent Extraction Processes: Factors Controlling Redox Speciation of Plutonium and Neptunium in Extraction Separation Processes 107

07-024 Materials and Design Methodology for Very High-Temperature Nuclear Systems 57

07-027 New Fission Product Waste Forms: Development and Characterization 109

07-030 Liquid Salts as Media for Process Heat Transfer from Very High-Temperature Reactors: Forced Convective Channel Flow Thermal Hydraulics, Materials, and Coatings 177

07-035 Computations for Advanced Nuclear Reactor Fuels 111

07-037 Experimental Development and Demonstration of Ultrasonic Measurement Diagnostics for Sodium Fast Reactor Thermohydraulics 113

07-046 Fundamental Processes of Coupled Radiation Damage and Mechanical Behavior in Nuclear Fuel Materials for High-Temperature Reactors 117

07-051 Economic, Depository, and Proliferation Impacts of Advanced Nuclear Fuel Cycles 119

07-057 Optimization of Heat Exchangers 179

07-058 Experimental and Computational Fluid Dynamics Analysis of Advanced Convective Cooling Systems 61

07-059 Analysis of Advanced Fuel Assemblies and Core Designs for the Current and Next Generations of Light-Water Reactors 121

07-060 Powder Metallurgy of Uranium Alloy Fuels for Transuranic-Burning Fast Reactors 123

07-063 Neutronic and Thermal-Hydraulic Coupling Techniques for Sodium-Cooled Fast Reactor Simulations 125

07-064 Fundamental Studies of Irradiation-Induced Defect Formation and Fission Product Dynamics in Oxide Fuels 127

07-069 Establishing a Scientific Basis for Optimizing Compositions, Processing Paths, and Fabrication Methods for Nanostructured Ferritic Alloys for Use in Advanced Fission Energy Systems 65

07-071 Identification and Analysis of Critical Gaps in Nuclear Fuel Cycle Codes Required by the SINEMA Program 129

FY 2007 NERI-C Projects

08-014 An Innovative Approach to Precision Fission Measurements Using a Time Projection Chamber 131

08-020 Risk-Informed Balancing of Safety, Non-Proliferation, and Economics for the Sodium-Cooled Fast Reactor 135

08-033 Deployment of a Suite of High-Performance Computational Tools for Multi-Scale Multi-Physics Simulation of Generation IV Reactors 137

08-039 Real-Time Detection Methods to Monitor TRU Compositions in UREX+ Process Streams 141

08-041 Performance of Actinide-Containing Fuel Matrices Under Extreme Radiation and Temperature Environments 145

08-043 A Research Program on Very High-Temperature Reactors 69

08-047 Advanced Electrochemical Technologies for Hydrogen Production by Alternative Thermochemical Cycles 181

08-051 Radiation Damage in Nuclear Fuel for Advanced Burner Reactors: Modeling and Experimental Validation 149

08-055 Cladding and Structural Materials for Advanced Nuclear Energy Systems 73

08-058 Advanced Instrumentation and Control Methods for Small and Medium Export Reactors with IRIS Demonstration 153

08-067 Advanced Aqueous Separation Systems for Actinide Partitioning 155